NASA TECHNICAL NOTE

NASA TN D-5700

NASA TN D-5700



# FULL-SCALE WIND-TUNNEL INVESTIGATION OF THE STATIC LONGITUDINAL AND LATERAL CHARACTERISTICS OF A LIGHT SINGLE-ENGINE AIRPLANE

*by Marvin P. Fink, Delma C. Freeman, Jr., and H. Douglas Greer*

*Langley Research Center*
*Langley Station, Hampton, Va.*

NATIONAL AERONAUTICS AND SPACE ADMINISTRATION • WASHINGTON, D. C. • MARCH 1970

| 1. Report No. NASA TN D-5700 | 2. Government Accession No. | 3. Recipient's Catalog No. |
|---|---|---|
| 4. Title and Subtitle<br>FULL-SCALE WIND-TUNNEL INVESTIGATION OF THE STATIC LONGITUDINAL AND LATERAL CHARACTERISTICS OF A LIGHT SINGLE-ENGINE AIRPLANE | | 5. Report Date<br>March 1970<br>6. Performing Organization Code |
| 7. Author(s)<br>Marvin P. Fink, Delma C. Freeman, Jr., and H. Douglas Greer | | 8. Performing Organization Report No.<br>L-7012<br>10. Work Unit No.<br>736-01-10-01-23 |
| 9. Performing Organization Name and Address<br>NASA Langley Research Center<br>Hampton, Va. 23365 | | 11. Contract or Grant No.<br>13. Type of Report and Period Covered<br>Technical Note |
| 12. Sponsoring Agency Name and Address<br>National Aeronautics and Space Administration<br>Washington, D.C. 20546 | | 14. Sponsoring Agency Code |

15. Supplementary Notes

16. Abstract

The airplane was a light single-engine low-wing monoplane. Tests were made over an angle-of-attack range of $-4^{0}$ to $20^{0}$ and over a sideslip range of $\pm 8^{0}$ at thrust coefficients of $T_C' = 0$, 0.20, and 0.46. Control effectiveness was taken for a full range of deflections on the aileron, elevator, rudder, and flap. Downwash measurements at tail were also obtained for the range of thrust coefficient and flap deflection.

| 17. Key Words Suggested by Author(s)<br>Light single-engine airplane<br>Stability and control<br>Tail downwash | 18. Distribution Statement<br>Unclassified – Unlimited | | |
|---|---|---|---|
| 19. Security Classif. (of this report)<br>Unclassified | 20. Security Classif. (of this page)<br>Unclassified | 21. No. of Pages<br>138 | 22. Price*<br>$3.00 |

*For sale by the Clearinghouse for Federal Scientific and Technical Information
Springfield, Virginia 22151

# FULL-SCALE WIND-TUNNEL INVESTIGATION OF THE STATIC LONGITUDINAL AND LATERAL CHARACTERISTICS OF A LIGHT SINGLE-ENGINE AIRPLANE

By Marvin P. Fink, Delma C. Freeman, Jr.,
and H. Douglas Greer
Langley Research Center

## SUMMARY

A force test investigation has been conducted in the Langley full-scale tunnel to determine the static longitudinal and lateral stability and control characteristics of a full-scale, light, single-engine airplane. The investigation was made over an angle-of-attack range of $-4^{\circ}$ to $20^{\circ}$ at various angles of sideslip between $\pm 8^{\circ}$ for various power and flap settings. The power conditions were a thrust coefficient $T_c'$ of zero which represents either a low-power or a high-speed condition (where the thrust coefficient approaches zero), $T_c' = 0.20$ which corresponds to a climb condition, and $T_c' = 0.46$ which corresponds to a take-off condition.

The investigation showed that the airplane has stick-fixed longitudinal stability for angles of attack up to and through the stall for all configurations tested with the center of gravity located at 0.10 mean aerodynamic chord. Power generally has a small destabilizing effect but the airplane is statically stable even with the most rearward center-of-gravity location. The airplane is directionally stable and has positive effective dihedral through the stall for all conditions tested. The aileron and rudder effectiveness was maintained through the stall and was powerful enough to trim out all airplane moments through the stall.

## INTRODUCTION

For the past several years the NASA Flight Research Center has been conducting a program to evaluate the flying qualities of a number of general aviation aircraft. The results of these investigations have been reported in reference 1. As a part of the continuing investigation, one of the airplanes investigated in reference 1, a light twin-engine configuration, was tested in the Langley full-scale tunnel, and the results have been reported in reference 2. The next phase of the wind-tunnel program was to investigate the characteristics of the single-engine version of the airplane of reference 2. The investigation was made to determine the static longitudinal and lateral stability and

control characteristics with various power and flap settings over a range of angles of attack from $-4^{o}$ to $20^{o}$ and over a range of sideslip angles of $\pm 8^{o}$. The tests except those at thrust coefficients of 0.46 and 0.55 were made at a tunnel speed of about 93 feet per second which gives a Reynolds number of approximately $2.96 \times 10^{6}$. Tests at 0.46 and 0.55 thrust coefficient were made at tunnel speeds of 54.8 and 77.0 feet per second, respectively.

## SYMBOLS

Figure 1 shows the stability-axis system used in the presentation of the data and the positive direction of forces, moments, and angles. The data are computed about the moment center shown in figure 2 which is at airplane longitudinal station 85, or 10.0 percent of the mean aerodynamic chord and 1.0 ft (0.30 m) below the reference line.

| | |
|---|---|
| $b$ | wing span, 35.98 ft (10.97 m) |
| $C_D$ | drag coefficient, Drag/qS |
| $C_L$ | lift coefficient, Lift/qS |
| $C_m$ | pitching-moment coefficient, Pitching moment/$qS\bar{c}$ |
| $C_n$ | yawing-moment coefficient, Yawing moment/qSb |
| $C_l$ | rolling-moment coefficient, Rolling moment/qSb |
| $C_Y$ | side-force coefficient, Side force/qS |
| $C_{L_\alpha}$ | lift-curve slope at $\alpha = 0^{o}$, untrimmed |
| $C_{l_\beta}$ | lateral stability parameter |
| $C_{n_\beta}$ | directional stability parameter |
| $\frac{\partial C_m}{\partial C_L}$ | longitudinal stability parameter |
| $C_{l_{\delta,a}}$ | aileron effectiveness parameter $\frac{\partial C_l}{\partial \delta_a}$, per deg |
| $C_{l_{\delta,r}}$ | rolling effectiveness of rudder |

| | |
|---|---|
| $C_{m_{\delta,t}}$ | horizontal-tail effectiveness parameter, $\frac{\partial C_m}{\partial \delta_t}$, per deg |
| $C_{n_{\delta,a}}$ | yawing effectiveness of aileron |
| $C_{n_{\delta,r}}$ | rudder effectiveness parameter, $\frac{\partial C_n}{\partial \delta_r}$, per deg |
| $\bar{c}$ | mean aerodynamic chord, 5 ft (1.53 m) |
| D | propeller diameter, 6.42 ft (1.96 m) |
| n | propeller speed, revolutions/sec |
| q | free-stream dynamic pressure, $lbf/ft^2$ $(N/m^2)$ |
| $\frac{q_t}{q}$ | ratio of dynamic pressure at tail to free-stream dynamic pressure |
| S | wing area, 178 $ft^2$ $(16.50\ m^2)$ |
| T | effective thrust, $Drag_{\text{propellers removed}} - Drag_{\text{propellers operating}}$ |
| $T_c'$ | thrust coefficient, $T/qS$ at $\alpha = 0^o$ |
| V | free-stream velocity, ft/sec (m/sec) |
| $\frac{V}{nD}$ | propeller advance ratio |
| x | longitudinal axis |
| $\alpha$ | angle of attack of fuselage reference line, deg |
| $\beta$ | angle of sideslip, positive when nose is to left, deg |
| $\delta_a$ | total aileron deflection, positive when right aileron is down, $(\delta_a)_{\text{Left}} - (\delta_a)_{\text{Right}}$, deg |
| $\delta_f$ | flap deflection, positive when trailing edge is down, deg |
| $\delta_r$ | rudder deflection, positive when trailing edge is left, deg |

$\delta_t$ horizontal-tail deflection, positive when trailing edge is down, deg

$\epsilon$ downwash angle at tail, deg

Subscript:

max maximum

## AIRPLANE

The airplane tested was a light, single-engine, low-wing monoplane having a maximum take-off weight of 3100 lb (13 800 N). Figure 2 gives the principal dimensions and figure 3 shows the airplane mounted in the tunnel test section. The airplane had a wing span of 35.98 feet (10.97 m), a wing area of 178 $ft^2$ (16.50 $m^2$), an aspect ratio of 7.3, and a mean aerodynamic chord of 5 feet (1.53 m) based on projection of the outboard leading edge of the wing through the fuselage. The wing airfoil section was a modified NACA $64_2A215$ airfoil with the trailing-edge cusp faired out. The wing had $5^o$ of geometric dihedral and was at $2^o$ positive incidence with respect to the fuselage reference line. Normally the airplane wing has no twist, but measurements of the test vehicle taken at the wing root and wing tip showed that the left wing tip had $1^o$ of positive incidence with respect to the wing root. Power was provided by a variable-frequency electric motor. The thrust axis was canted $3^o$ to right and $2.75^o$ downward to the reference line. The airplane had a standard three-control system. The horizontal tail was of the all-movable type with a travel of $3.4^o$ to $-12.8^o$. The horizontal tail had a geared trailing-edge tab which moved in the same direction as the tail with a deflection ratio (tab deflection/tail deflection) of 1.5. The travel of each aileron was from $15^o$ to $-17.8^o$. The rudder travel was $\pm 25^o$.

## TESTS

The tests were made to determine the static longitudinal and lateral stability and control characteristics of the airplane over a wide range of flight conditions. The airplane was tested over an angle-of-attack range of $-4^o$ to $20^o$ and over a sideslip range of $\pm 8^o$ for the clean condition ($\delta_f = 0^o$, gear up) and for $15^o$ and $32^o$ flap deflections with gear down. A range of tail incidence angles from $3.4^o$ to $-18.8^o$ was investigated at zero sideslip, and the aileron and rudder effectiveness was measured over the sideslip range. The tests were made at thrust coefficients of $T_C' = 0$, 0.20, and 0.46 which represent flight conditions of low power or high speed, a climb at best angle at about 90-percent power, and at full power as in take-off, respectively. The test thrust coefficients were based on

installed horsepower of 260. Several tests were made at a thrust coefficient of 0.55 which would be representative of a 355 horsepower engine. The propeller blade angle, and consequently the advance ratio, for each thrust coefficient was set at a fixed value which was representative of that for flight conditions at which the particular value of thrust coefficient could be achieved. The values of $V/nD$ were 0.98, 0.49, 0.33, and 0.33 for values of $T_C'$ of 0, 0.20, 0.46, and 0.55, respectively. A propeller blade angle of 19.5° was set for $T_C' = 0$ and 0.46; and 23° was used for $T_C' = 0.20$. Tail downwash surveys were made along the horizontal tail hinge axis with the tail off at zero sideslip for flap deflections of 0°, 15°, and 32° for $T_C' = 0$, 0.20, and 0.46.

## PRESENTATION OF DATA

The data from these tests have been corrected for airstream misalinement, horizontal buoyancy effects, mounting strut tares, and wind-tunnel jet-boundary effects.

The data are presented in the following figures:

## RESULTS AND DISCUSSION

The basic data obtained during the wind-tunnel investigation are presented in figures 4 to 37 without analysis. Summary plots have been prepared from some of these data to illustrate the general static stability and control characteristics of the airplane. Only the summary plots are discussed.

### Longitudinal Characteristics

The longitudinal characteristics of the airplane with various power conditions are presented in figure 38 for flap deflections of $0^{\circ}$, $15^{\circ}$, and $32^{\circ}$. As might be expected, increasing power results in an increase in lift-curve slope and maximum lift coefficient because of the increased slipstream velocity over the wing. This effect of power on the lift characteristics is summarized in figure 39 where lift-curve slope and maximum lift coefficient are shown as functions of thrust coefficient.

The pitching-moment curves shown in figure 38 are virtually linear through the stall and do not exhibit the nose-down pitching moment at the stall usually associated with a straight-wing airplane. The variation of the pitching-moment curves with angle of attack indicates that increasing thrust has little effect on the longitudinal characteristics except for a trim change. These power effects are further illustrated in figure 40 where the variation in static margin $\partial C_m/\partial C_L$ with thrust coefficient is presented. These data are a measure of the stick-fixed stability and show that power is destabilizing. The effects are generally small, however, and the airplane would have high static stability even at the aft center-of-gravity location (longitudinal station 92 or $0.22\bar{c}$).

The variation of horizontal-tail effectiveness with angle of attack is presented in figure 41 for flap deflections of $0^{\circ}$, $15^{\circ}$, and $32^{\circ}$. These data show that there is a relatively small reduction in tail effectiveness at the higher angles of attack, particularly with flaps down, and that the general level of tail effectiveness is little affected by flap deflection for a given power condition. The tail effectiveness is presented as a function of

thrust coefficient in figure 42 for each flap deflection of the tests. These data show that power increased the tail effectiveness as would be expected, the slipstream acting on part of the tail.

Presented in figure 43 is the variation of the average downwash angle and the dynamic pressure ratio at the tail with angle of attack for the flap and power conditions investigated. These data were obtained from surveys and show a large increase in downwash angle with flap deflection. Also, there is little effect of power on the downwash angle except for $\delta_f = 32^o$ and $T_c' = 0.46$. The dynamic-pressure ratio is relatively unaffected by flap deflection but increases with power, as might be expected.

## Lateral Characteristics

The variation of the effective-dihedral parameter $C_{l_\beta}$ with angle of attack is shown in figure 44 for the various flap and power conditions of the test. The data show that the airplane has positive effective dihedral $\left(-C_{l_\beta}\right)$ in all conditions except for $\delta_f = 32^o$ and $T_c' = 0.55$ where $C_{l_\beta}$ is about zero in the middle angle-of-attack range. The value of $-C_{l_\beta}$ varies widely depending upon the angle of attack, flap, or power condition; this statement means the response of the airplane to gusts or to rudder inputs to raise a wing could vary with the airplane configuration and flight condition.

The variation of the directional stability parameter $C_{n_\beta}$ with angle of attack is shown in figure 45 for the various flap and power conditions. These data show that the airplane is directionally stable in all conditions over the entire angle-of-attack range. As was the case for the effective dihedral, the value of $C_{n_\beta}$ varies considerably for the different conditions. The effect of power on the directional stability characteristics is presented in figure 46 and shows that power causes a large increase in the directional stability as would be expected because of the increase in dynamic pressure at the tail caused by the slipstream.

The variation of the aileron rolling moments with angle of attack for sideslip angles of $0^o$ and $\pm 8^o$ is presented in figure 47 for flaps deflected $0^o$ and $32^o$ and $T_c' = 0$ and 0.46. These data show that in general, the aileron effectiveness remains at a fairly constant level throughout the angle-of-attack range and is relatively unaffected by flap deflection, power, or angle of sideslip. The variation of the aileron yawing moments with angle of attack is presented in figure 48 for the same flap and power conditions. These data show that the ailerons produce adverse yaw for all conditions and the magnitude of the yawing moment increases with increasing angle of attack.

The variation of rudder effectiveness with angle of attack for sideslip angles from $8^o$ to $-8^o$ is presented in figures 49 to 51 for all power conditions tested and for flap deflections of $0^o$ and $32^o$. These data show that rudder effectiveness is maintained throughout the angle-of-attack range for all test conditions although there is some

decrease in effectiveness near the stall, particularly for the negative sideslip conditions with high power. The effect of power on the rudder effectiveness is presented in figure 51. The data show that the rudder effectiveness is more than doubled at maximum power because of the increased dynamic pressure at the tail caused by the slipstream.

The basic lateral characteristics of the airplane, as shown by the variation of the lateral coefficients $C_l$ and $C_n$ with angle of attack for $0^\circ$ sideslip, are presented in figure 52 for the various flap and power conditions of the test. The data show that below the stall, there is an out-of-trim positive rolling moment for all conditions that gradually reduces with an increase in angle of attack. The rolling moment becomes negative near the stall. Tufts showed that the left wing starts to stall in the area aft of the intersection of the inboard glove and the wing leading edge. After the stall, the rolling moment might become positive again, depending upon the configuration. In any case, the rolling moments generated at the stall are not unusually large. The data also show that the application of power creates a negative yawing moment that increases with angle of attack up to about the stall and then decreases above the stall. This yawing moment is caused by the action of the slipstream on the vertical tail.

An attempt has been made to determine whether the controls are powerful enough to overcome the asymmetric moments near the stall, and the results of the analysis are presented in figure 53. In this figure is plotted the variation of the rolling and yawing moments with angle of attack at $0^\circ$ sideslip for $T_c' = 0.46$ and $\delta_f = 32^\circ$. Added to these curves are the moments available from full opposite aileron and rudder deflection (including the adverse yaw of the ailerons and the roll due to rudder deflection). These data show that based on static wind-tunnel results, the rolling and yawing moments available from aileron and rudder are more than adequate to trim out the airplane moments.

## CONCLUSIONS

A full-scale wind-tunnel investigation has been made to determine the static longitudinal and lateral stability and control characteristics of a light single-engine airplane. The investigation was made over an angle-of-attack range of $-4^\circ$ to $20^\circ$ at various angles of sideslip between $\pm 8^\circ$ for various power and flap settings. The following conclusions were drawn from the results of the investigation:

1. The airplane has stick-fixed longitudinal stability through the stall for all configurations of the test, the center of gravity being located at 0.10 mean aerodynamic chord. Power generally has a small destabilizing effect, but the airplane is statically stable even with the aft center-of-gravity location.

2. The airplane is directionally stable and has positive effective dihedral through the stall for all conditions of the test.

3. Aileron and rudder effectiveness is maintained through the stall.

4. Aileron and rudder controls are powerful enough to trim out all asymmetric airplane moments through the stall.

Langley Research Center,
National Aeronautics and Space Administration,
Langley Station, Hampton, Va., December 19, 1969.

## REFERENCES

1. Barber, Marvin R.; Jones, Charles K.; Sisk, Thomas R.; and Haise, Fred W.: An Evaluation of the Handling Qualities of Seven General-Aviation Aircraft. NASA TN D-3726, 1966.

2. Fink, Marvin P.; and Freeman, Delma C., Jr.: Full-Scale Wind-Tunnel Investigation of Static Longitudinal and Lateral Characteristics of a Light Twin-Engine Airplane. NASA TN D-4983, 1969.

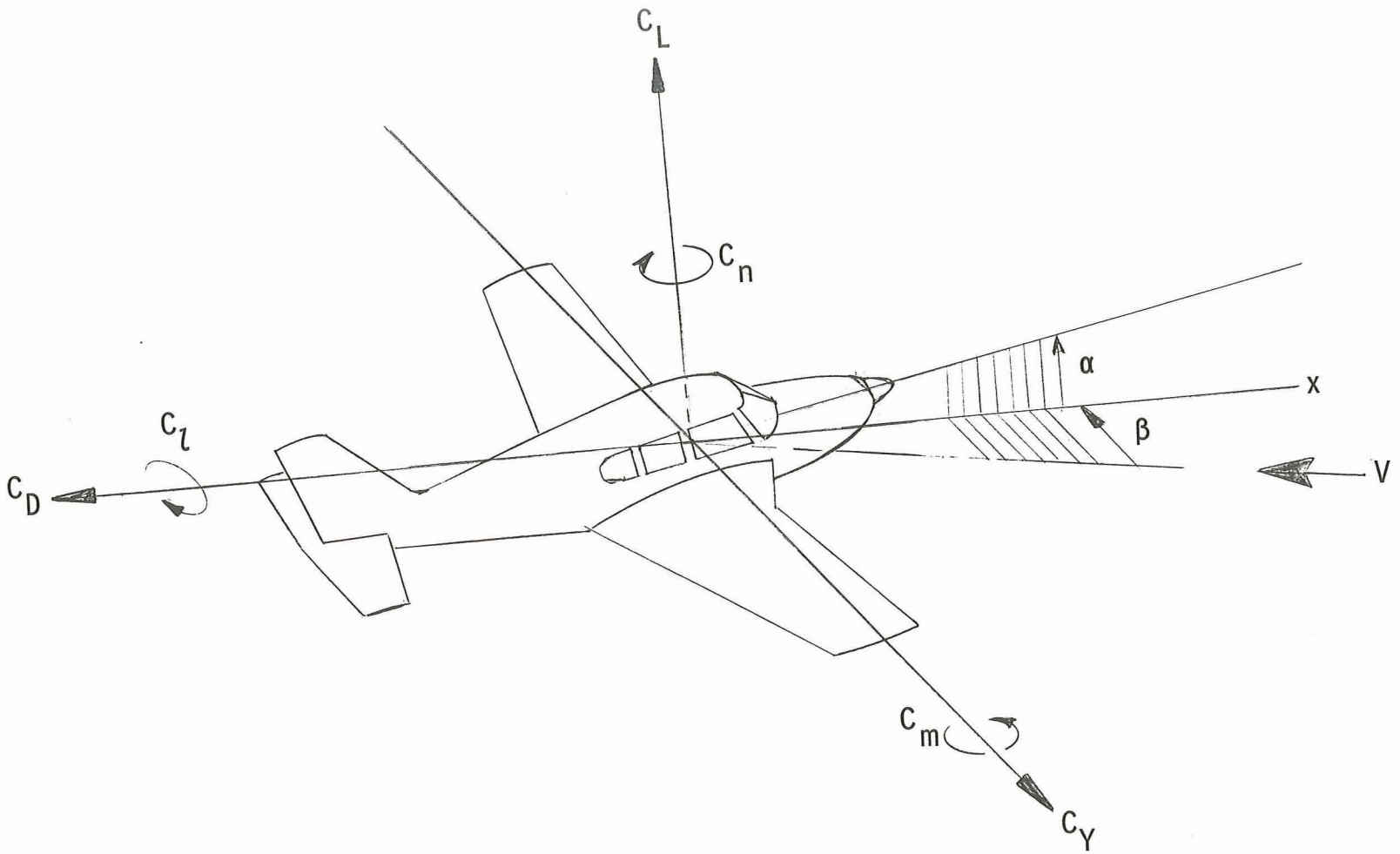


Figure 1.- System of axes and positive sense of angles, forces, and moments.

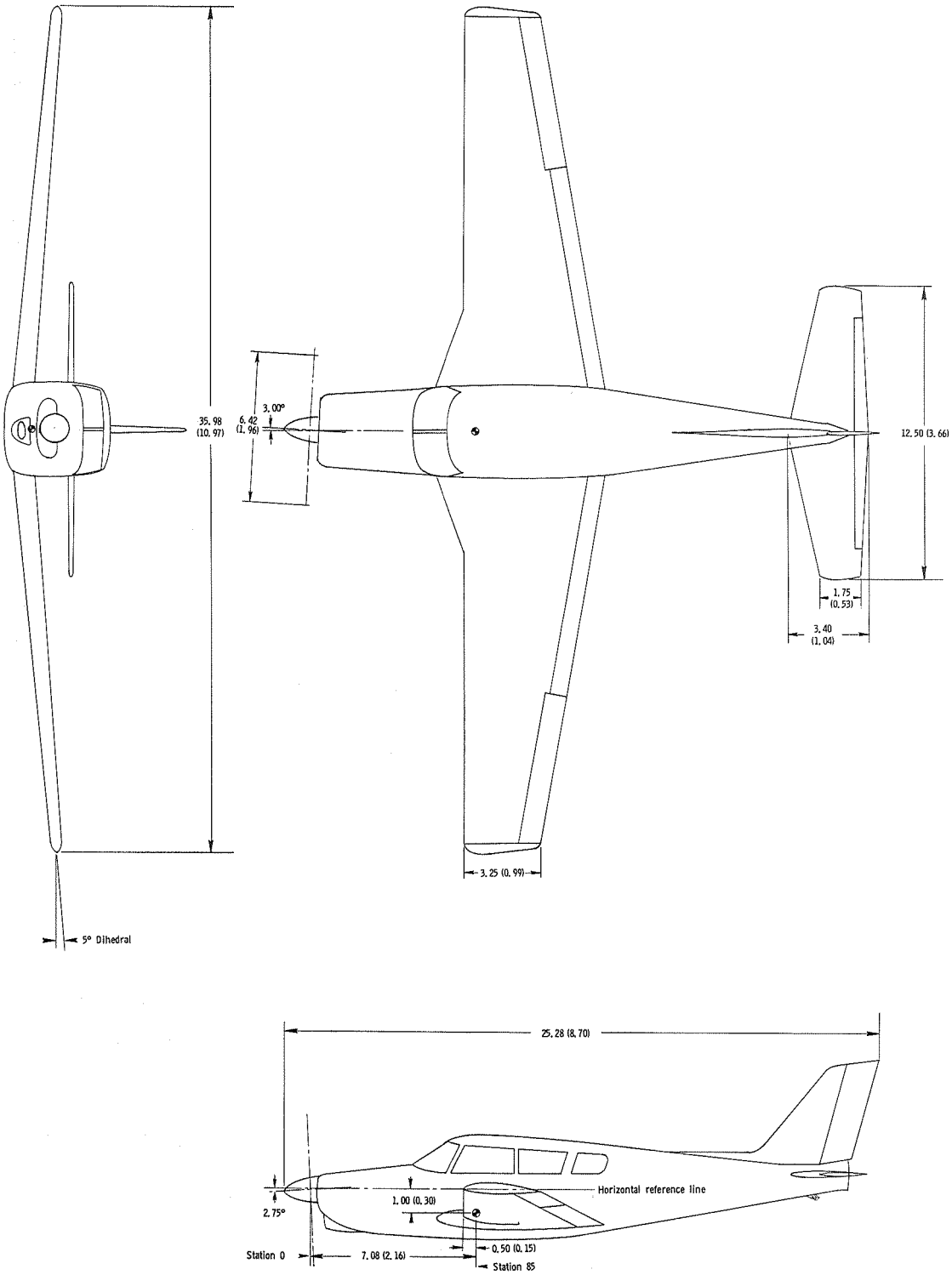


Figure 2.- Three-view drawing of airplane. All dimensions are in feet (meters).

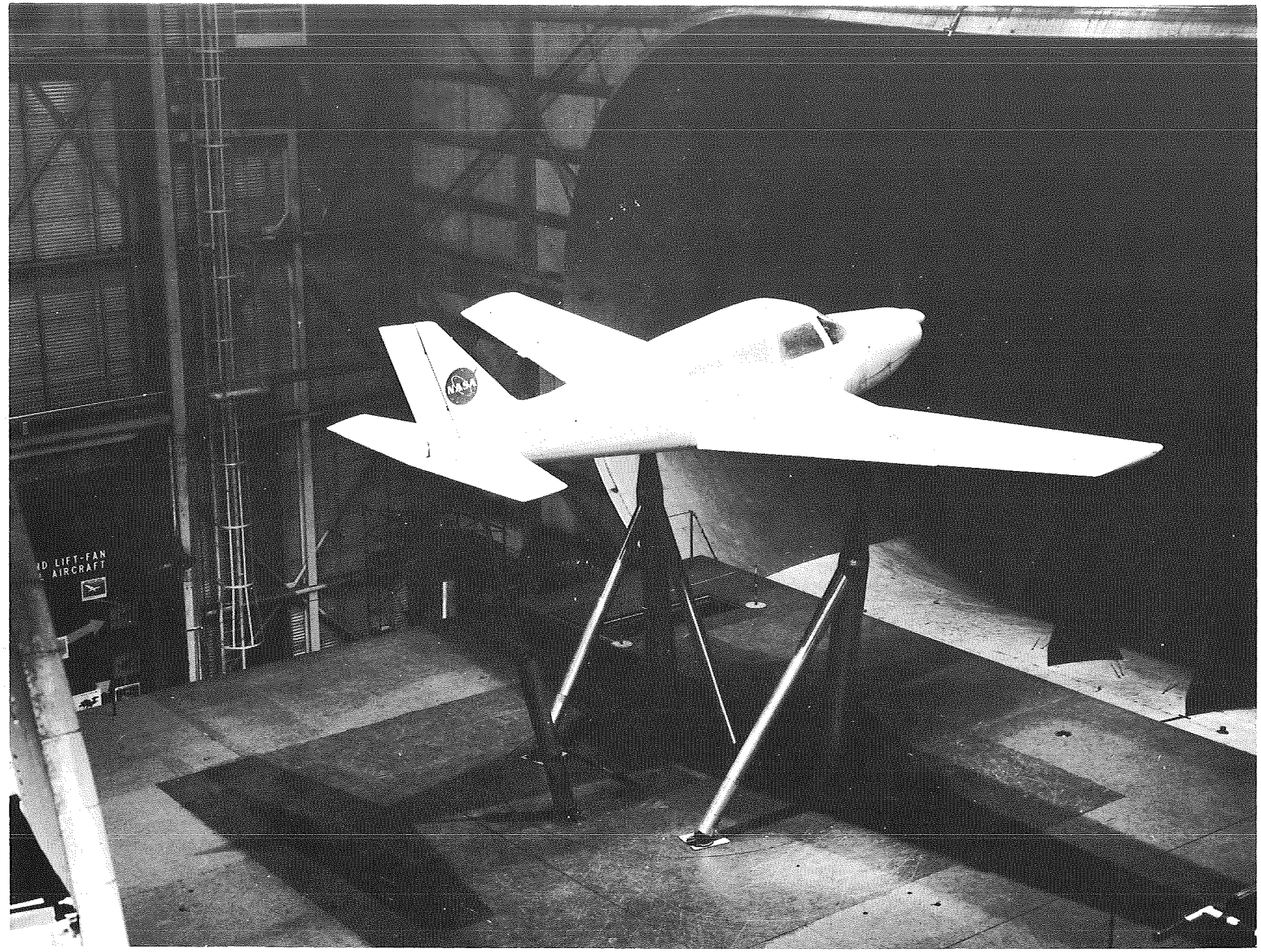


Figure 3.- Photograph of airplane mounted in Langley full-scale tunnel.

L-69-3193

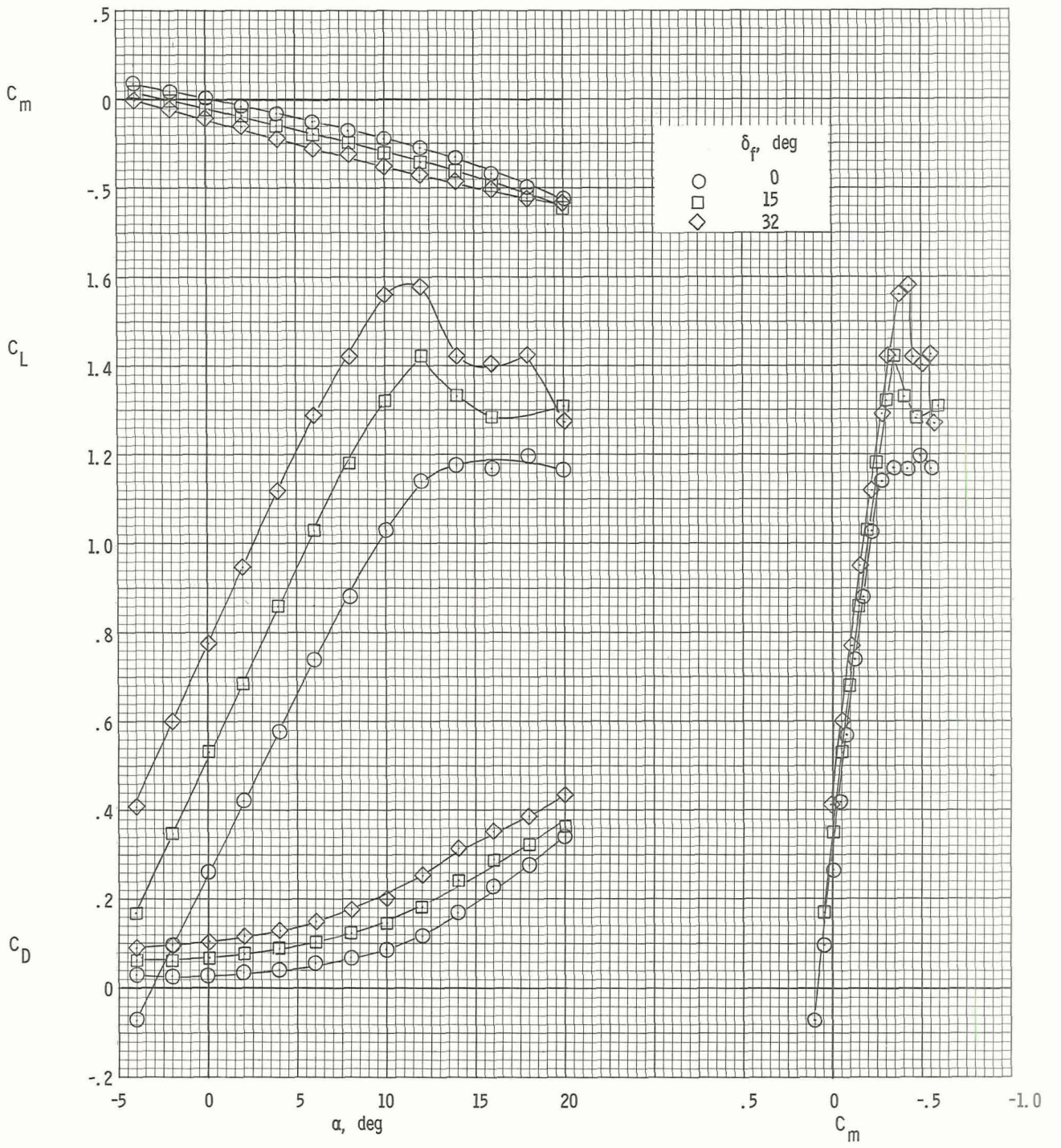


Figure 4.- Longitudinal aerodynamic characteristics of the airplane with propellers removed for several flap deflections.

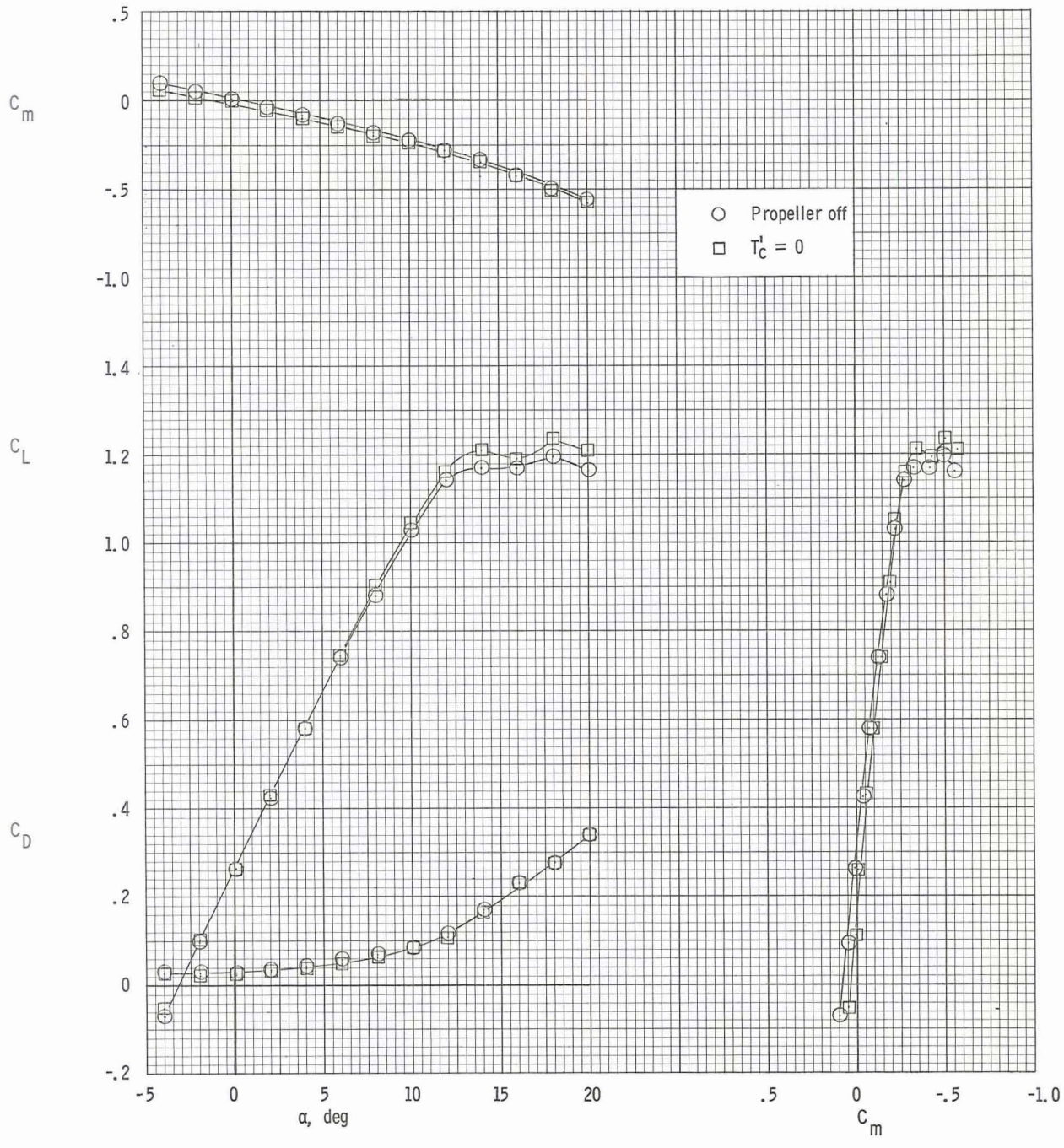


(a) $\delta_f = 0^o$.

Figure 5.- Comparison of the longitudinal characteristics of the airplane with propeller removed and zero thrust coefficient.

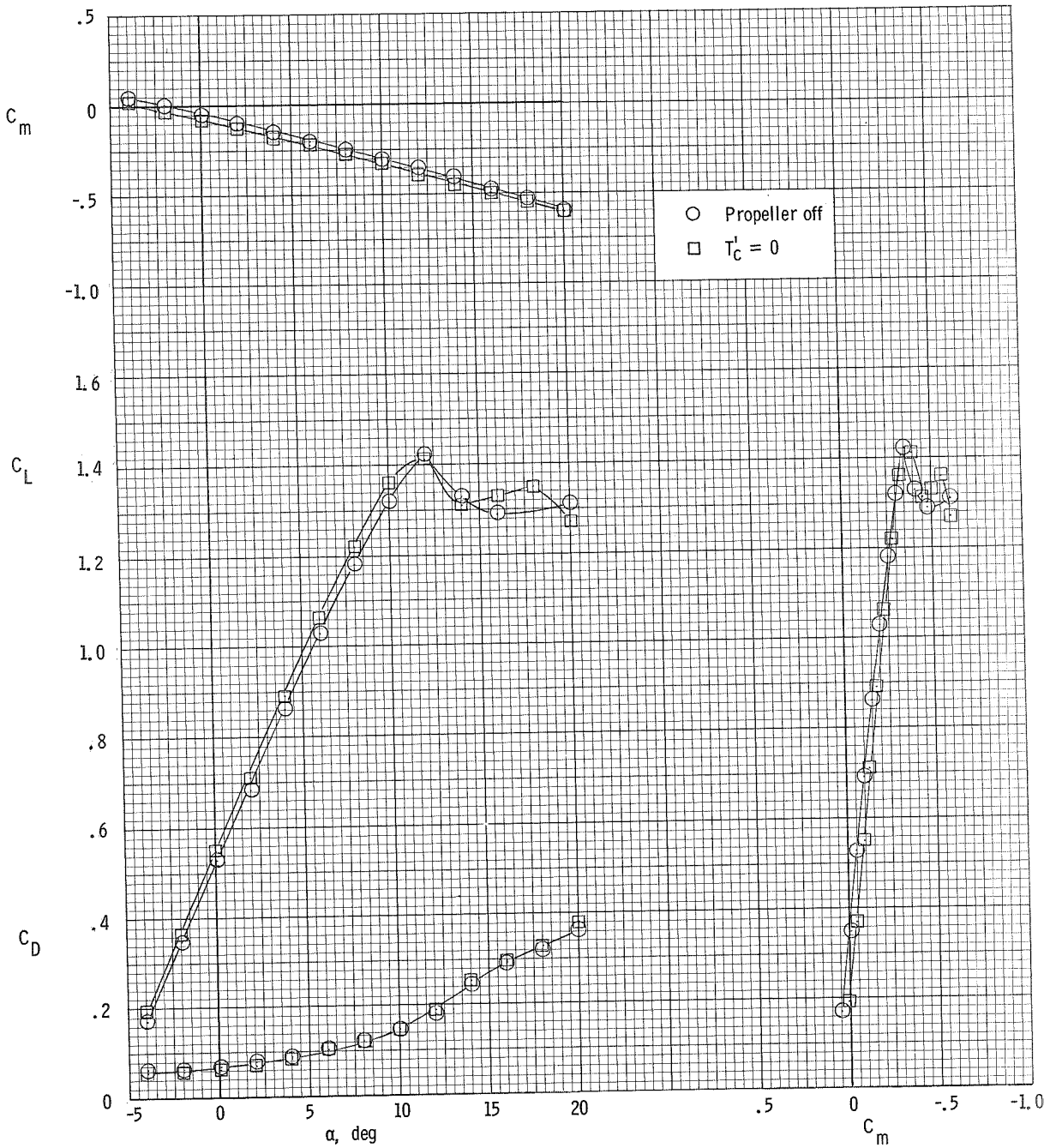


(b) $\delta_f = 15^o$.

Figure 5.- Continued.

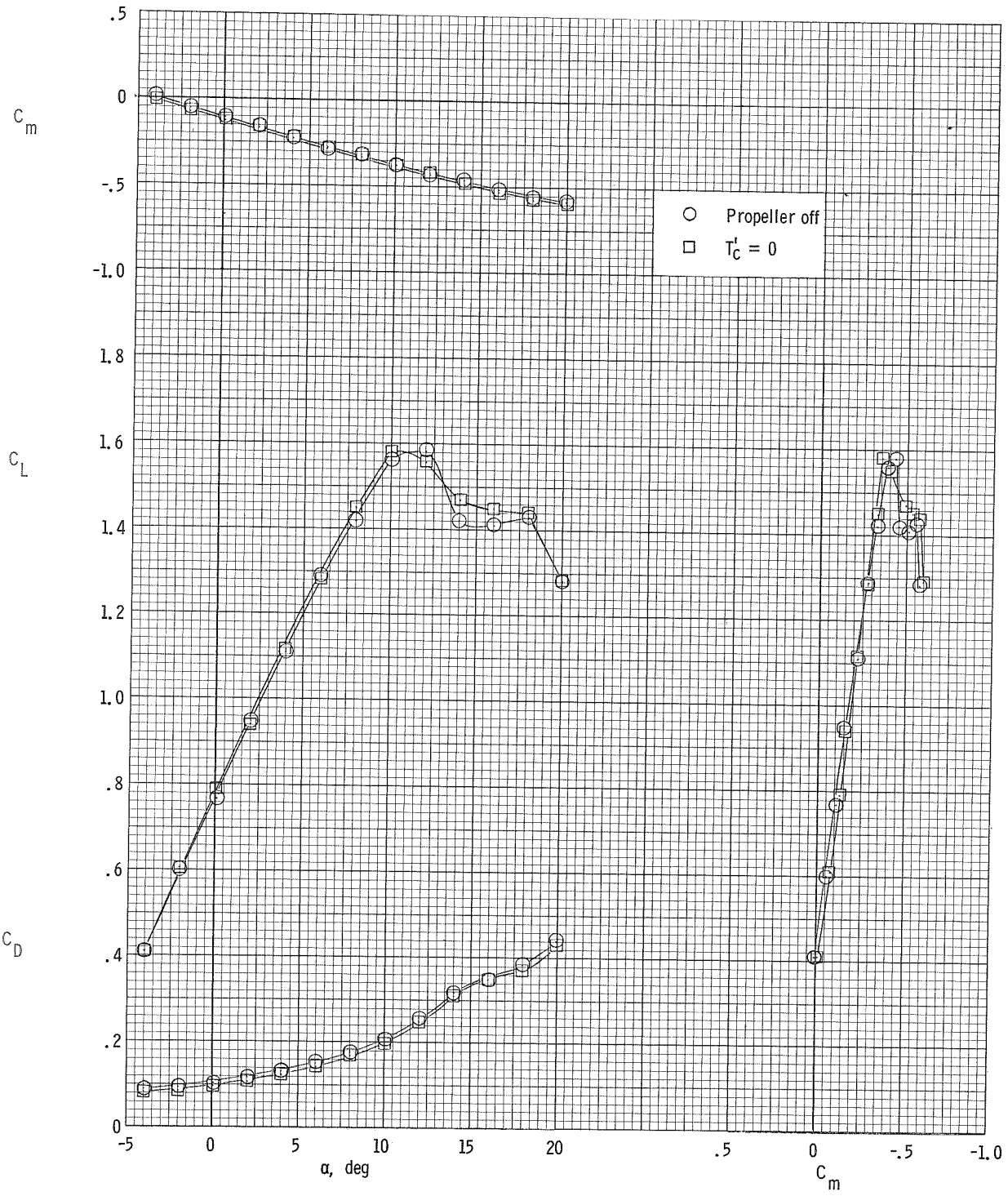


(c) $\delta_f = 32^o$.

Figure 5.- Concluded.

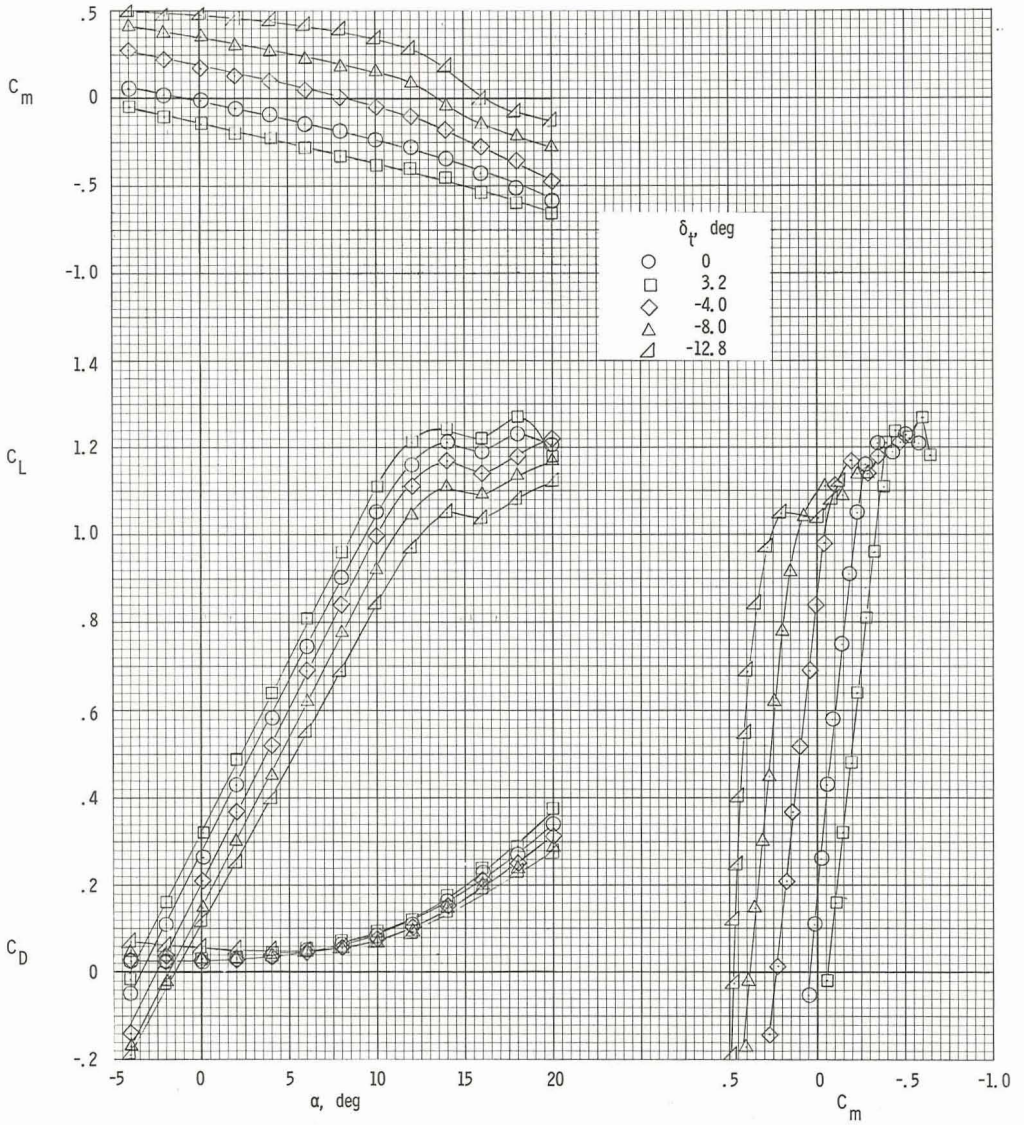


(a) $T_C' = 0.$

Figure 6.- Longitudinal aerodynamic characteristics of the airplane for several thrust coefficients for $\delta_f = 0^o$.

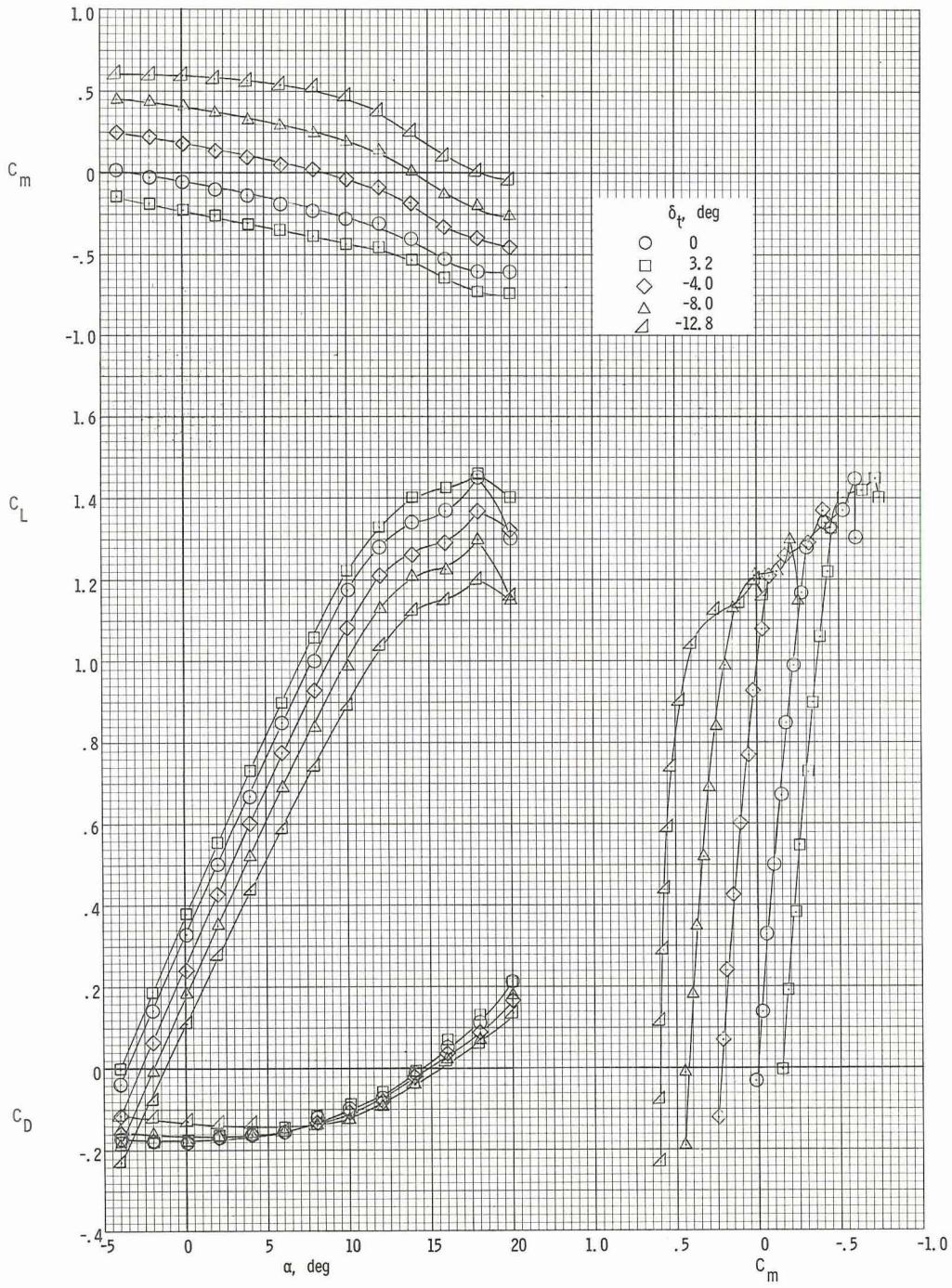


(b) $T_c' = 0.20$.

Figure 6.- Continued.

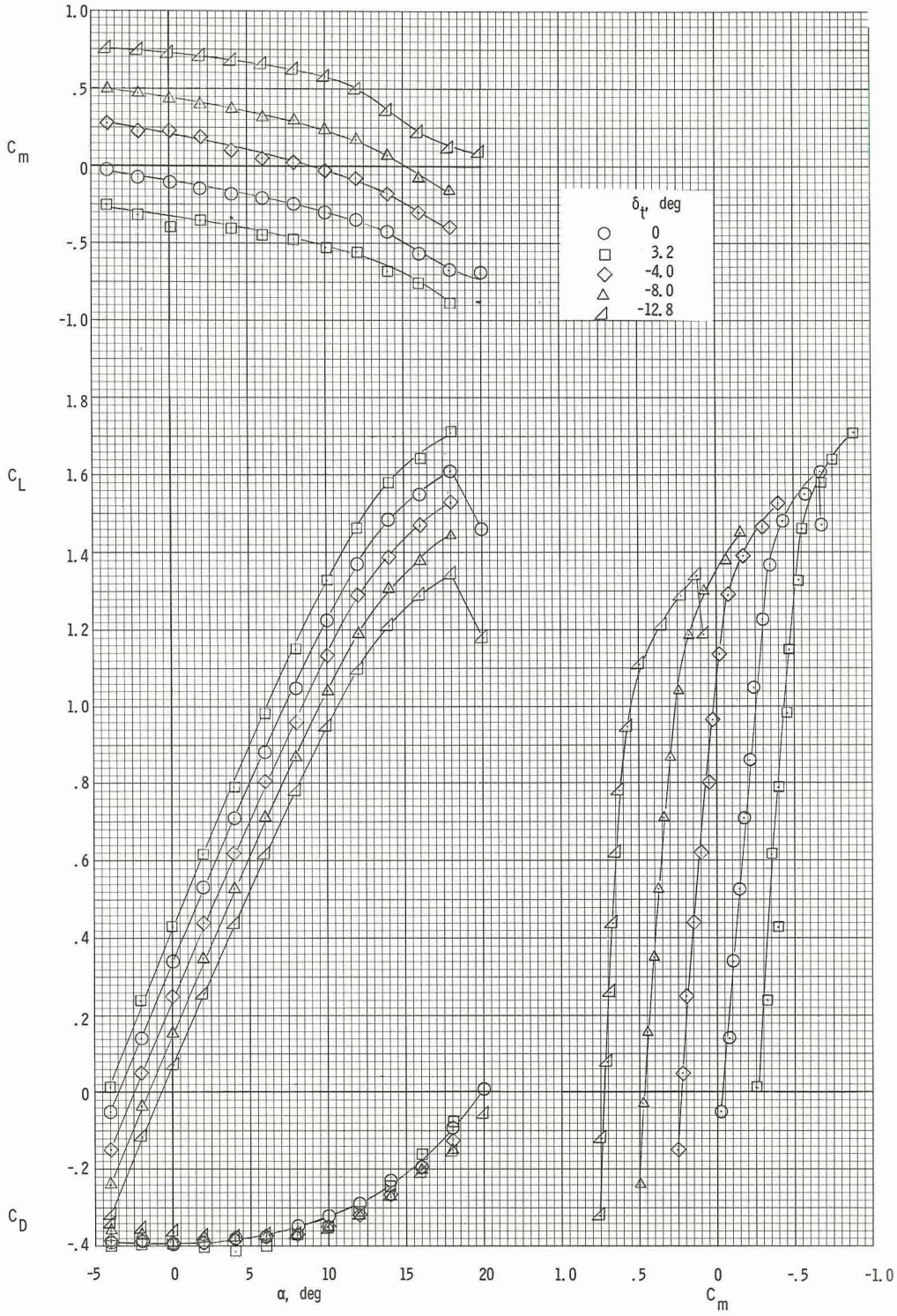


(c) $T_C' = 0.46$.

Figure 6.- Concluded.

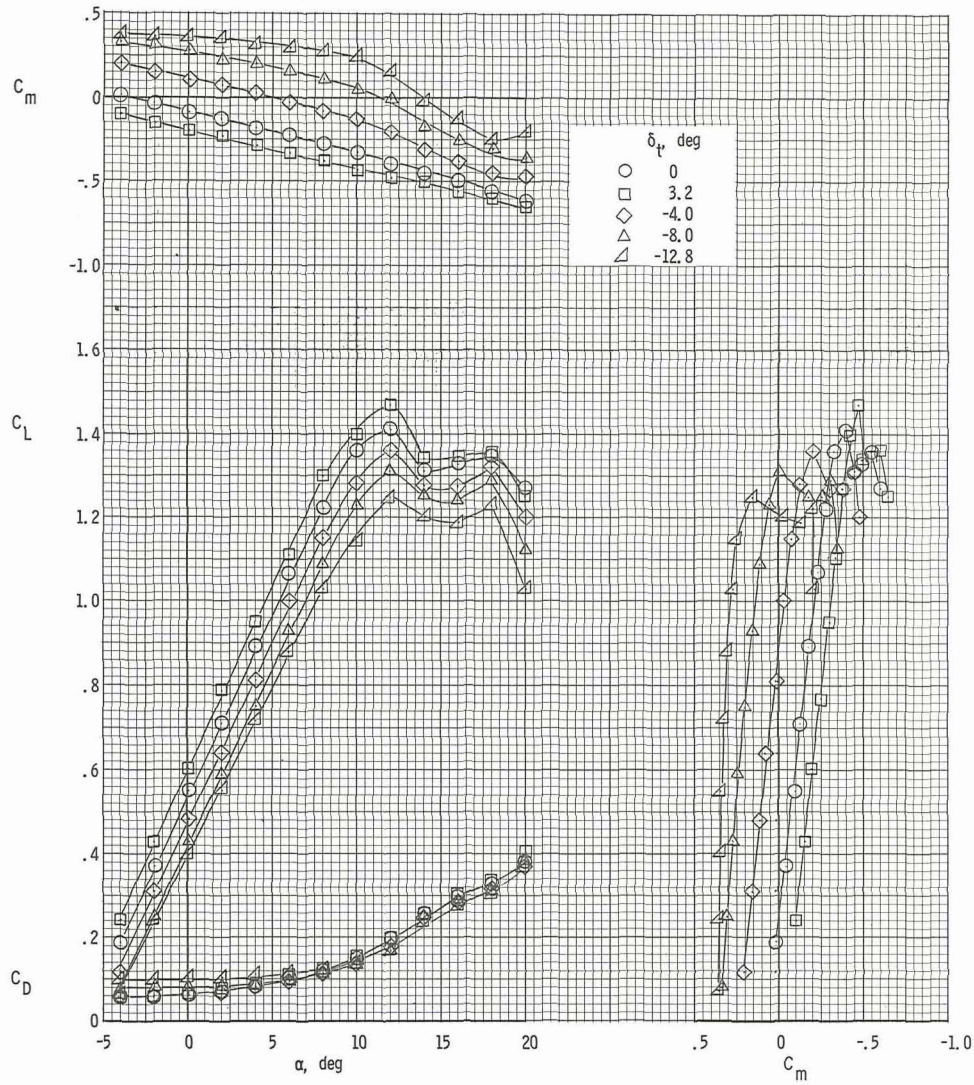


(a) $T_C' = 0$.

Figure 7.- Longitudinal aerodynamic characteristics of the airplane for several thrust coefficients. $\delta_f = 15^0$.

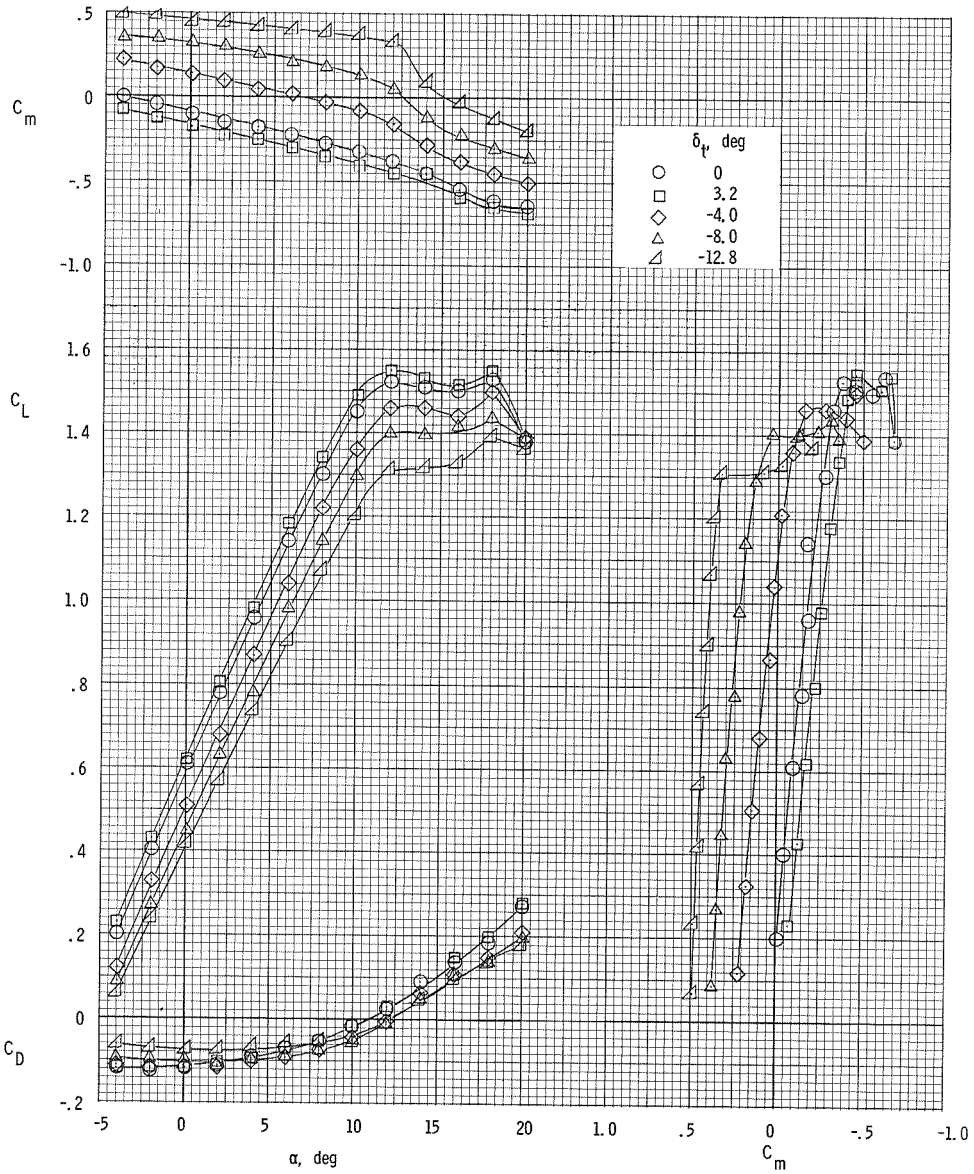


(b) $T_C' = 0.20$.

Figure 7.- Continued.

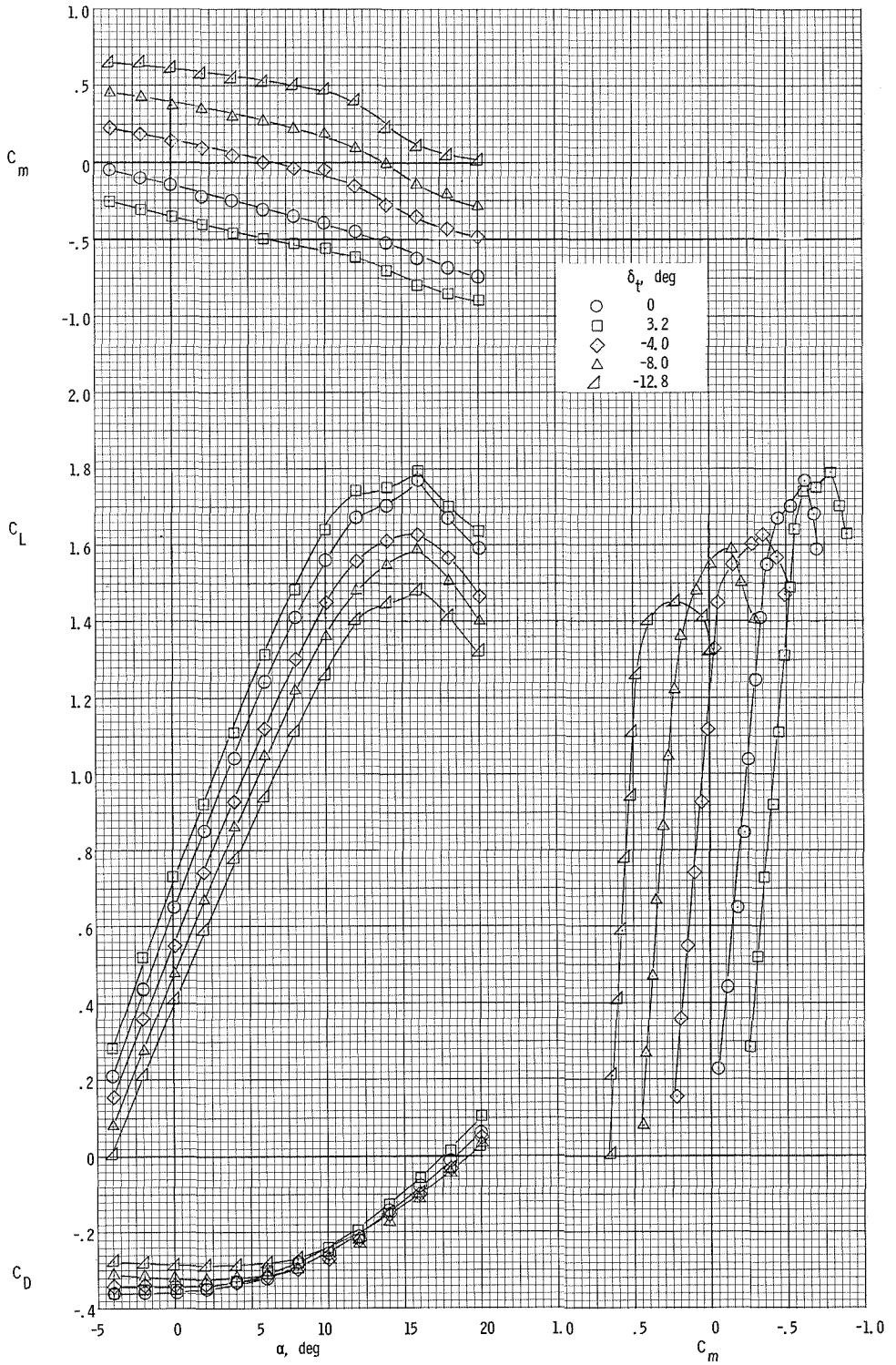


(c) $T_C' = 0.46$.

Figure 7.- Concluded.

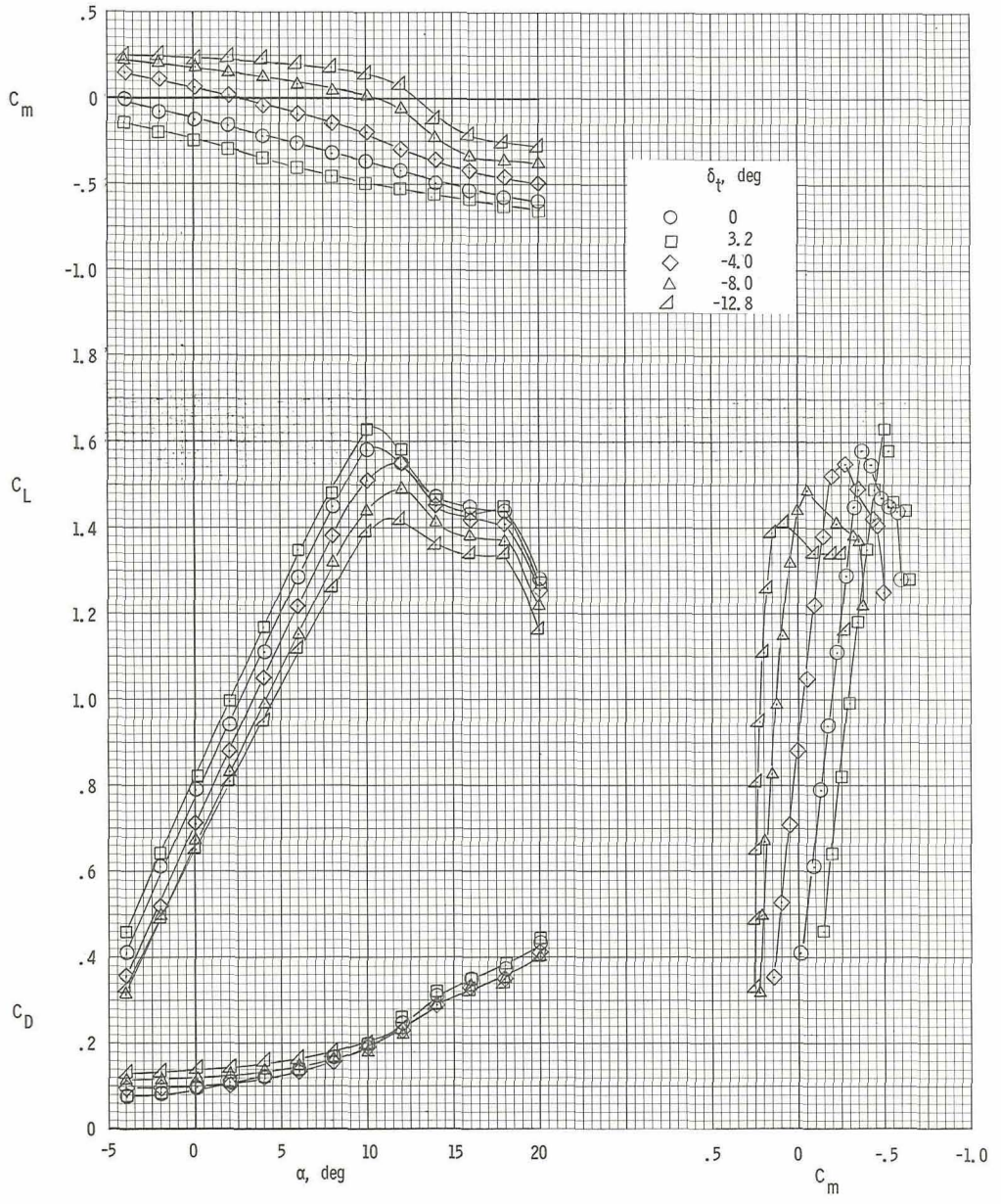


(a) $T_C' = 0$.

Figure 8.- Longitudinal aerodynamic characteristics of the airplane for several thrust coefficients. $\delta_f = 32^o$.

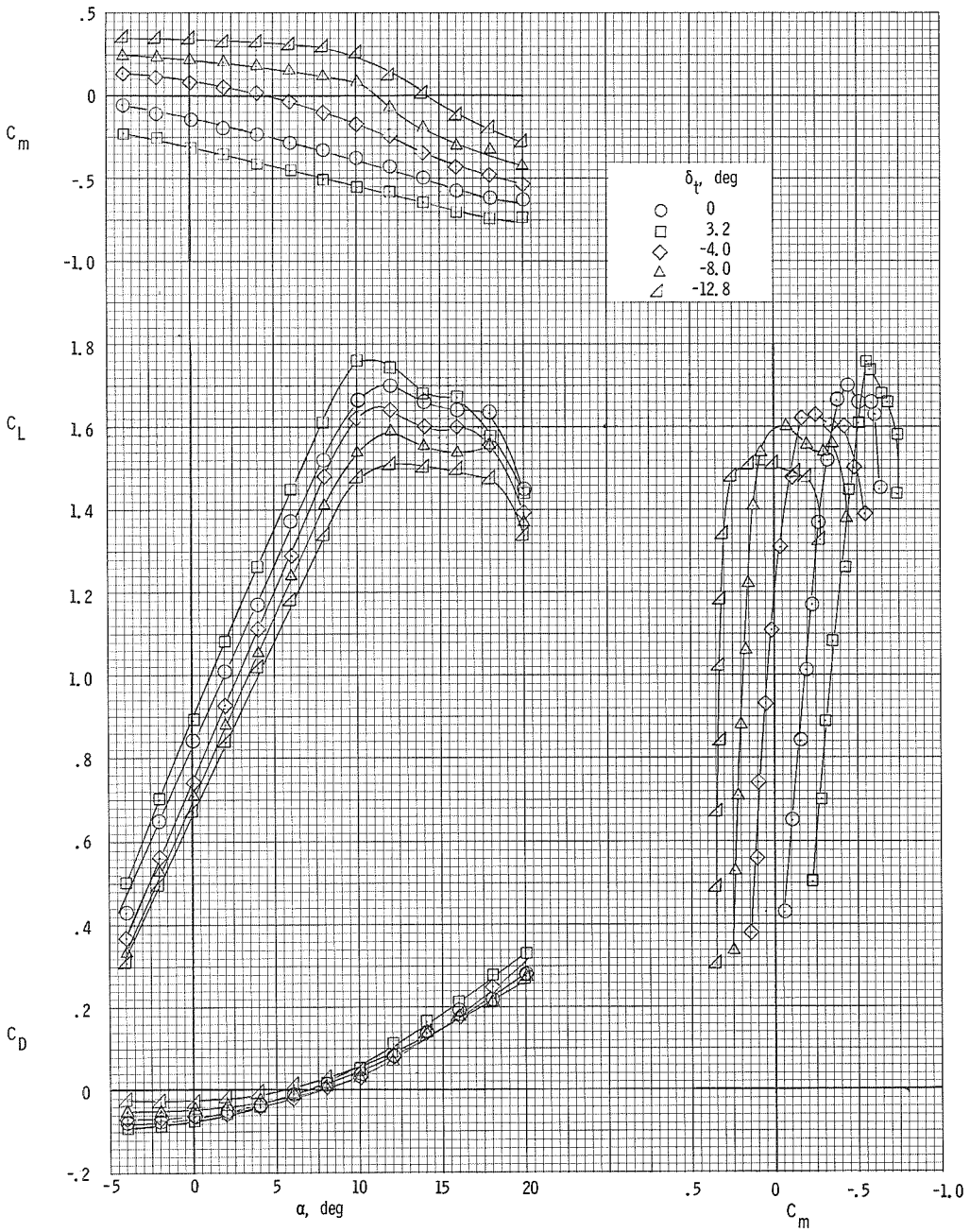


(b) $T_C' = 0.20$.

Figure 8.- Continued.

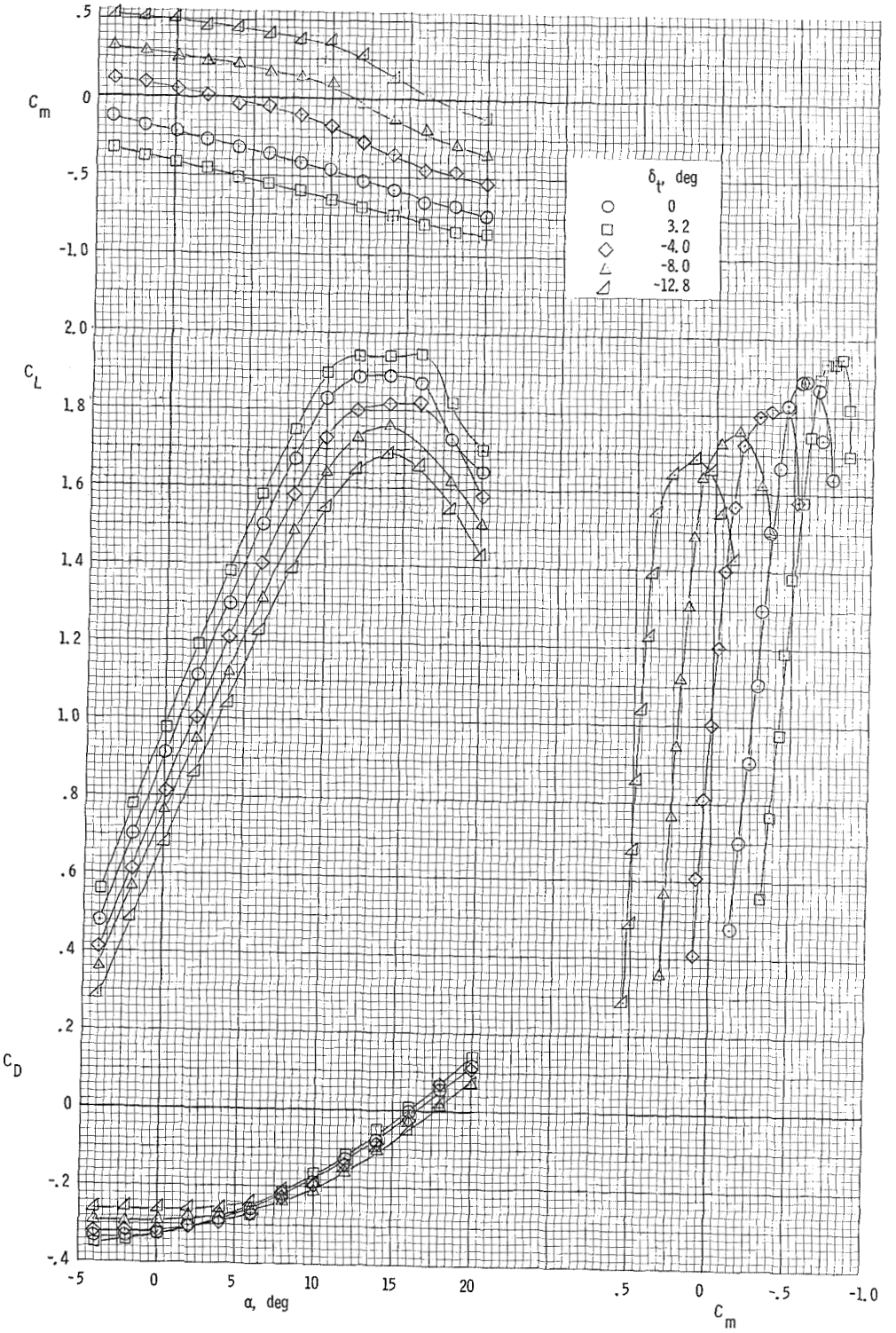


(c) $T_C' = 0.46$.

Figure 8.- Concluded.

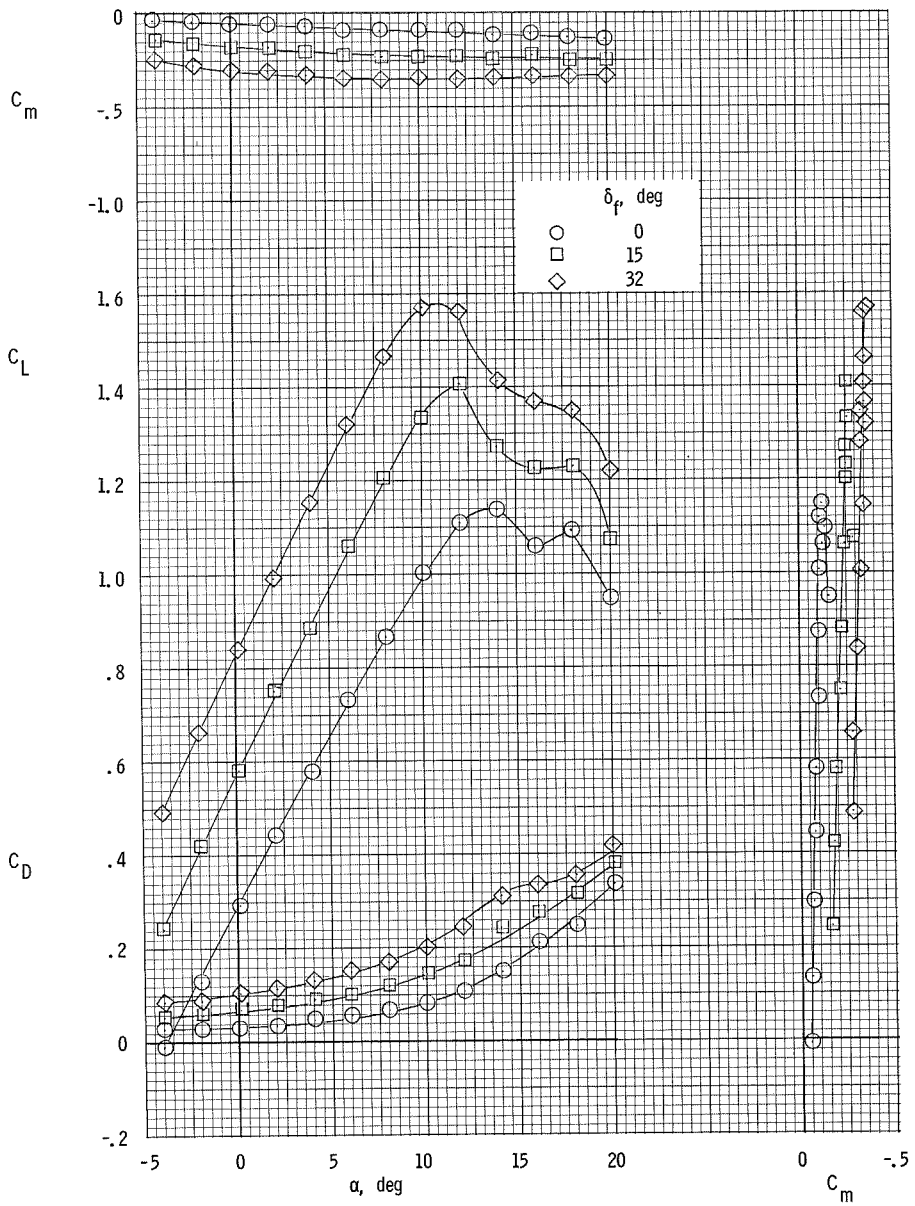


(a) $T_c' = 0$.

Figure 9.- Longitudinal aerodynamic characteristics of the airplane with horizontal tail removed.

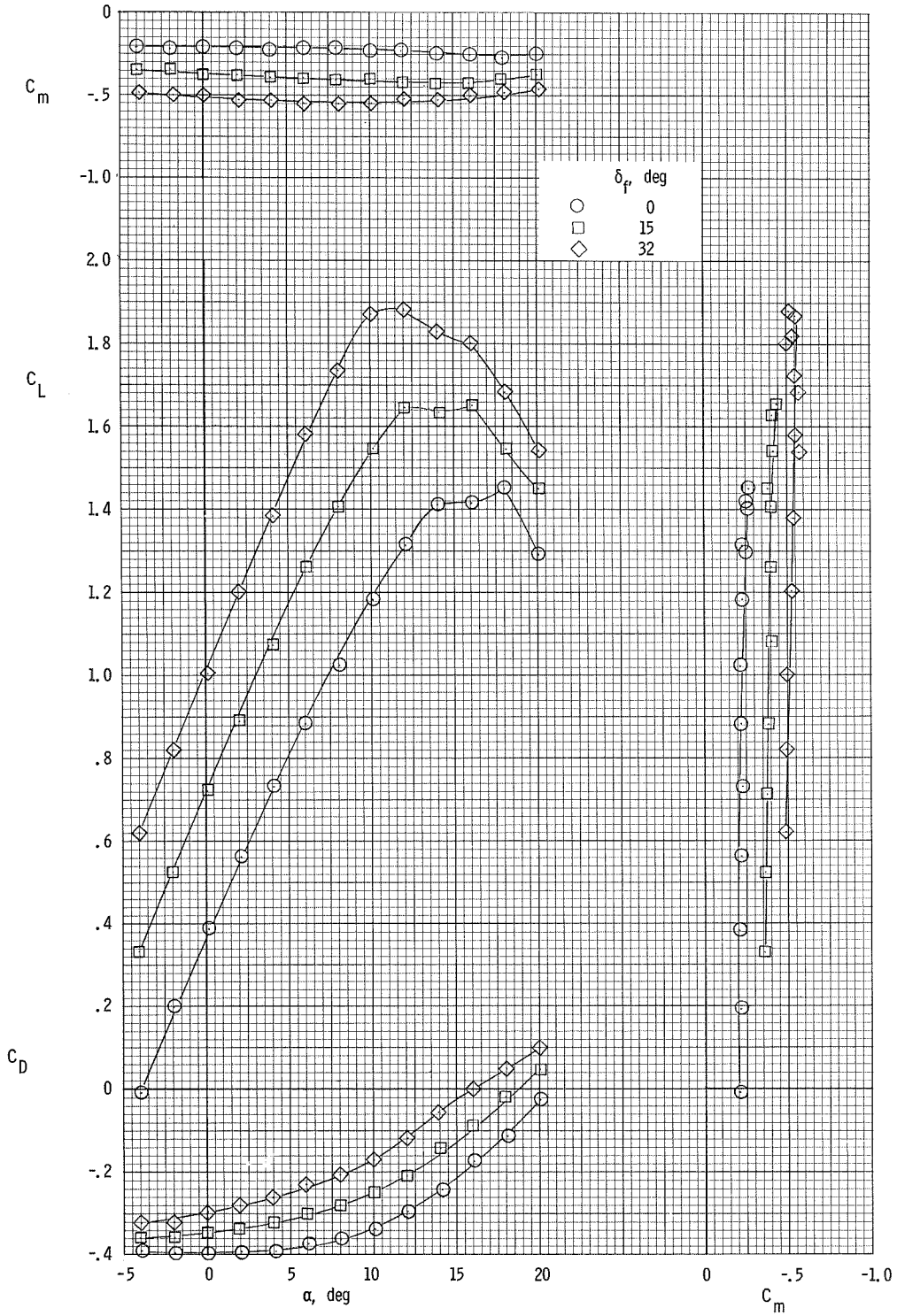


(b) $T_C' = 0.46$.

Figure 9.- Concluded.

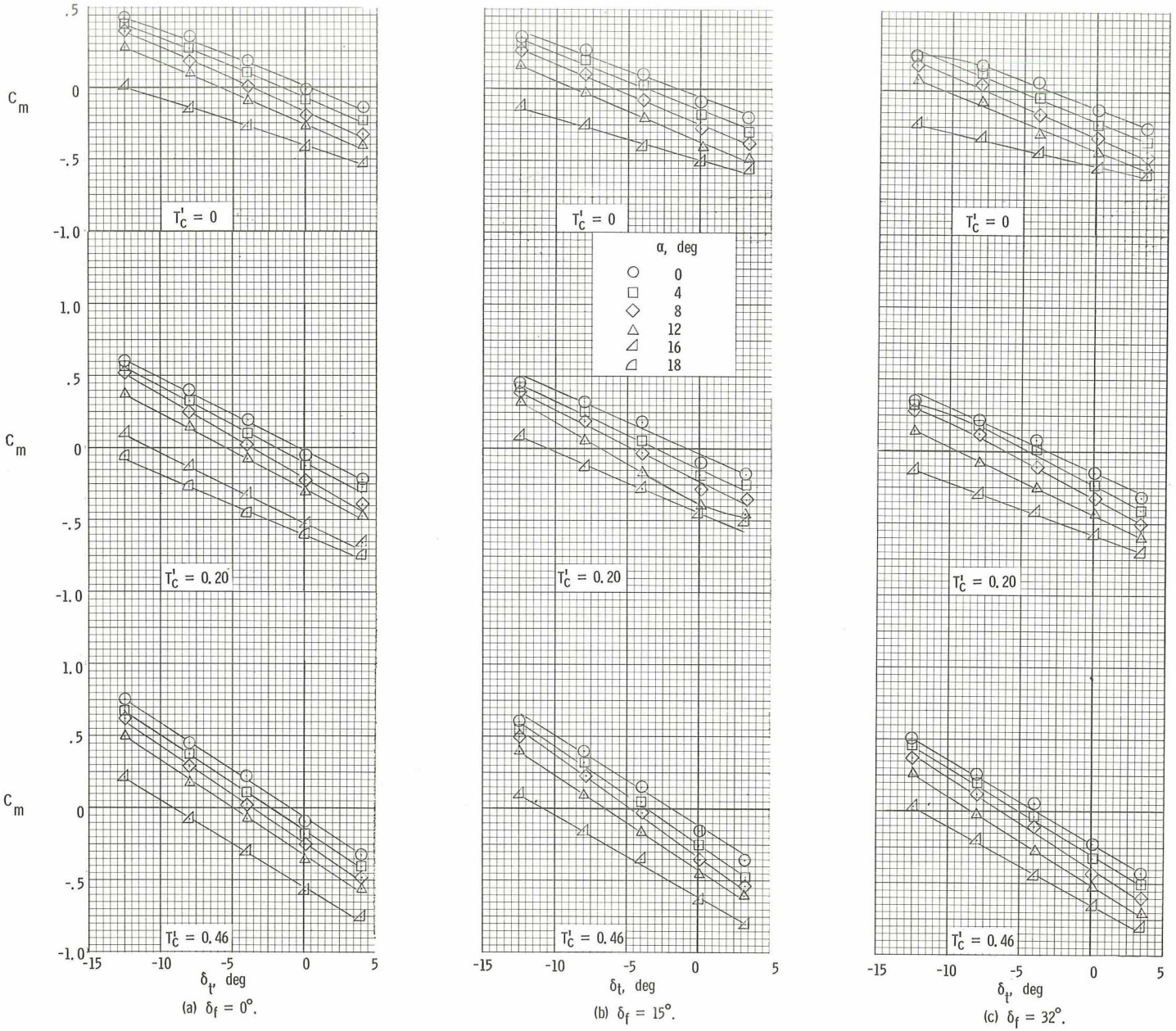


(a) $\delta_f = 0°$.

(b) $\delta_f = 15°$.

(c) $\delta_f = 32°$.

Figure 10.- Variations of pitching-moment coefficient with horizontal-tail deflection for several power and flap deflections.

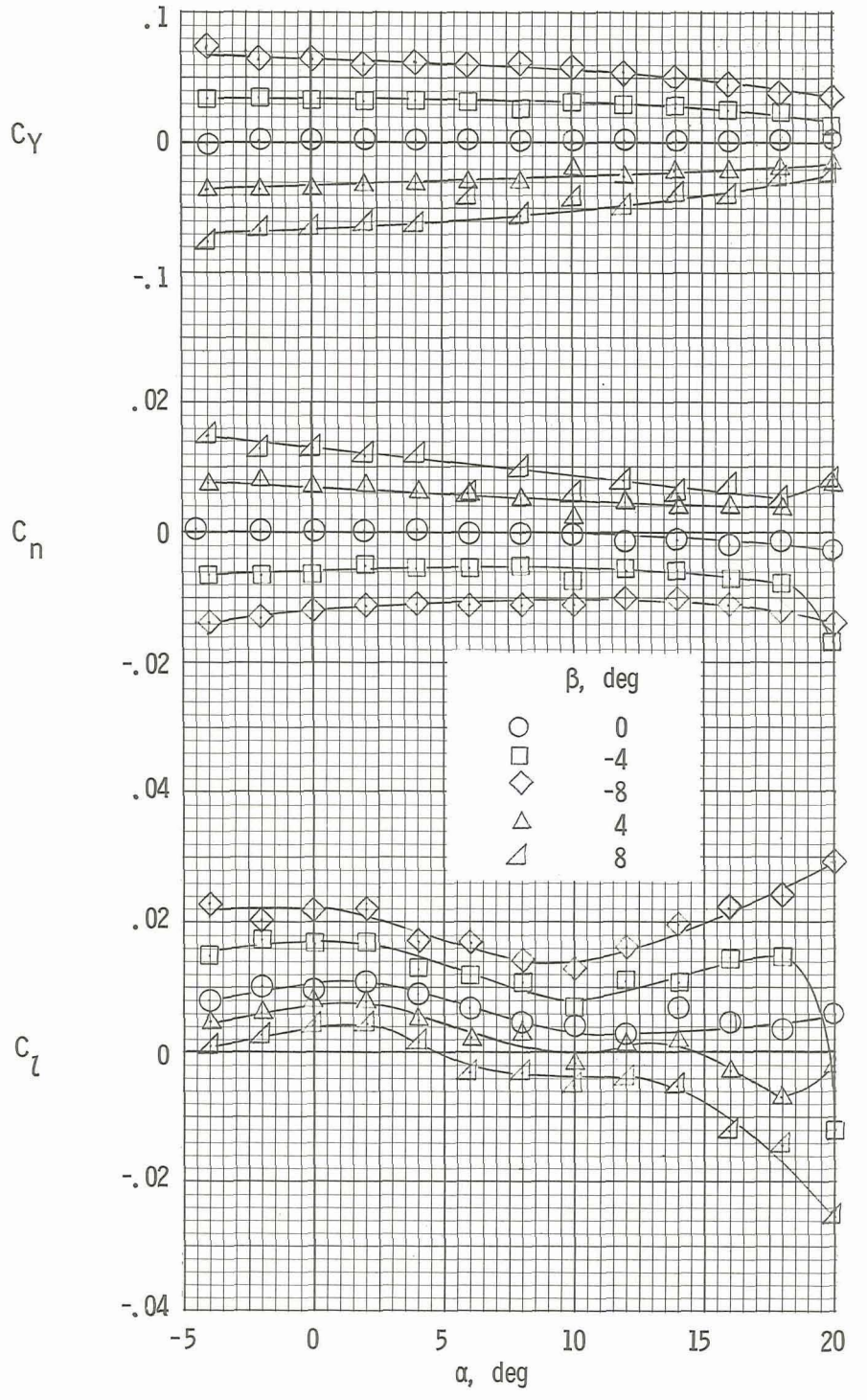


(a) $\delta_f = 0^0$.

Figure 11.- Lateral characteristics of the airplane with propellers removed for several flap deflections.

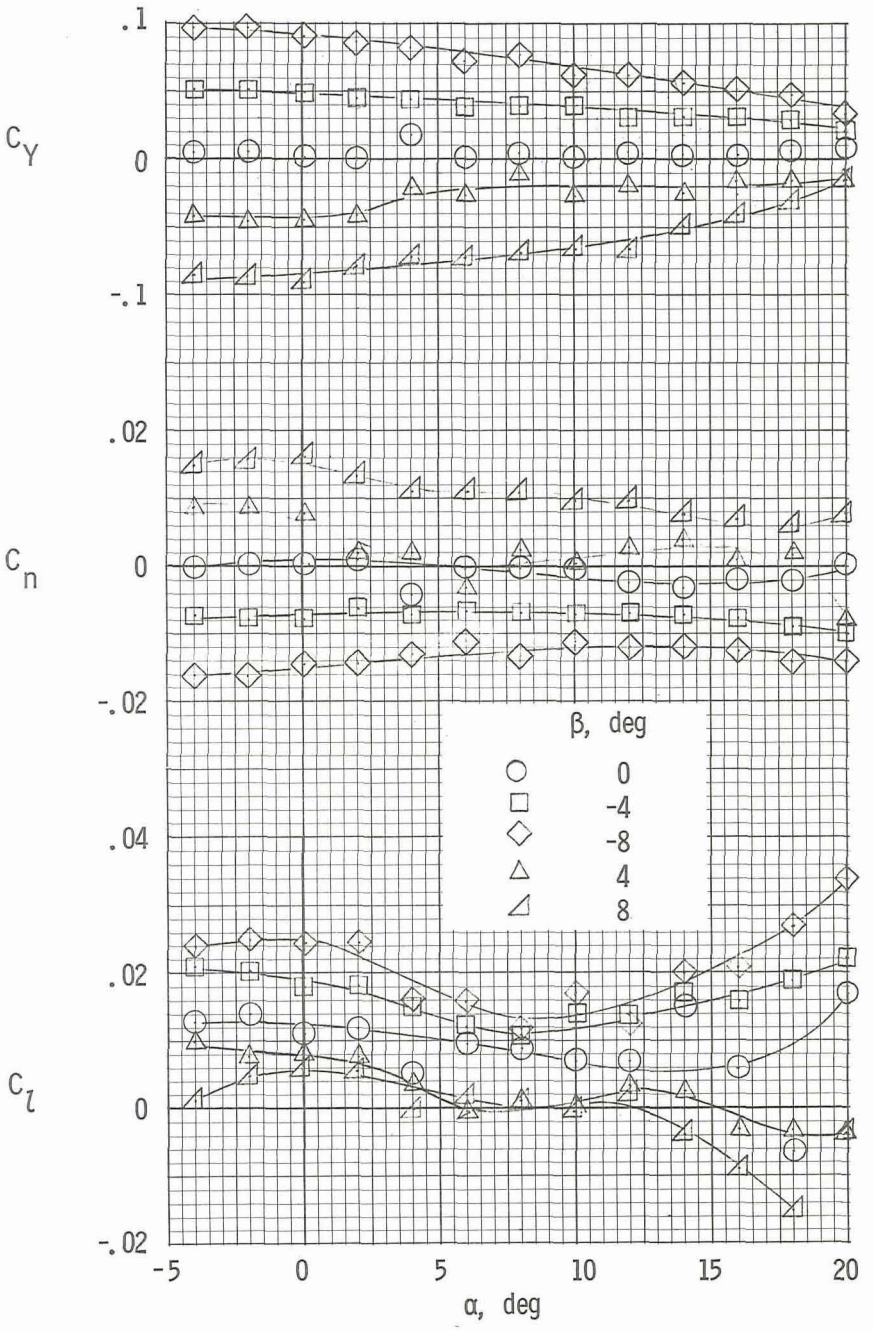


(b) $\delta_f = 15^0$.

Figure 11.- Continued.

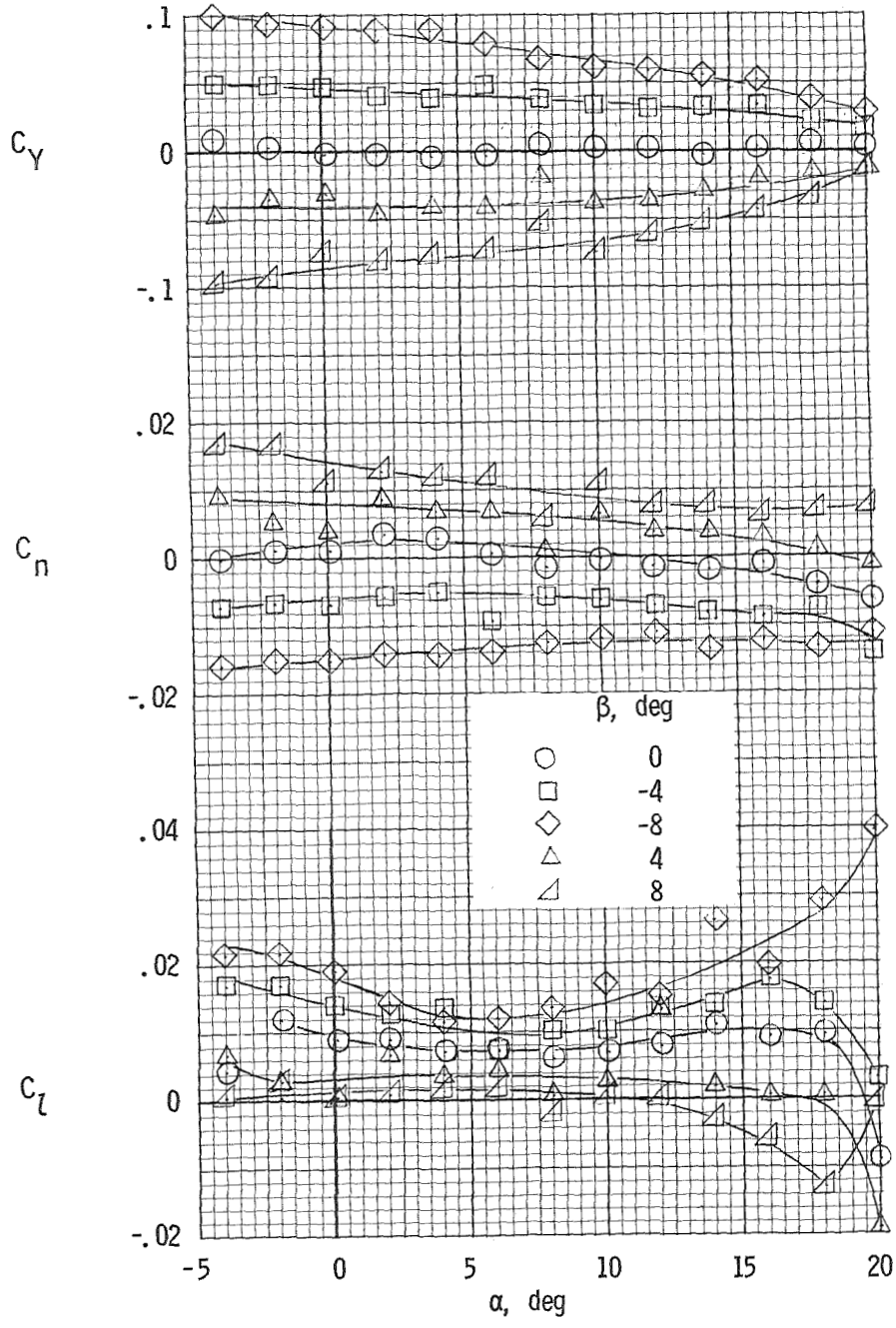


(c) $\delta_f = 32^0$.

Figure 11.- Concluded.

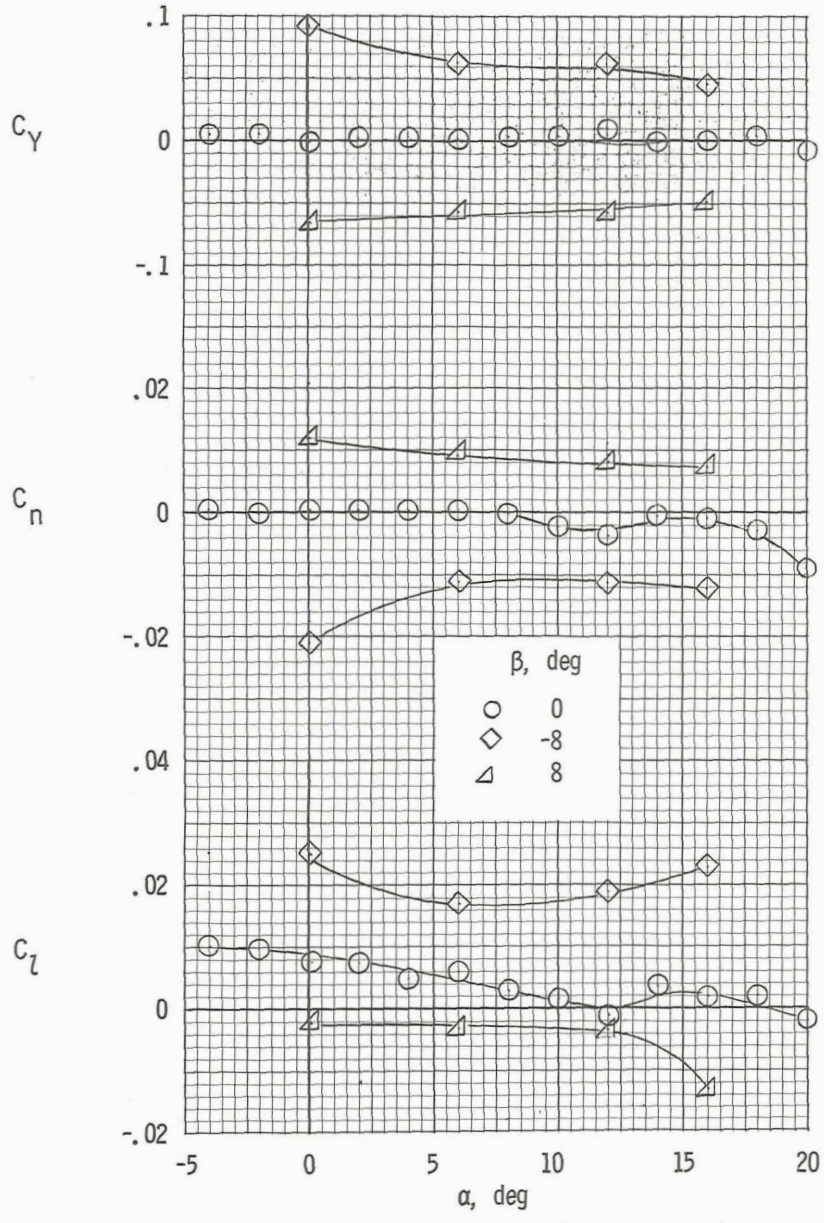


(a) $T_C' = 0$.

Figure 12.- Lateral characteristics of the airplane for several sideslip angles and thrust coefficients for $\delta_f = 0^0$.

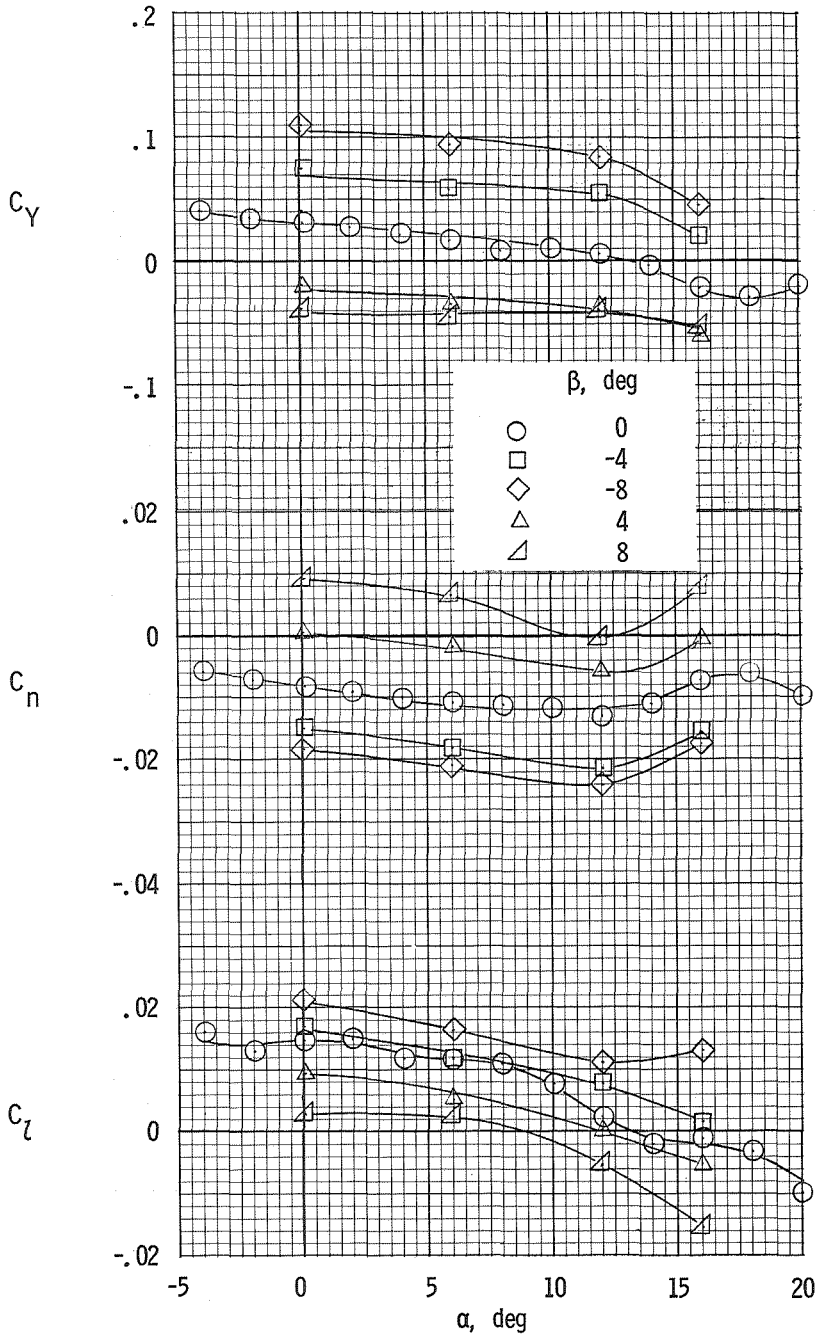


(b) $T_C' = 0.20$.

Figure 12.- Continued.

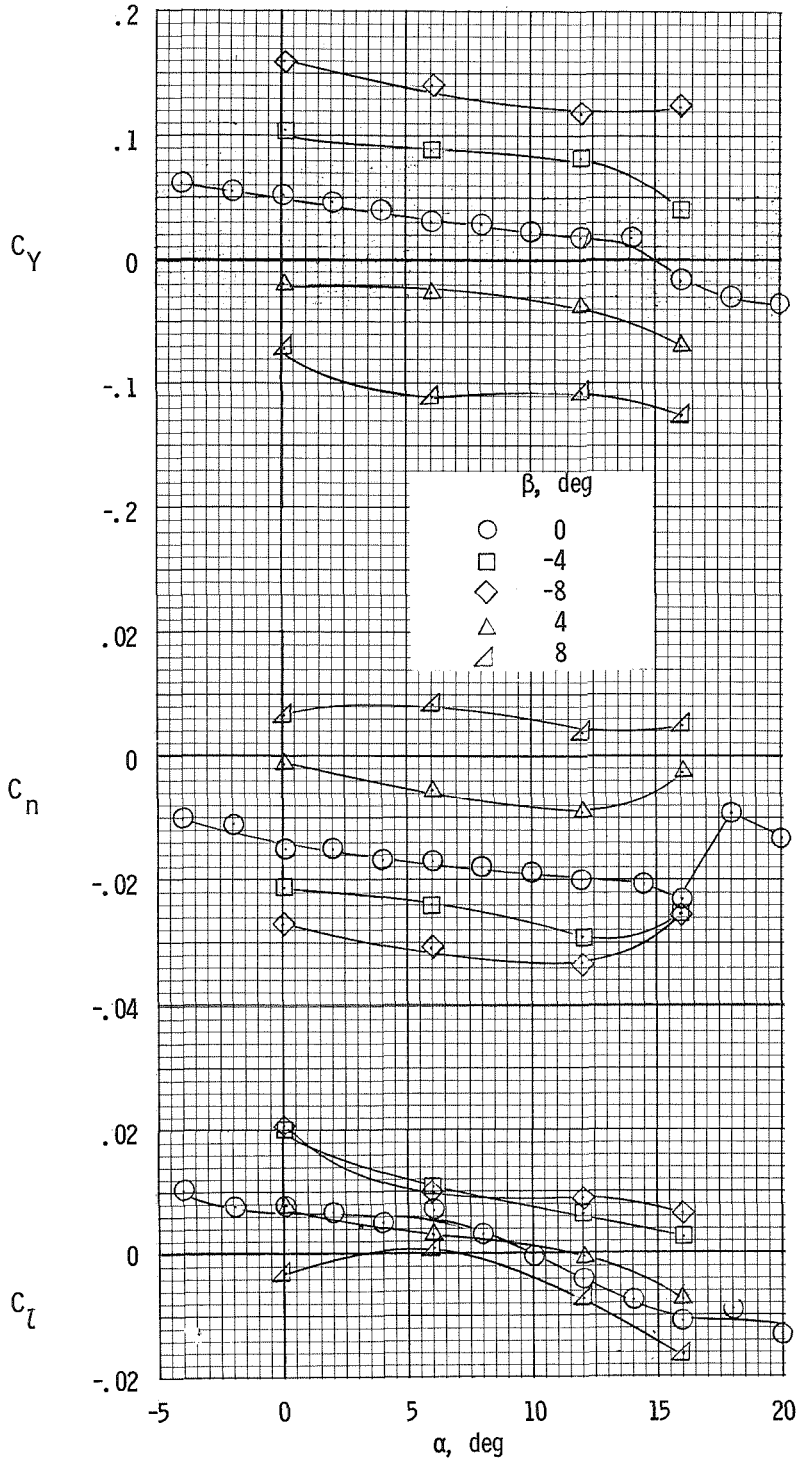


(c) $T_c' = 0.46$.

Figure 12.- Continued.

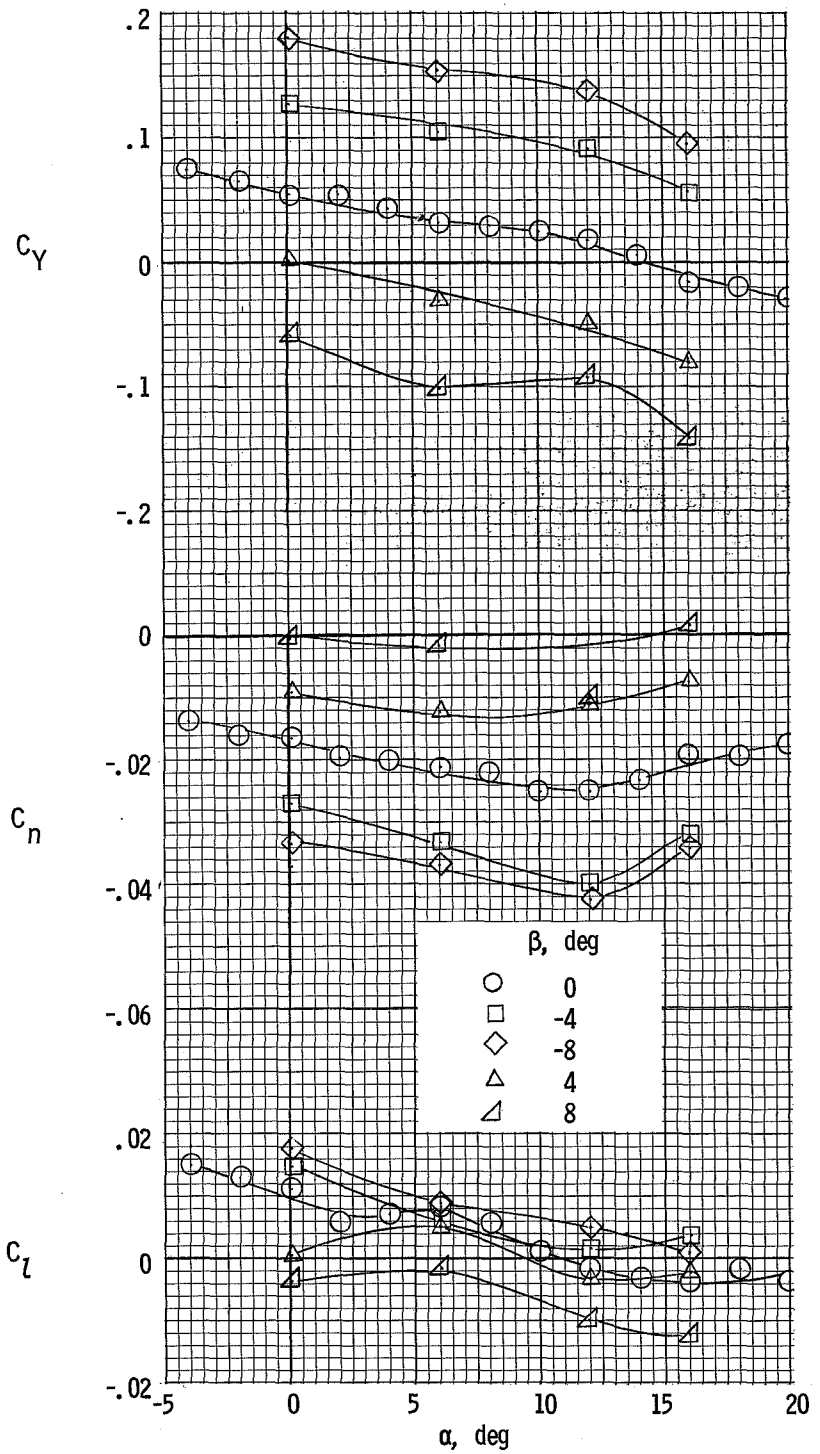


(d) $T_C' = 0.55$.

Figure 12.- Concluded.

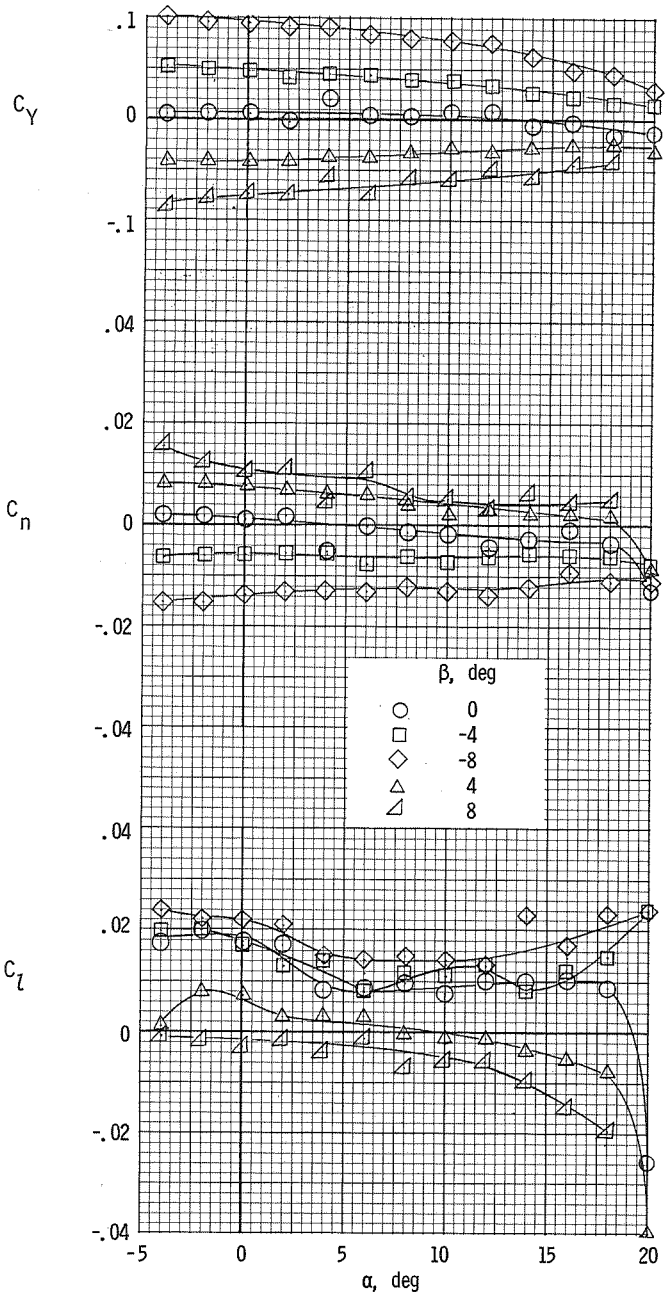


(a) $T_C' = 0$.

Figure 13.- Lateral characteristics of the airplane for several sideslip angles and thrust coefficients for $\delta_f = 15^o$.

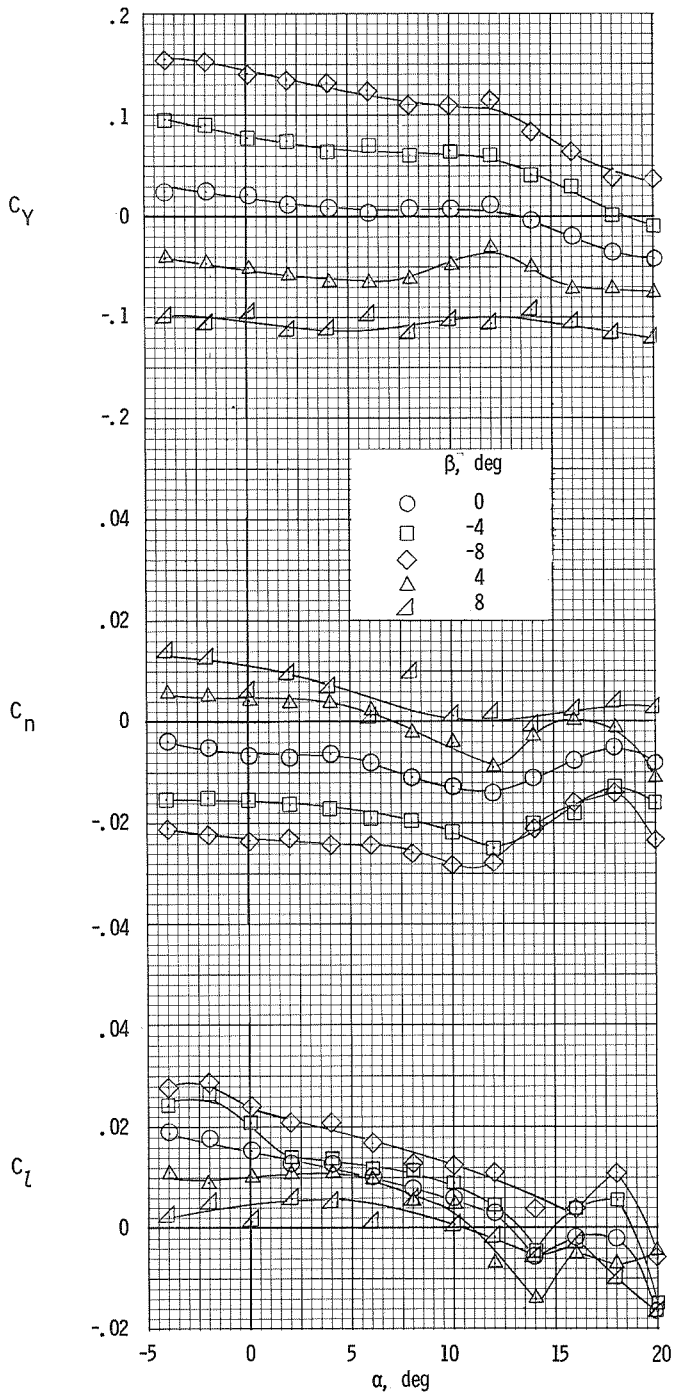


(b) $T_C' = 0.20$.

Figure 13.- Continued.

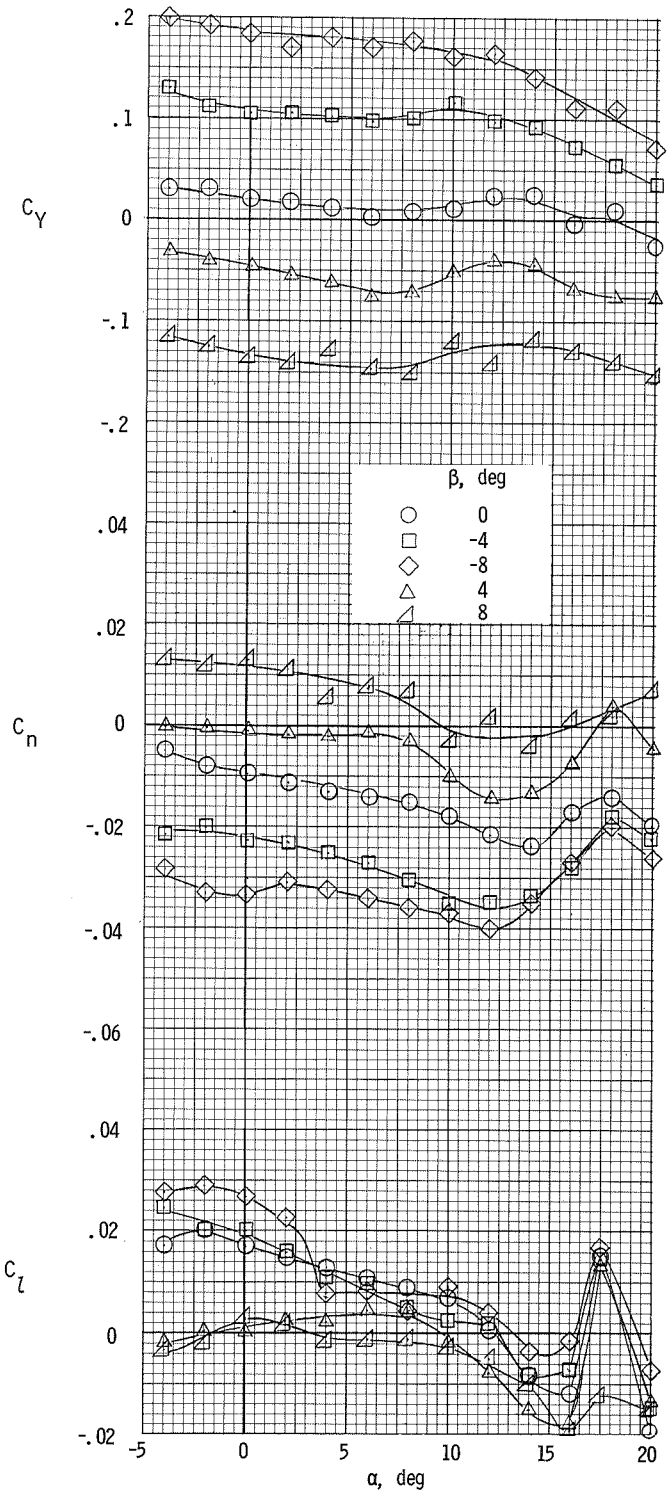


(c) $T_c' = 0.46$.

Figure 13.- Continued.

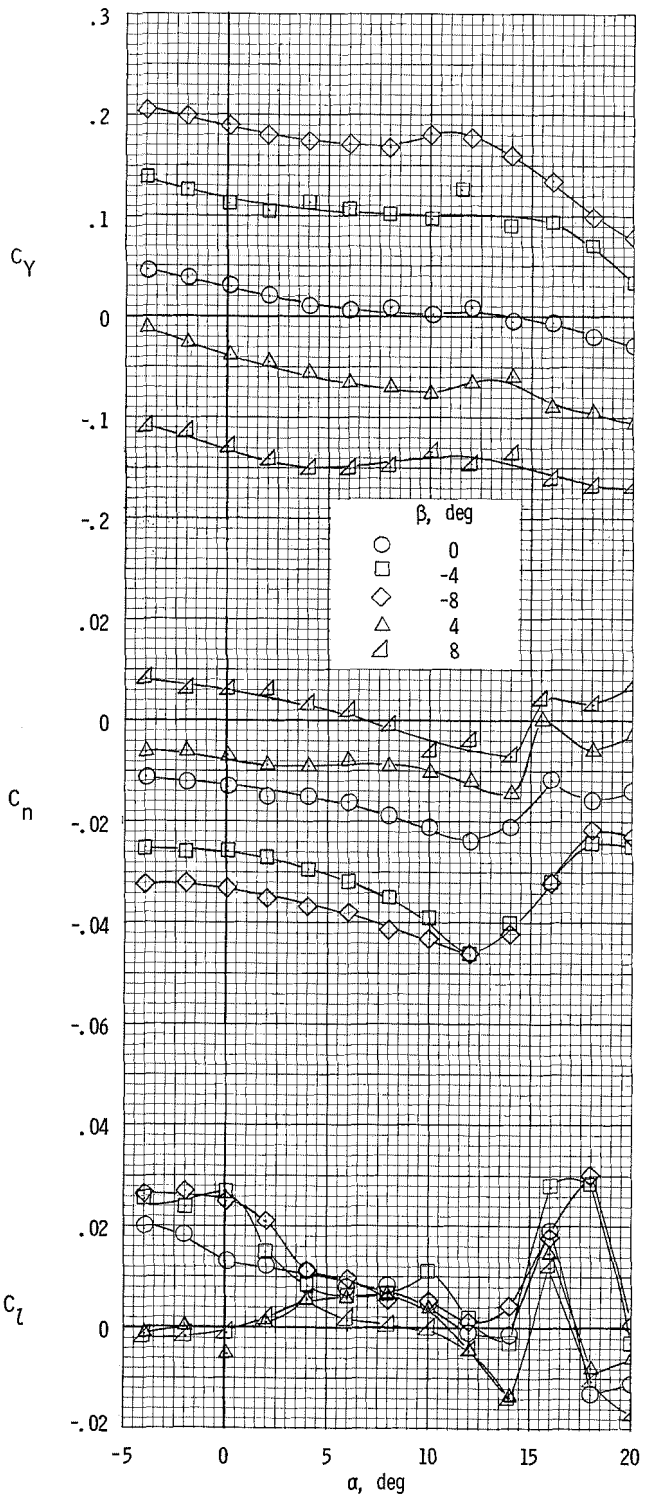


(d) $T_c' = 0.55$.

Figure 13.- Concluded.

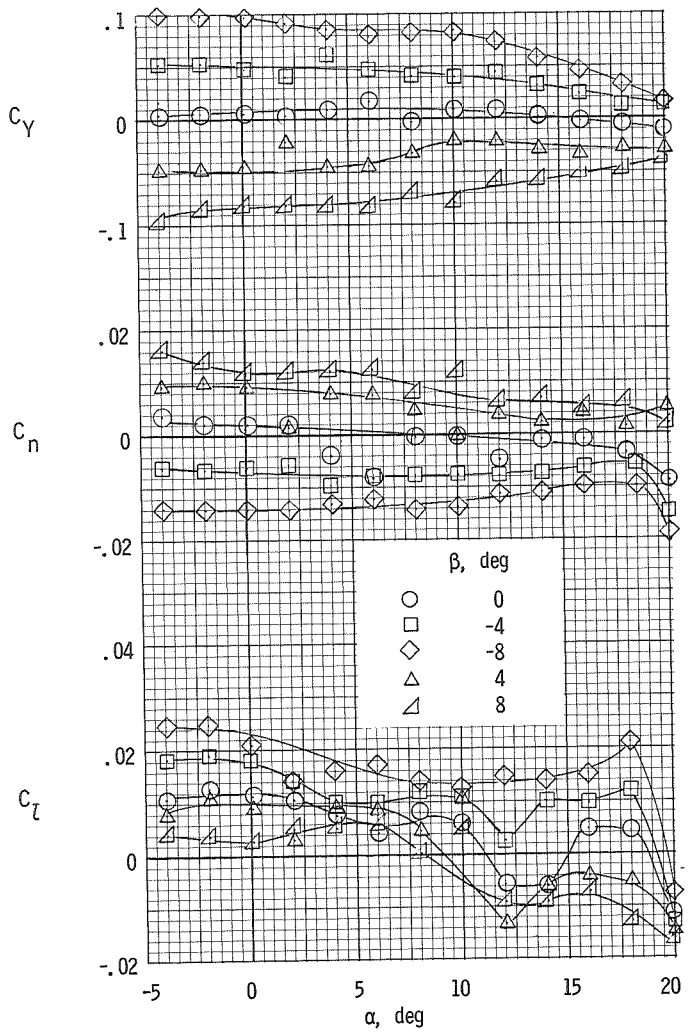


(a) $T_c' = 0$.

Figure 14.- Lateral characteristics of the airplane for several sideslip angles and thrust coefficients for $\delta_f = 32^o$.

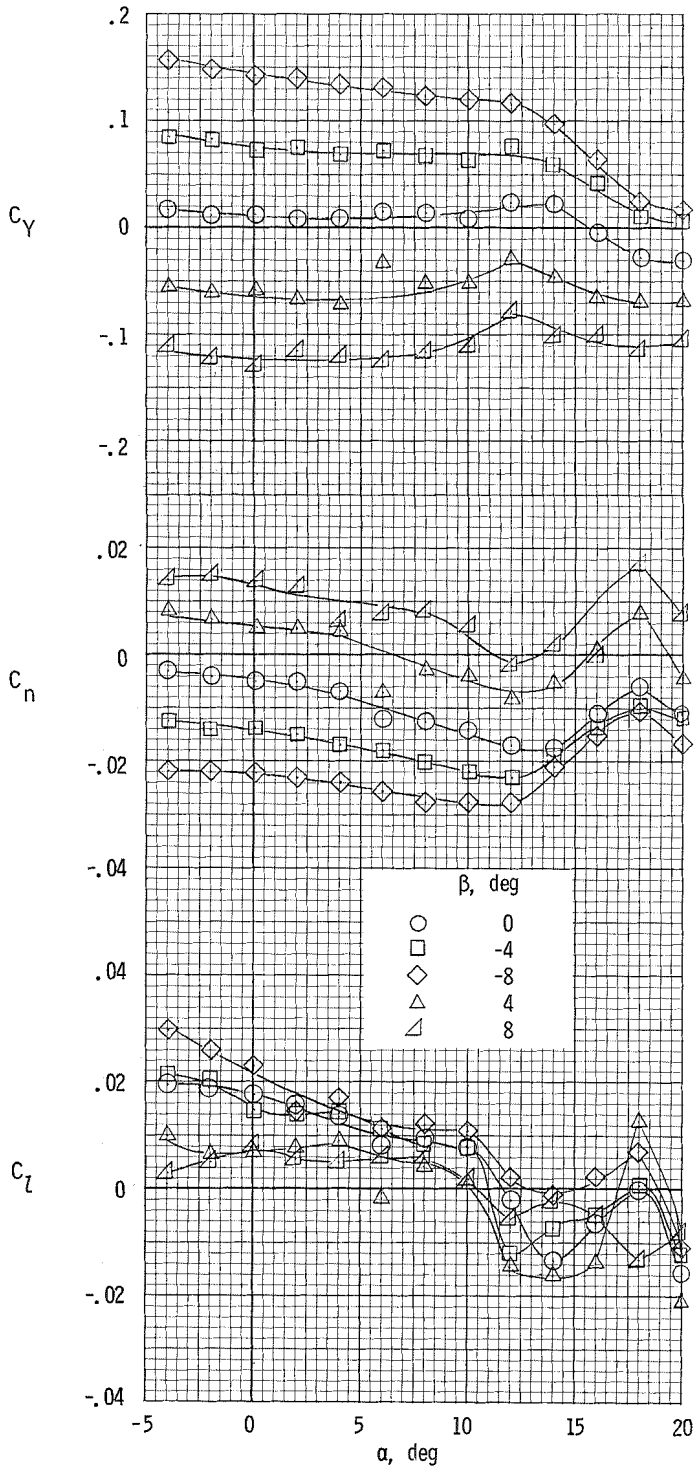


(b) $T_C' = 0.20$.

Figure 14.- Continued.

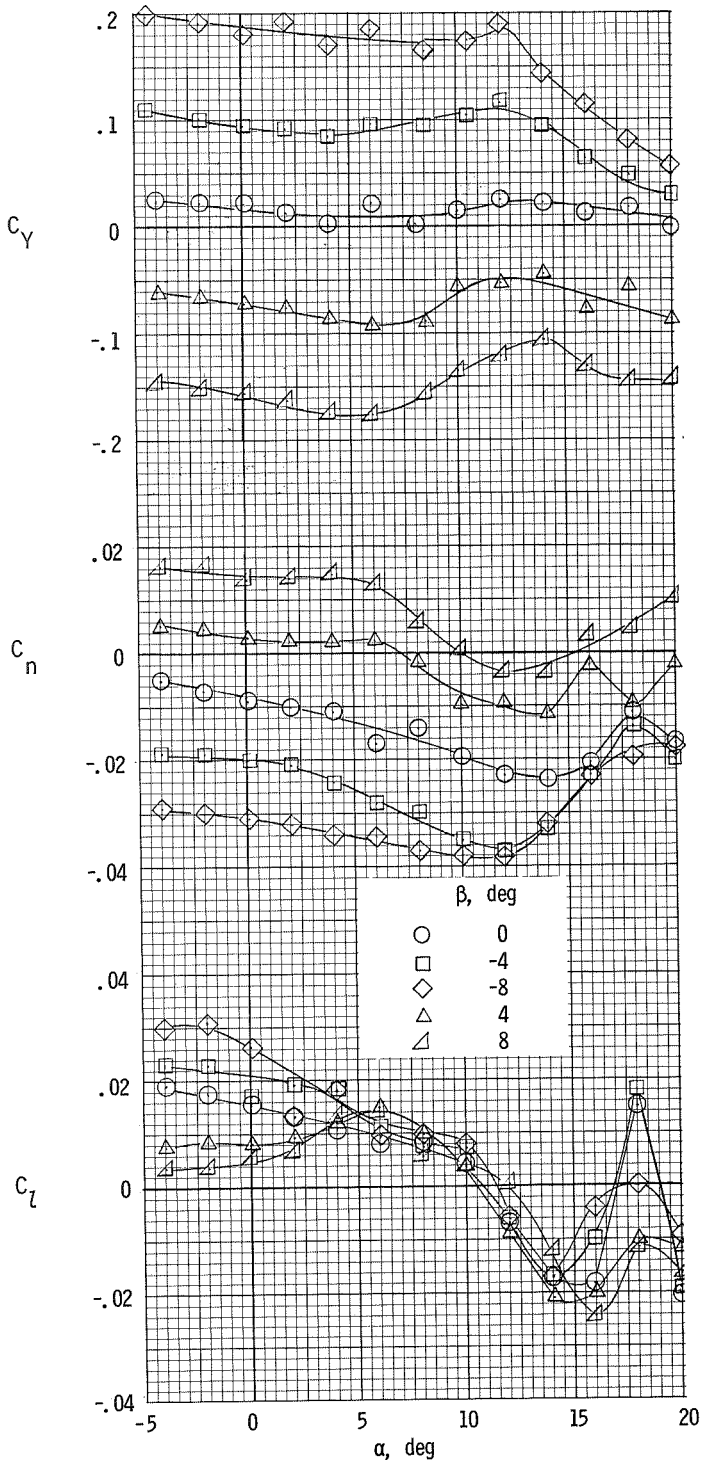


(c) $T_C' = 0.46$.

Figure 14.- Continued.

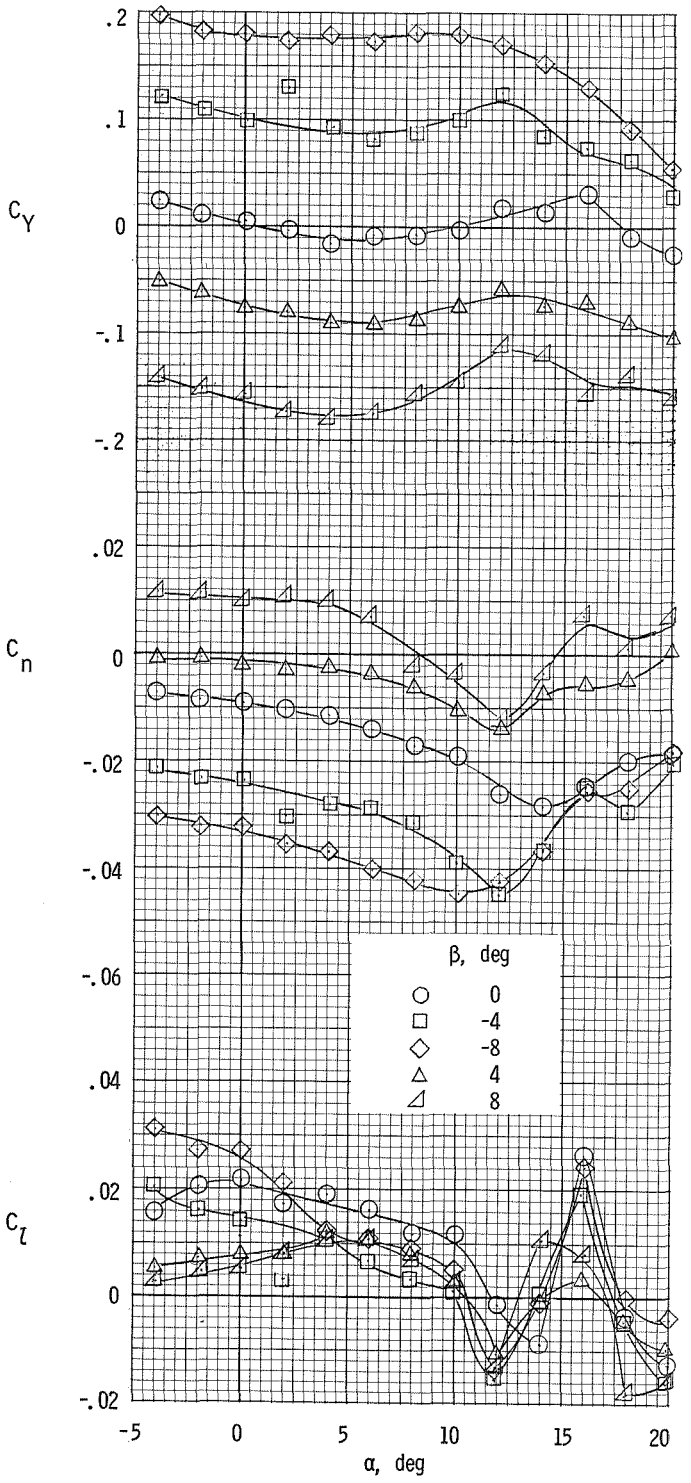


(d) $T_C' = 0.55$.

Figure 14.- Concluded.

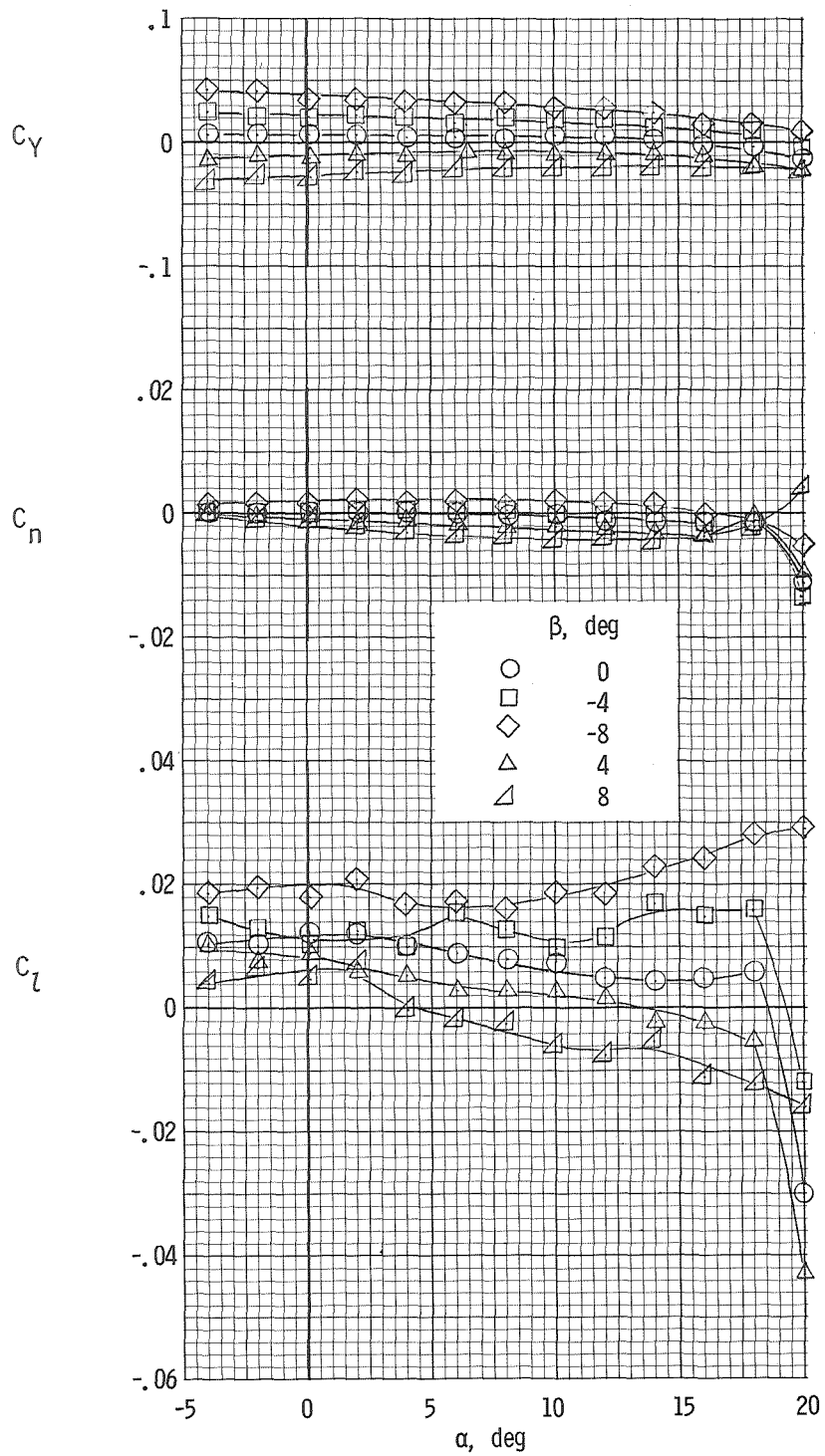


(a) $T_C' = 0$.

Figure 15.- Lateral characteristics of the airplane with the vertical tail removed for $\delta_f = 0^0$.

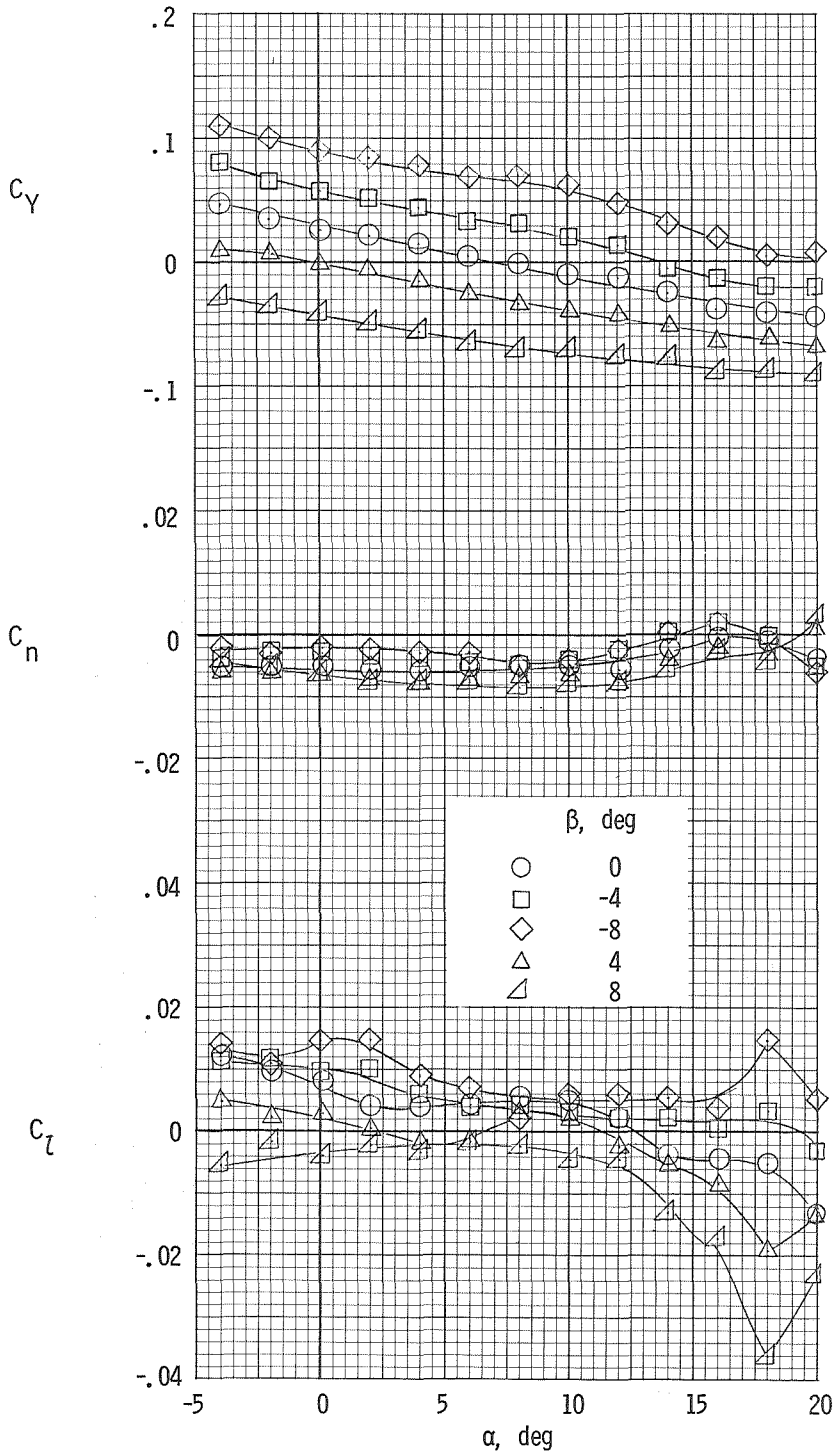


(b) $T_c' = 0.46$.

Figure 15.- Concluded.

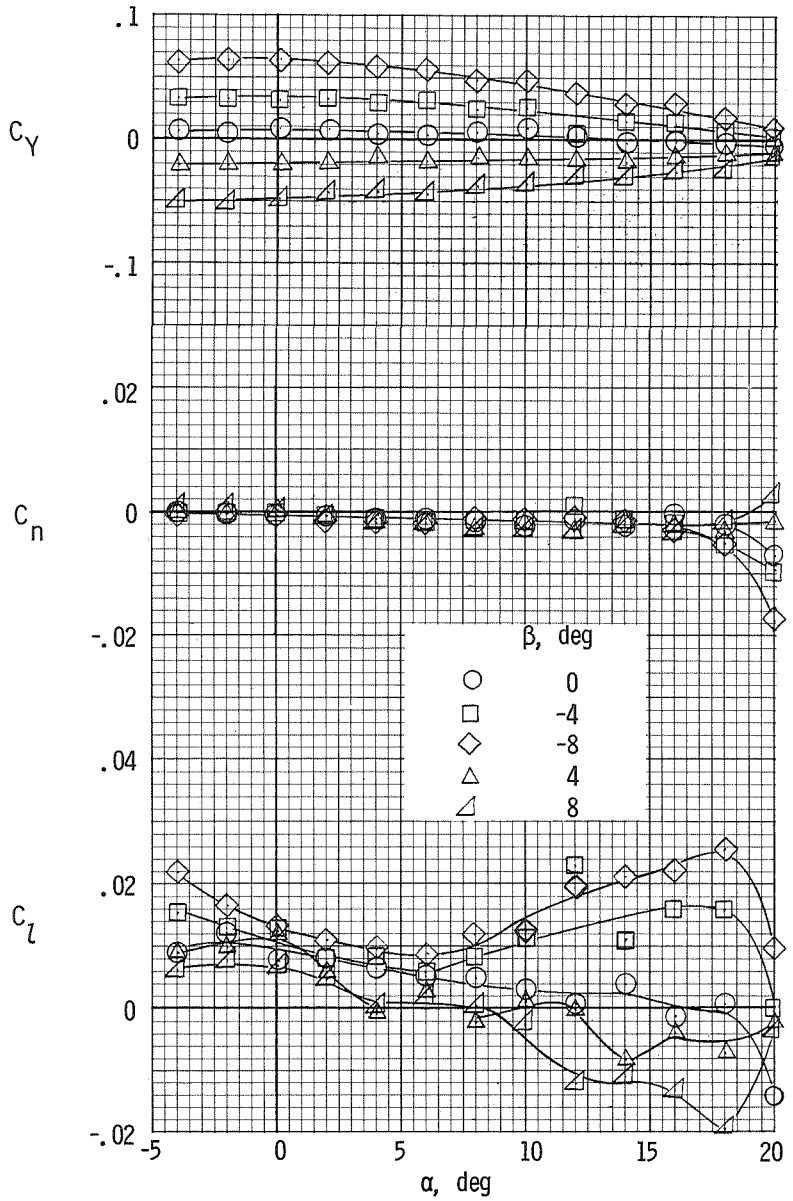


(a) $T_c' = 0$.

Figure 16.- Lateral characteristics of the airplane with the vertical tail removed for $\delta_f = 32^0$.

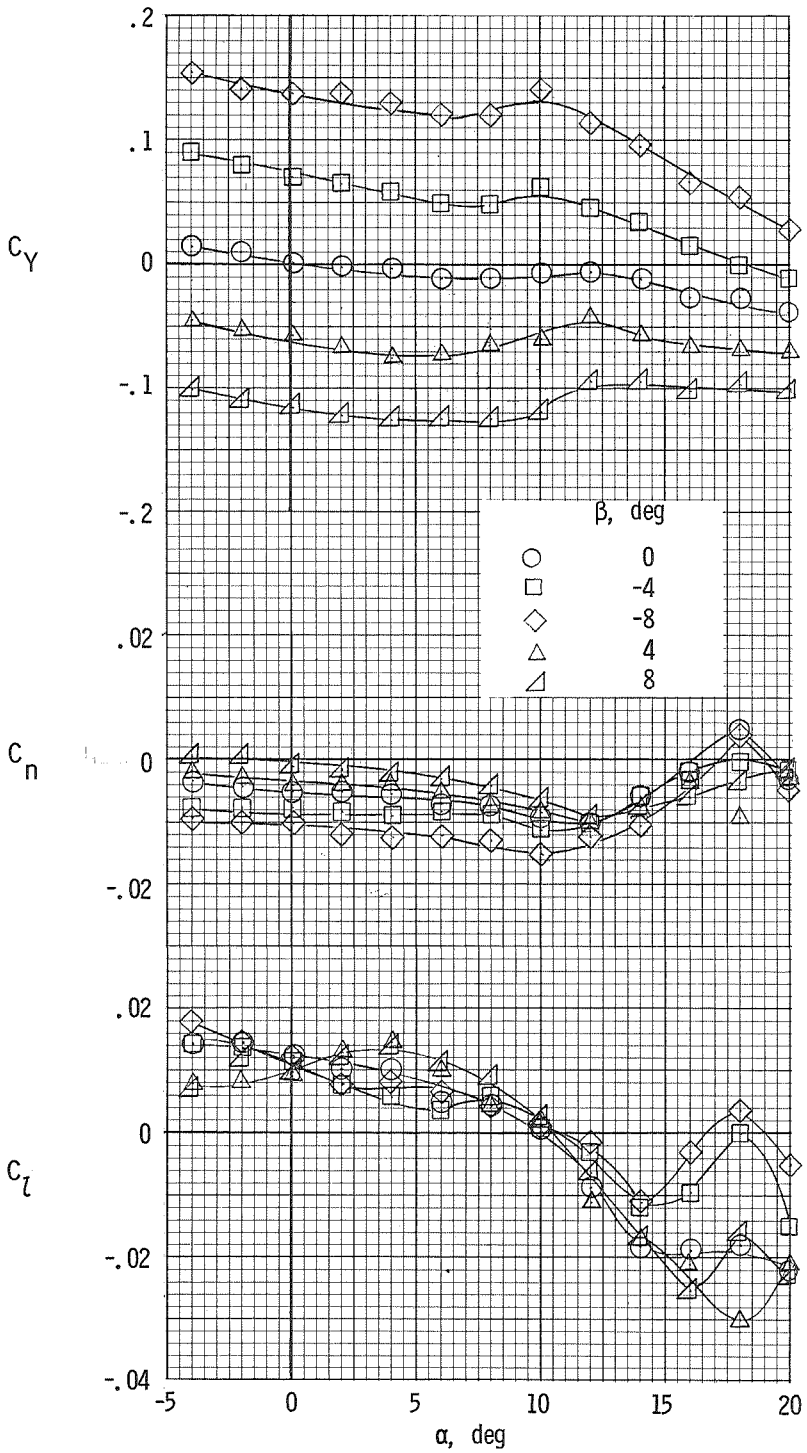


(b) $T_c' = 0.46$.

Figure 16.- Concluded.

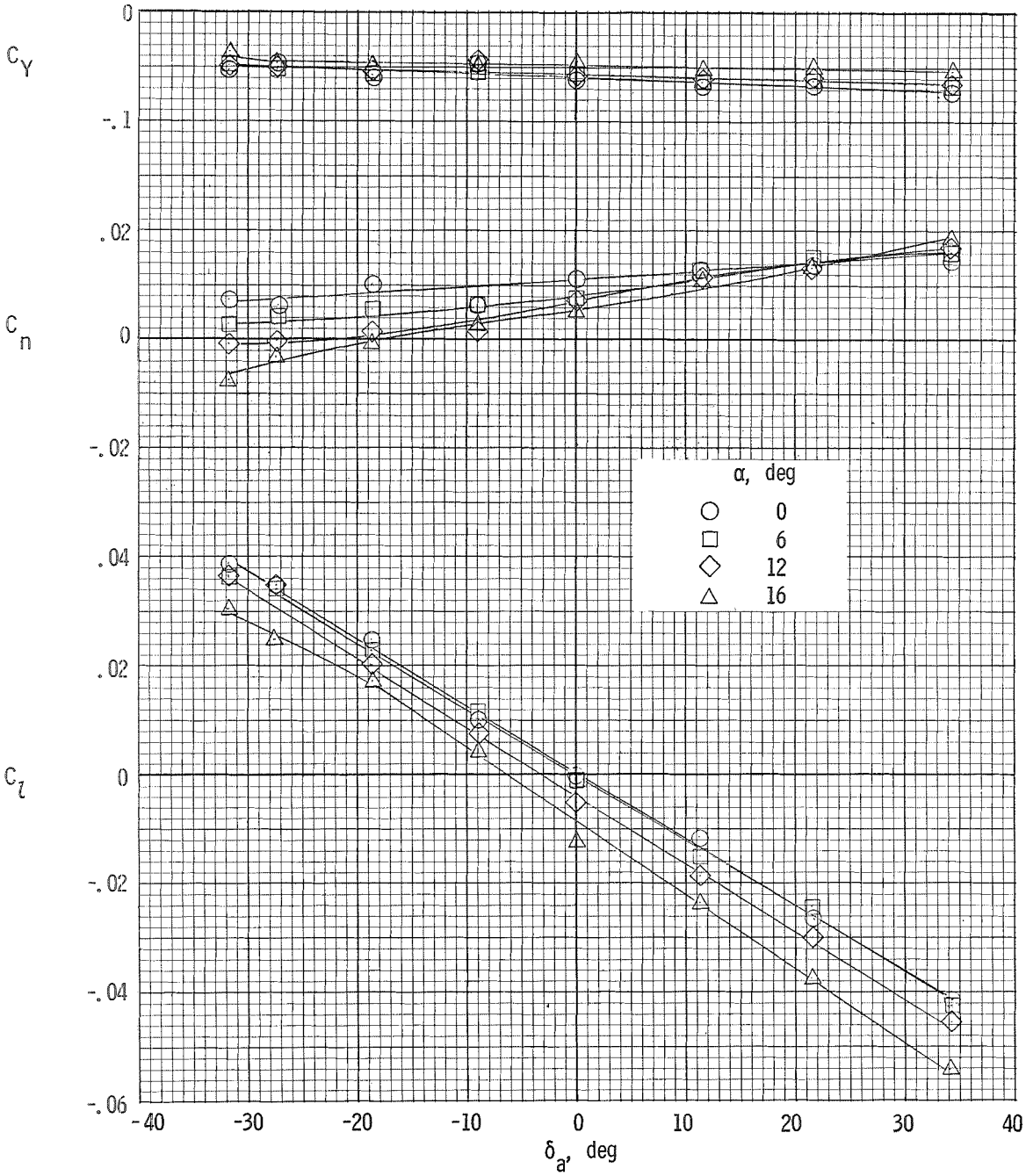


(a) $\beta = 8^{\circ}$.

Figure 17.- Variation of the lateral characteristics of the airplane with aileron deflection. $\delta_f = 0^{\circ}$; $T_c' = 0$.

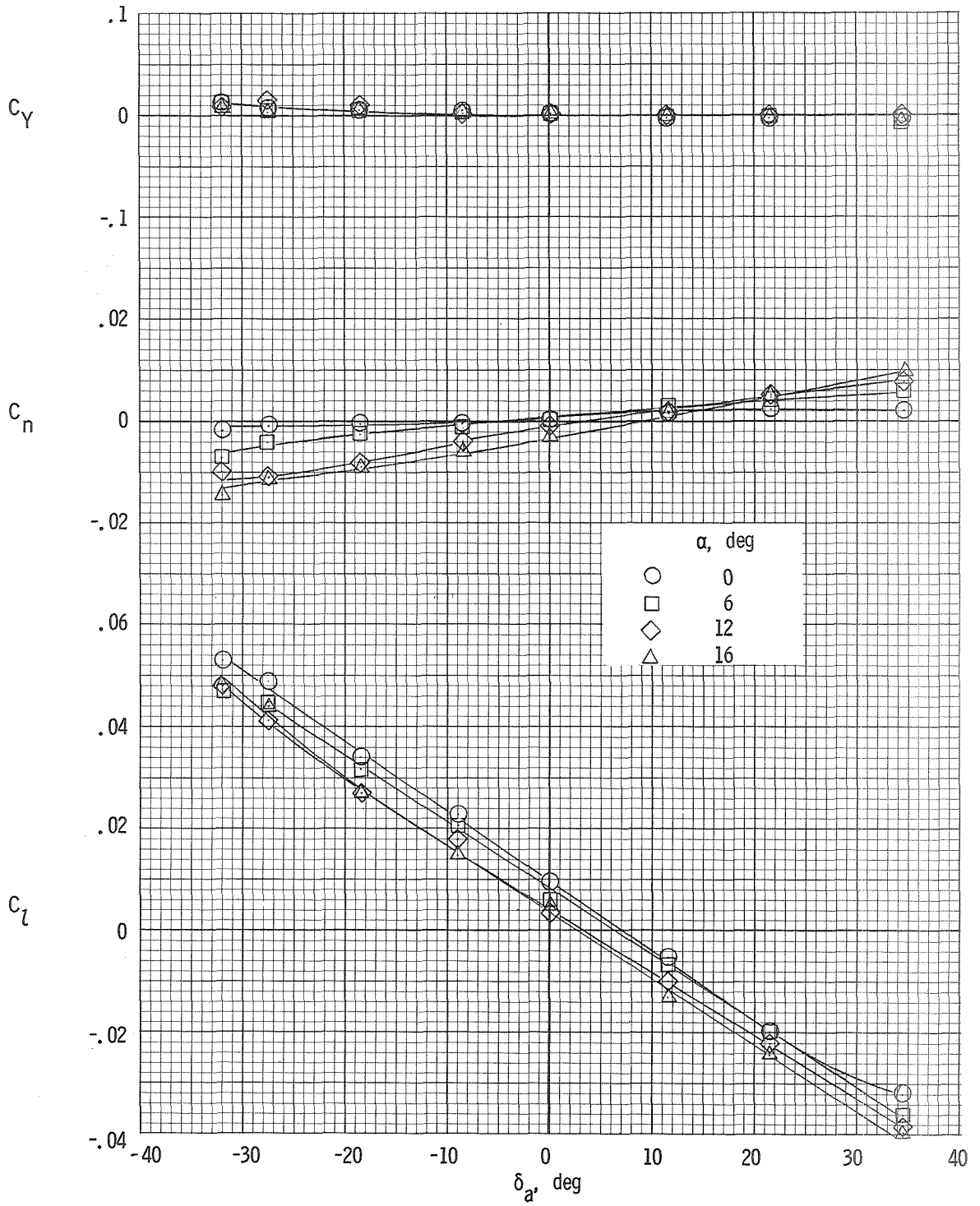


(b) $\beta = 0^0$.

Figure 17.- Continued.

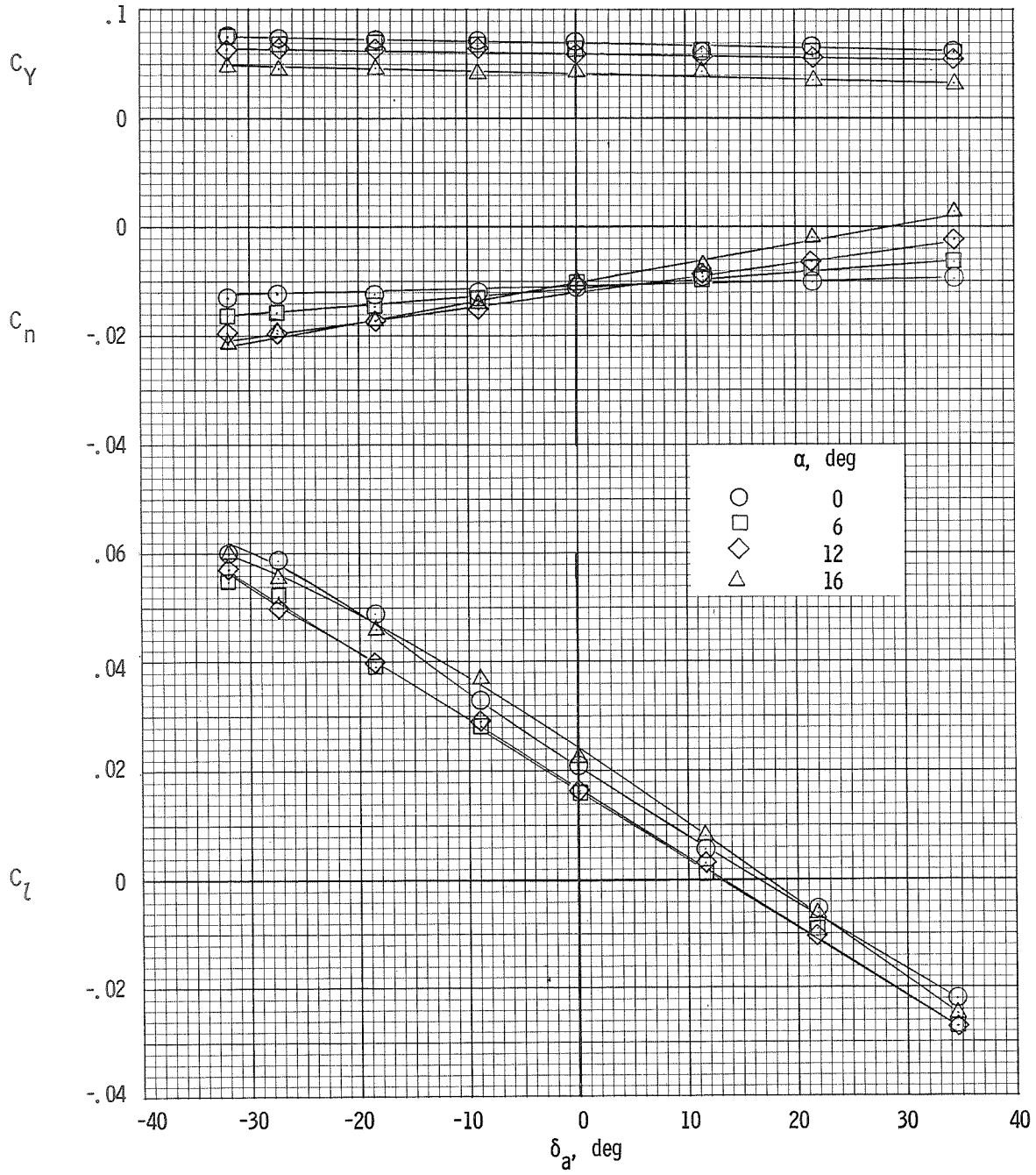


(c) $\beta = -8^0$.

Figure 17.- Concluded.

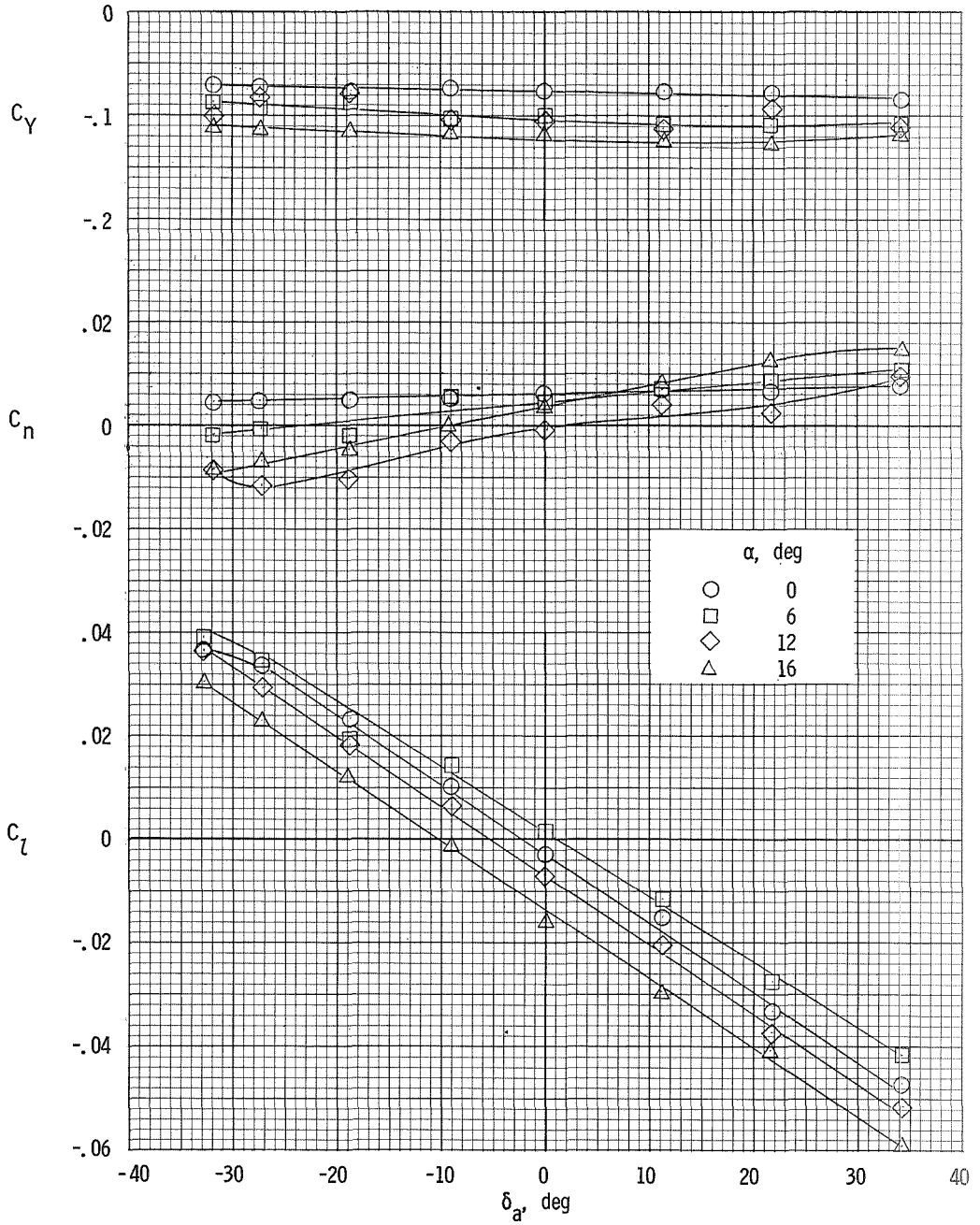


(a) $\beta = 8^0$.

Figure 18.- Variation of the lateral characteristics of the airplane with aileron deflection. $\delta_f = 0^0$; $T_C' = 0.46$.

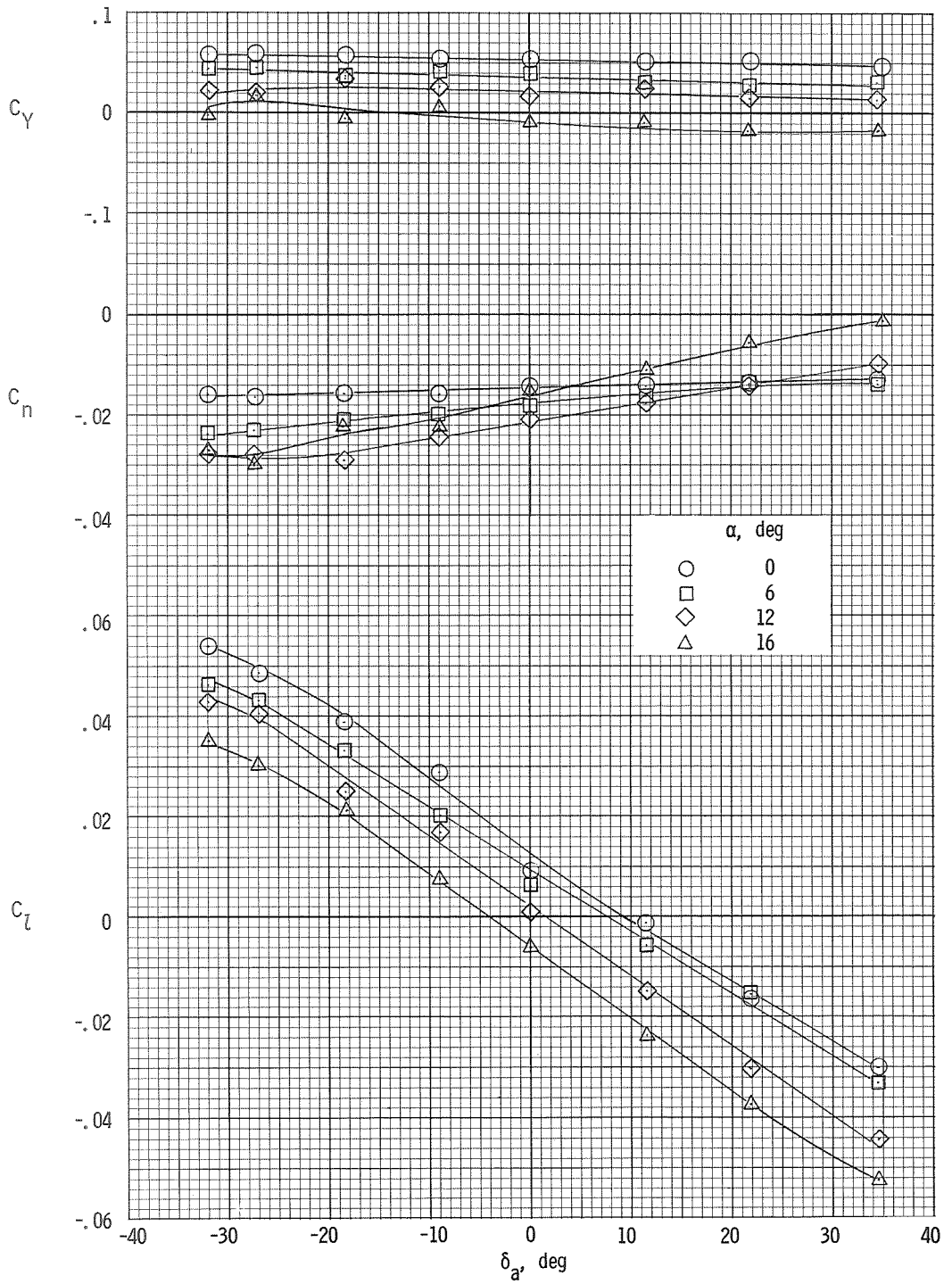


(b) $\beta = 0^0$.

Figure 18.- Continued.

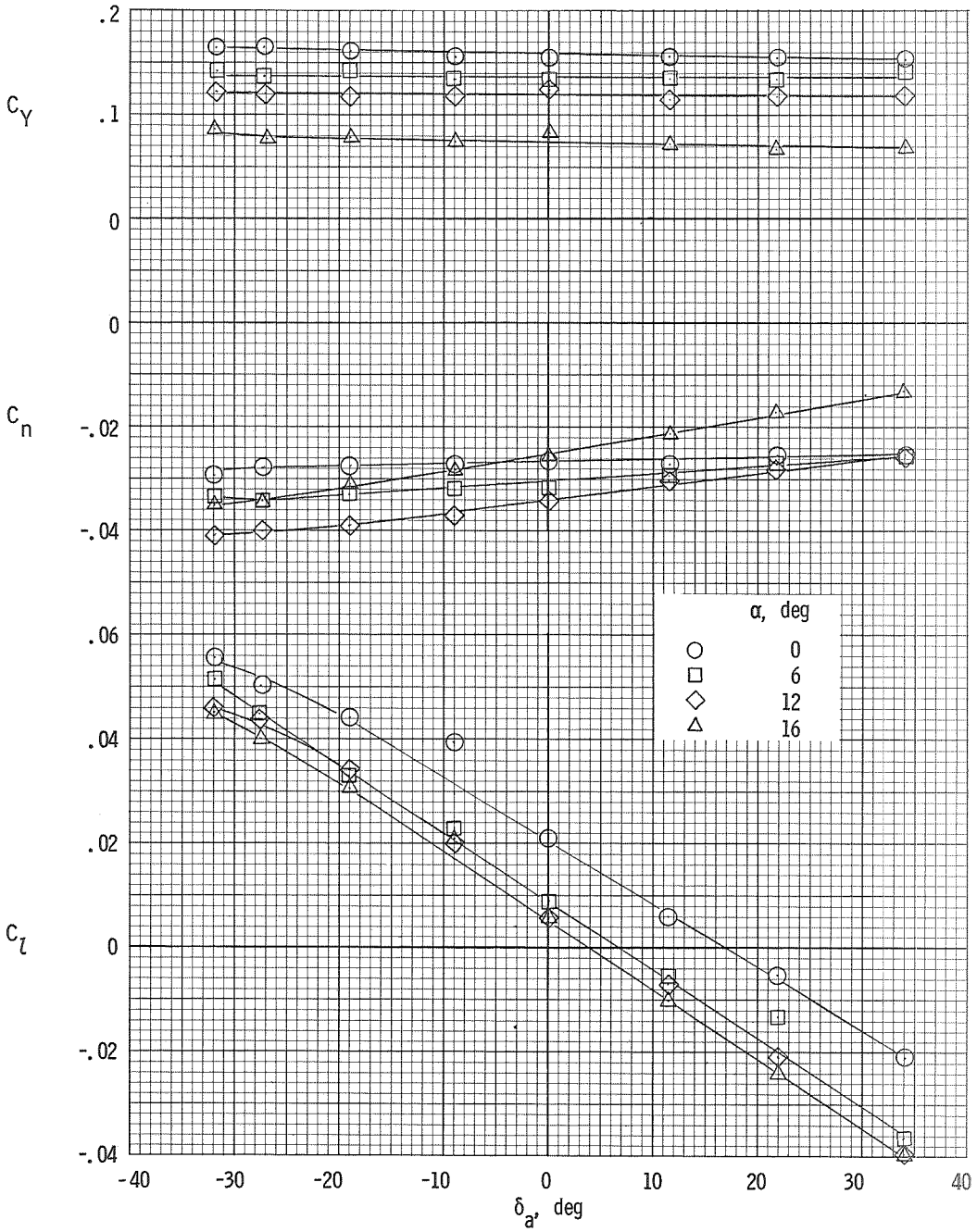


(c) $\beta = -8^{o}$.

Figure 18.- Concluded.

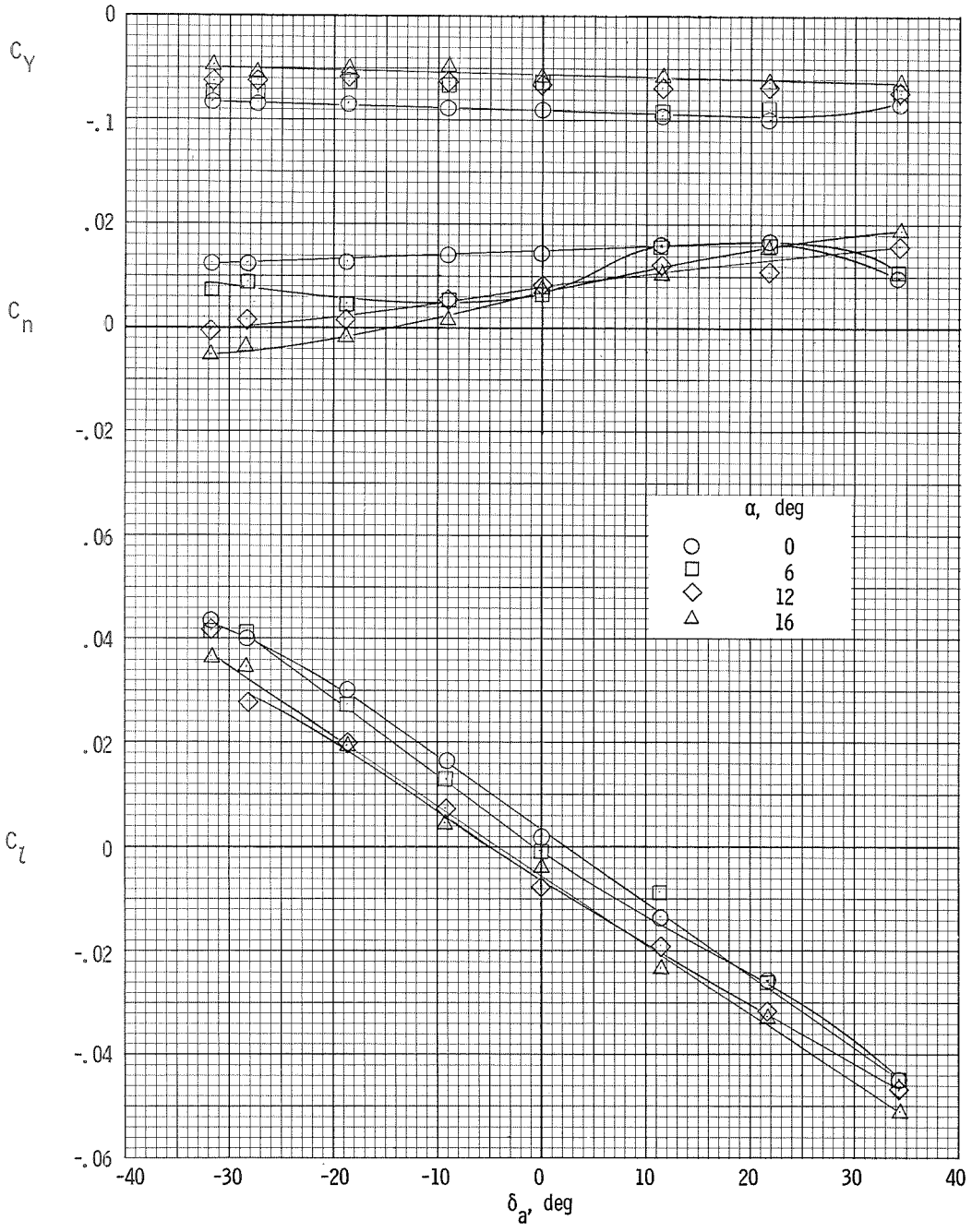


(a) $\beta = 8^0$.

Figure 19.- Variation of the lateral characteristics of the airplane with aileron deflection. $\delta_f = 32^0$; $T_c' = 0$.

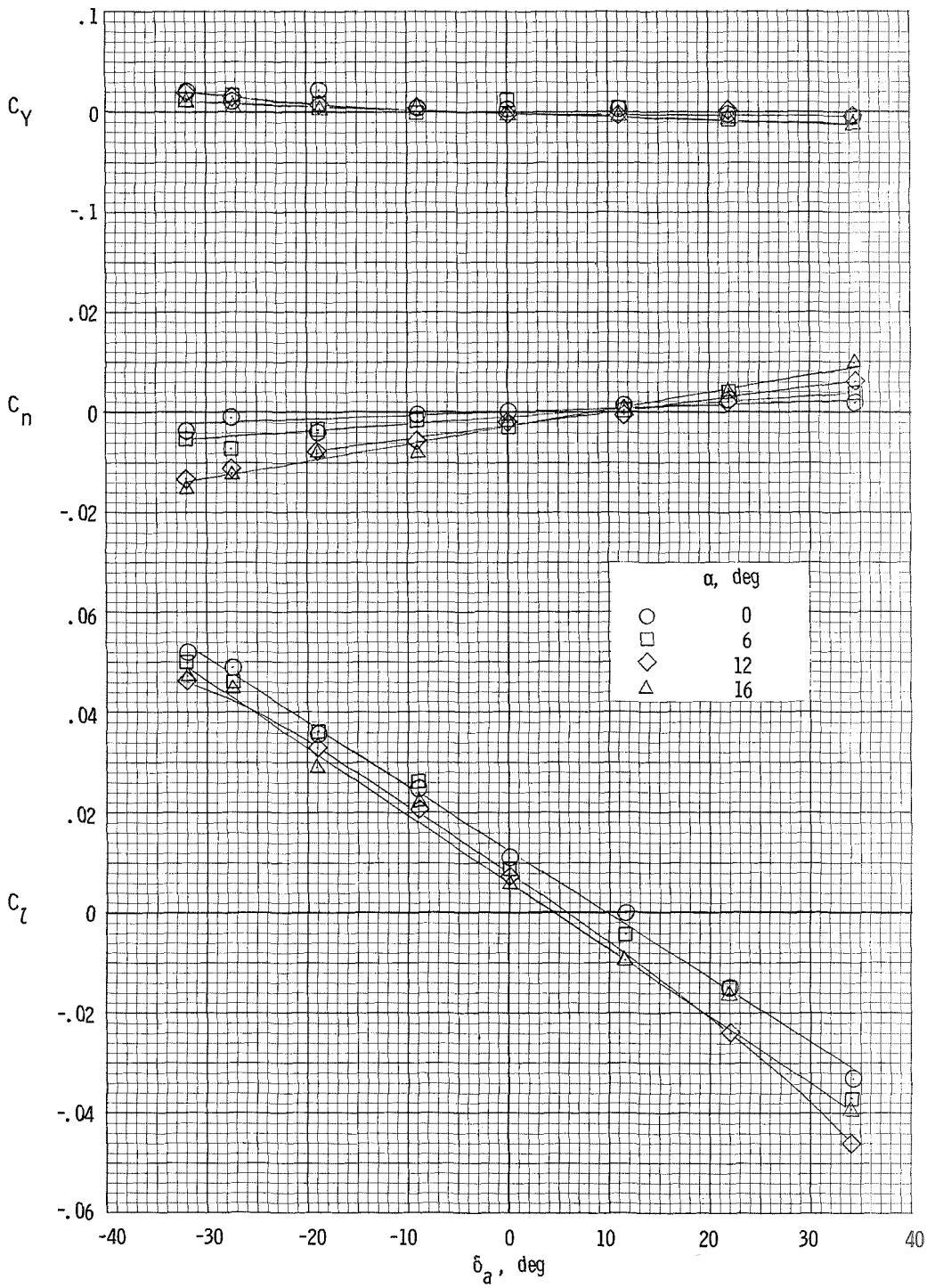


(b) $\beta = 0^o$.

Figure 19.- Continued.

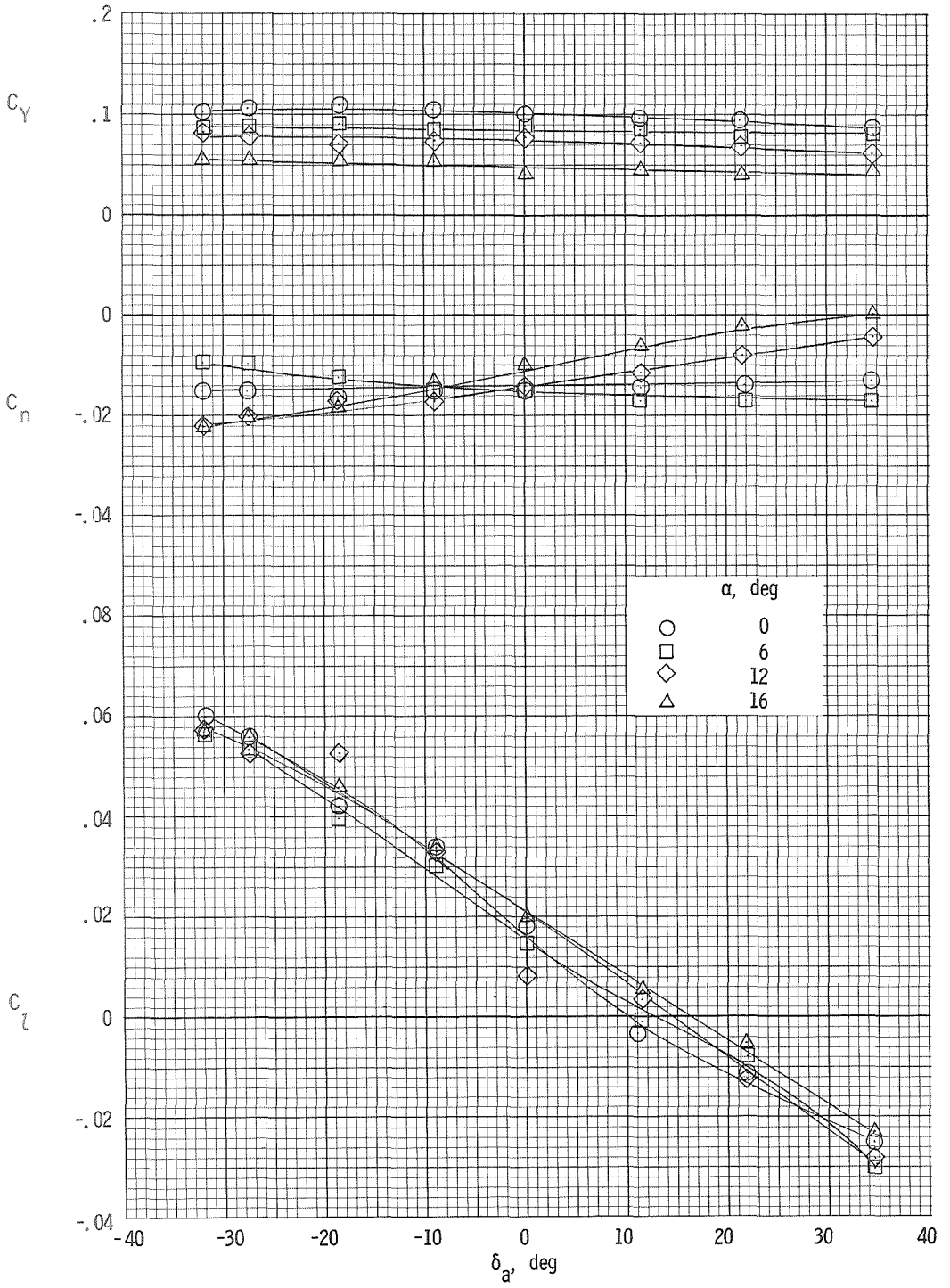


(c) $\beta = -8^{0}$.

Figure 19.- Concluded.

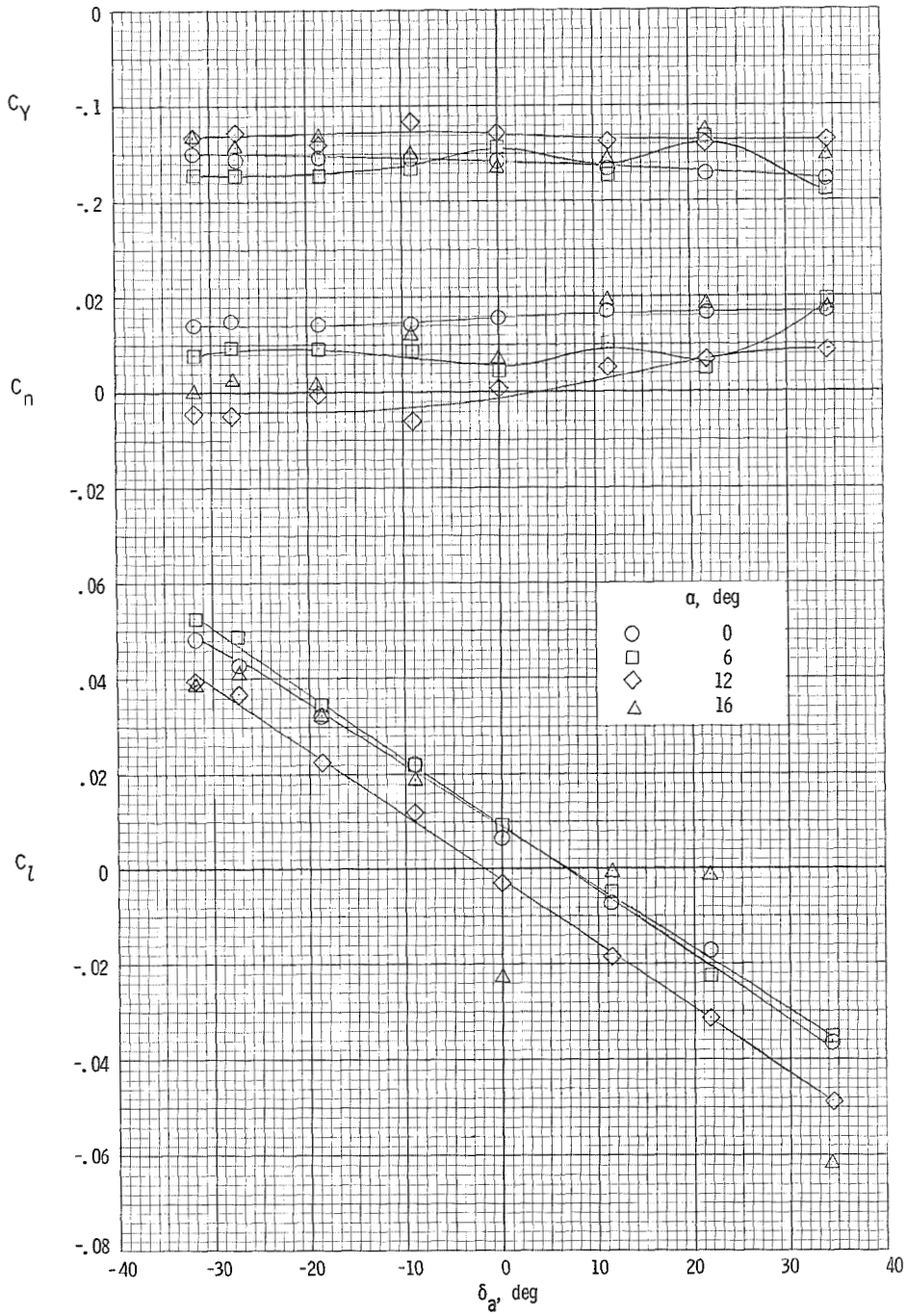


(a) $\beta = 8^{o}$.

Figure 20.- Variation of the lateral characteristics of the airplane with aileron deflection. $\delta_f = 32^{o}$; $T_C' = 0.46$.

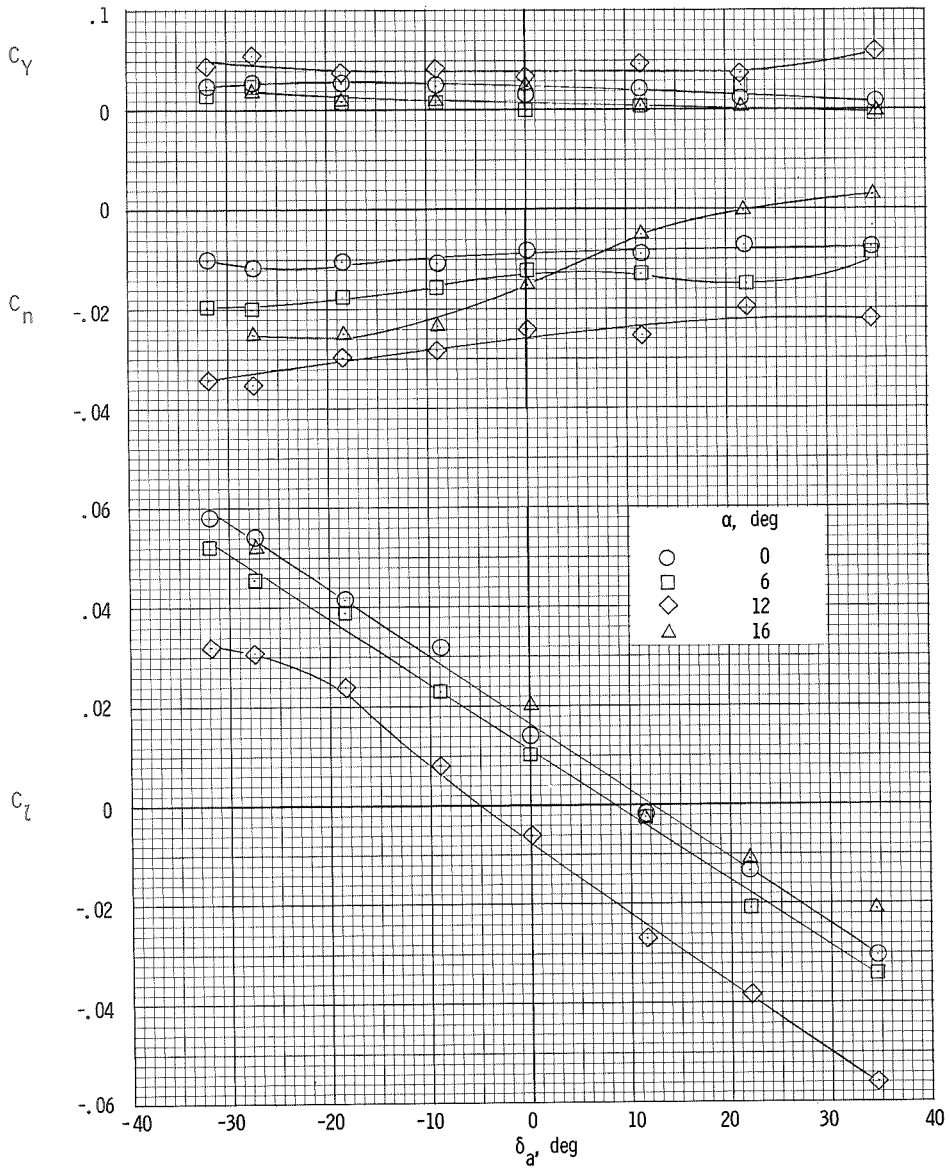


(b) $\beta = 0^o$.

Figure 20.- Continued.

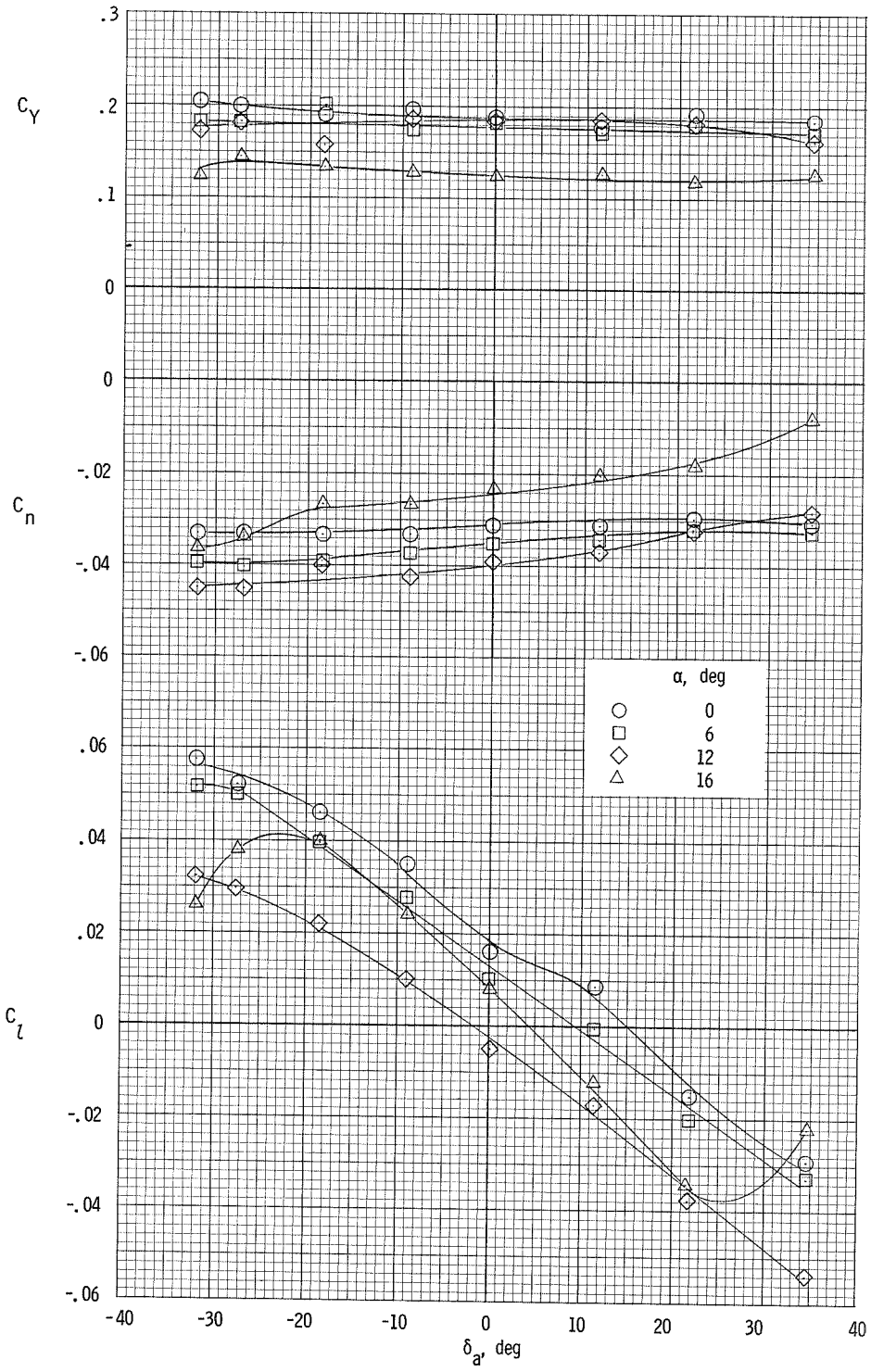


(c) $\beta = -8^{\circ}$.

Figure 20.- Concluded.

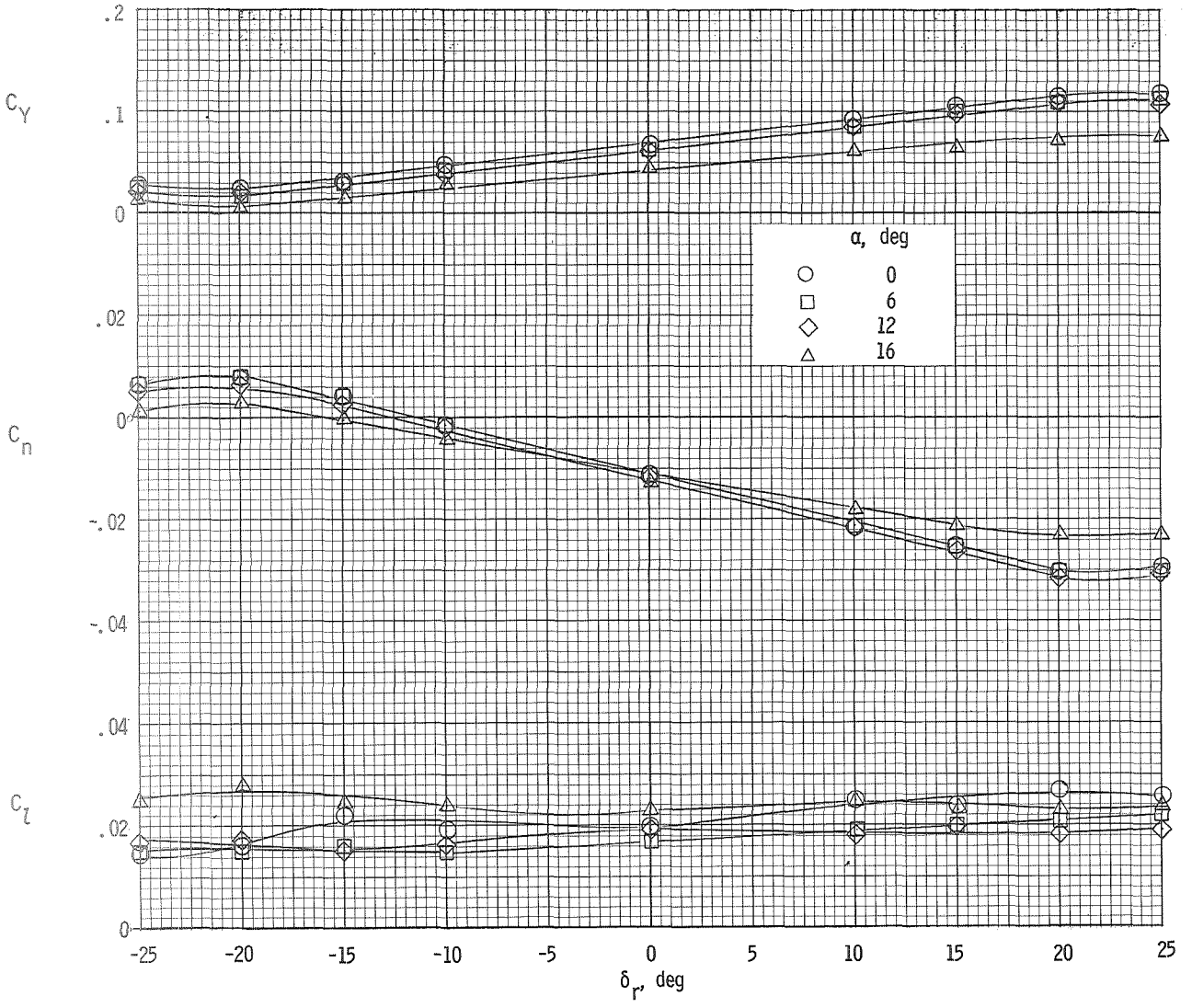


(a) $\beta = -8^0$.

Figure 21.- Variation of the lateral characteristics of the airplane with rudder deflection. $\delta_f = 0^0$; $T_C' = 0$.

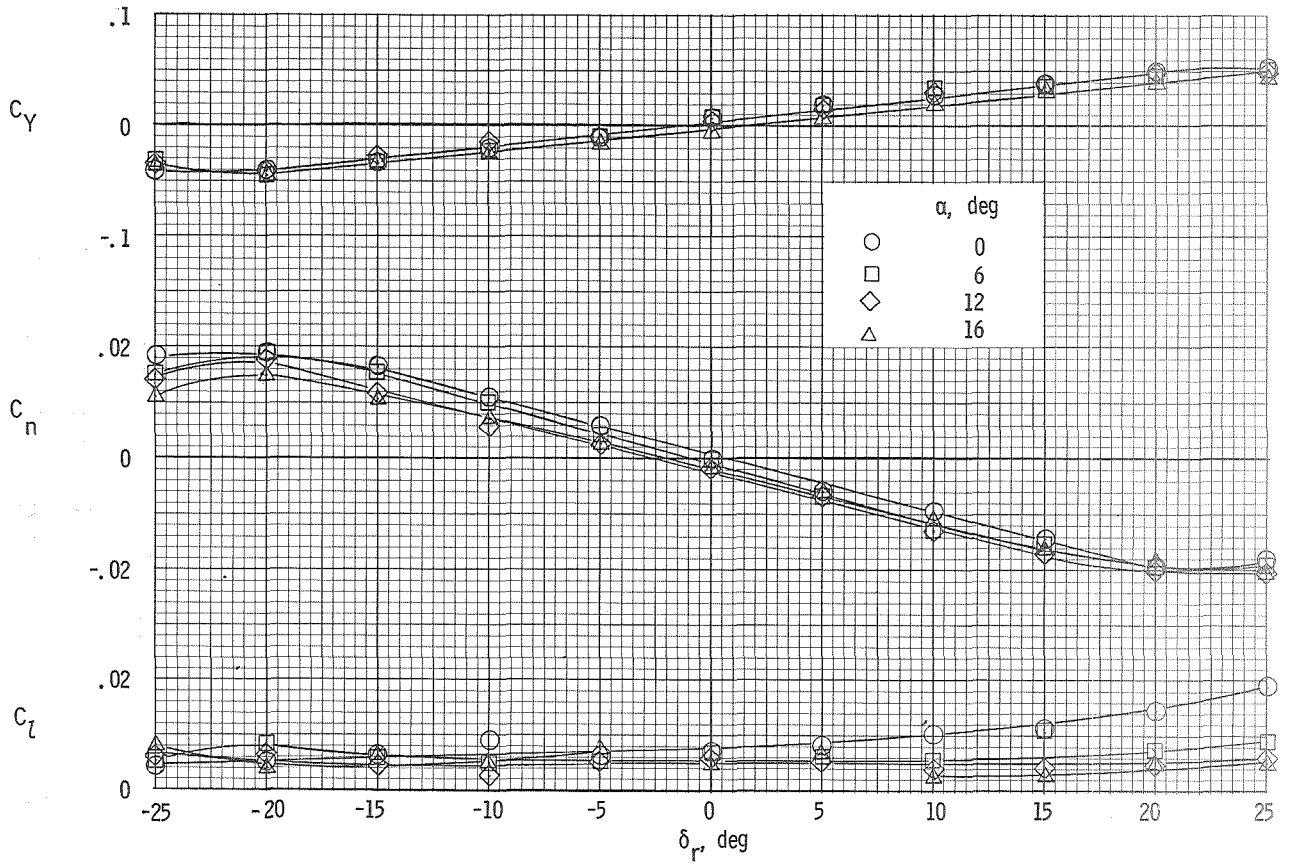


(b) $\beta = 0^0$.

Figure 21.- Continued.

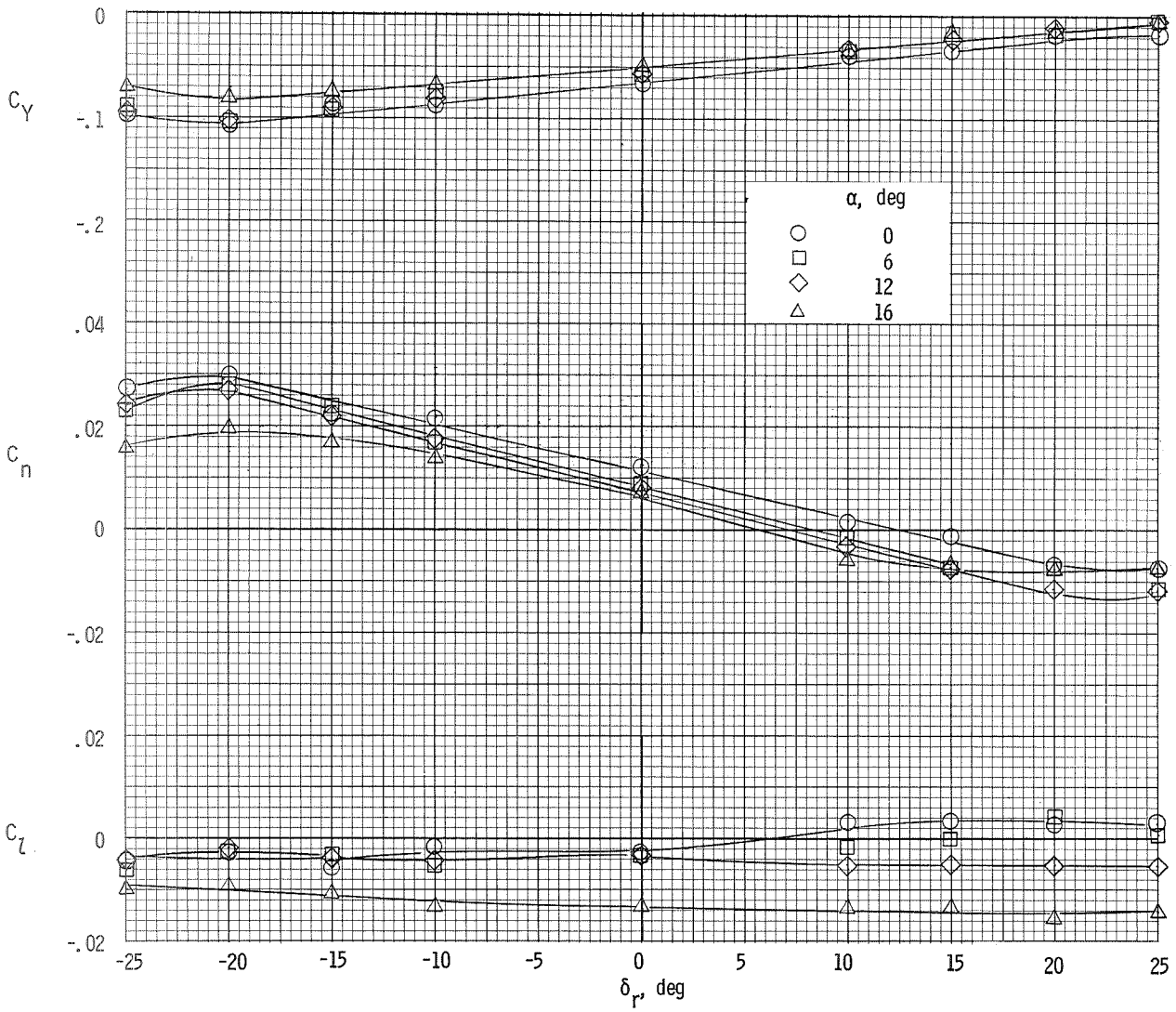


(c) $\beta = 8^{o}$.

Figure 21.- Concluded.

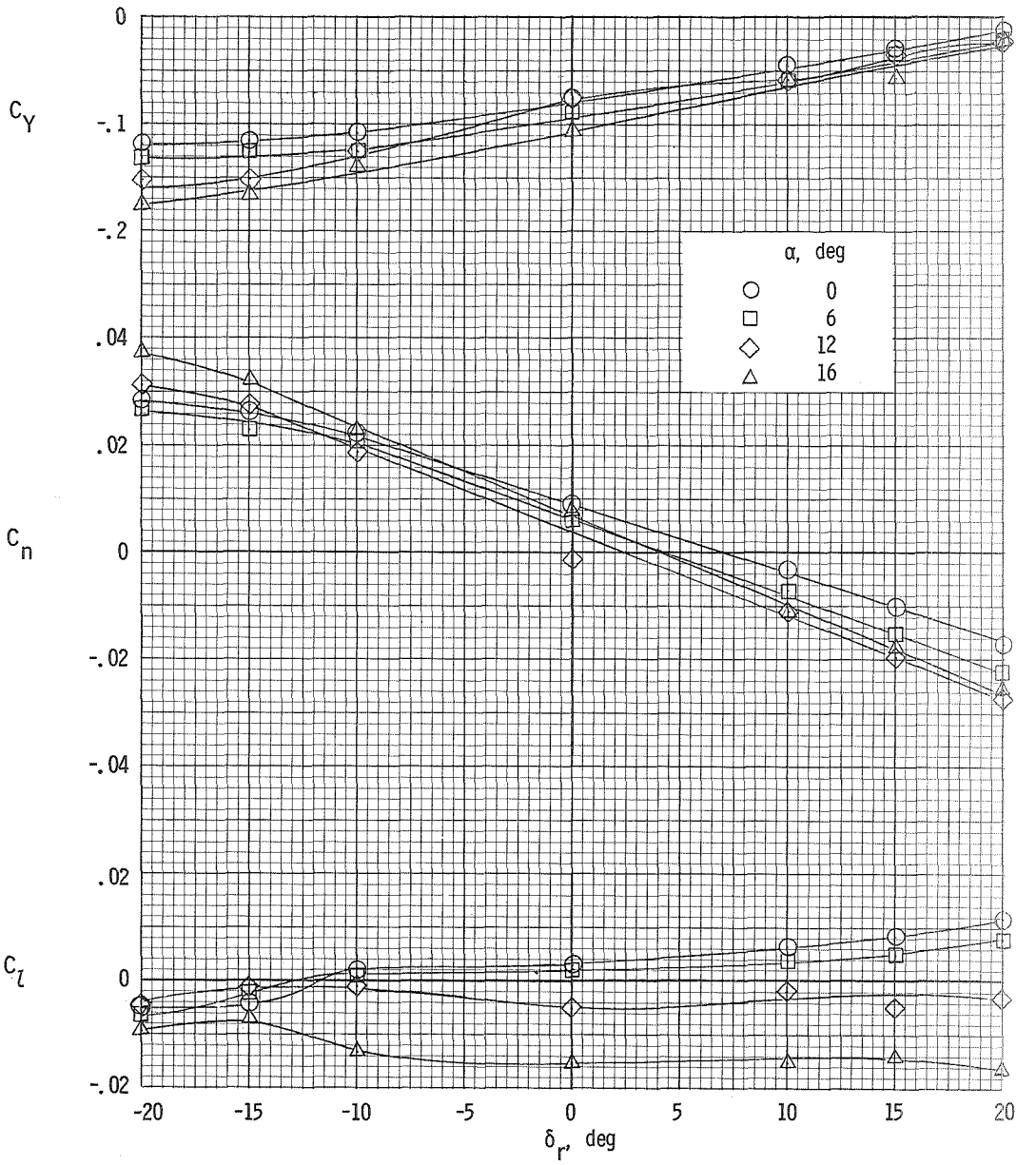


(a) $\beta = 8^0$.

Figure 22.- Variation of the lateral characteristics of the airplane with rudder deflection. $\delta_f = 0^0$; $T_c' = 0.20$.

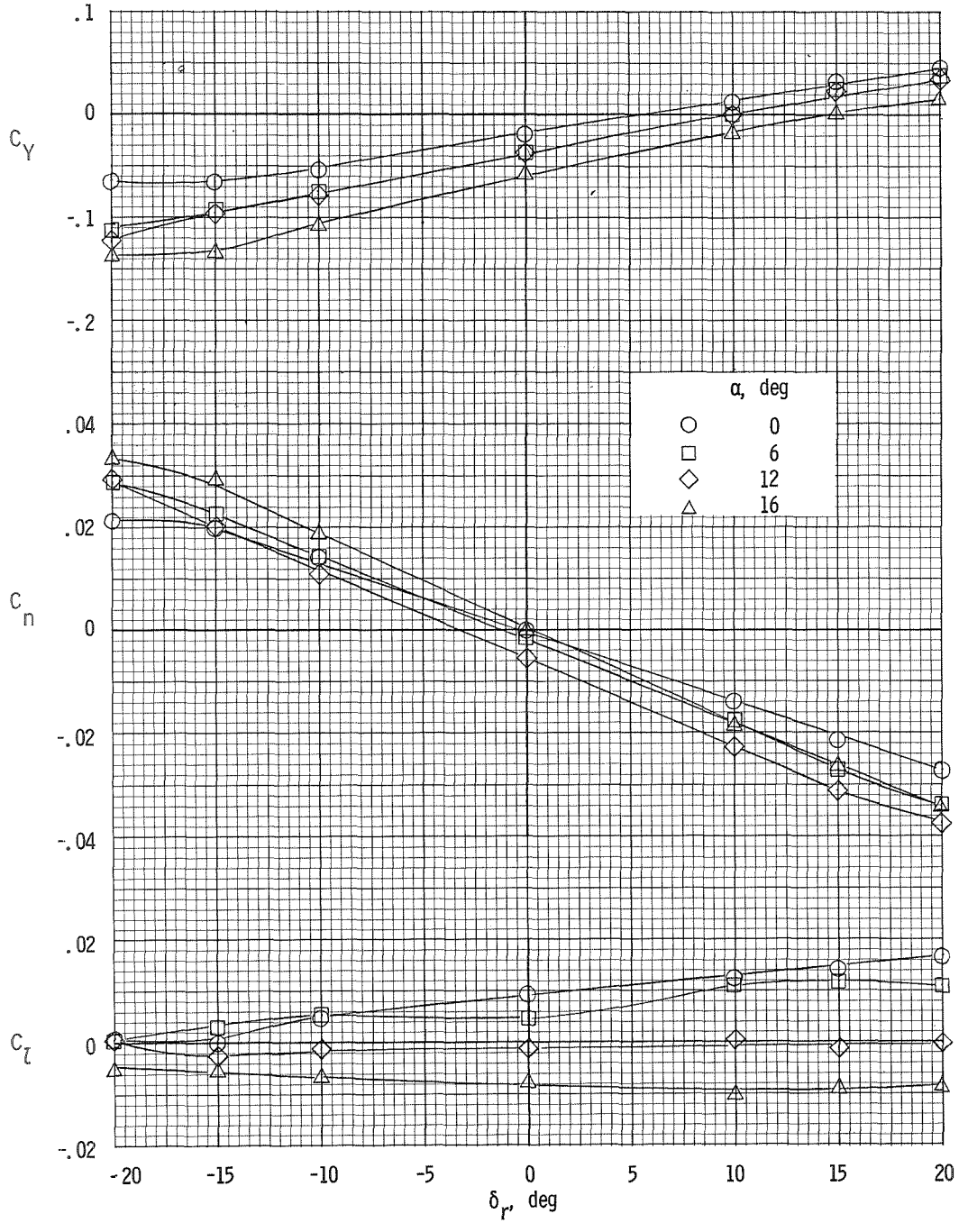


(b) $\beta = 4^o$.

Figure 22.- Continued.

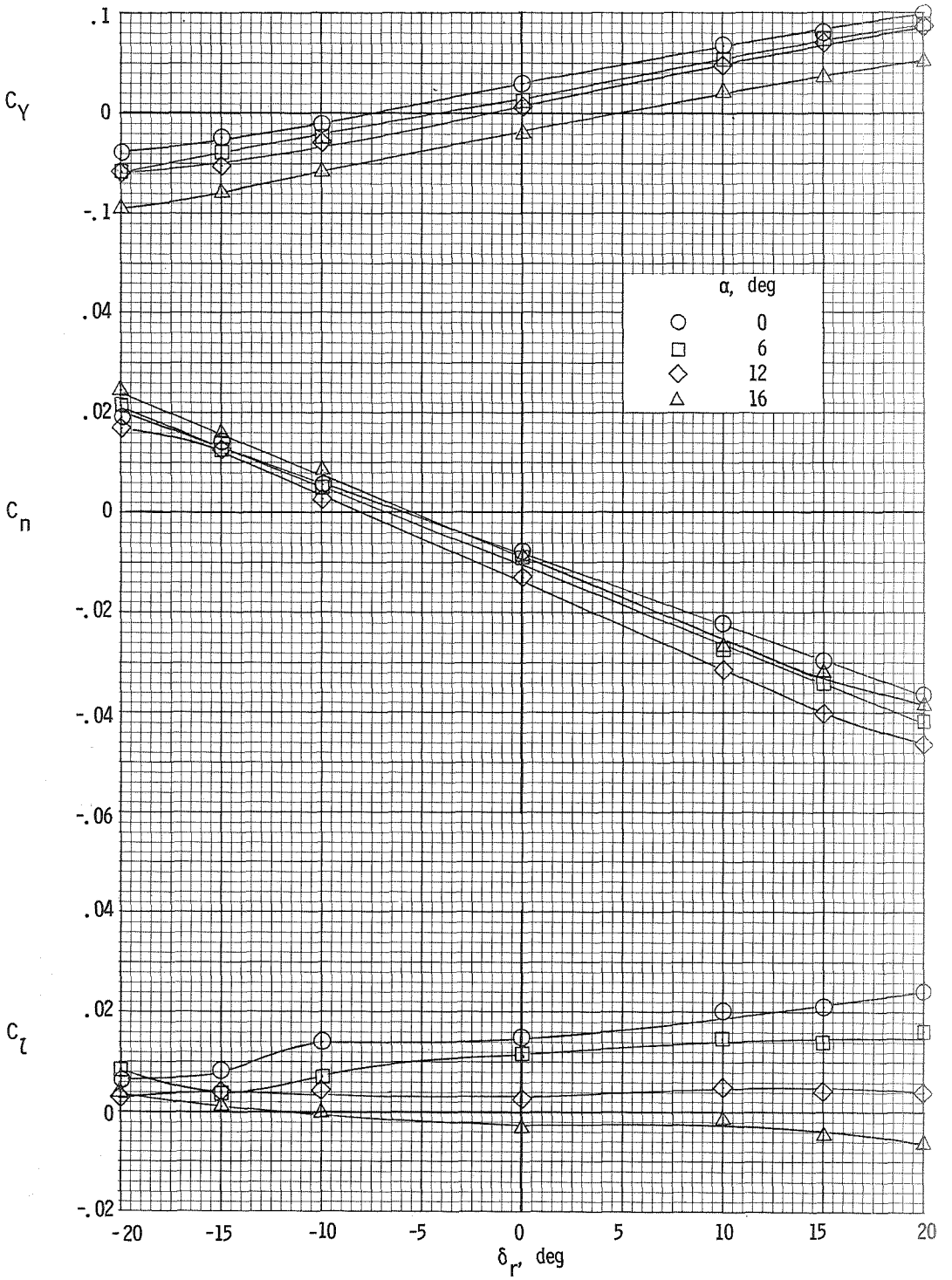


(c) $\beta = 0^0$.

Figure 22.- Continued.

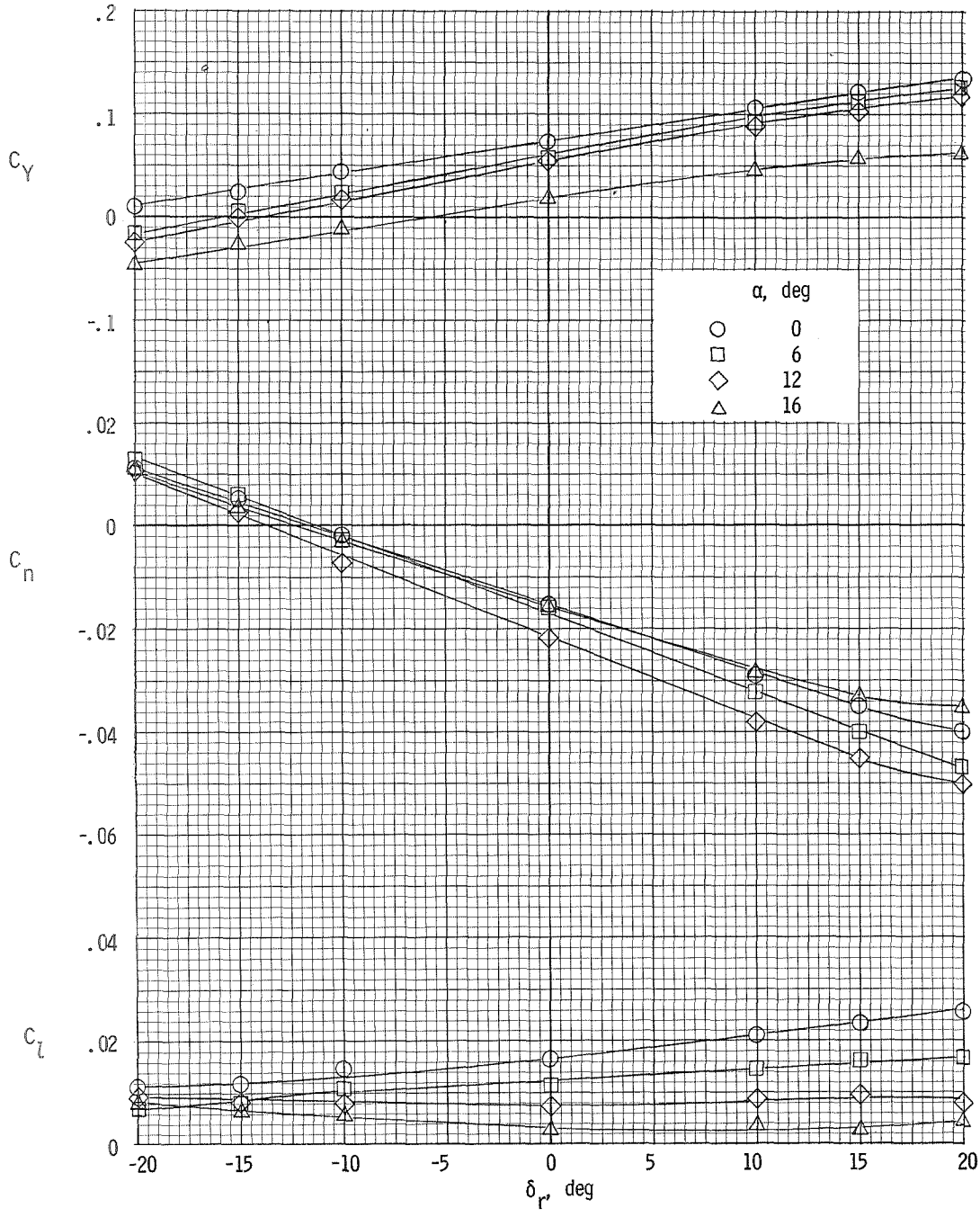


(d) $\beta = -4^{\circ}$.

Figure 22.- Continued.

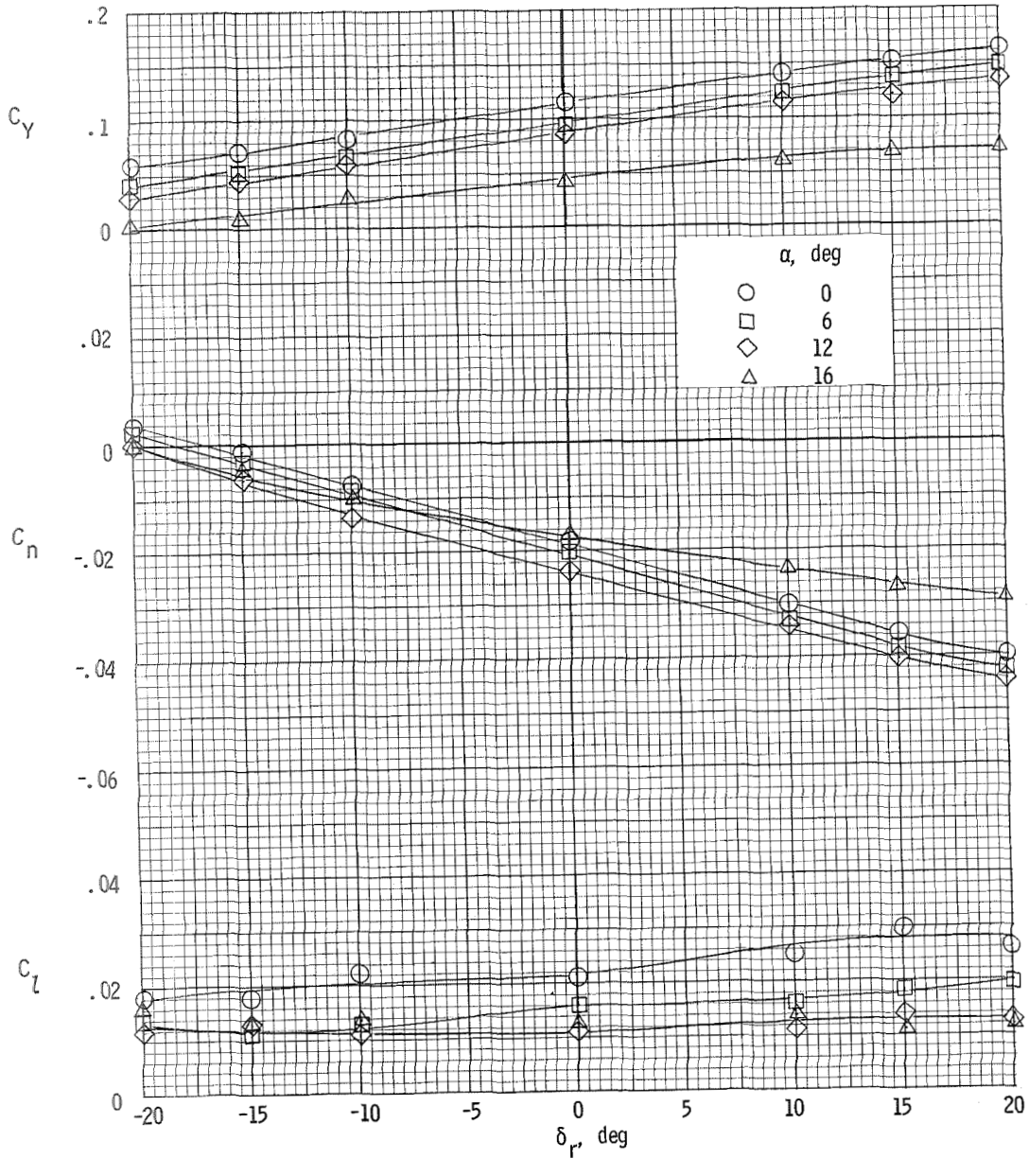


(e) $\beta = -8^{o}$.

Figure 22.- Concluded.

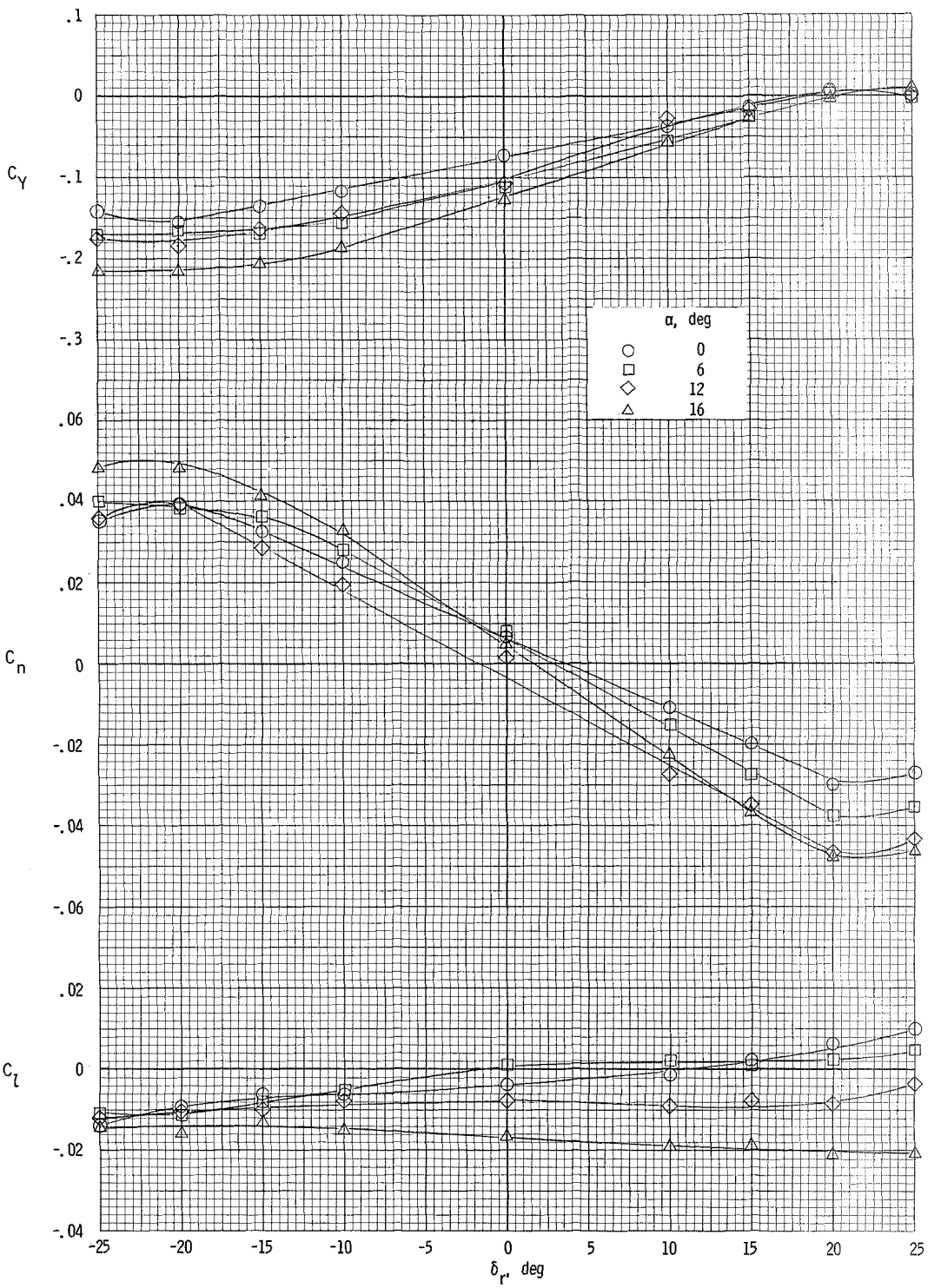


(a) $\beta = 8^{\circ}$.

Figure 23.- Variation of the lateral characteristics of the airplane with rudder deflection. $\delta_f = 0^{\circ}$; $T_C' = 0.46$.

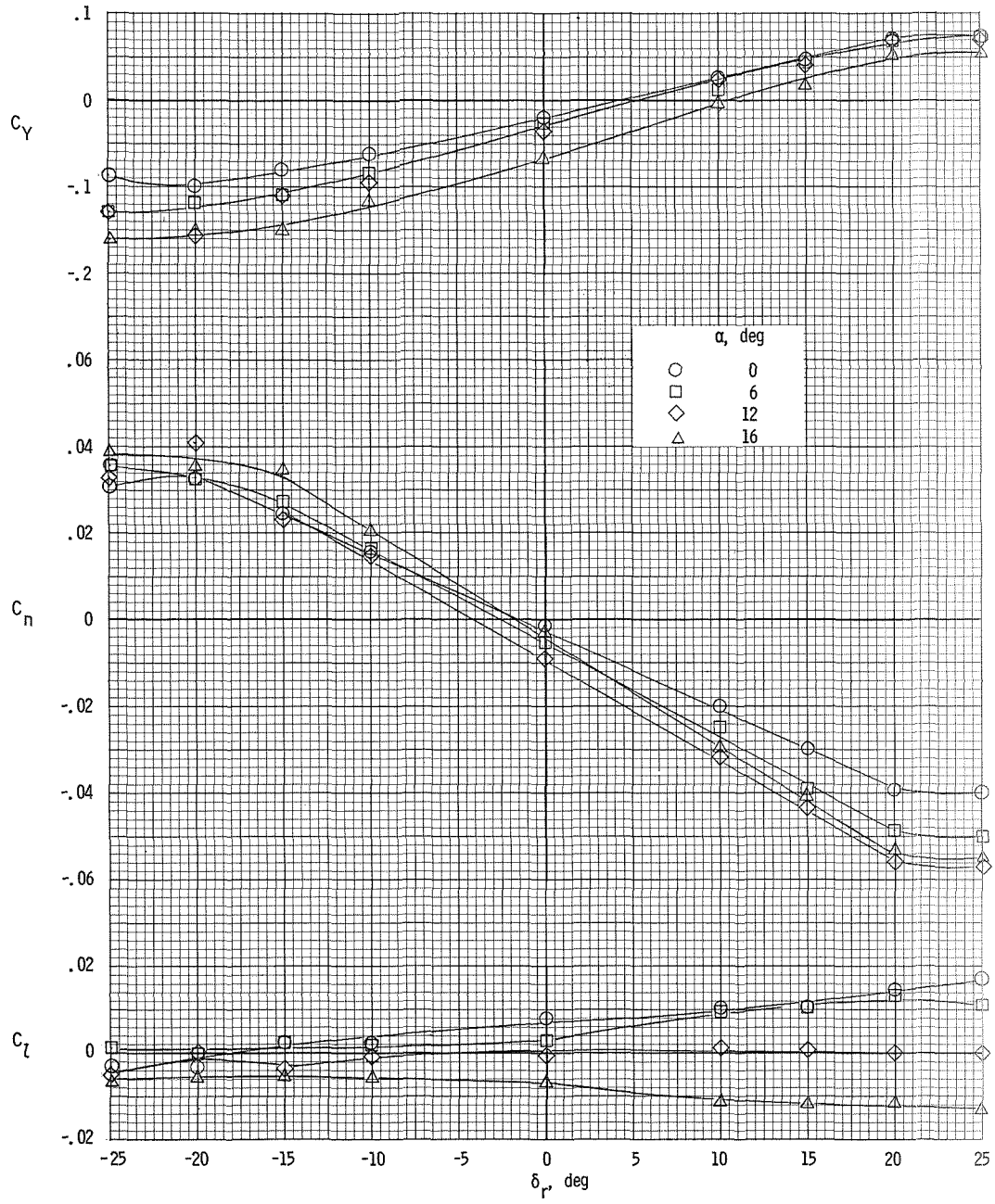


(b) $\beta = 4^0$.

Figure 23.- Continued.

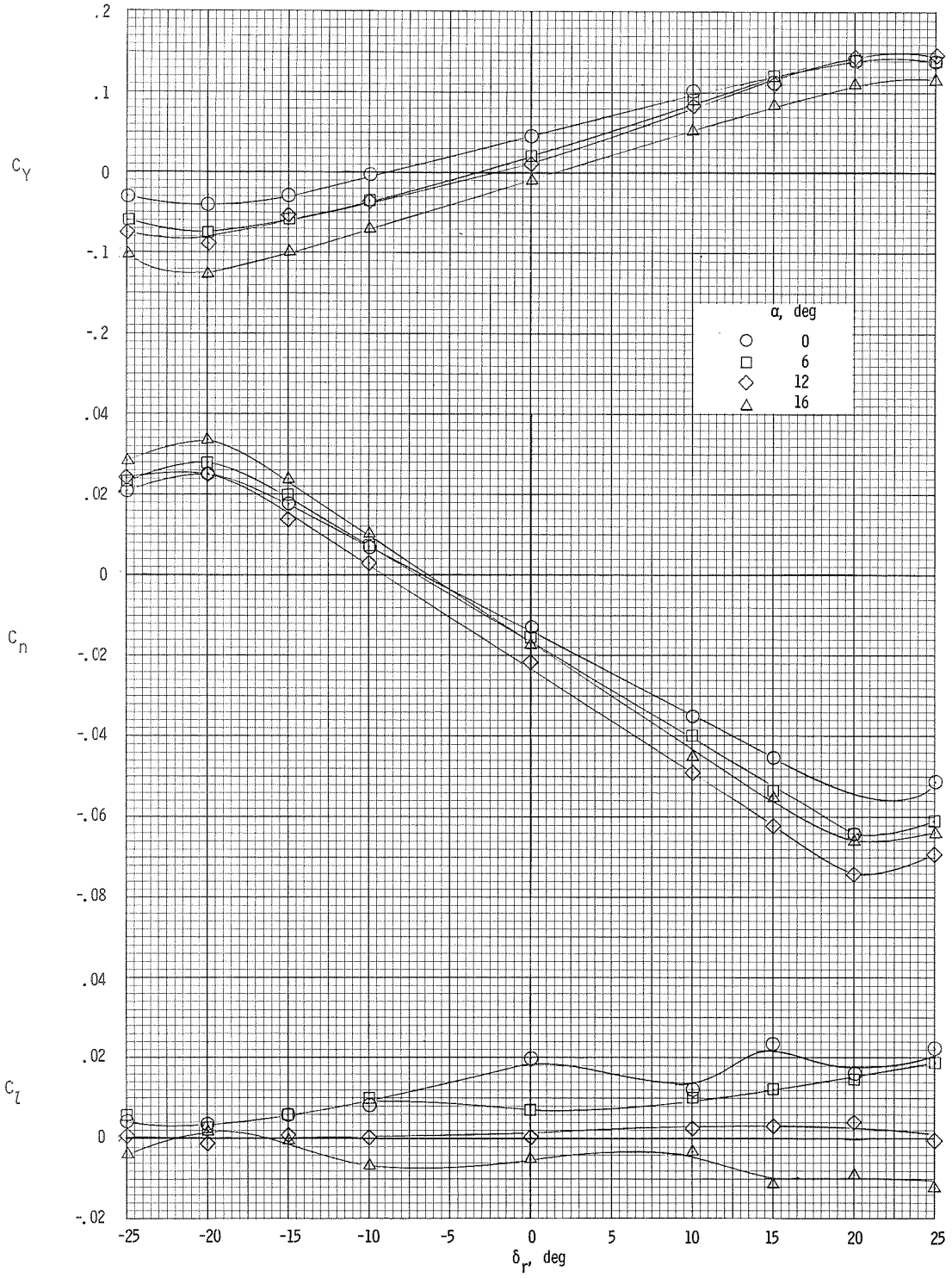


(c) $\beta = 0^o$.

Figure 23.- Continued.

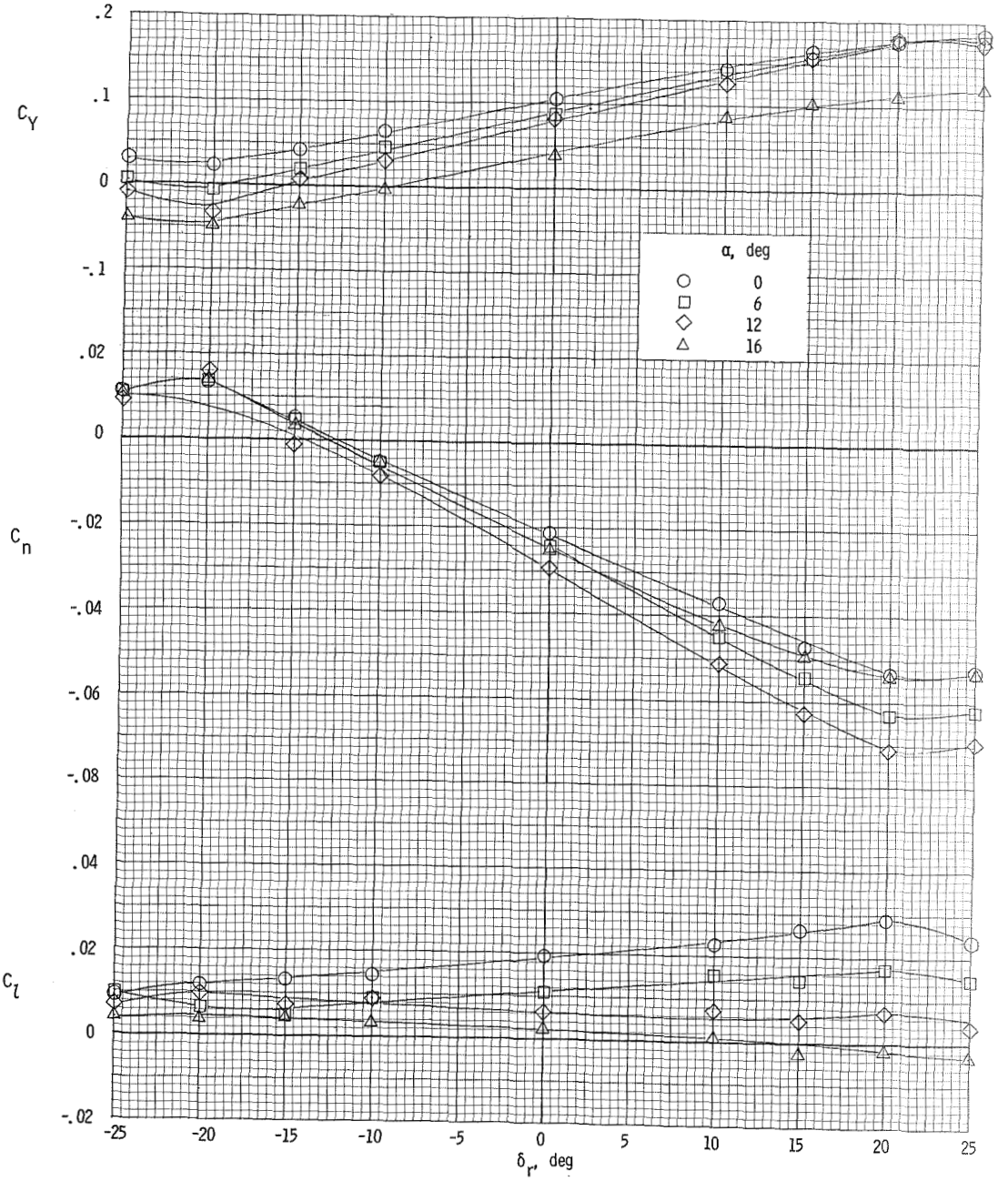


(d) $\beta = -4^0$.

Figure 23.- Continued.

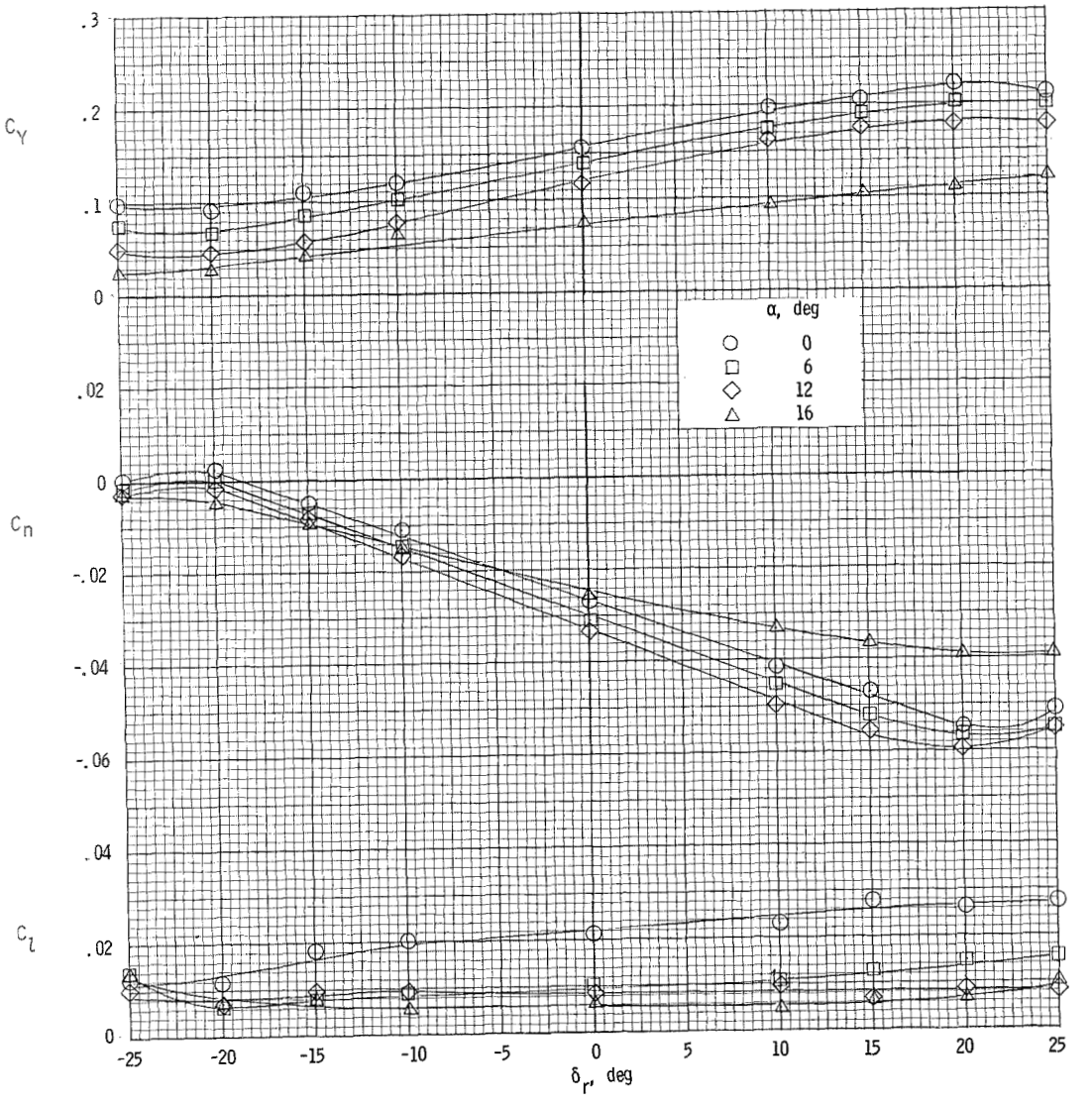


(e) $\beta = -8^{\circ}$.

Figure 23.- Concluded.

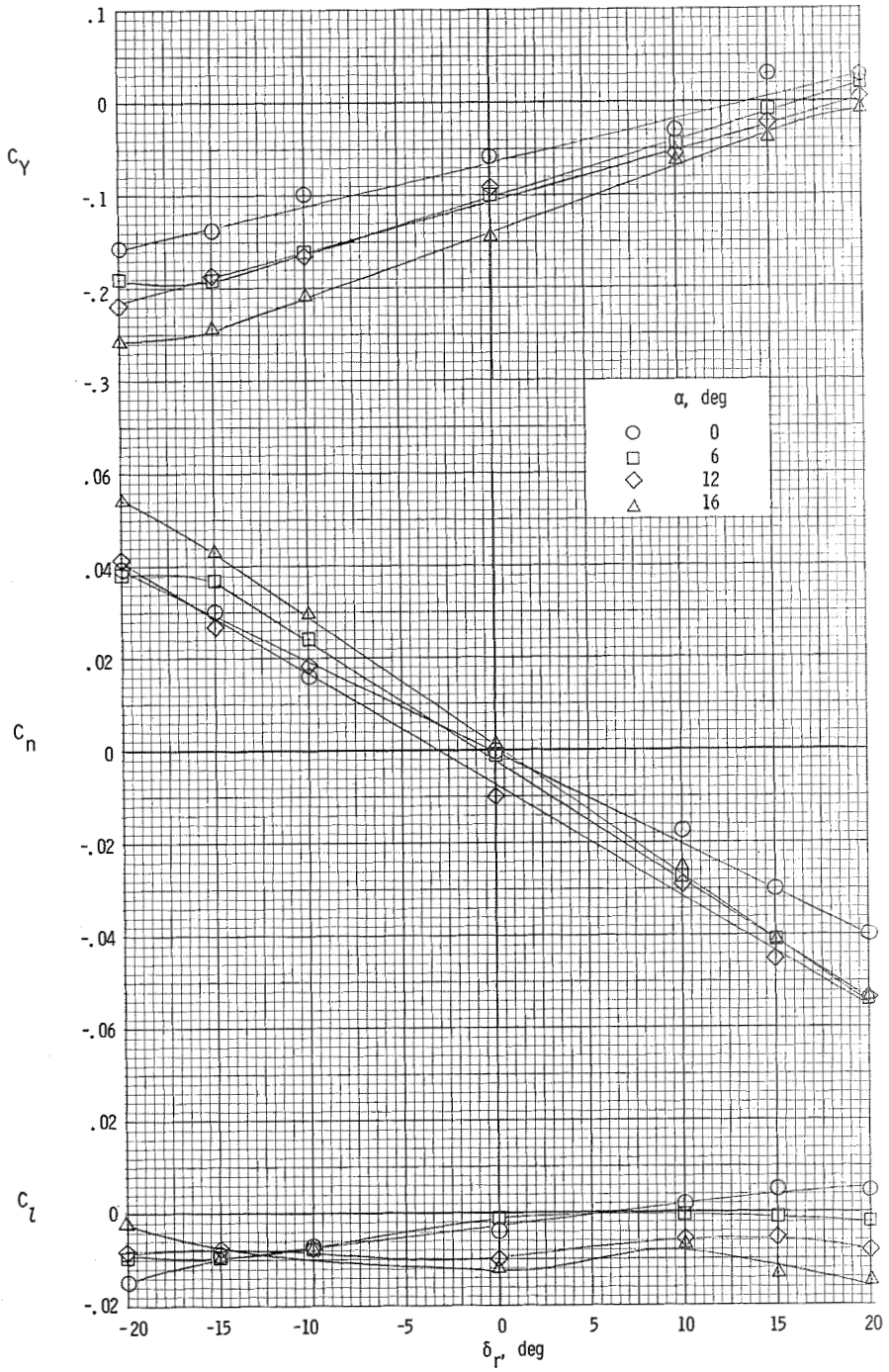


(a) $\beta = 8^0$.

Figure 24.- Variation of the lateral characteristics of the airplane with rudder deflection. $\delta_f = 0^0$; $T_C' = 0.55$.

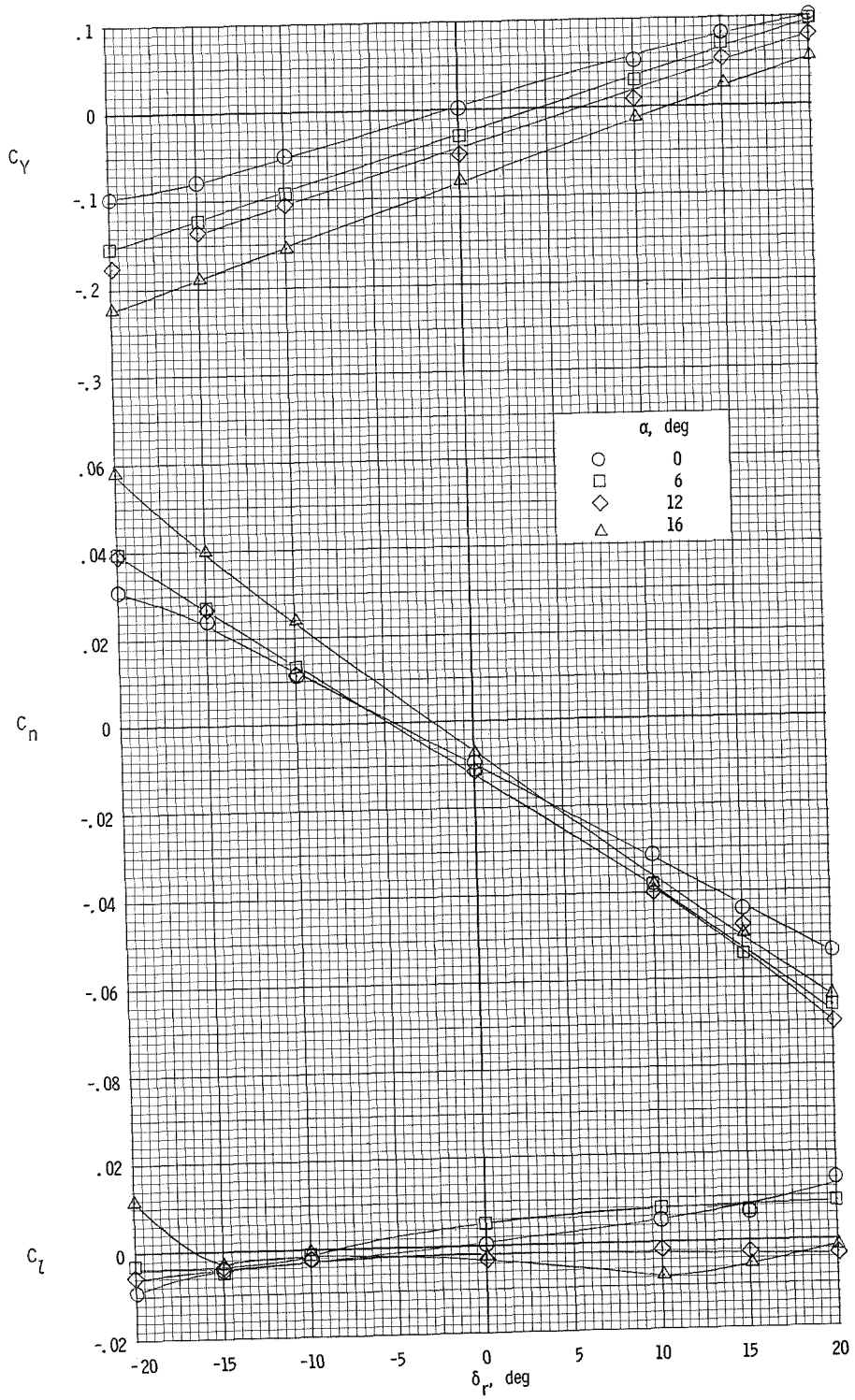


(b) $\beta = 4^0$.

Figure 24.- Continued.

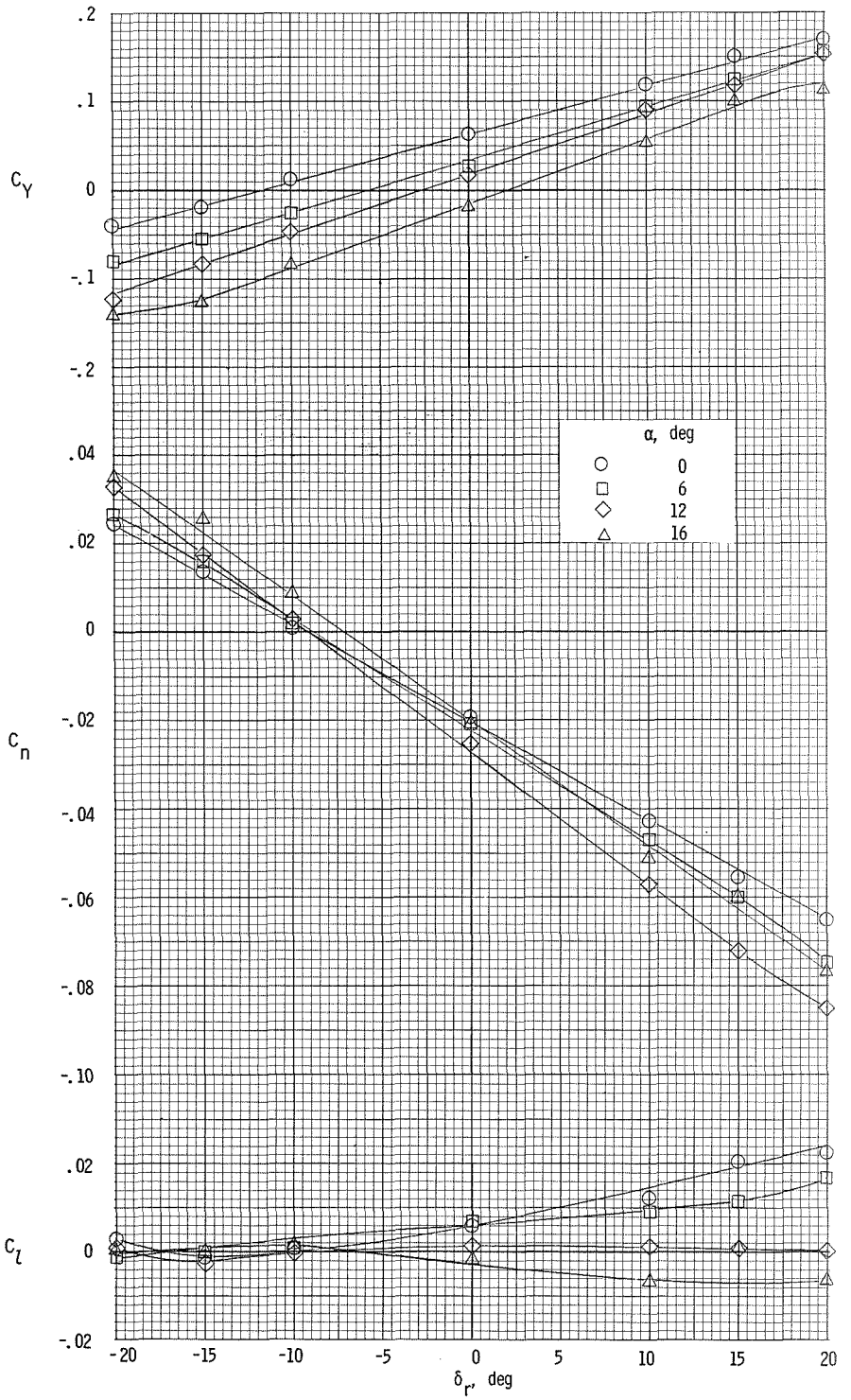


(c) $\beta = 0^{o}$.

Figure 24.- Continued.

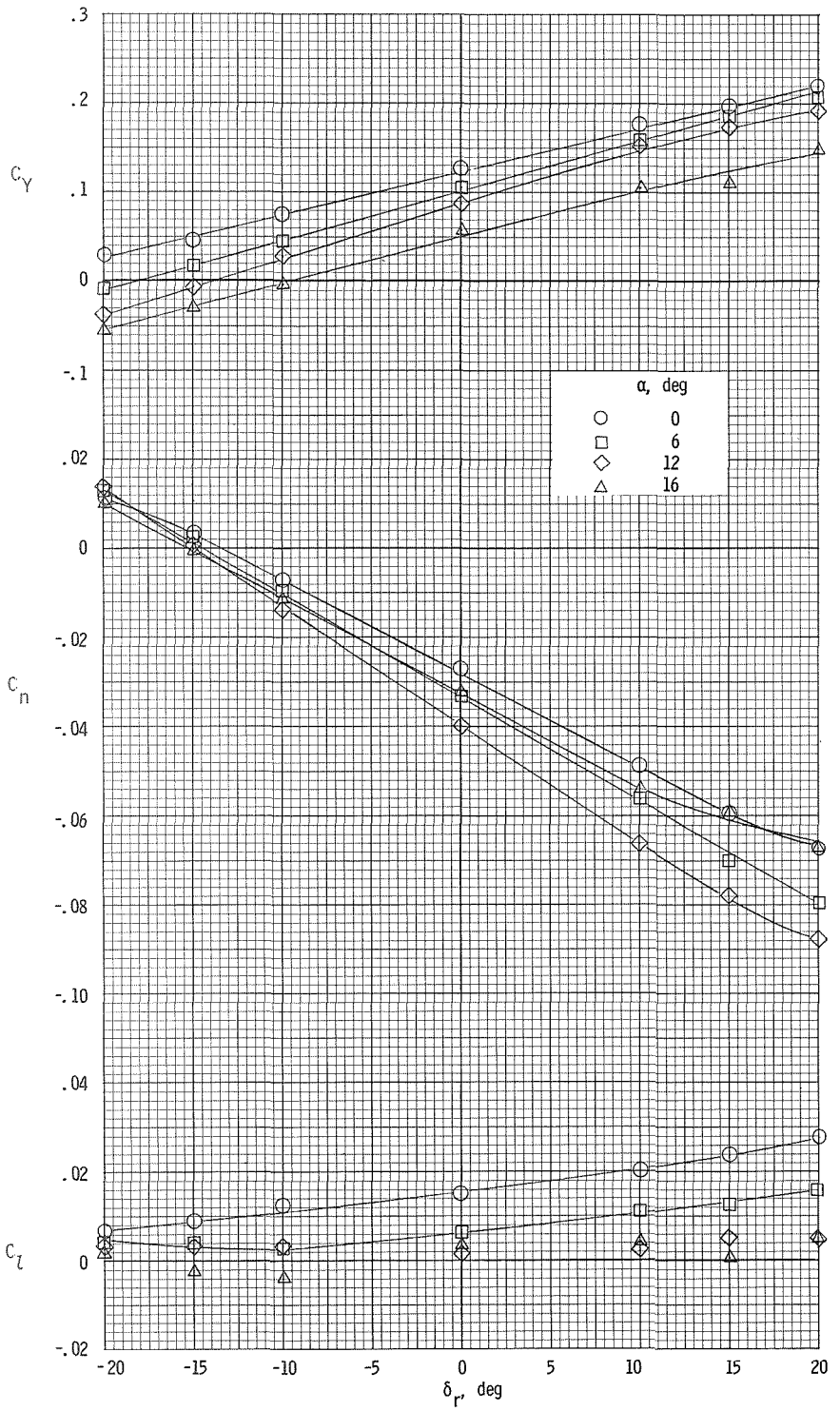


(d) $\beta = -4^{o}$.

Figure 24.- Continued.

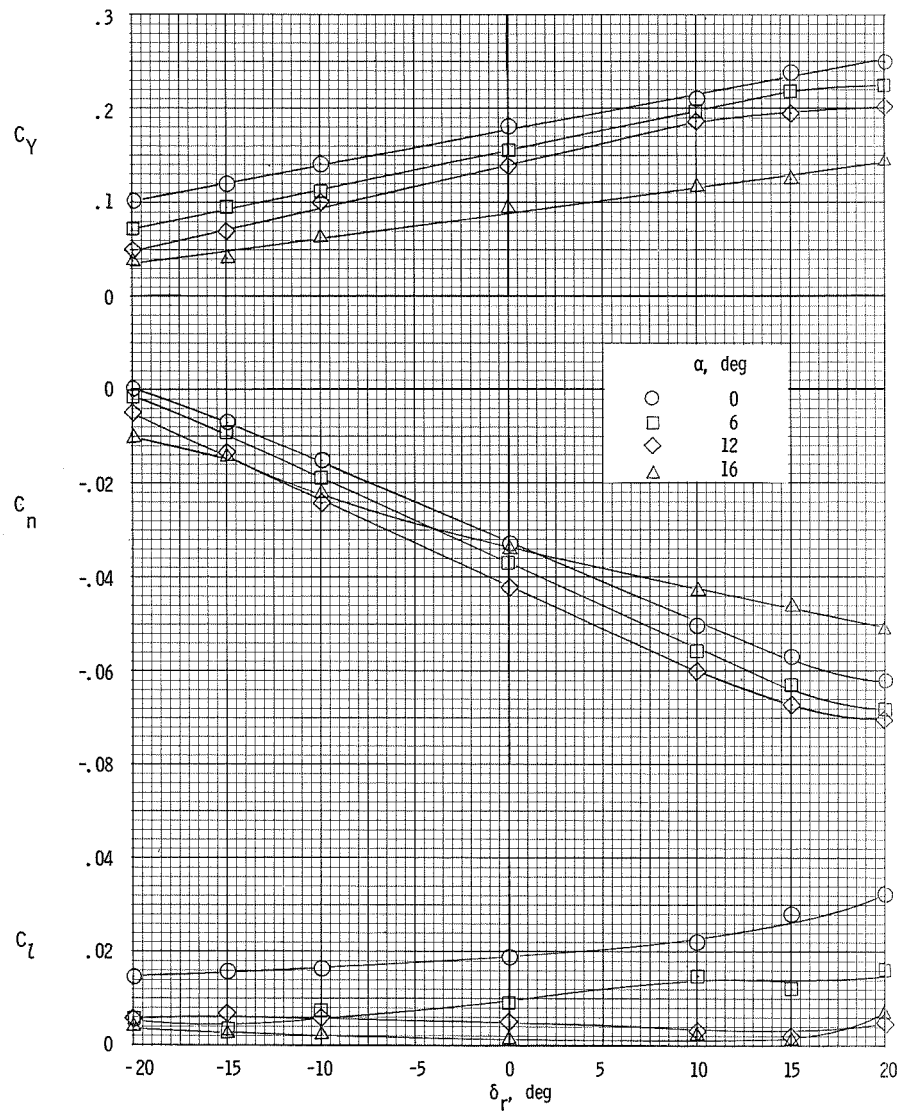


(e) $\beta = -8^0$.

Figure 24.- Concluded.

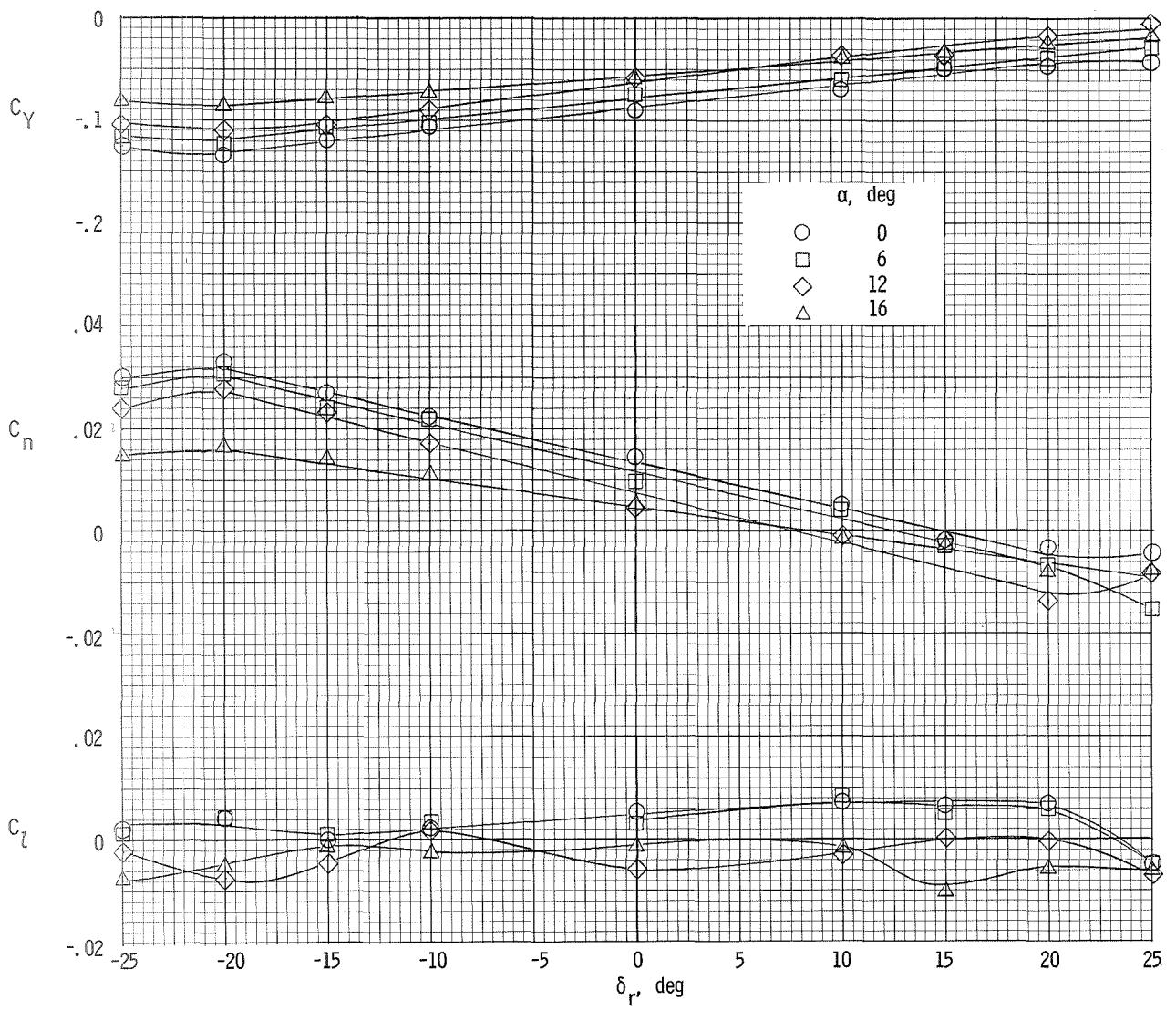


(a) $\beta = 8^0$.

Figure 25.- Variation of the lateral characteristics of the airplane with rudder deflection. $\delta_f = 32^0$; $T_c' = 0$.

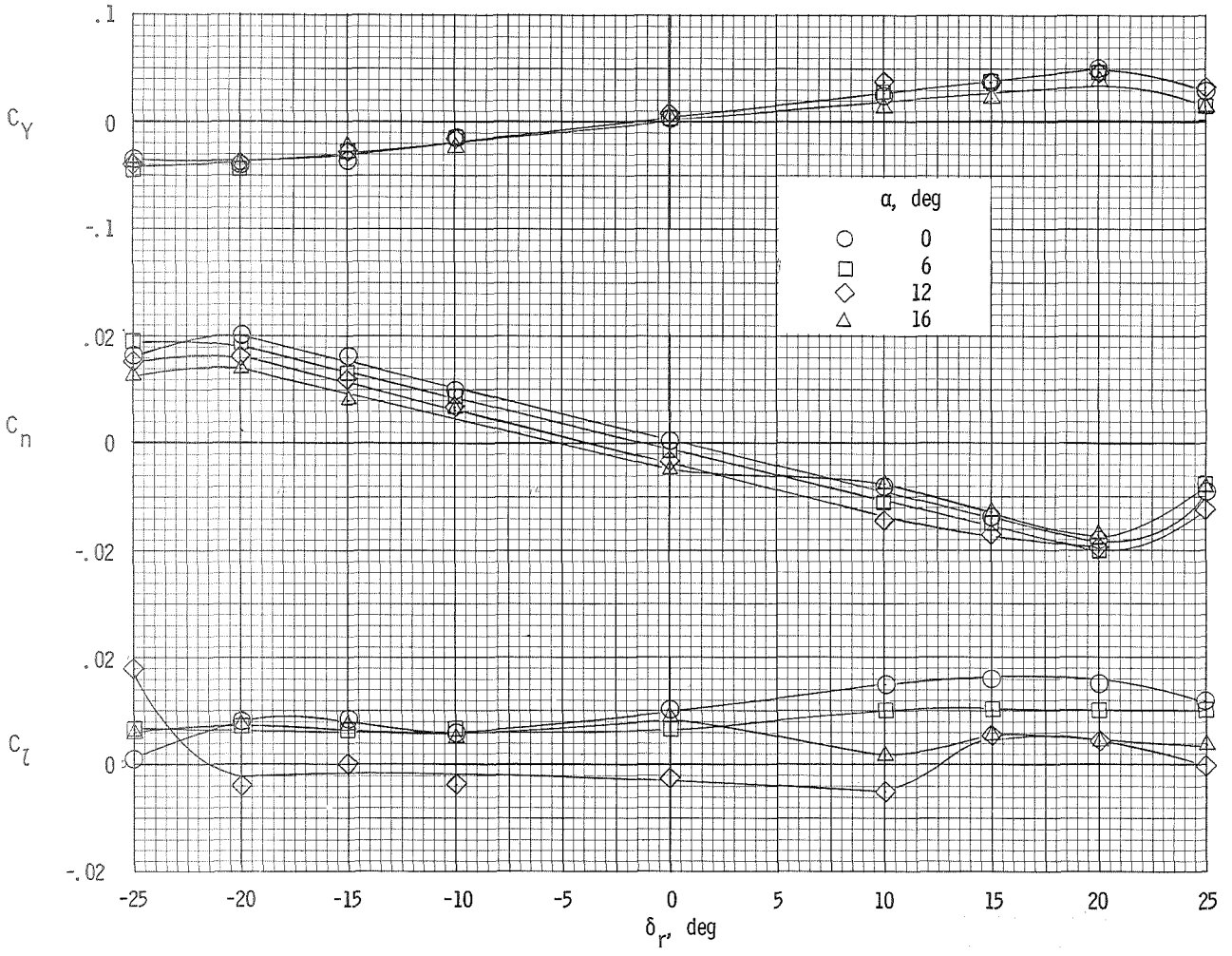


(b) $\beta = 0^0$.

Figure 25.- Continued.

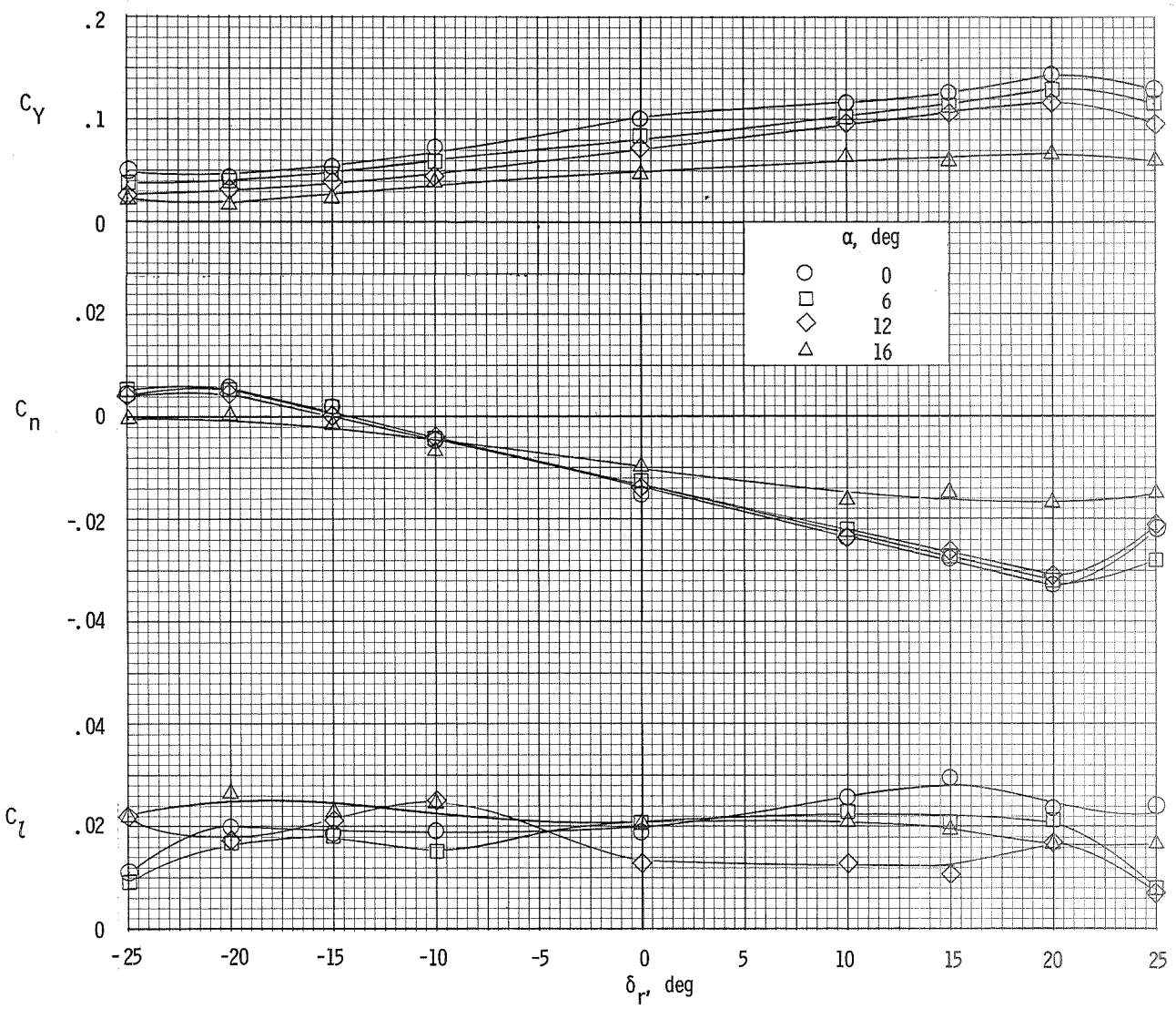


(c) $\beta = -8^0$.

Figure 25.- Concluded.

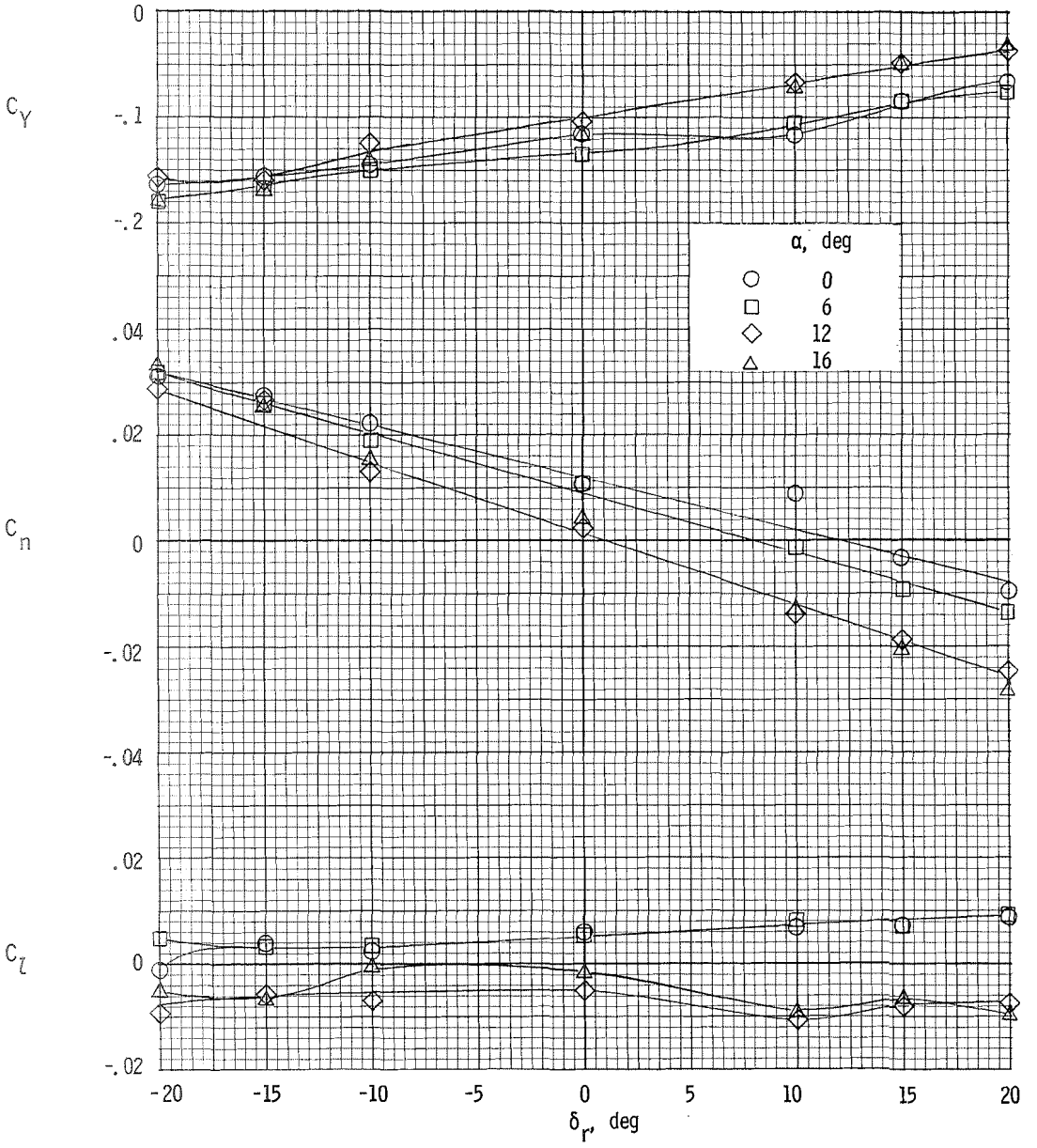


(a) $\beta = 8^0$.

Figure 26.- Variation of the lateral characteristics of the airplane with rudder deflection. $\delta_f = 32^0$; $T_C' = 0.20$.

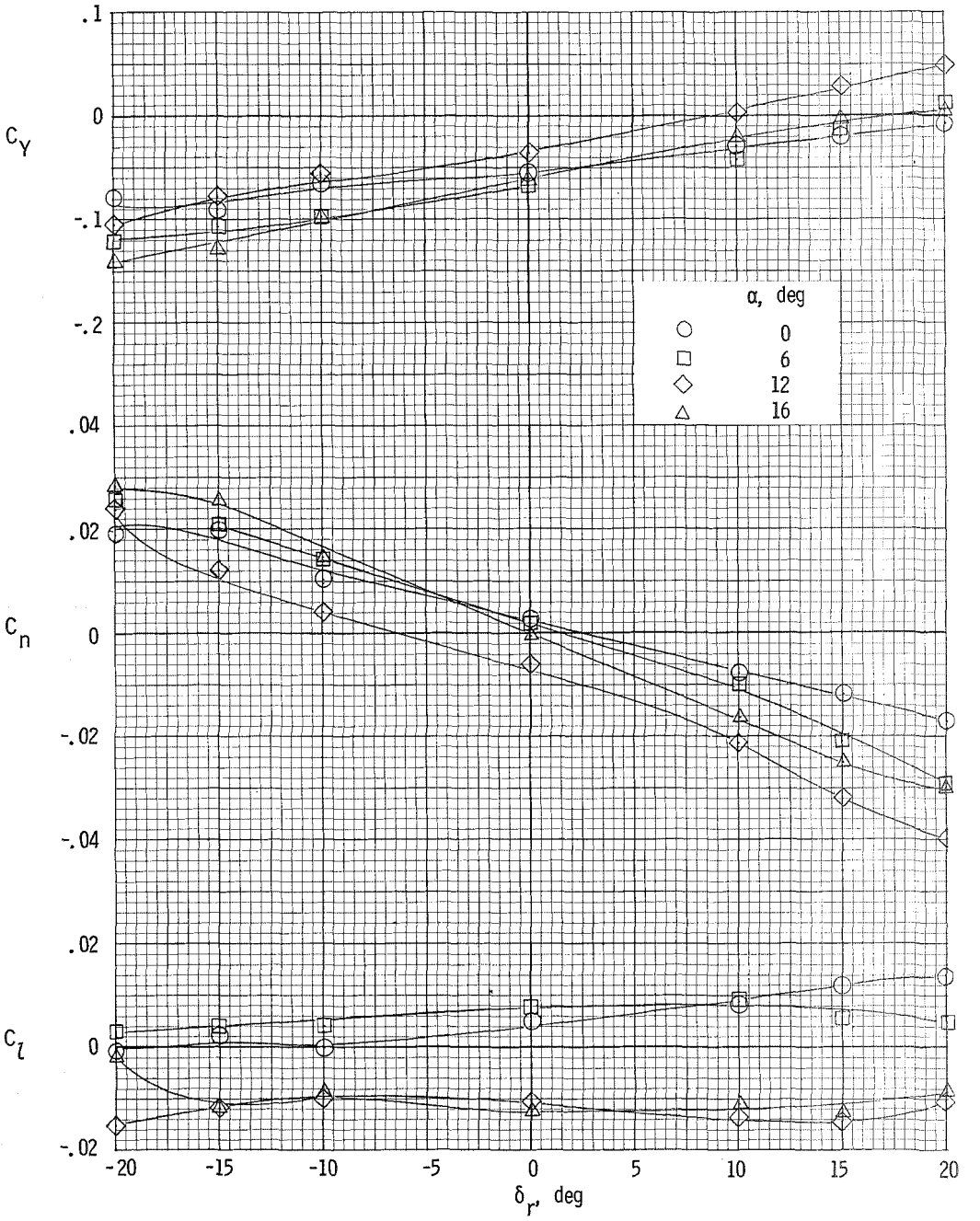


(b) $\beta = 4^0$.

Figure 26.- Continued.

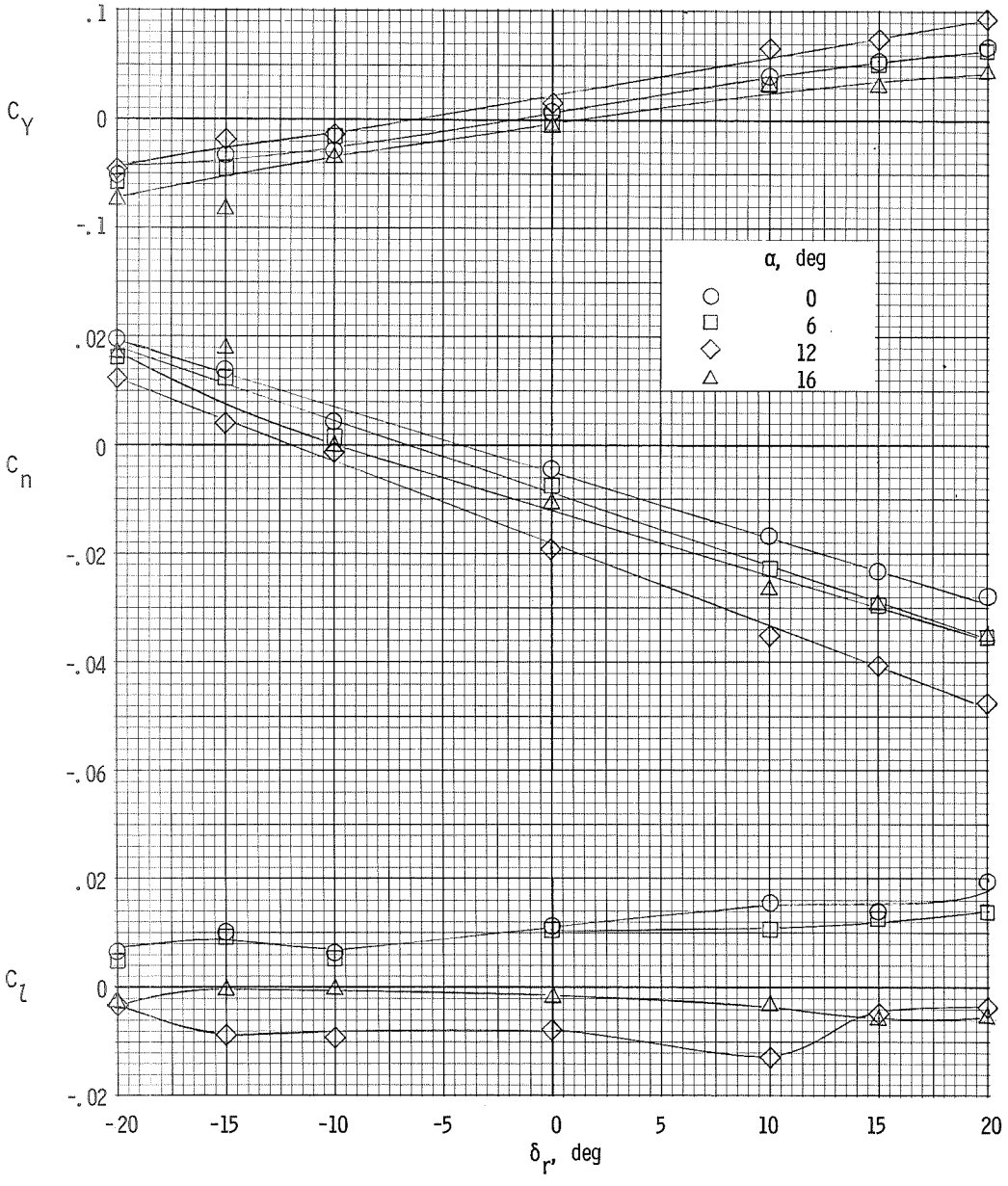


(c) $\beta = 0^0$.

Figure 26.- Continued.

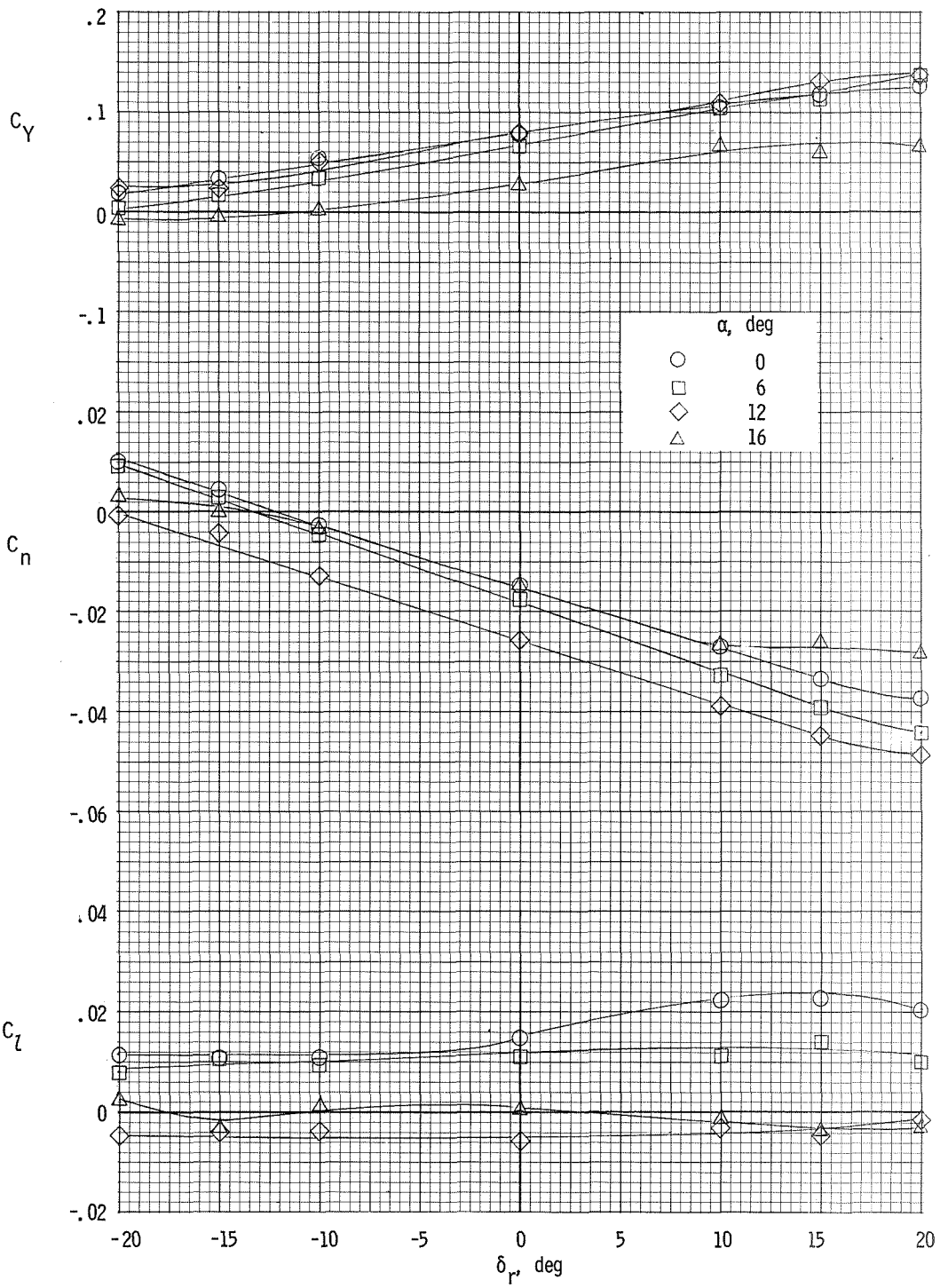


(d) $\beta = -4^0$.

Figure 26.- Continued.

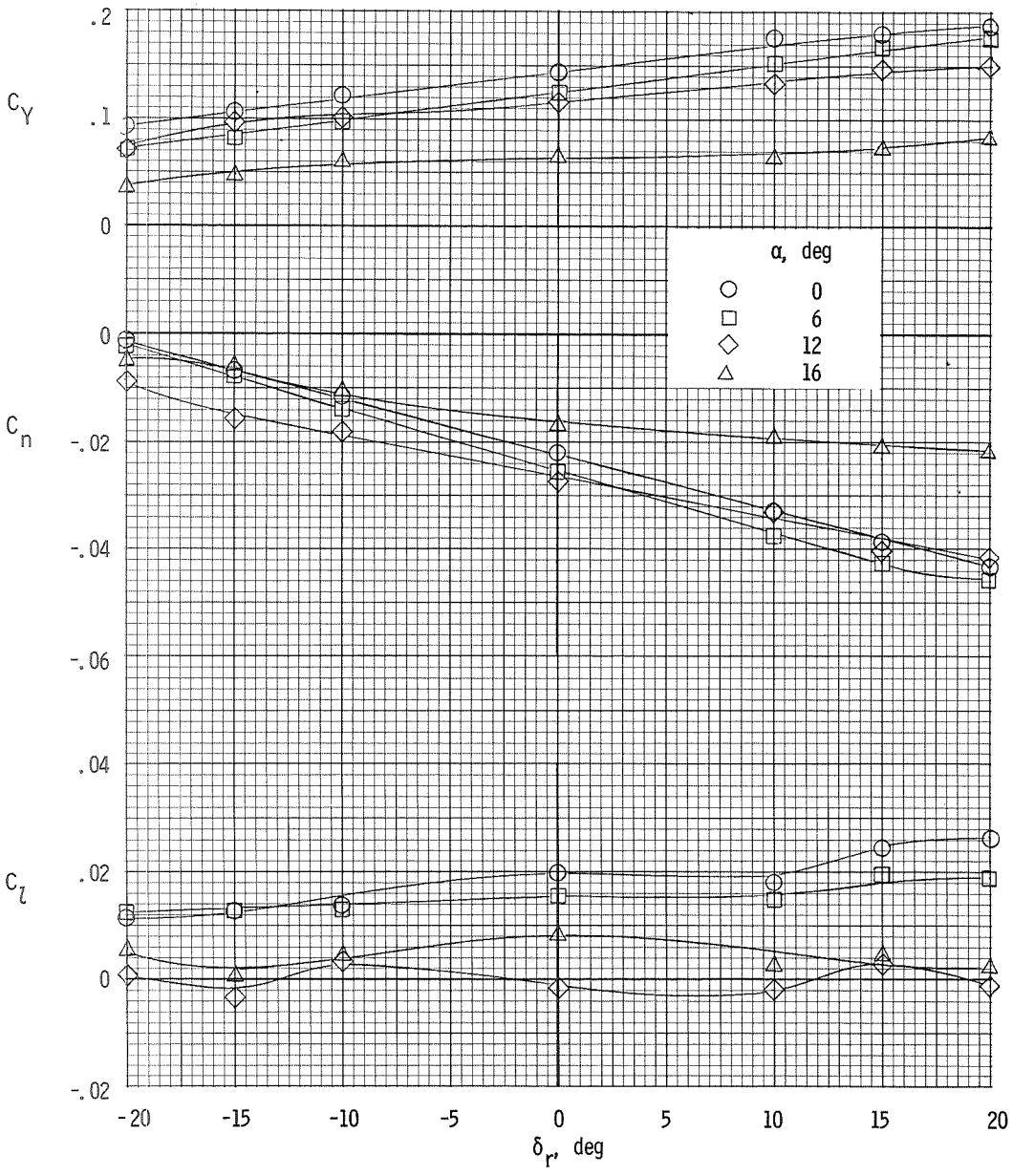


(e) $\beta = -8^{\circ}$.

Figure 26.- Concluded.

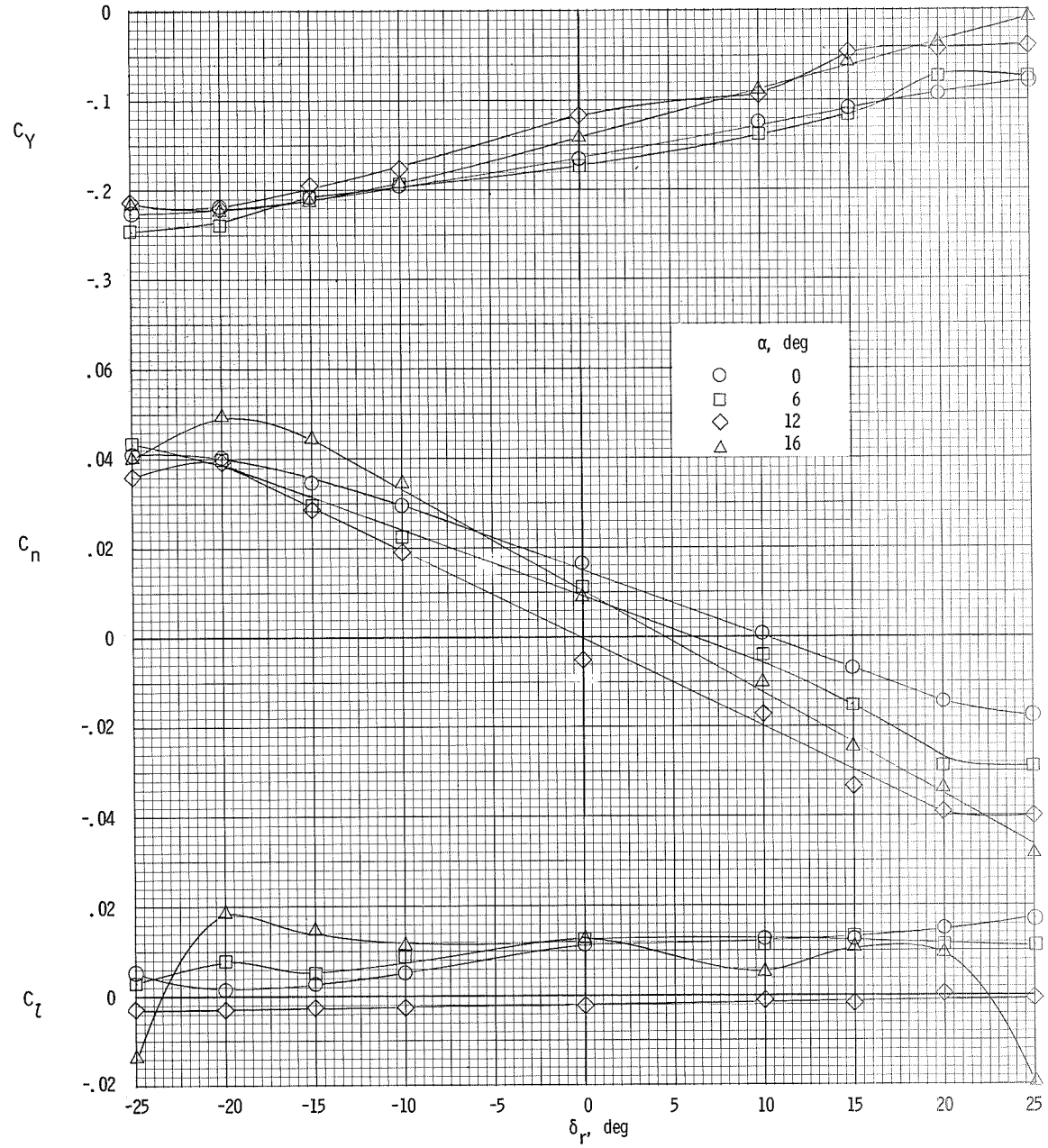


(a) $\beta = 8^0$.

Figure 27.- Variation of the lateral characteristics of the airplane with rudder deflection. $\delta_f = 32^0$; $T_C' = 0.46$.

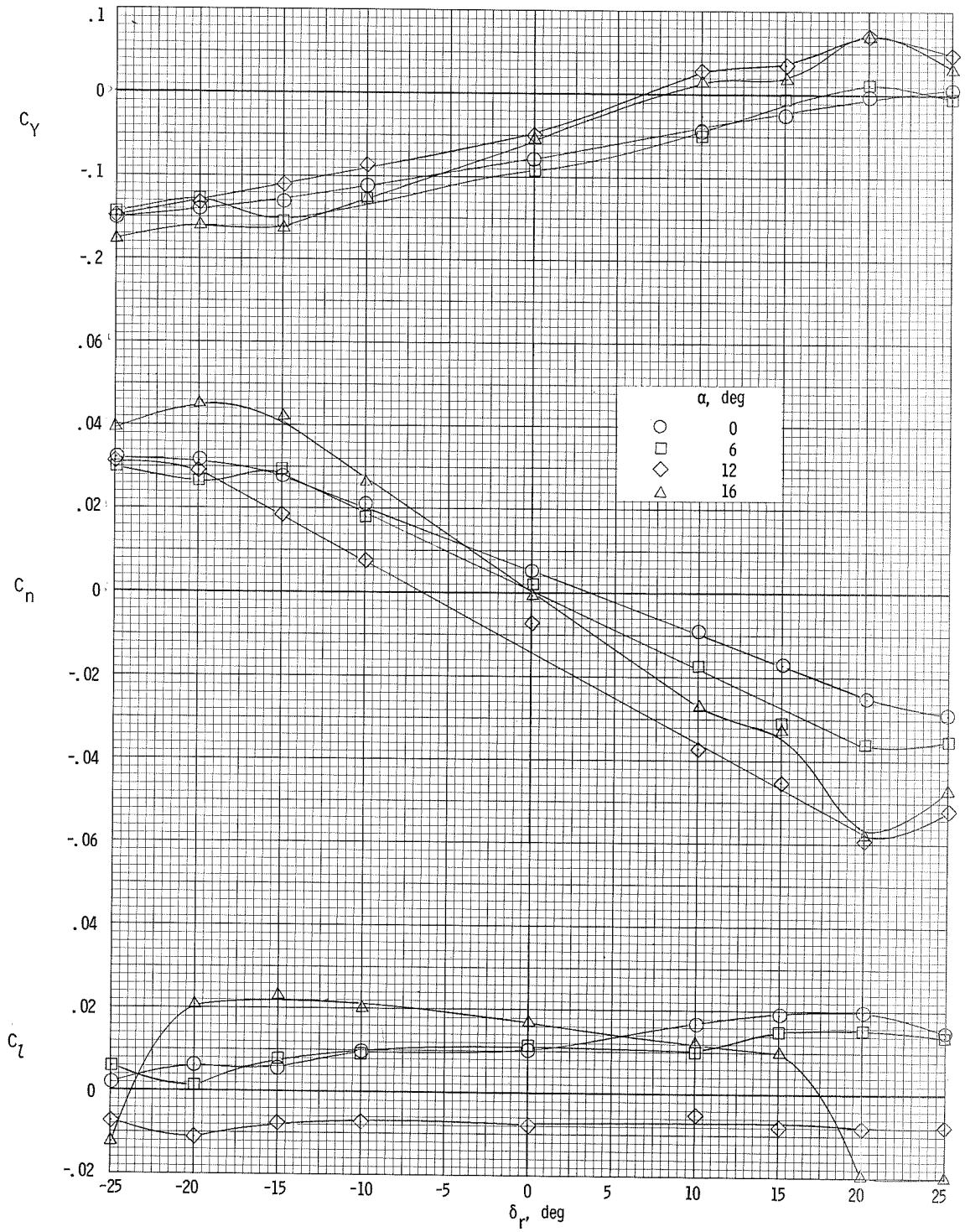


(b) $\beta = 4^{\circ}$.

Figure 27.- Continued.

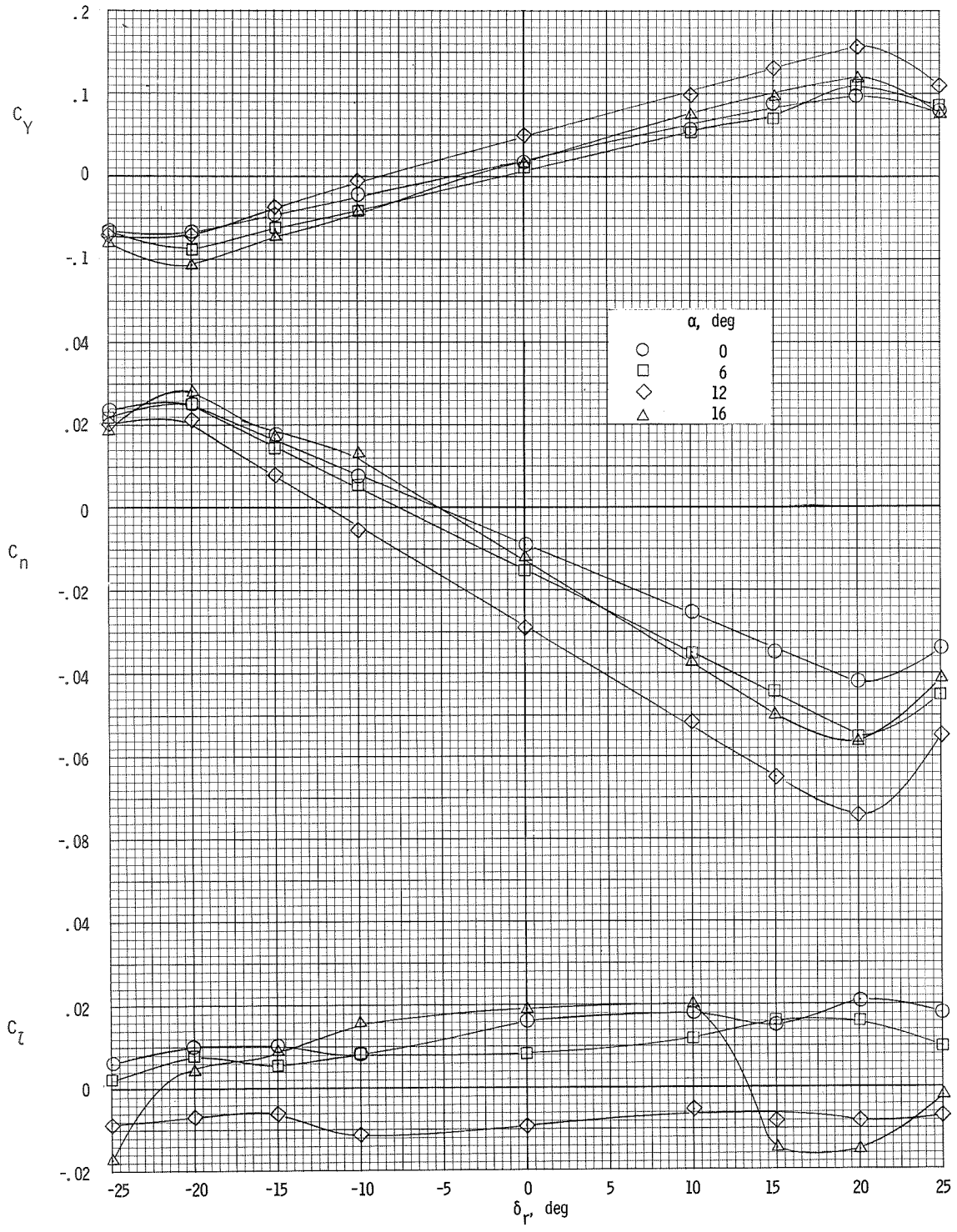


(c) $\beta = 0^0$.

Figure 27.- Continued.

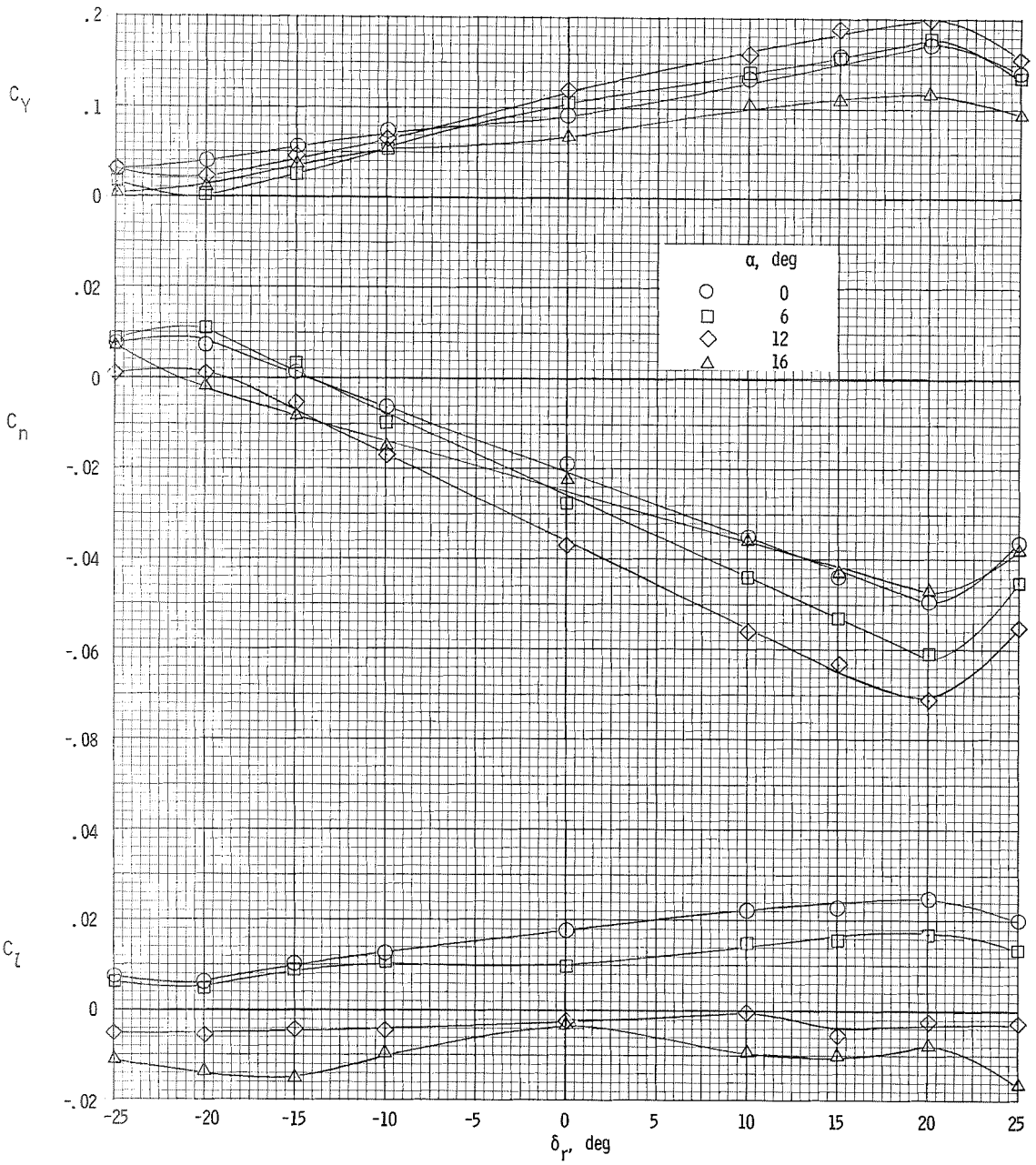


(d) $\beta = -4^0$.

Figure 27.- Continued.

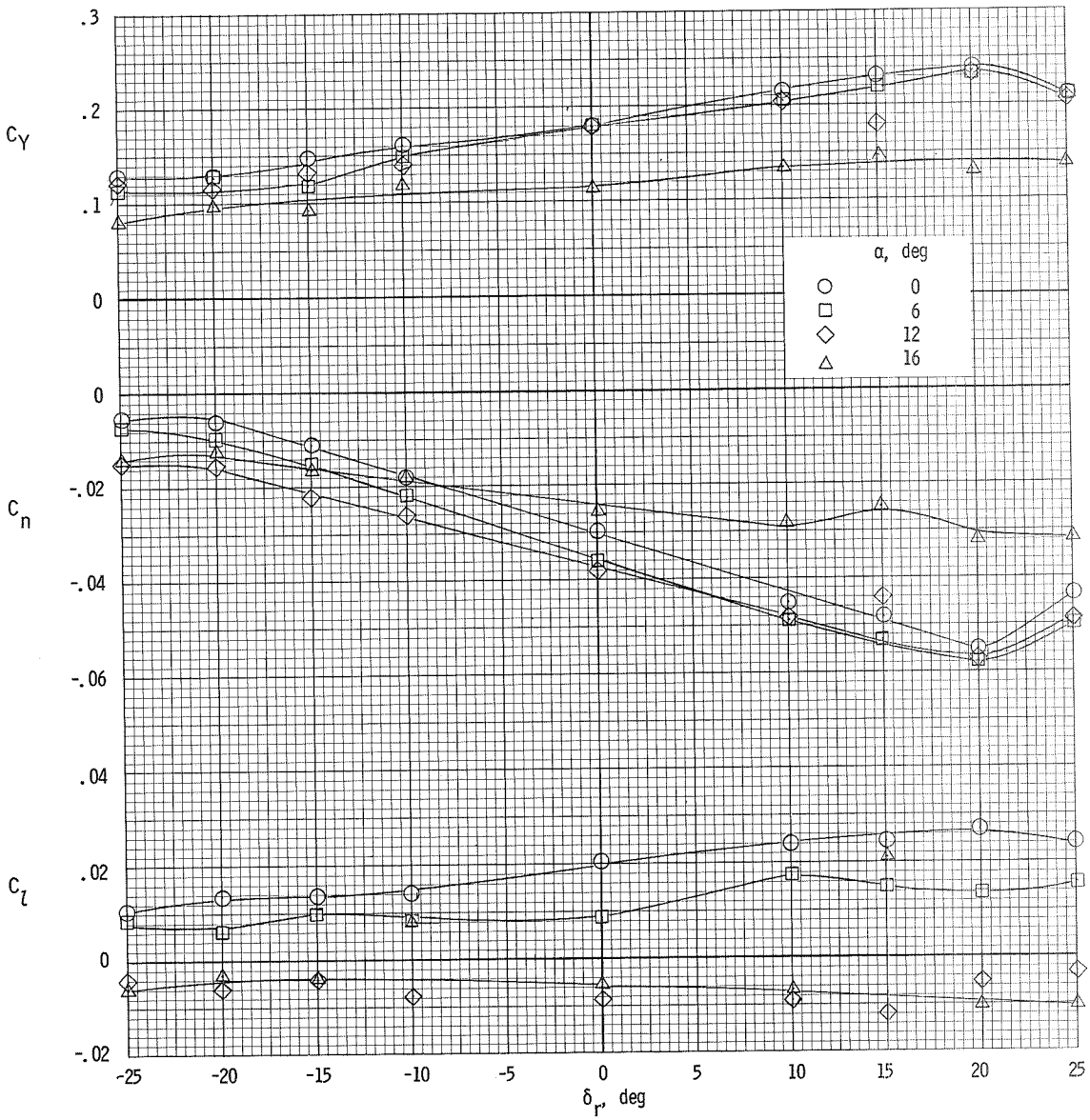


(e) $\beta = -8^{\circ}$.

Figure 27.- Concluded.

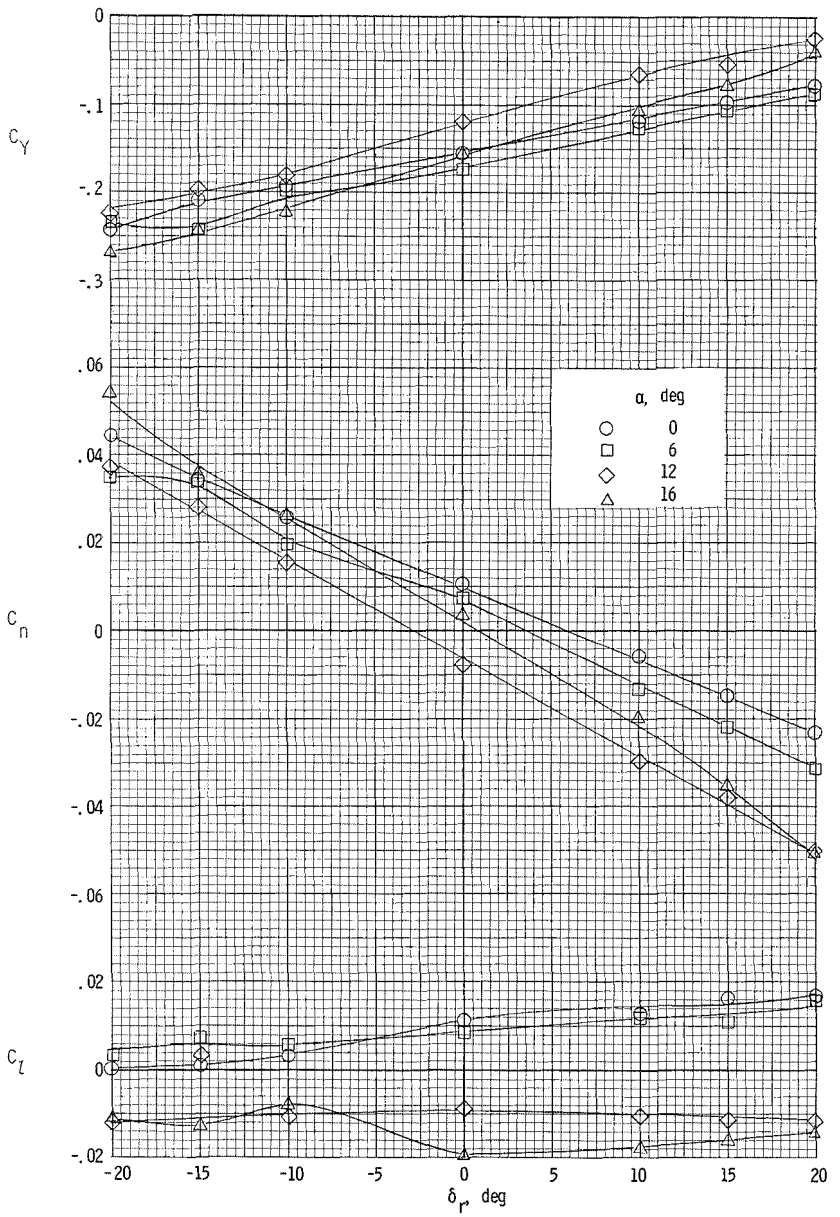


(a) $\beta = 8^0$.

Figure 28.- Variation of the lateral characteristics of the airplane with rudder deflection. $\delta_f = 32^0$; $T_C' = 0.55$.

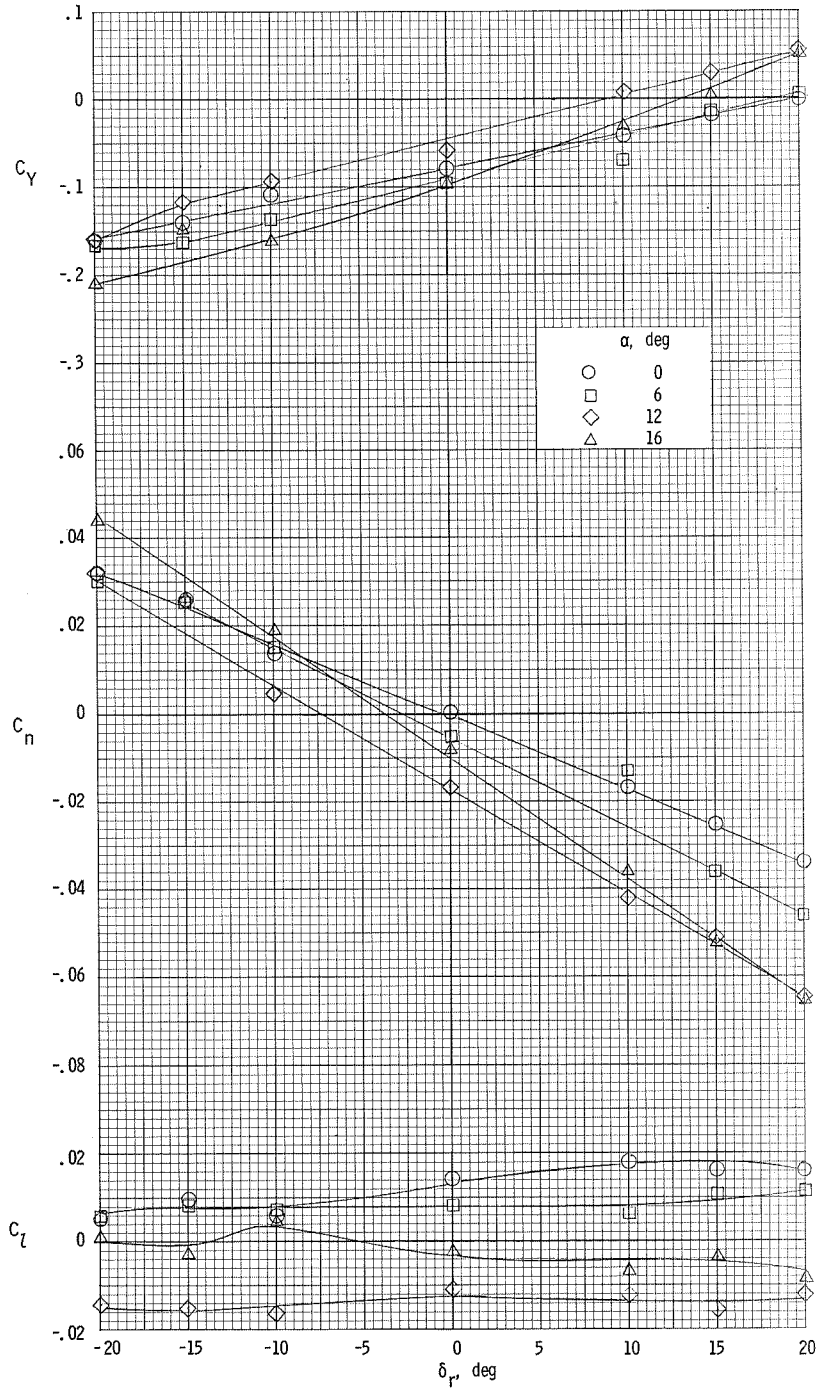


(b) $\beta = 4^o$.

Figure 28.- Continued.

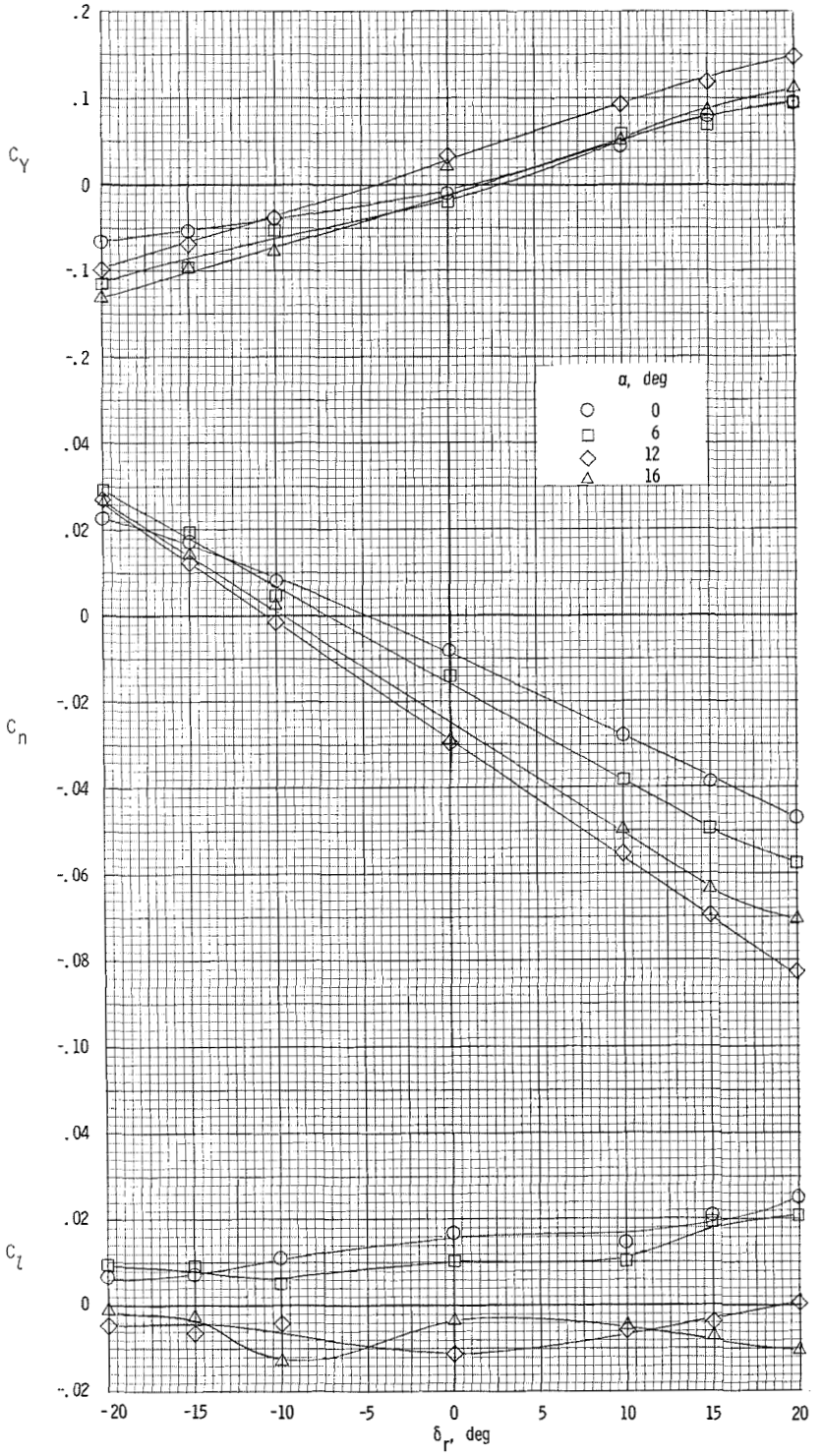


(c) $\beta = 0^0$.

Figure 28.- Continued.

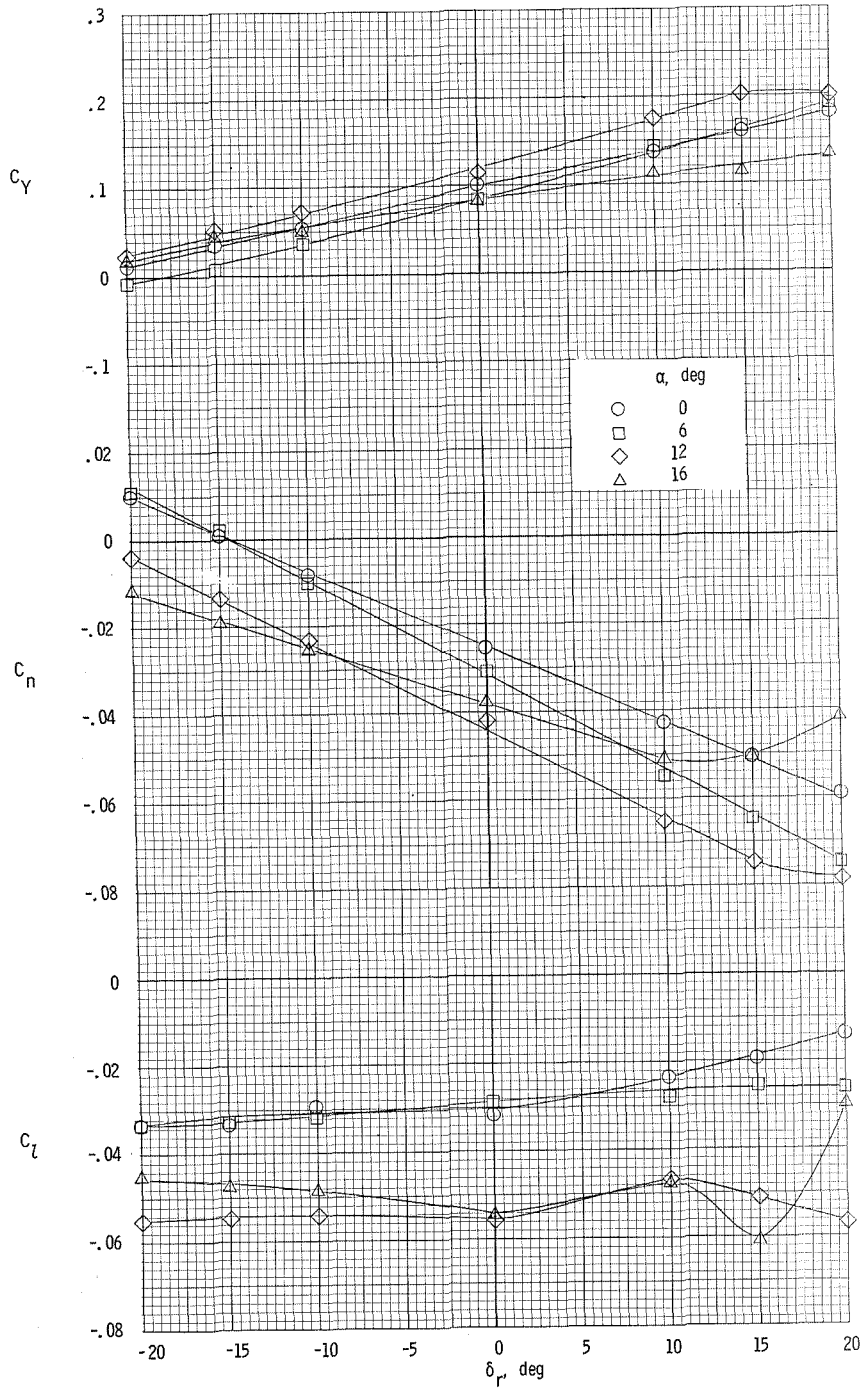


(d) $\beta = -4^0$.

Figure 28.- Continued.

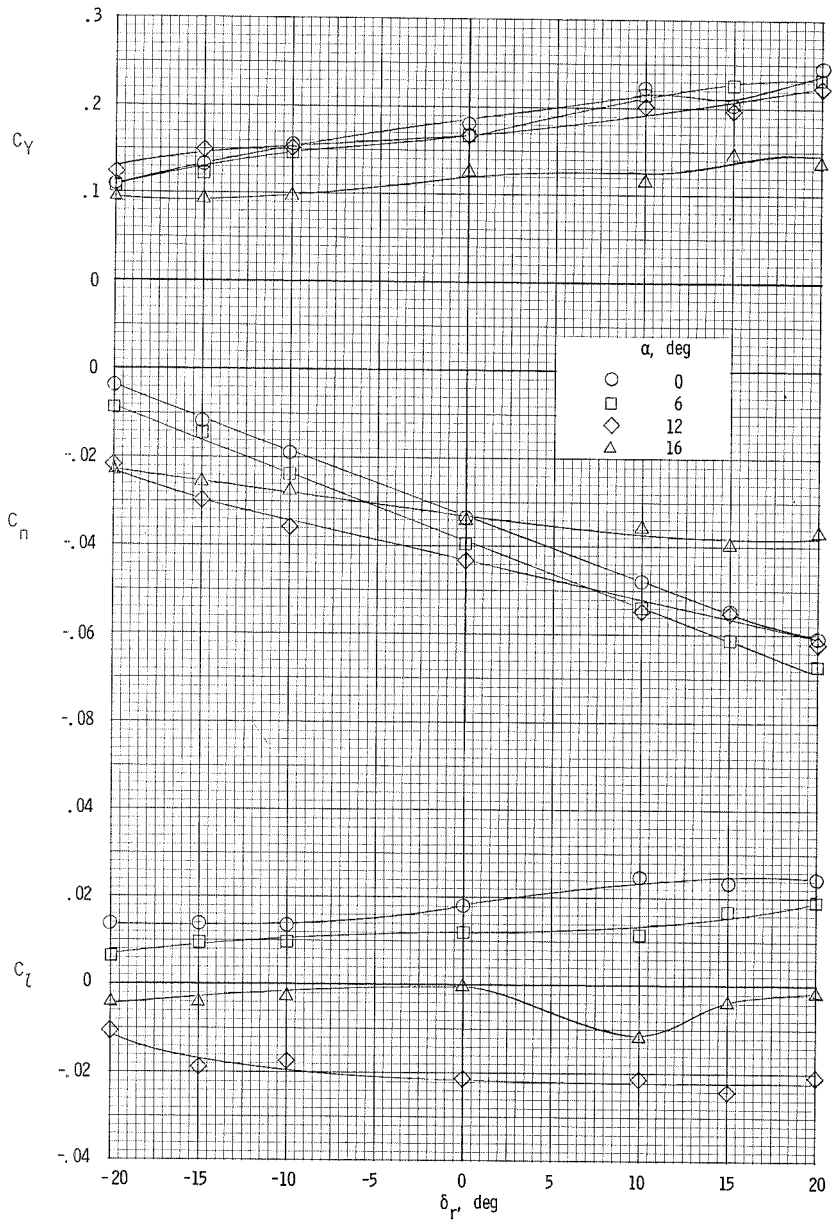


(e) $\beta = -8^{\circ}$.

Figure 28.- Concluded.

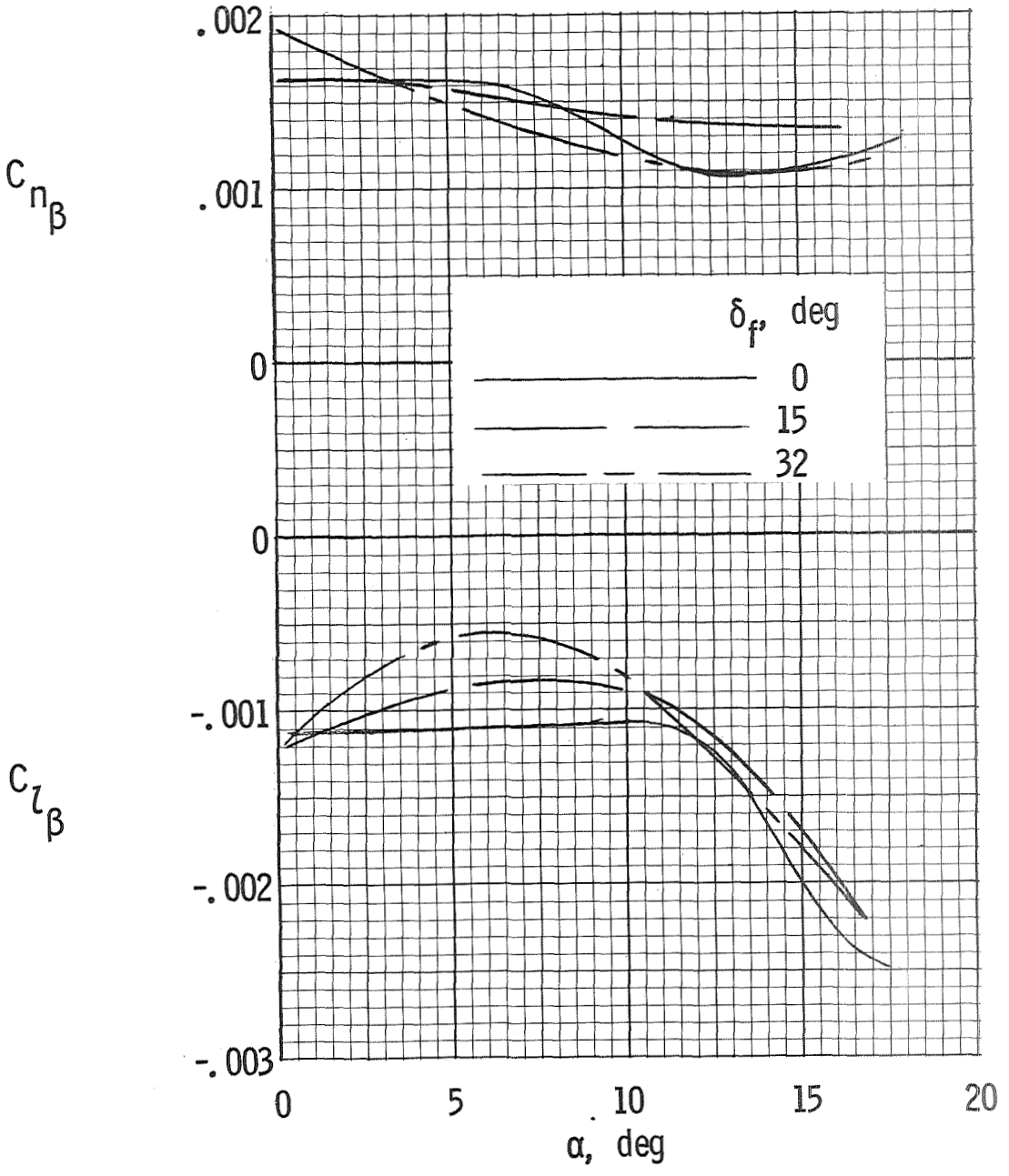


Figure 29.- Variation of effective dihedral and directional stability parameters with angle of attack. Propeller removed.

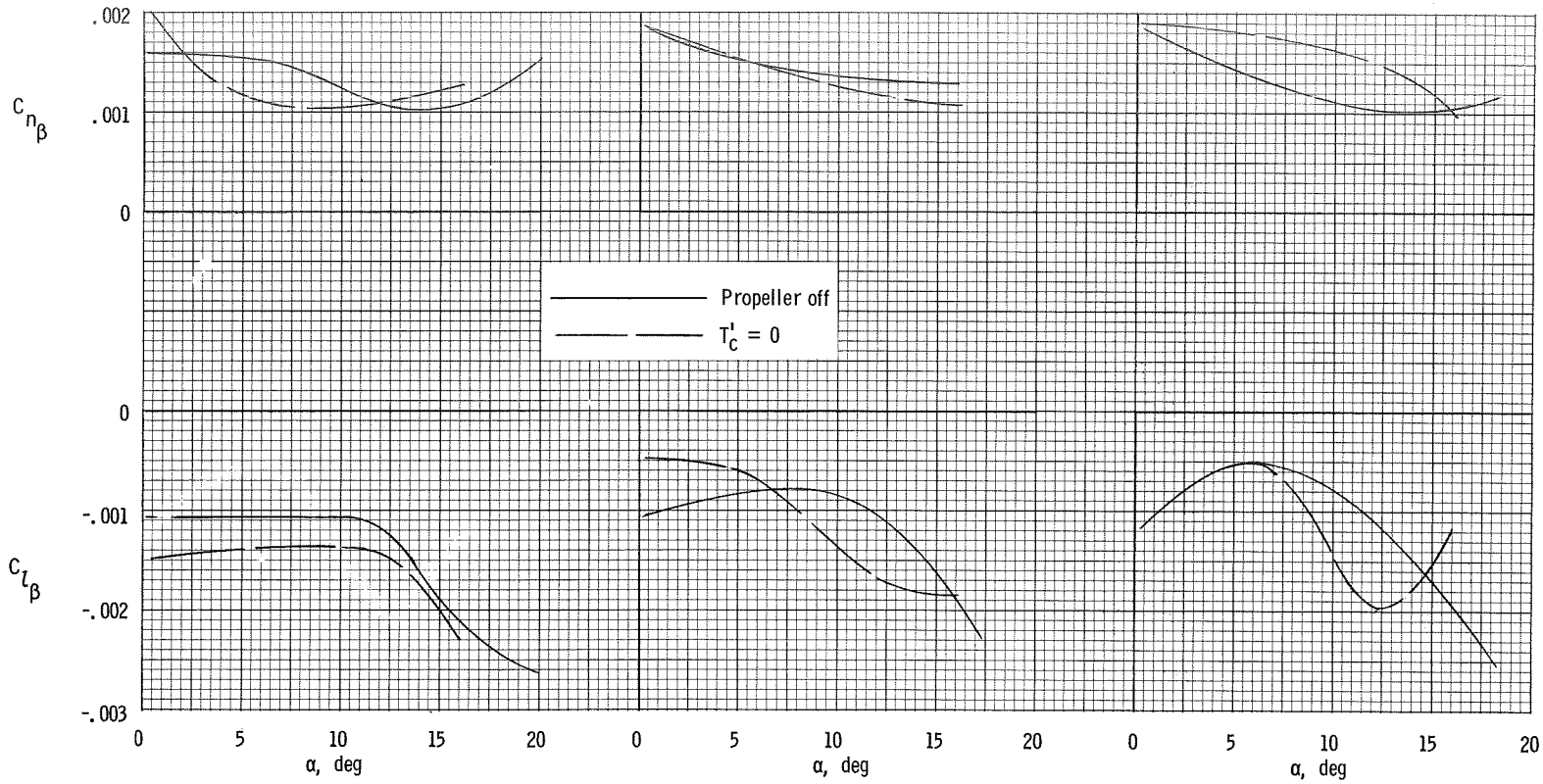


(a) $\delta_f = 0^0$. (b) $\delta_f = 15^0$. (c) $\delta_f = 32^0$.

Figure 30.- Comparison of the lateral characteristics of the airplane with propellers removed and zero thrust.

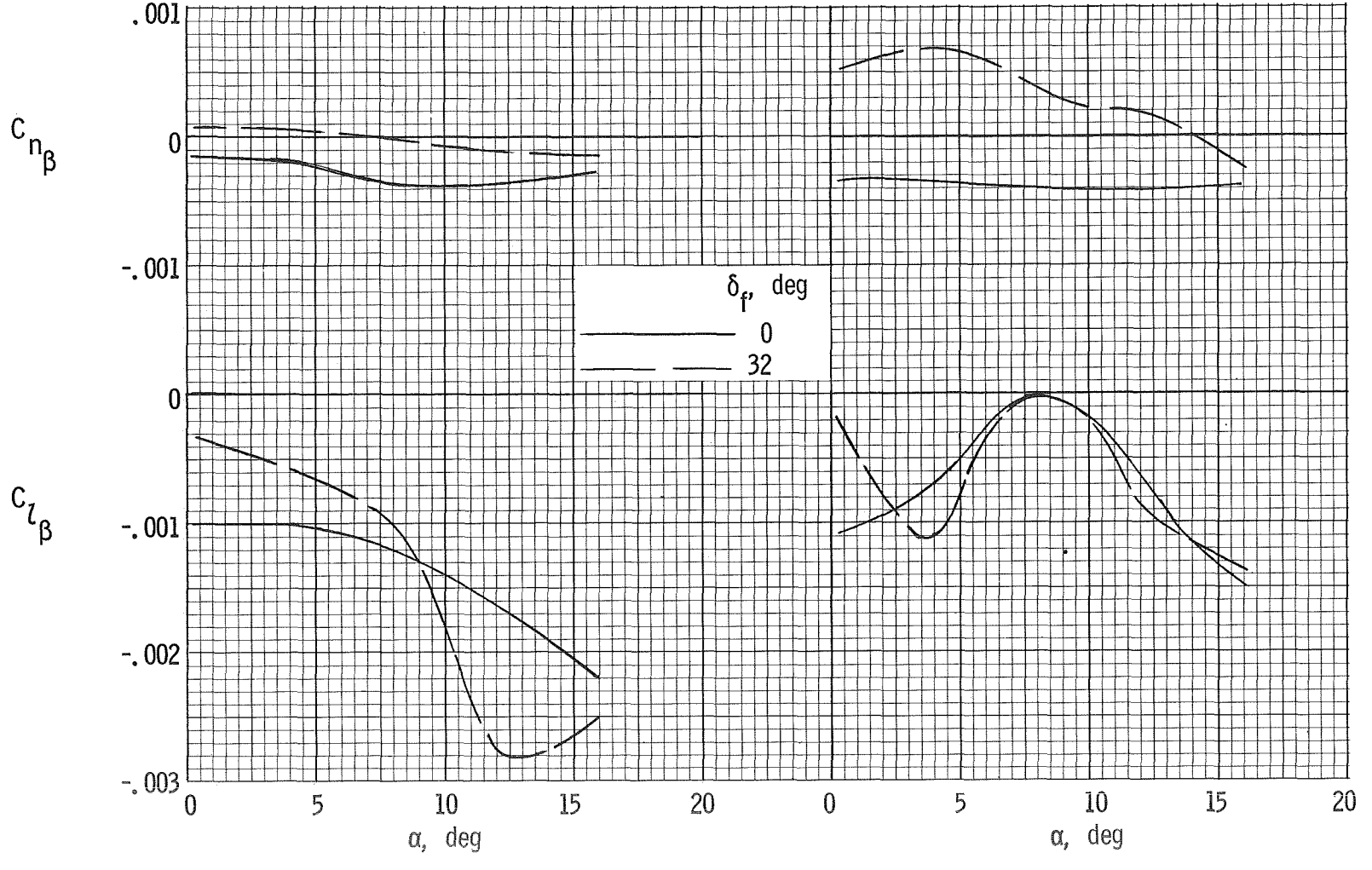


(a) $T_c' = 0.$

(b) $T_c' = 0.46.$

Figure 31.- Variation of effective dihedral and directional stability parameters with angle of attack with the vertical tail removed.

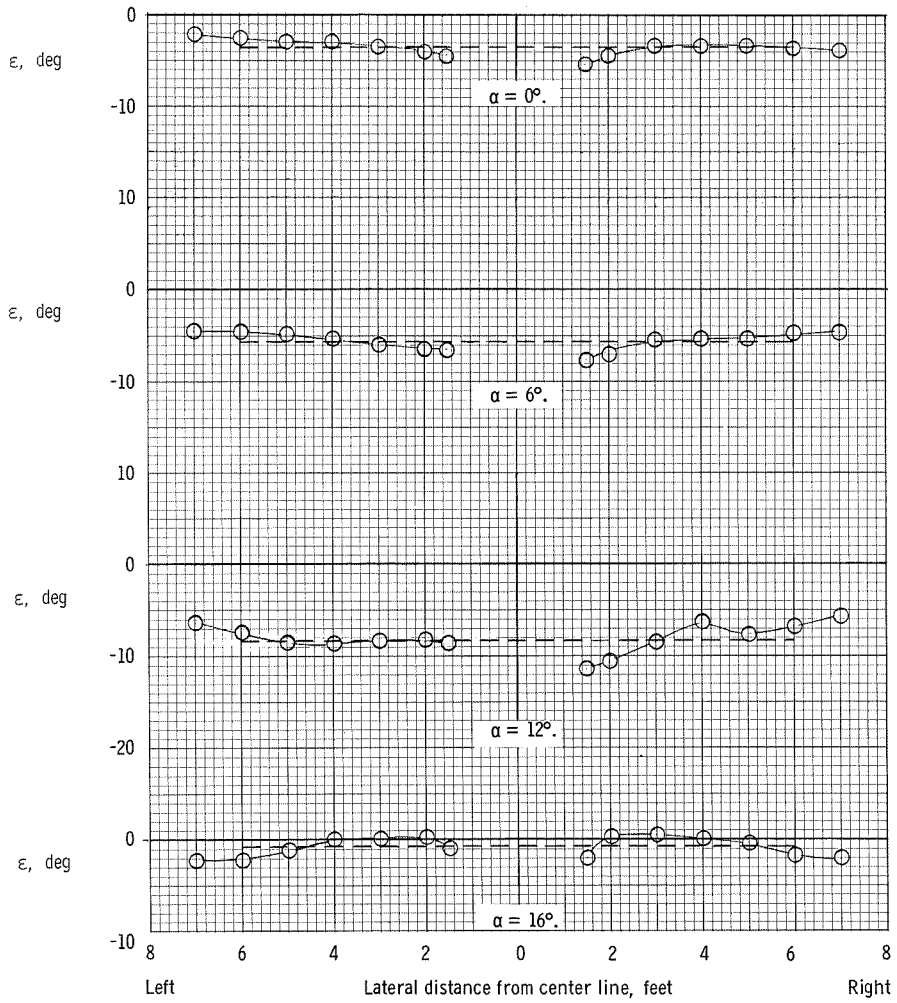


(a) $T_C' = 0$.

Figure 32.- Distribution of downwash across span of horizontal-tail surface. $\delta_f = 0^0$. Dashed lines are averages integrated over horizontal-tail span.

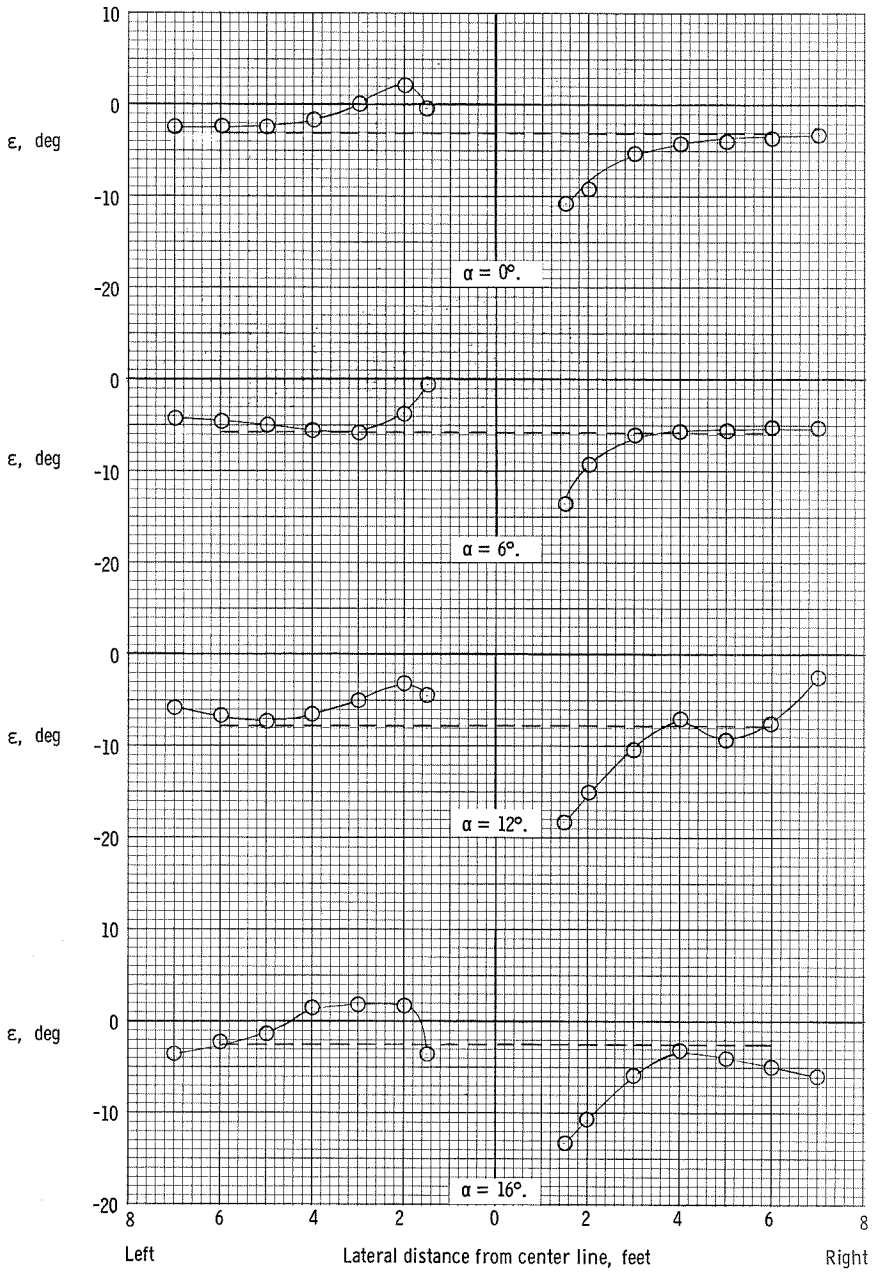


(b) $T_C' = 0.20$.

Figure 32.- Continued.

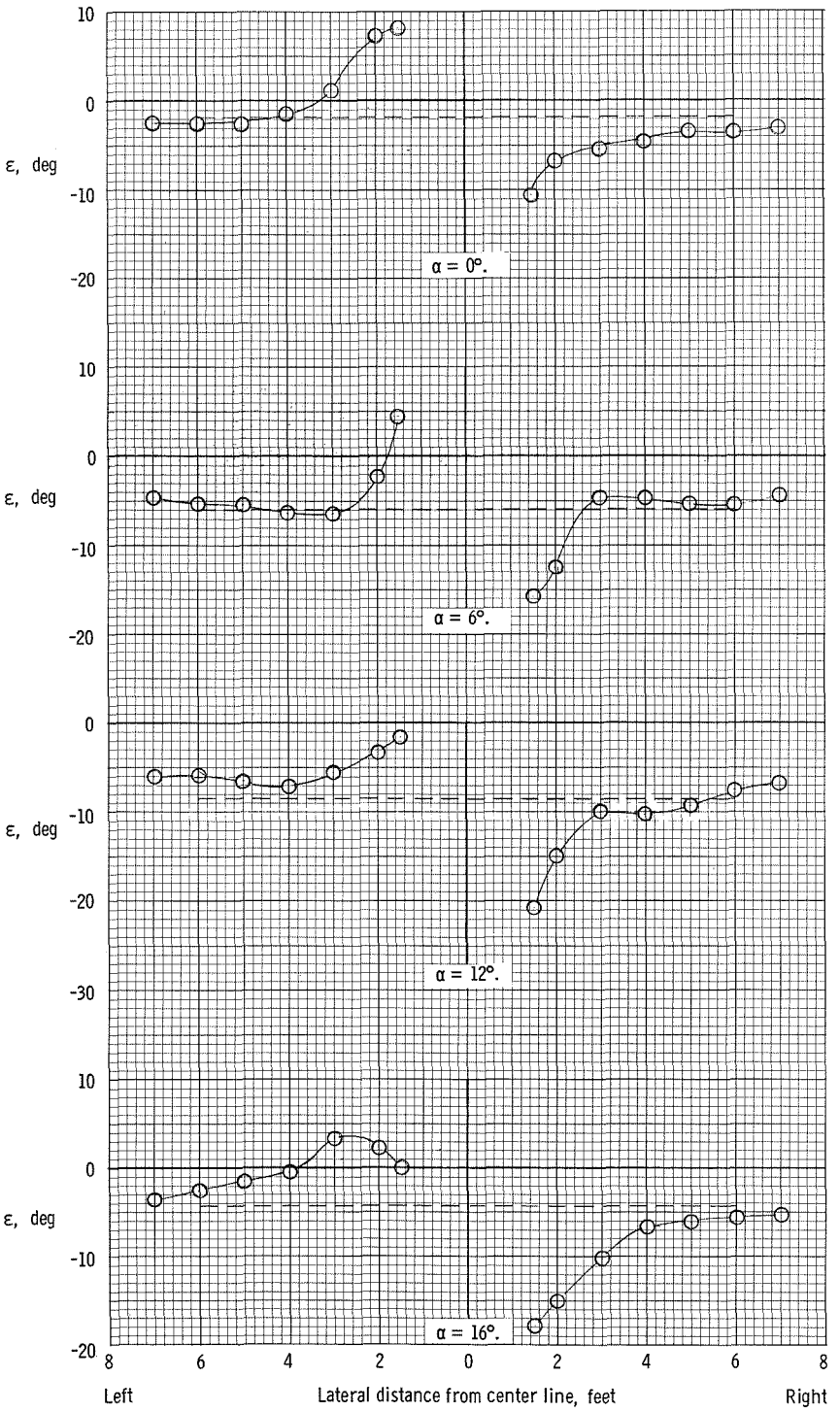


(c) $T_C' = 0.46$.

Figure 32.- Concluded.

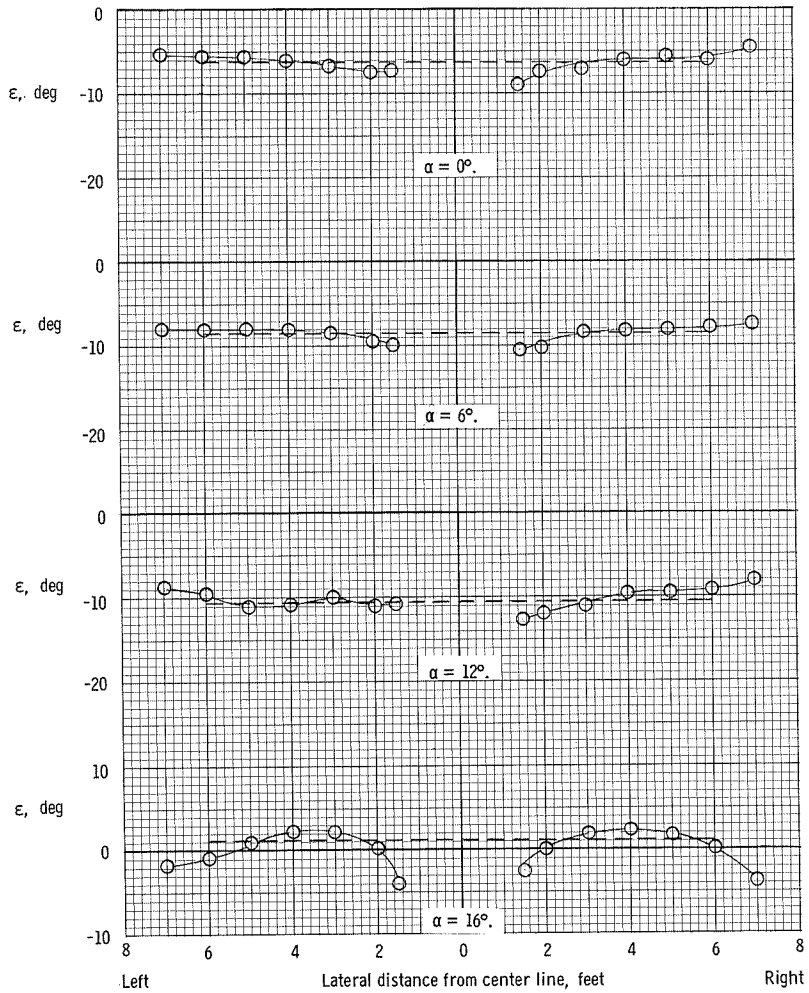


(a) $T_C' = 0$.

Figure 33.- Distribution of downwash across span of horizontal-tail surface. $\delta_f = 15^0$. Dashed lines are averages integrated over horizontal-tail span.

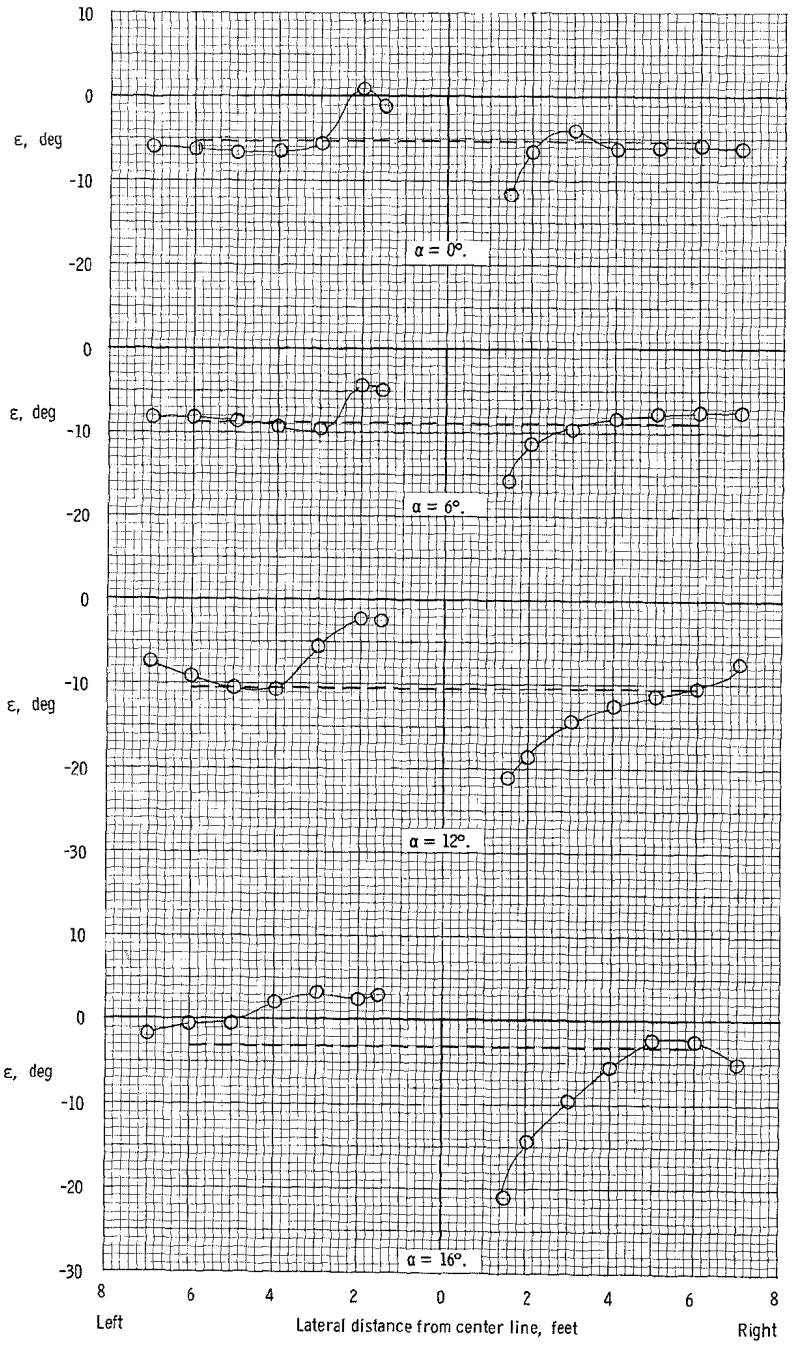


(b) $T_c' = 0.20$.

Figure 33.- Continued.

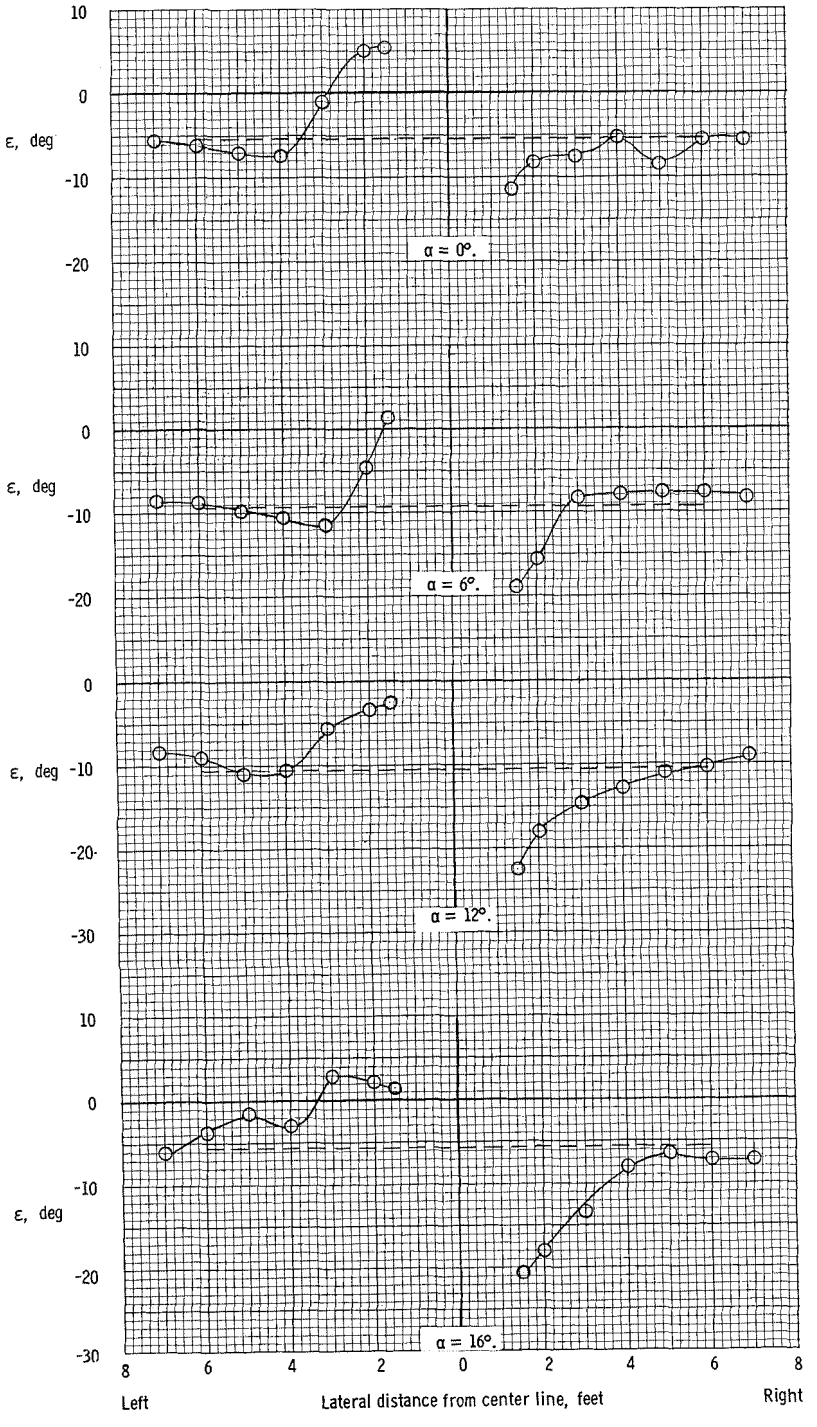


(c) $T_C' = 0.46$.

Figure 33.- Concluded.

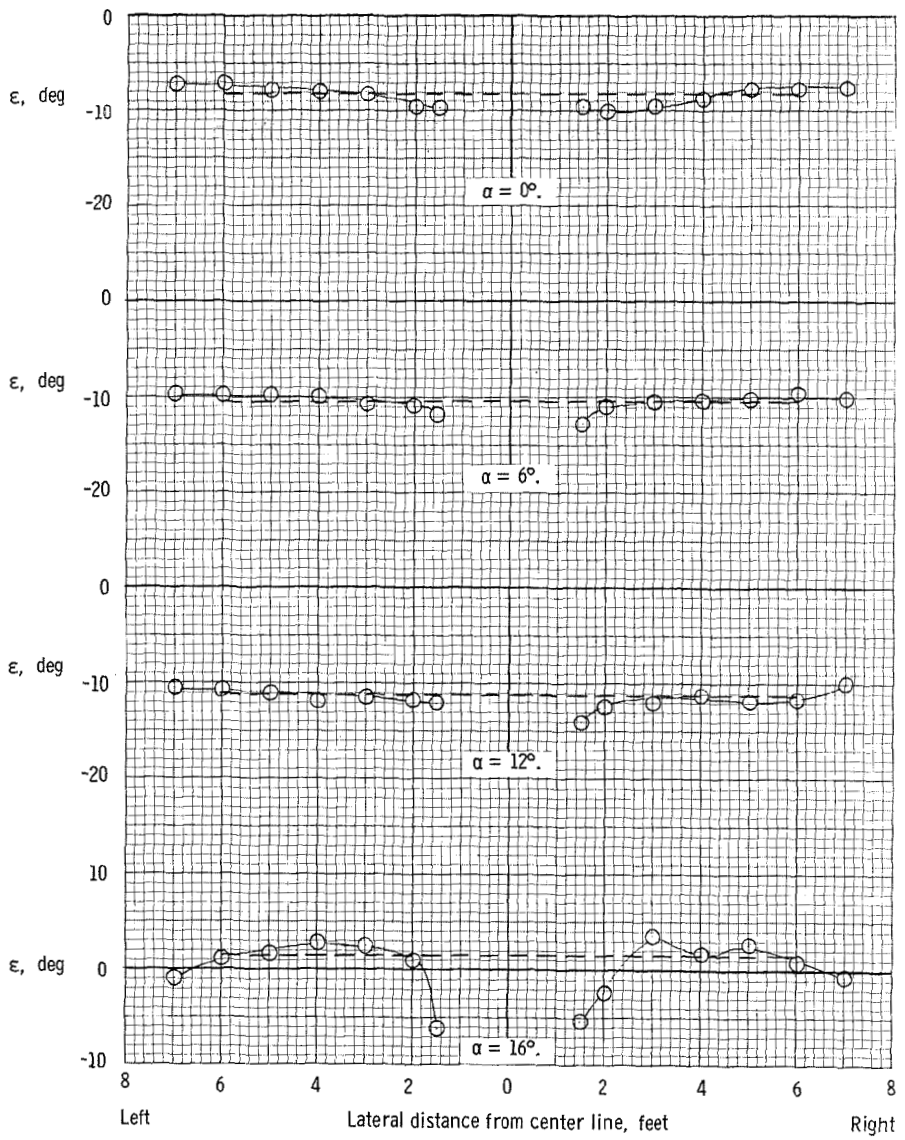


(a) $T_C' = 0$.

Figure 34.- Distribution of downwash across span of horizontal-tail surface. $\delta_f = 32^o$. Dashed lines are averages integrated over horizontal-tail span.

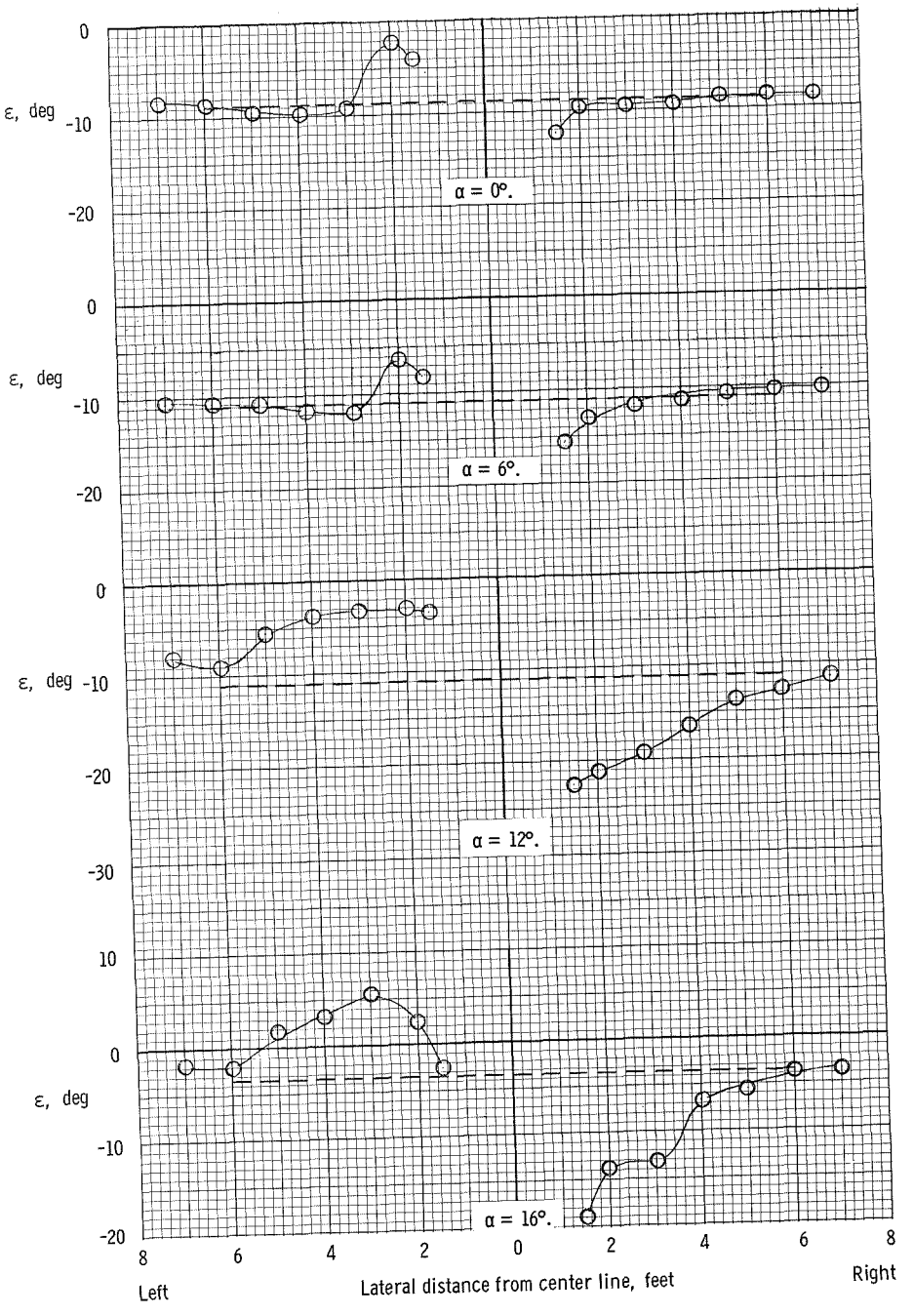


(b) $T_C' = 0.20$.

Figure 34.- Continued.

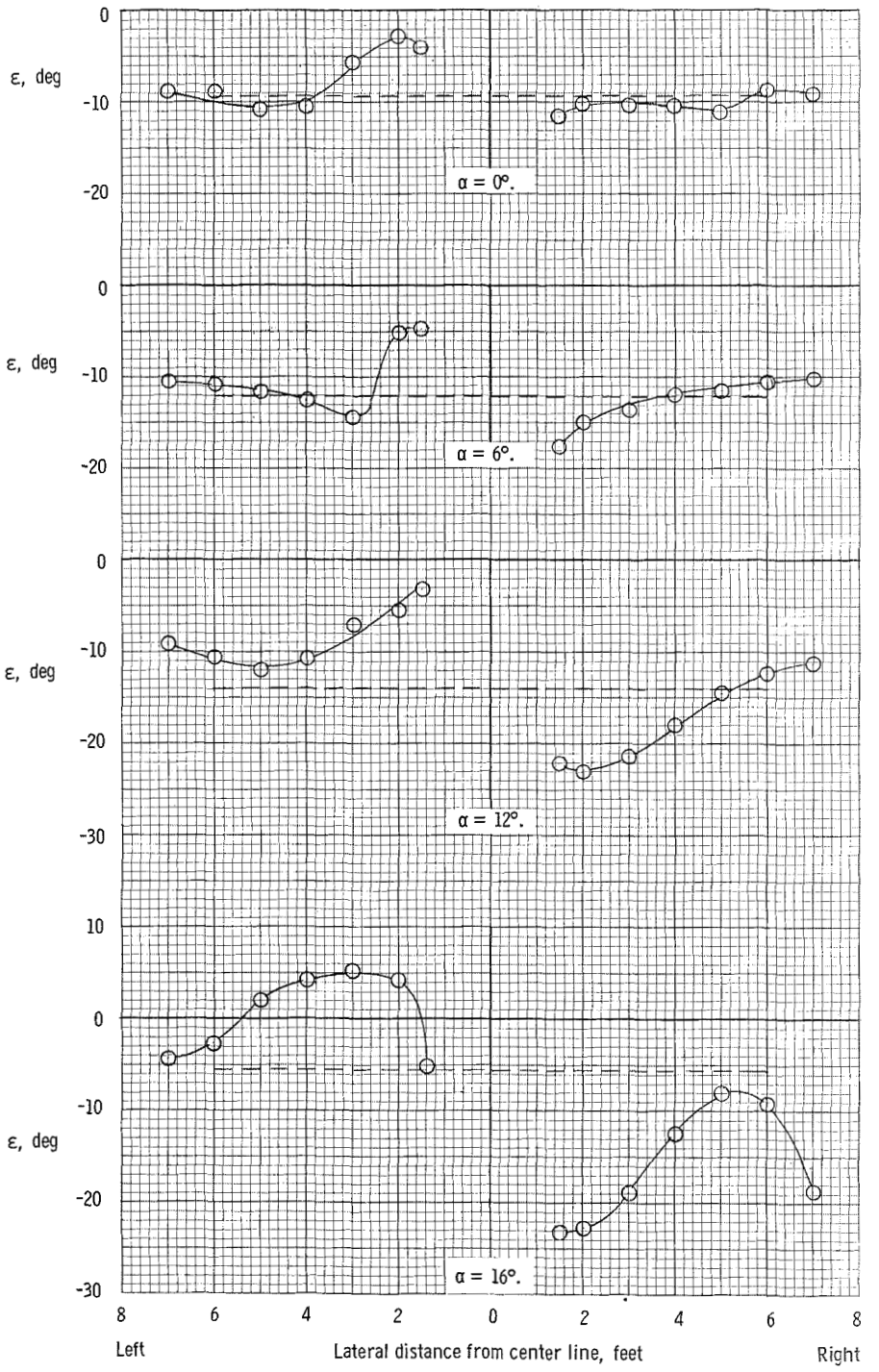


(c) $T_C' = 0.46$.

*Figure 34.- Concluded.*

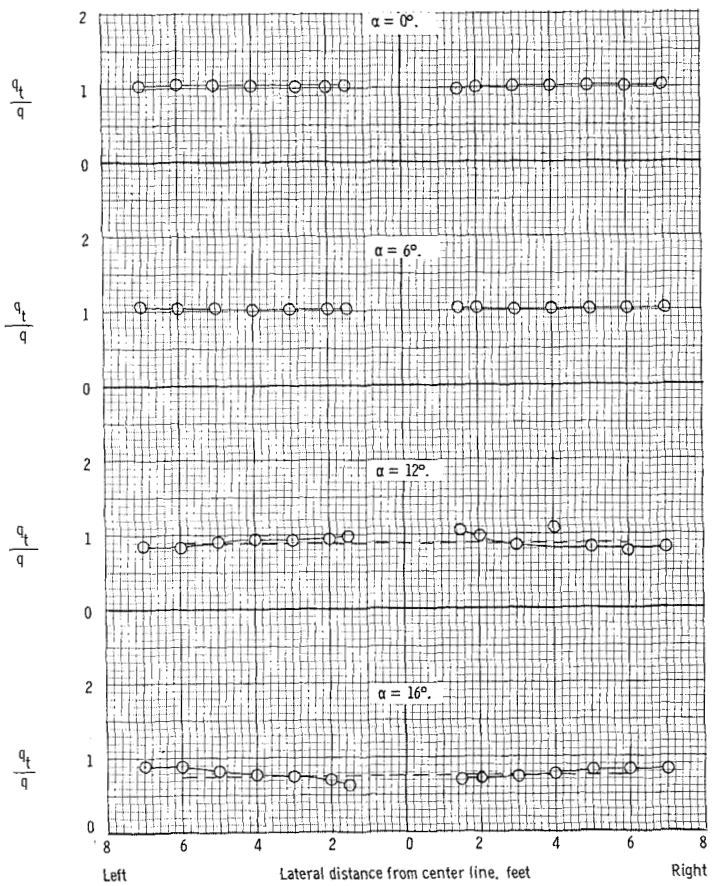


(a) $T_c' = 0.$

Figure 35.- Distribution of dynamic pressure across span of horizontal-tail surface. $\delta_f = 0^0$. Dashed lines are averages integrated over horizontal-tail span.

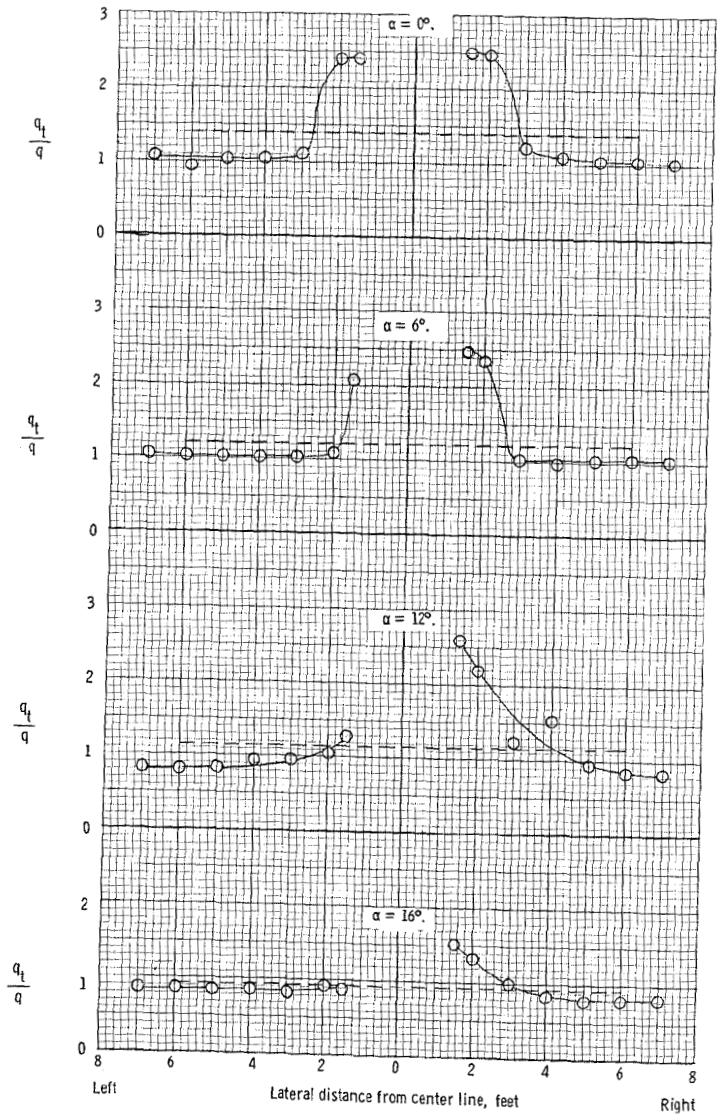


(b) $T_c' = 0.20$.

Figure 35.- Continued.

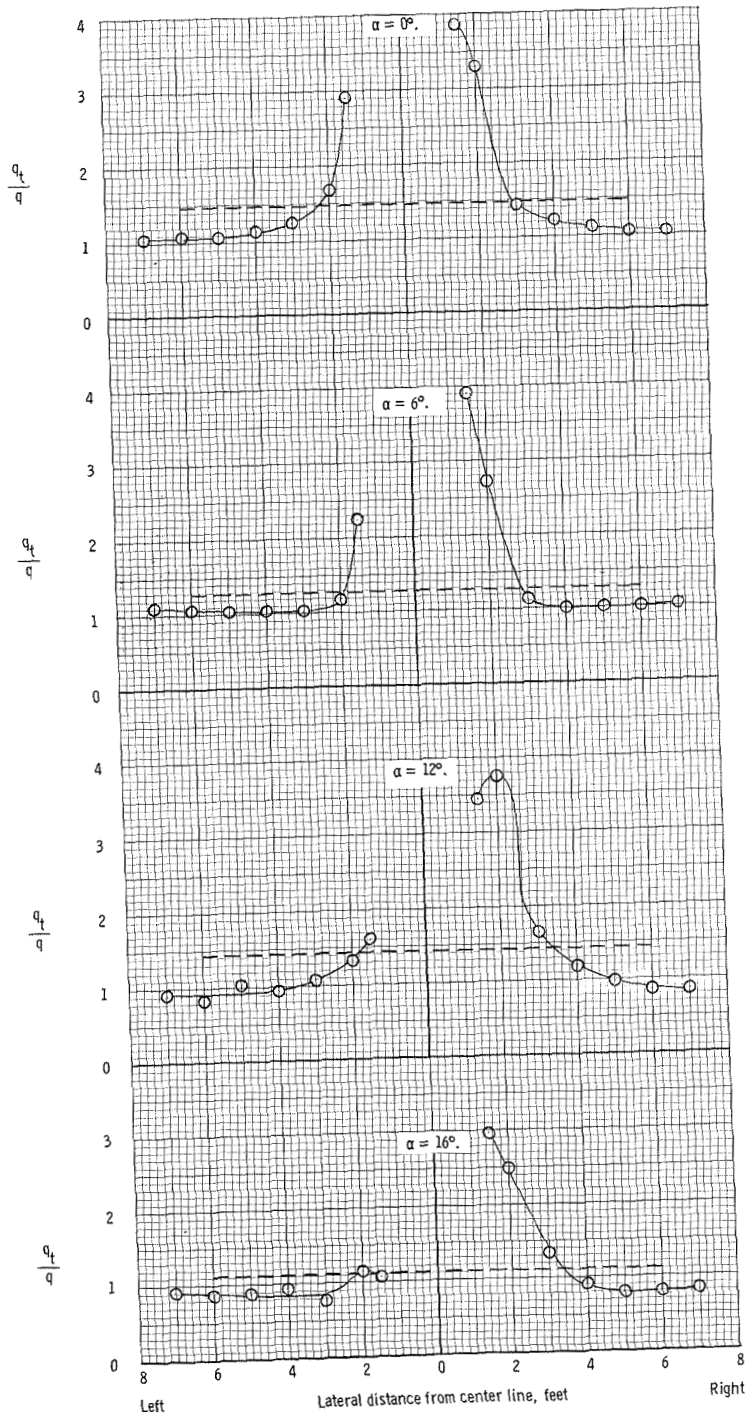


(c) $T_C' = 0.46$.

Figure 35.- Concluded.

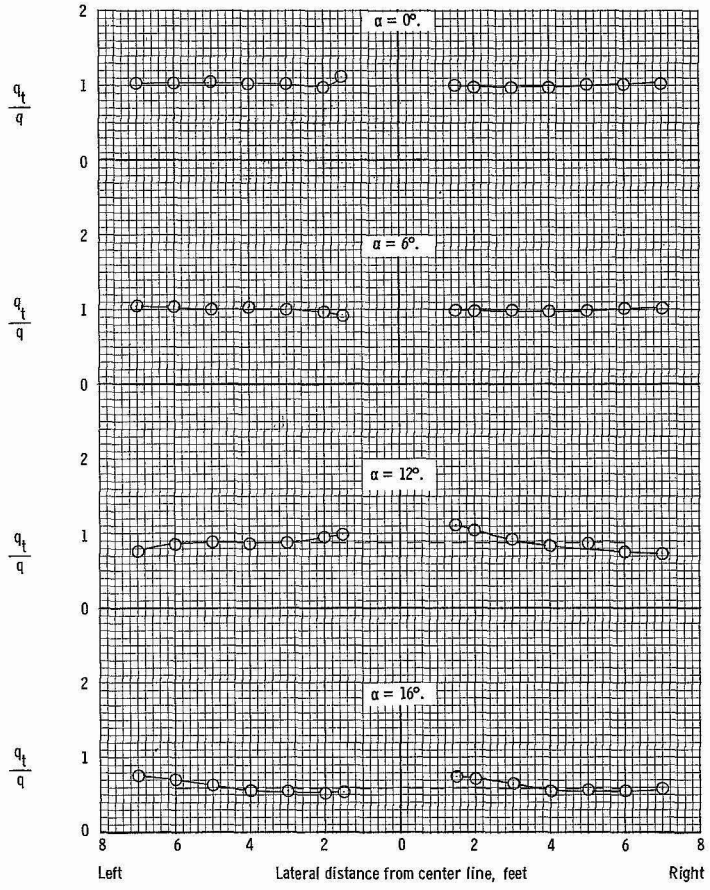


(a) $T_c' = 0$.

Figure 36.- Distribution of dynamic pressure across span of horizontal-tail surface. $\delta_f = 15^0$. Dashed lines are averages integrated over span of horizontal tail.

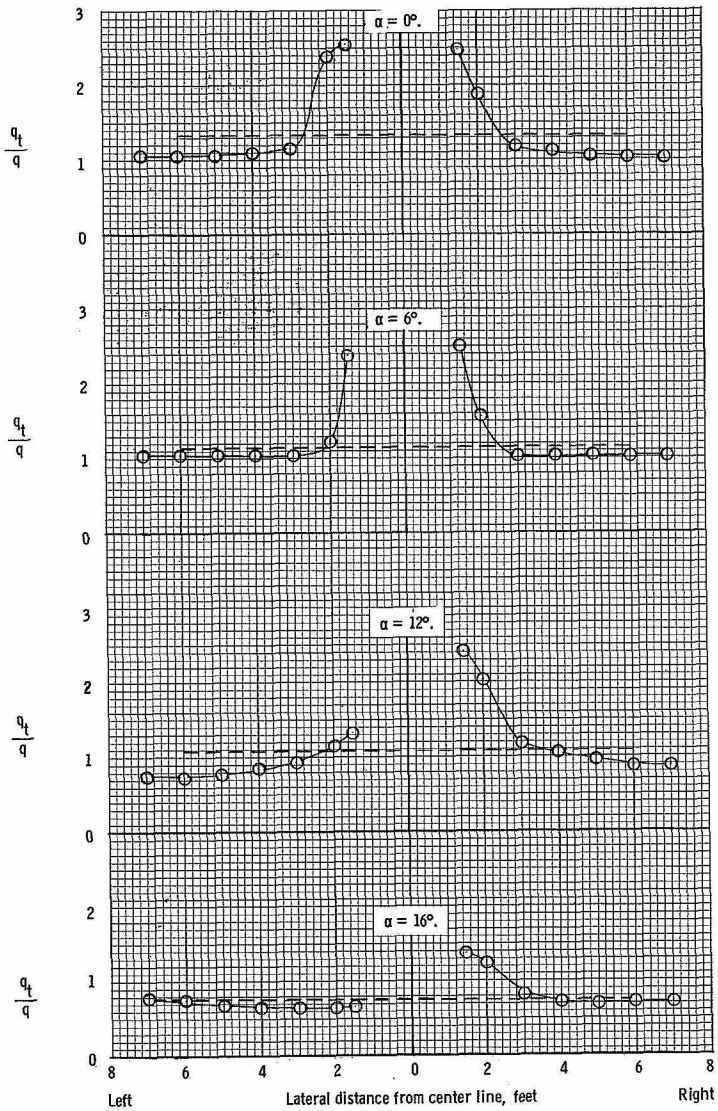


(b) $T_C' = 0.20$.

Figure 36.- Continued.

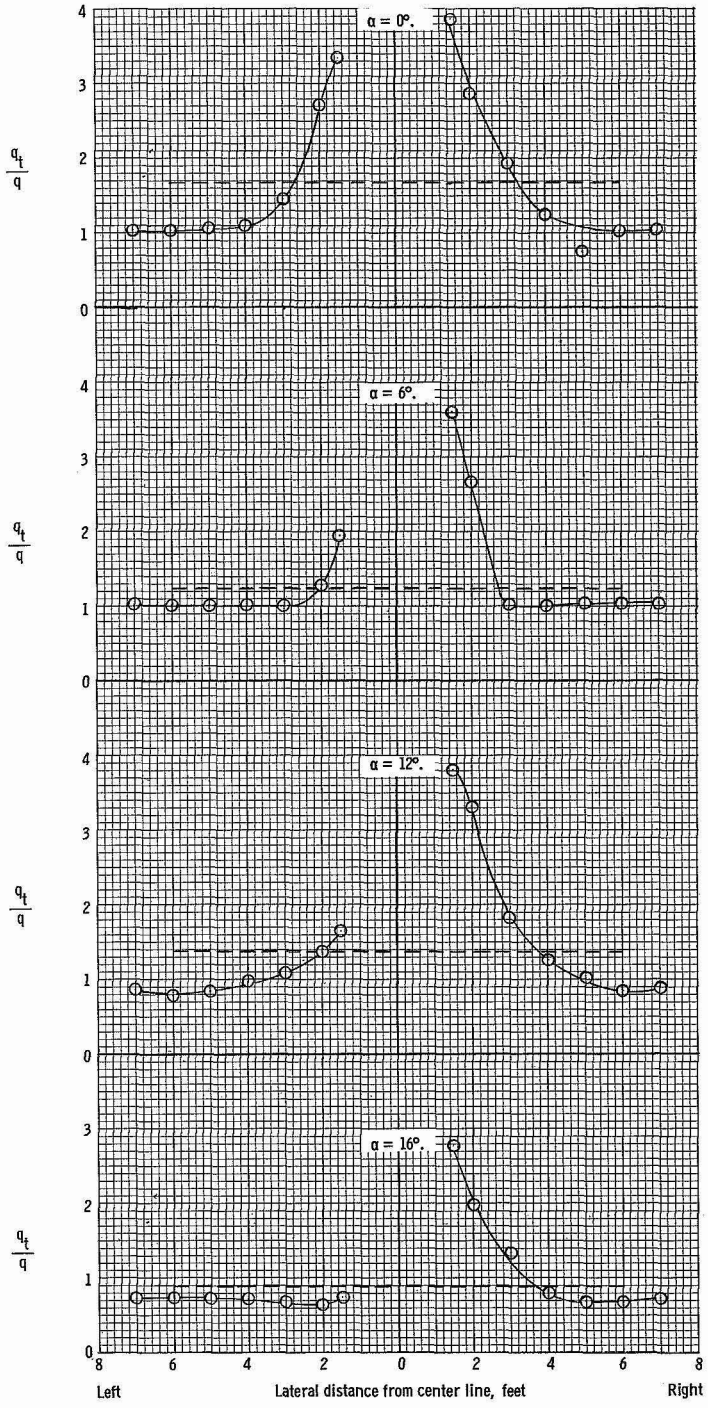


(c) $T_c' = 0.46$.

Figure 36.- Concluded.

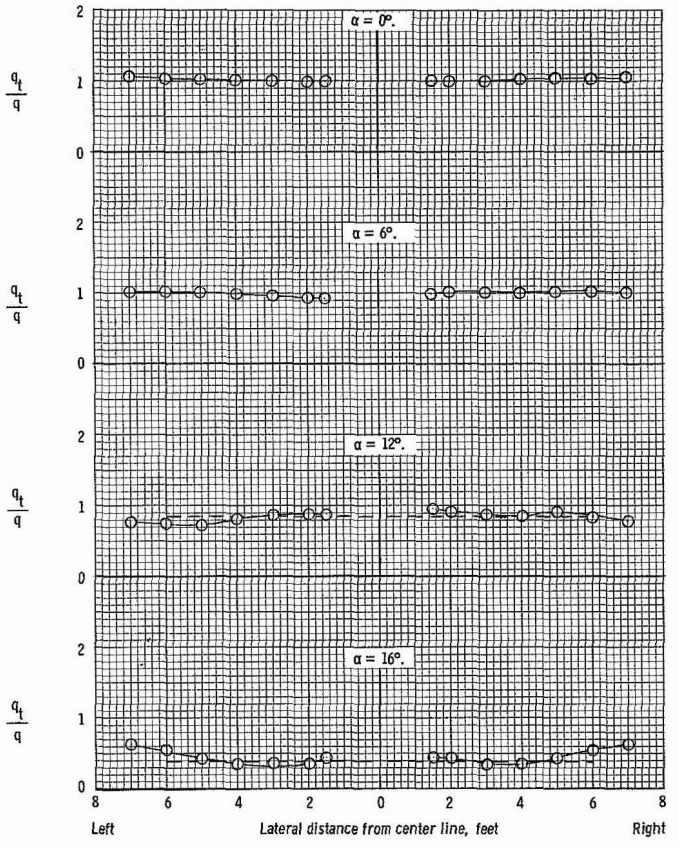


(a) $T_C' = 0$.

Figure 37.- Distribution of dynamic pressure across span of horizontal-tail surface. $\delta_f = 32^0$. Dashed lines are averages integrated over span of horizontal tail.

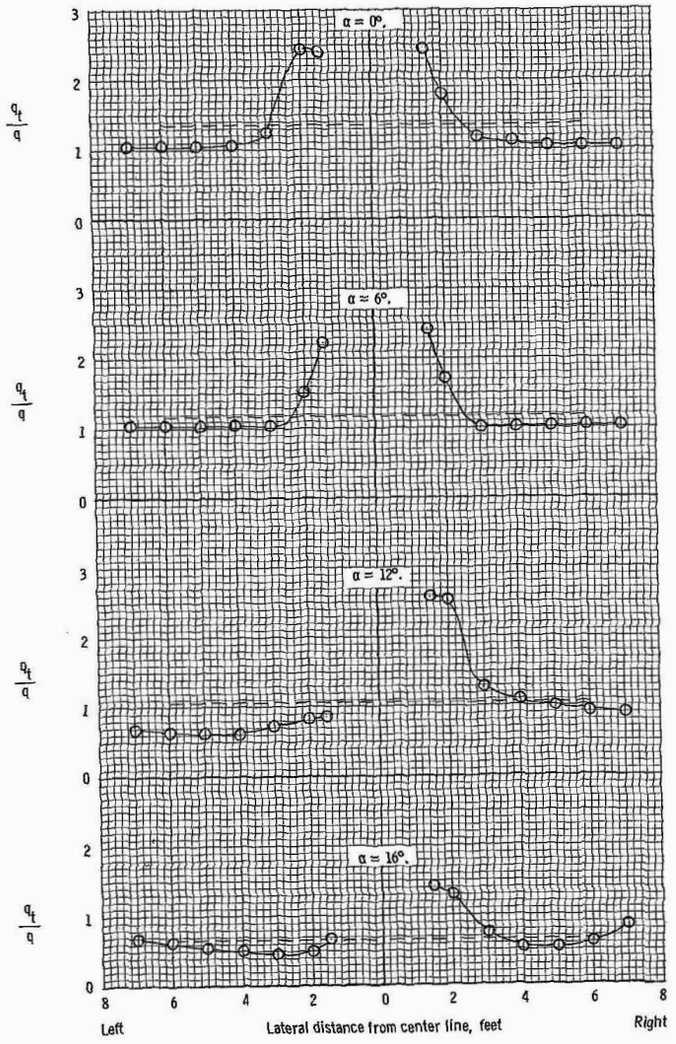


(b) $T_C' = 0.20$.

Figure 37.- Continued.

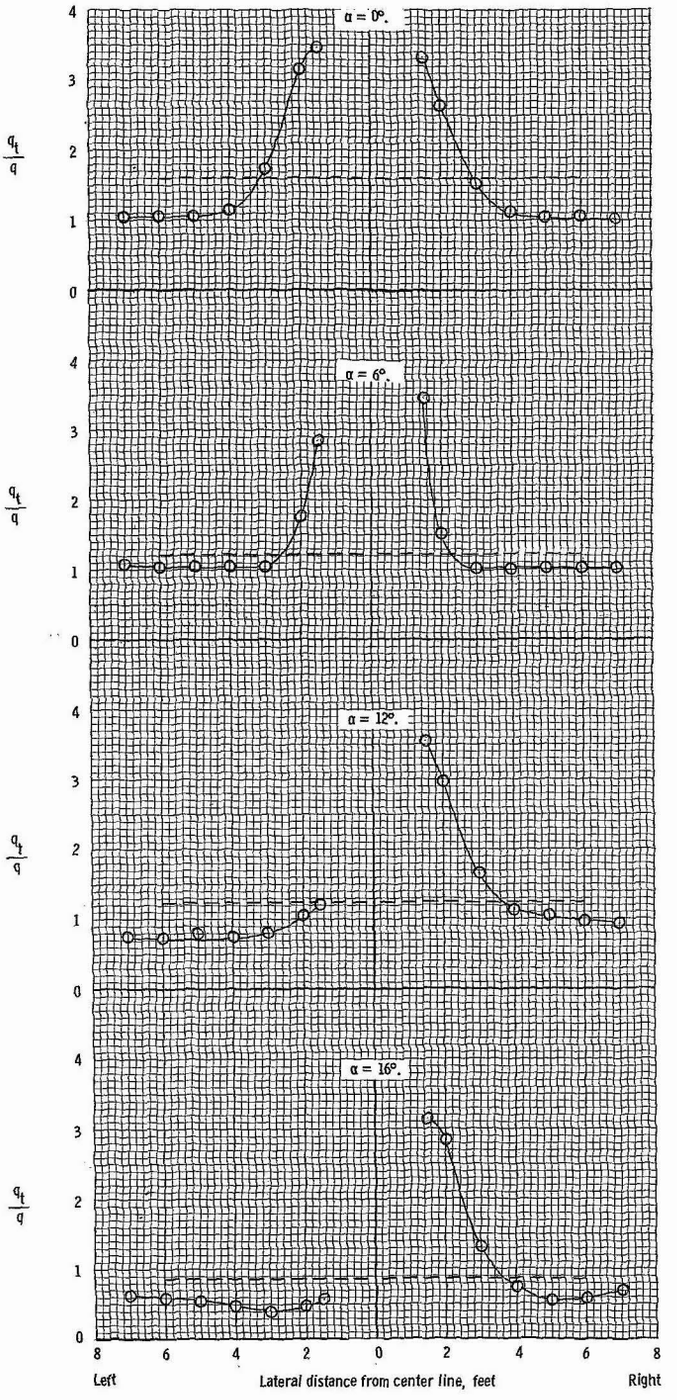


(c) $T_c' = 0.46$.

Figure 37.- Concluded.

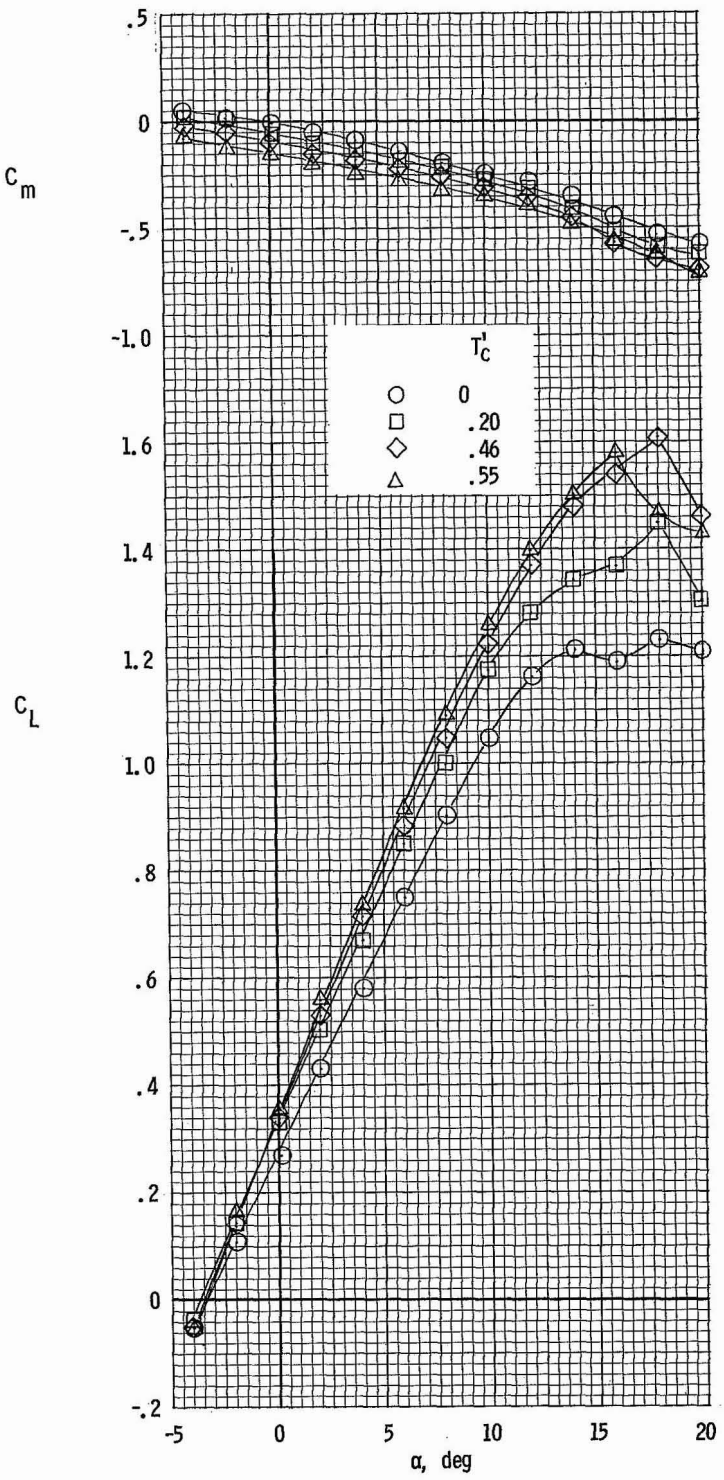


(a) $\delta_f = 0^0$.

Figure 38.- Effect of power on longitudinal characteristics. $\beta = 0^0$.

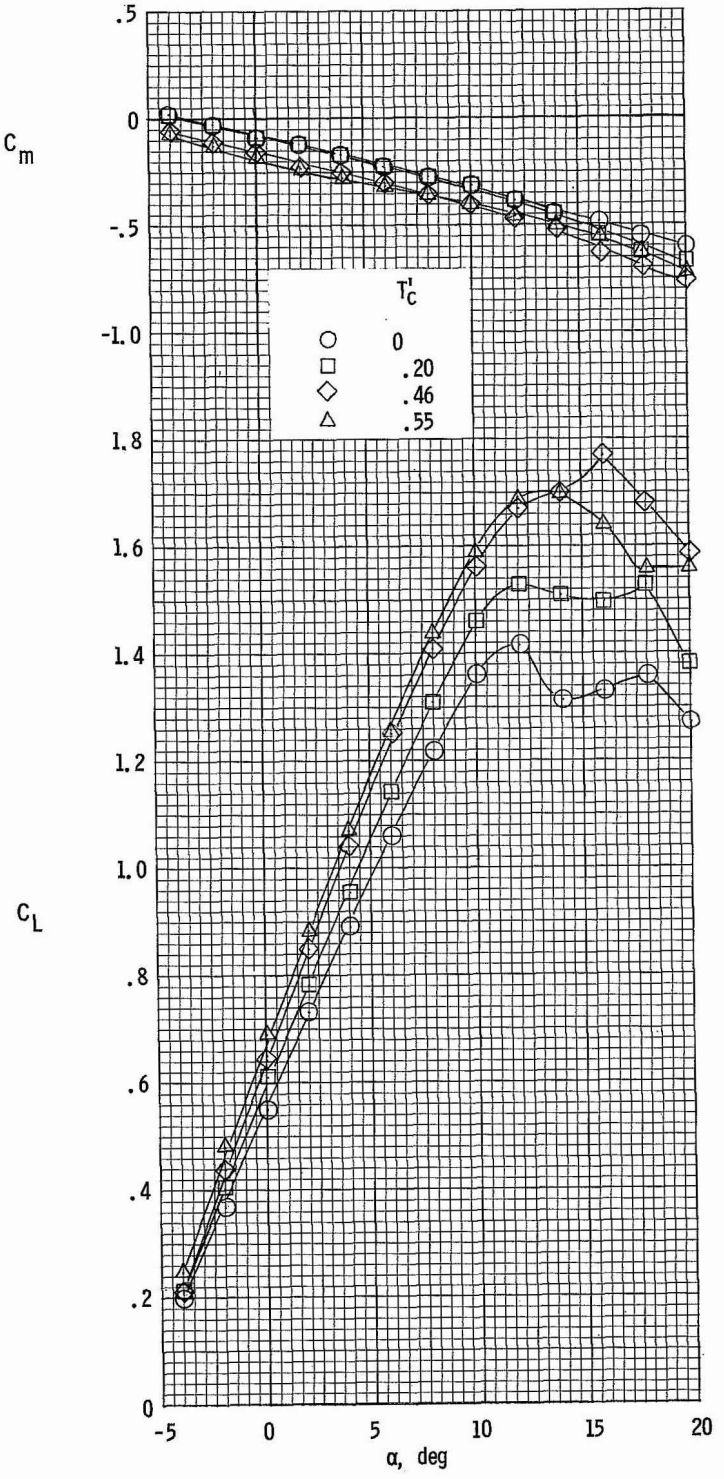


(b) $\delta_f = 15^o$.

Figure 38.- Continued.

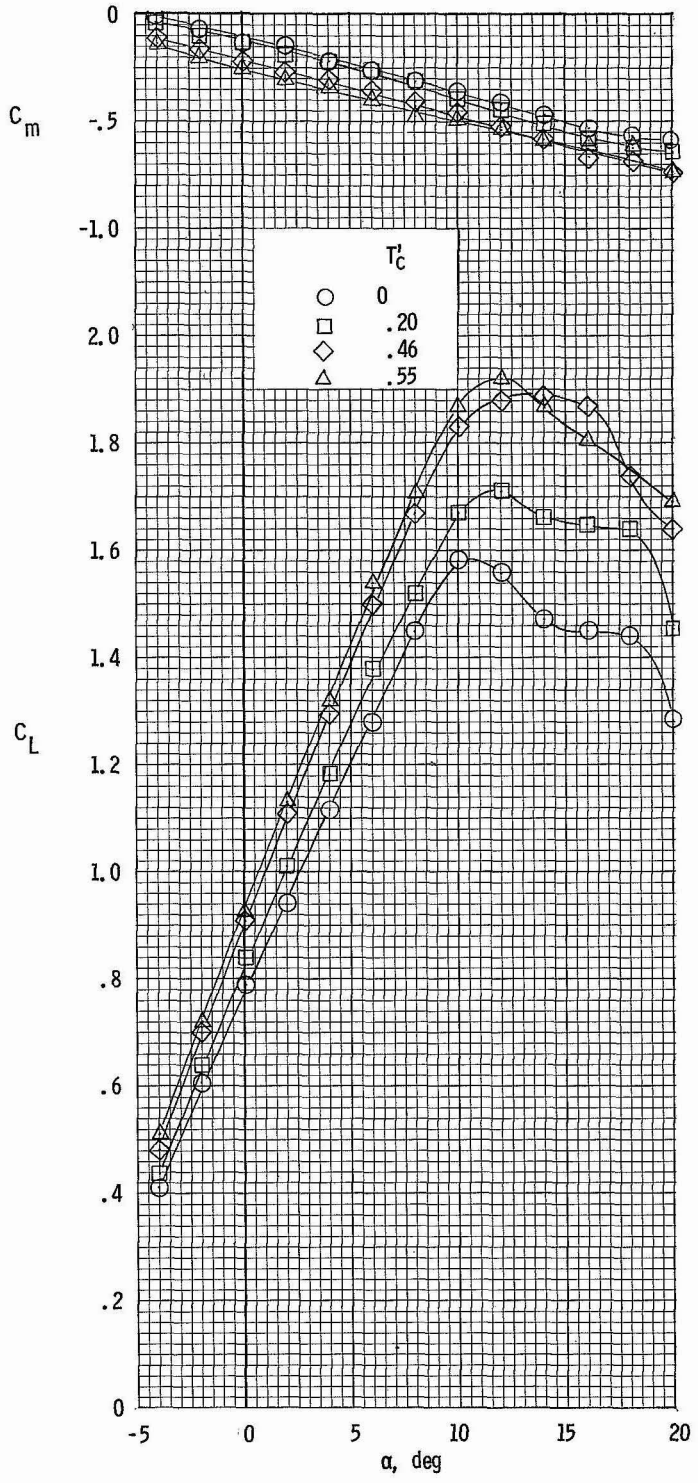


(c) $\delta_f = 32^0$.

Figure 38.- Concluded.

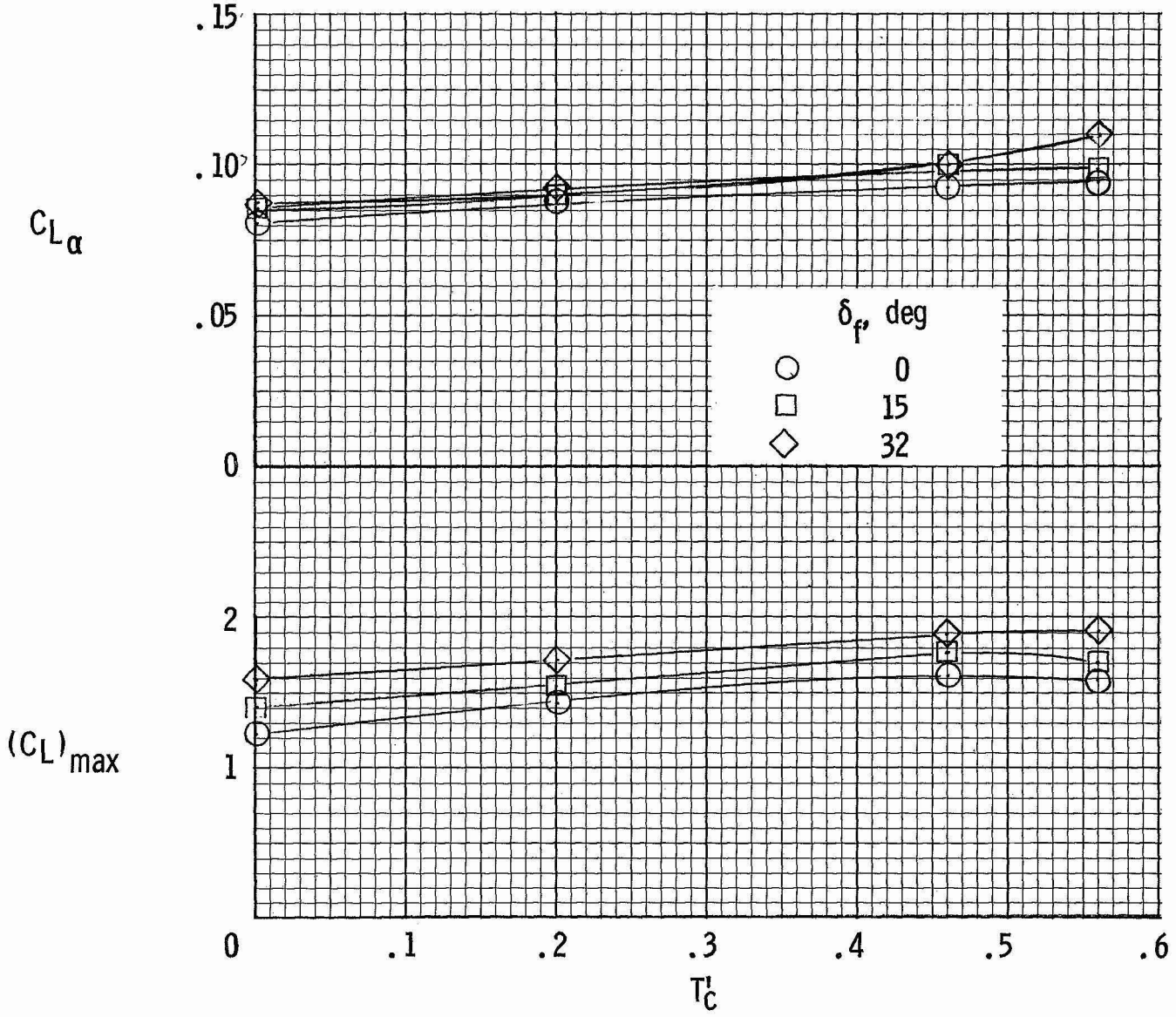


Figure 39.- Effect of power on lift-curve slope and maximum lift coefficient. $\delta_t = 0^0$.

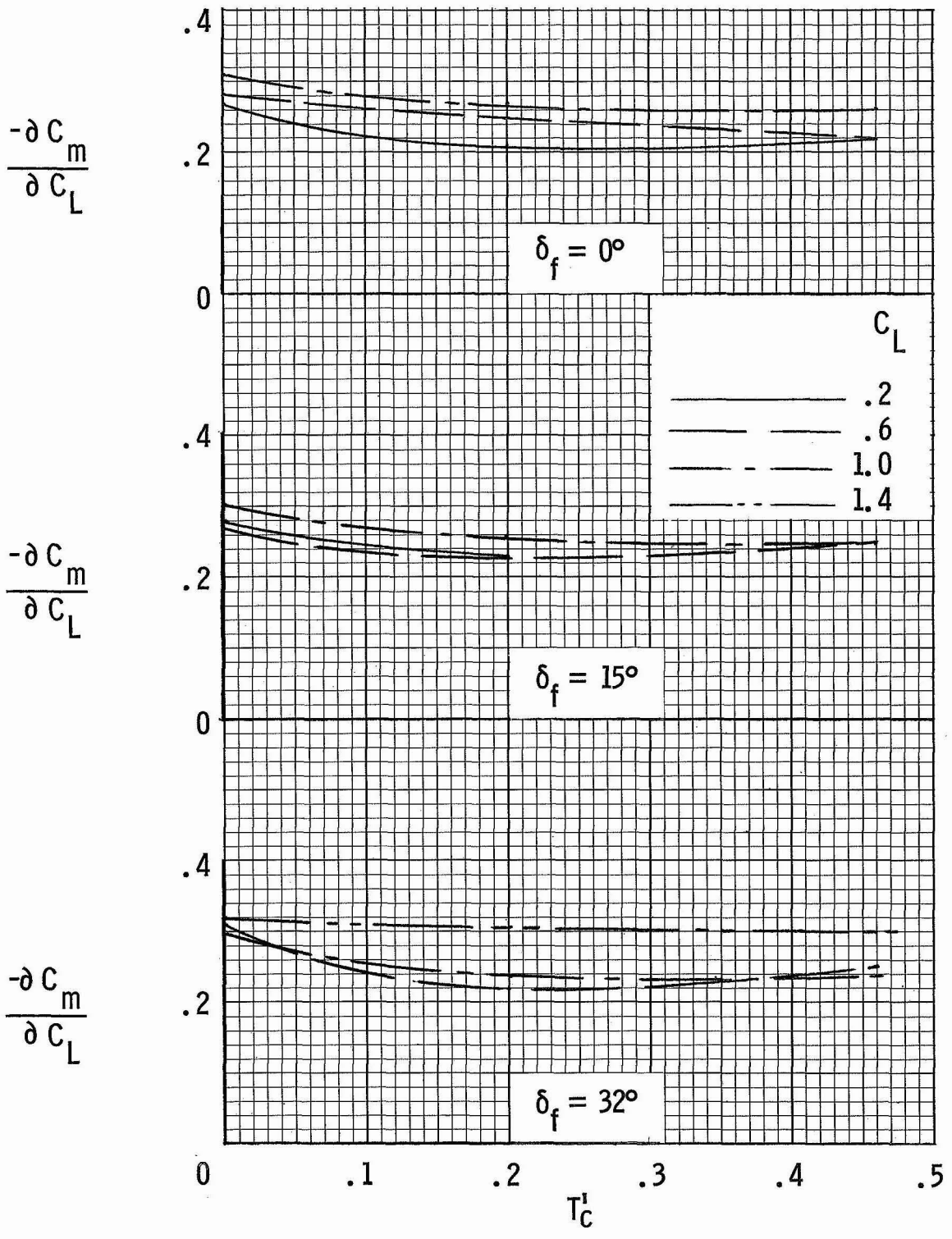


Figure 40.- Stick-fixed power-on longitudinal stability characteristics for 0.10$\bar{c}$ center-of-gravity location.

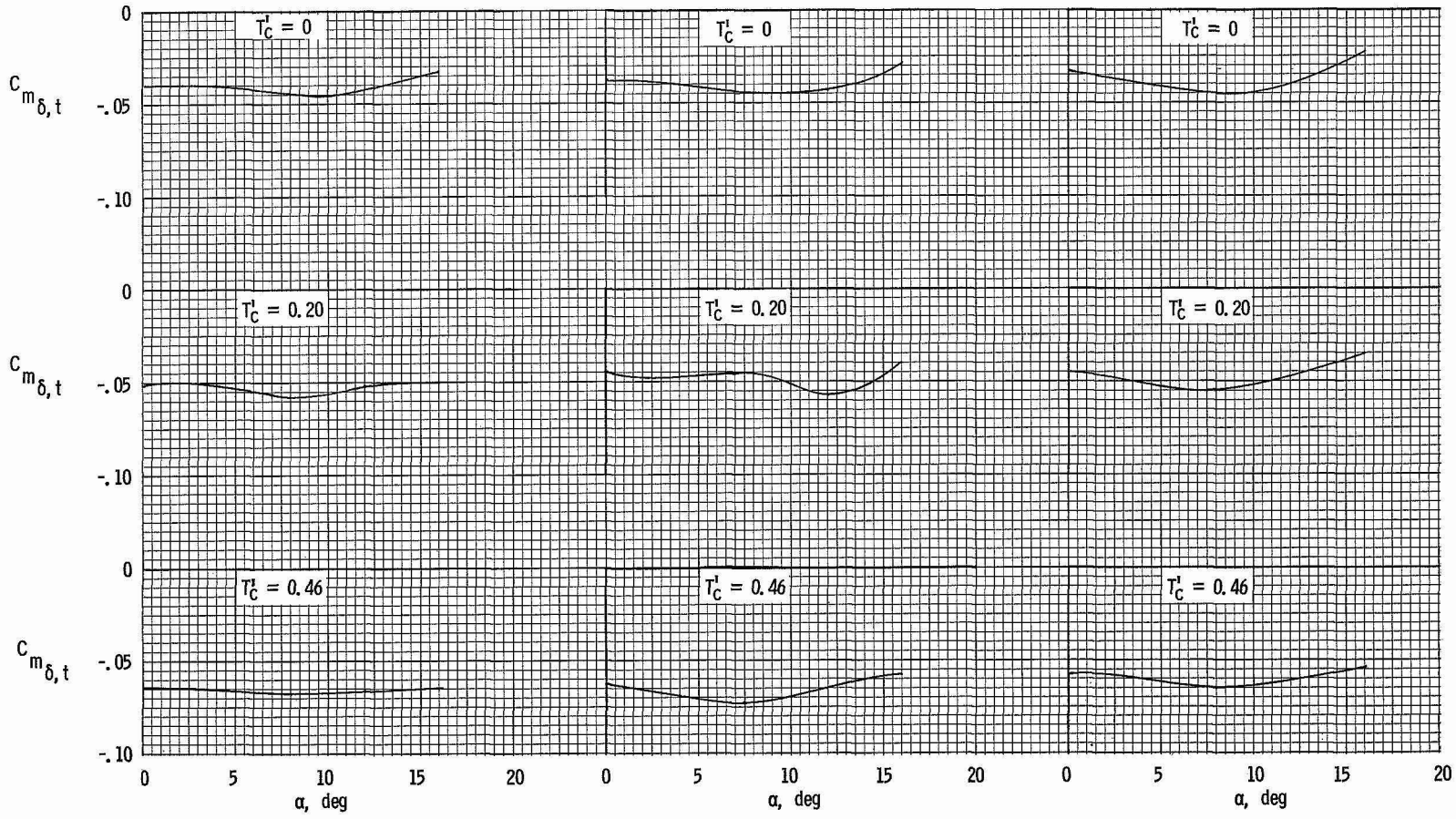


(a) $\delta_f = 0^o$. (b) $\delta_f = 15^o$. (c) $\delta_f = 32^o$.

Figure 41.- Variation of horizontal-tail effectiveness with angle of attack.

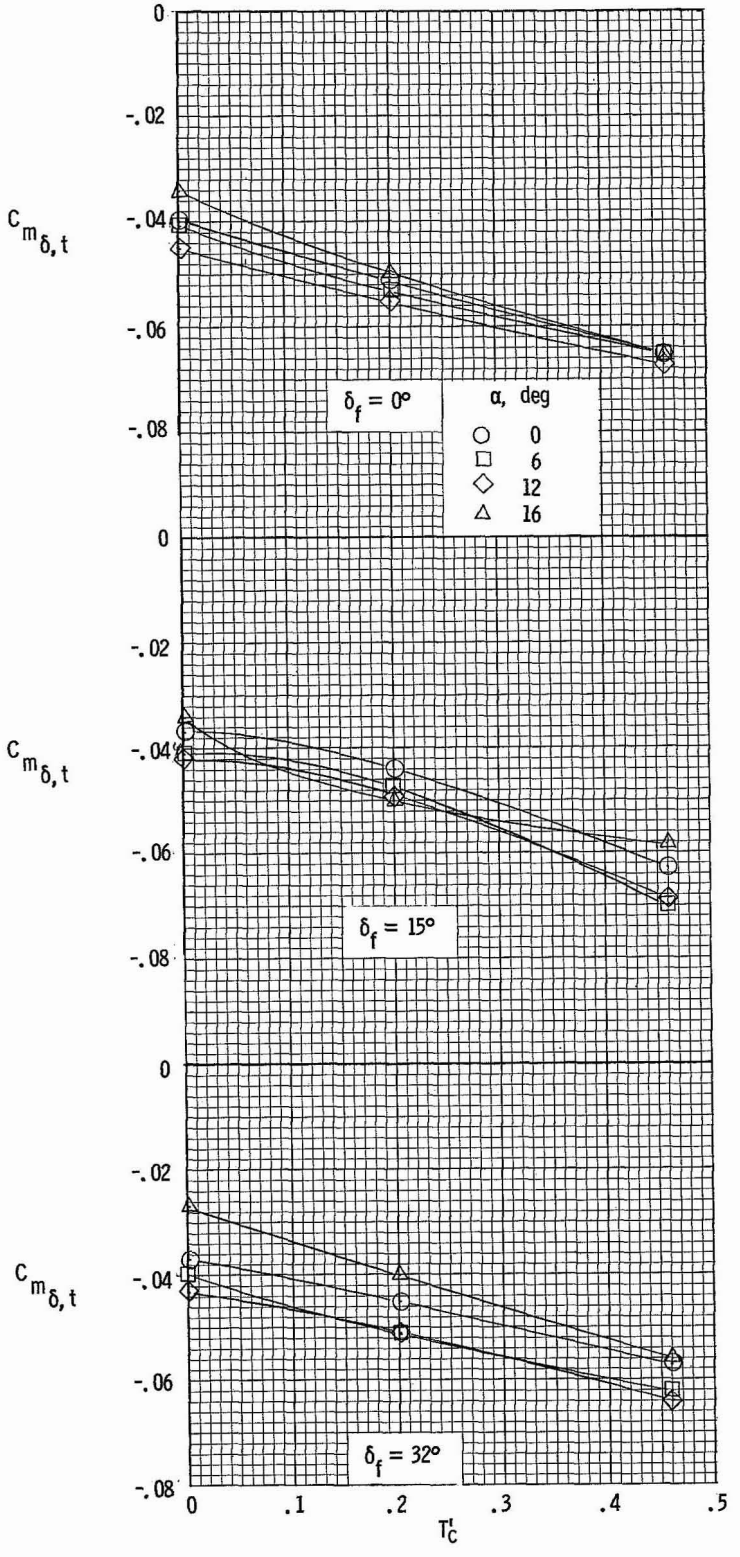


Figure 42.- Effect of power on horizontal-tail effectiveness.

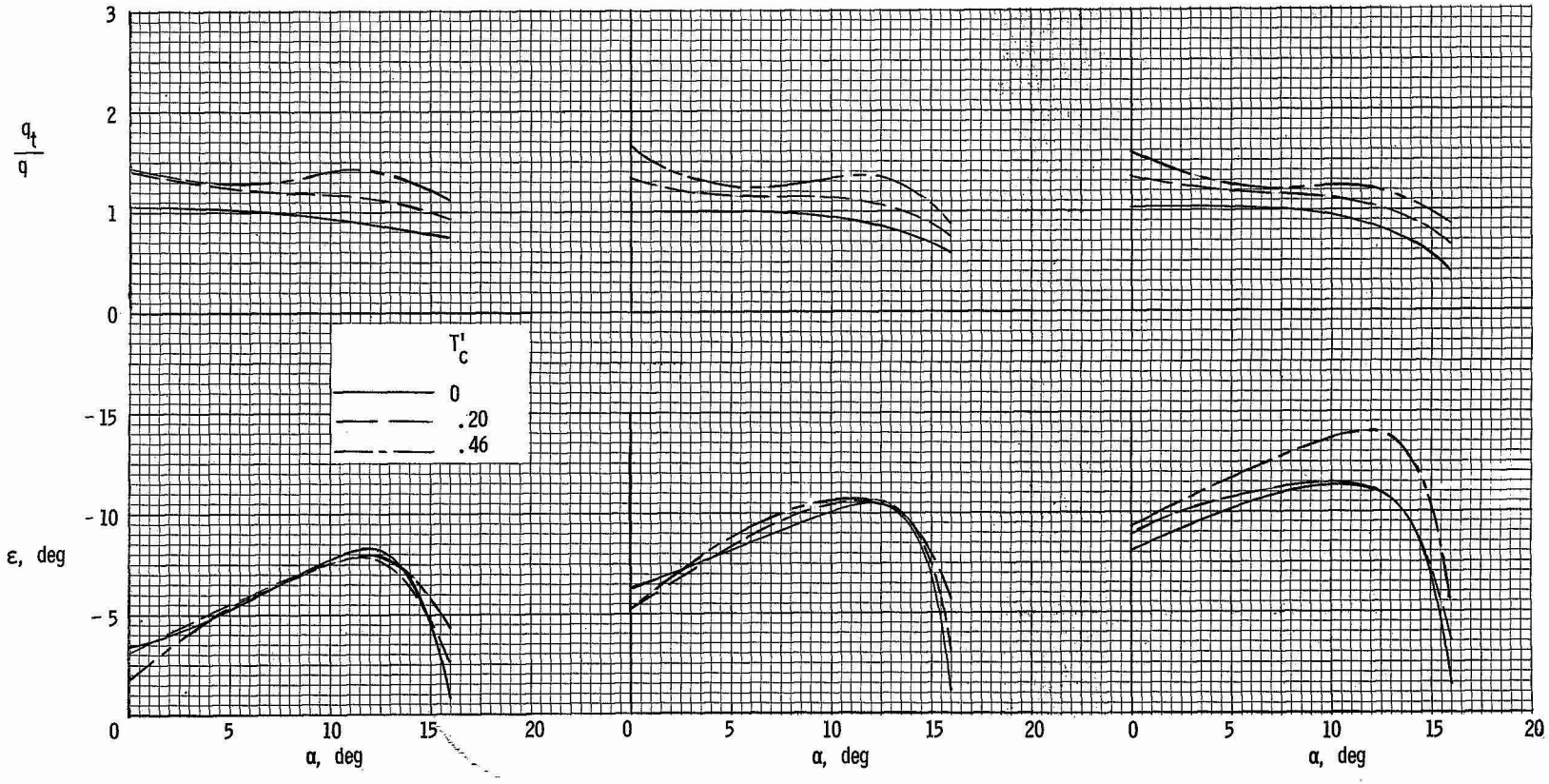


(a) $\delta_f = 0^o$. (b) $\delta_f = 15^o$. (c) $\delta_f = 32^o$.

Figure 43.- Variations of average tail downwash angle and dynamic pressure ratio with angle of attack for several power and flap settings.

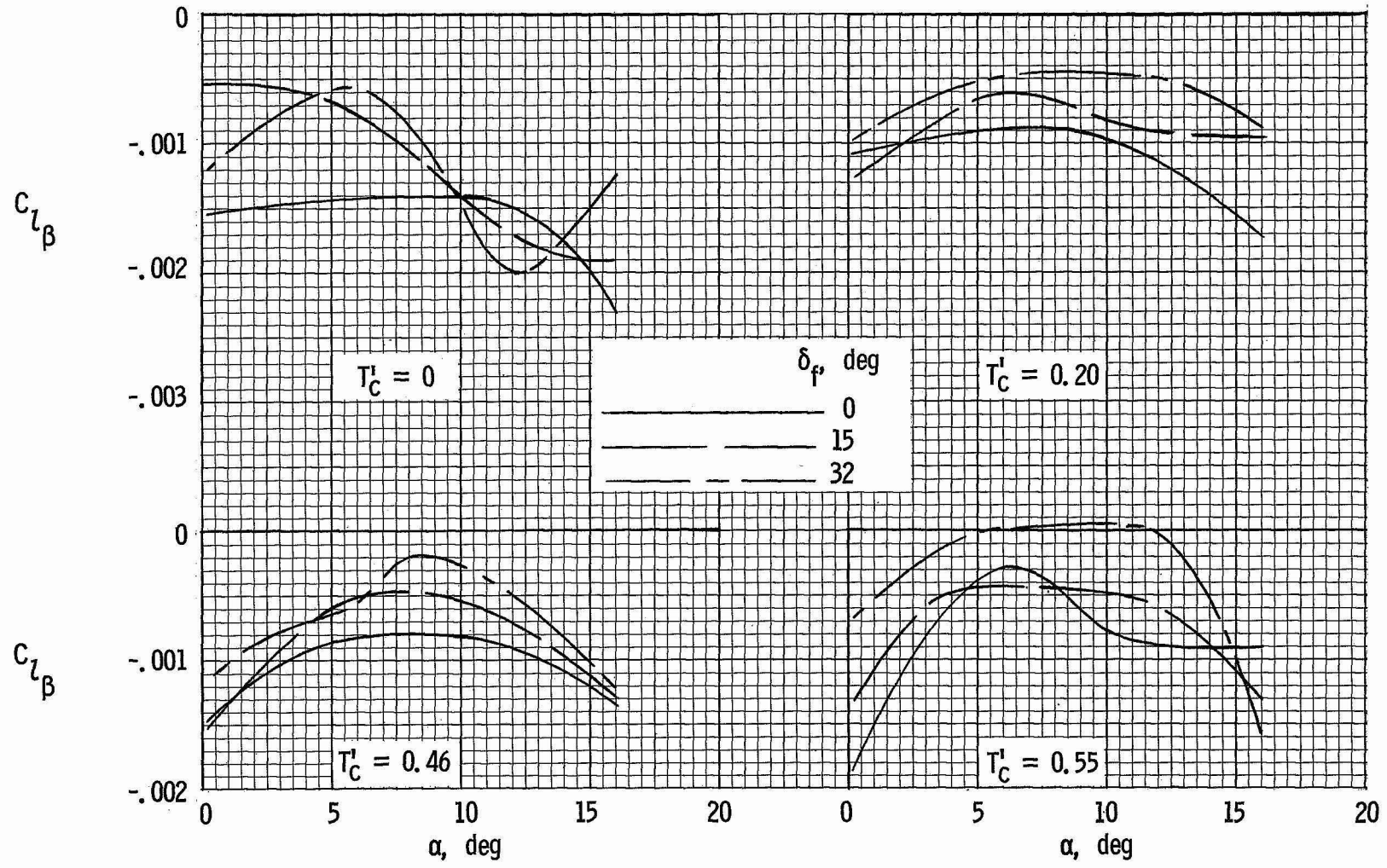


Figure 44.- Effective dihedral characteristics.

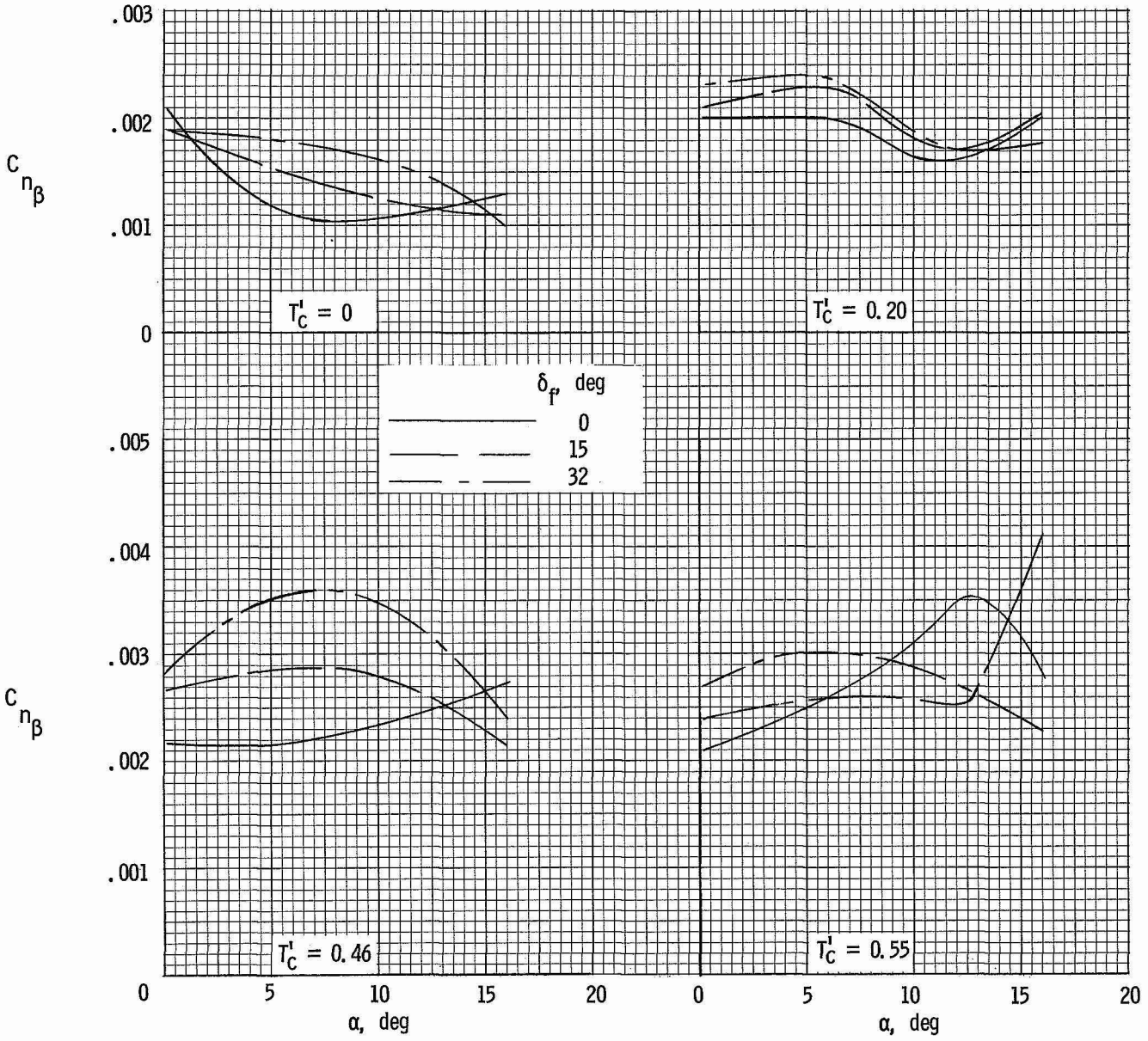


Figure 45.- Directional stability characteristics.

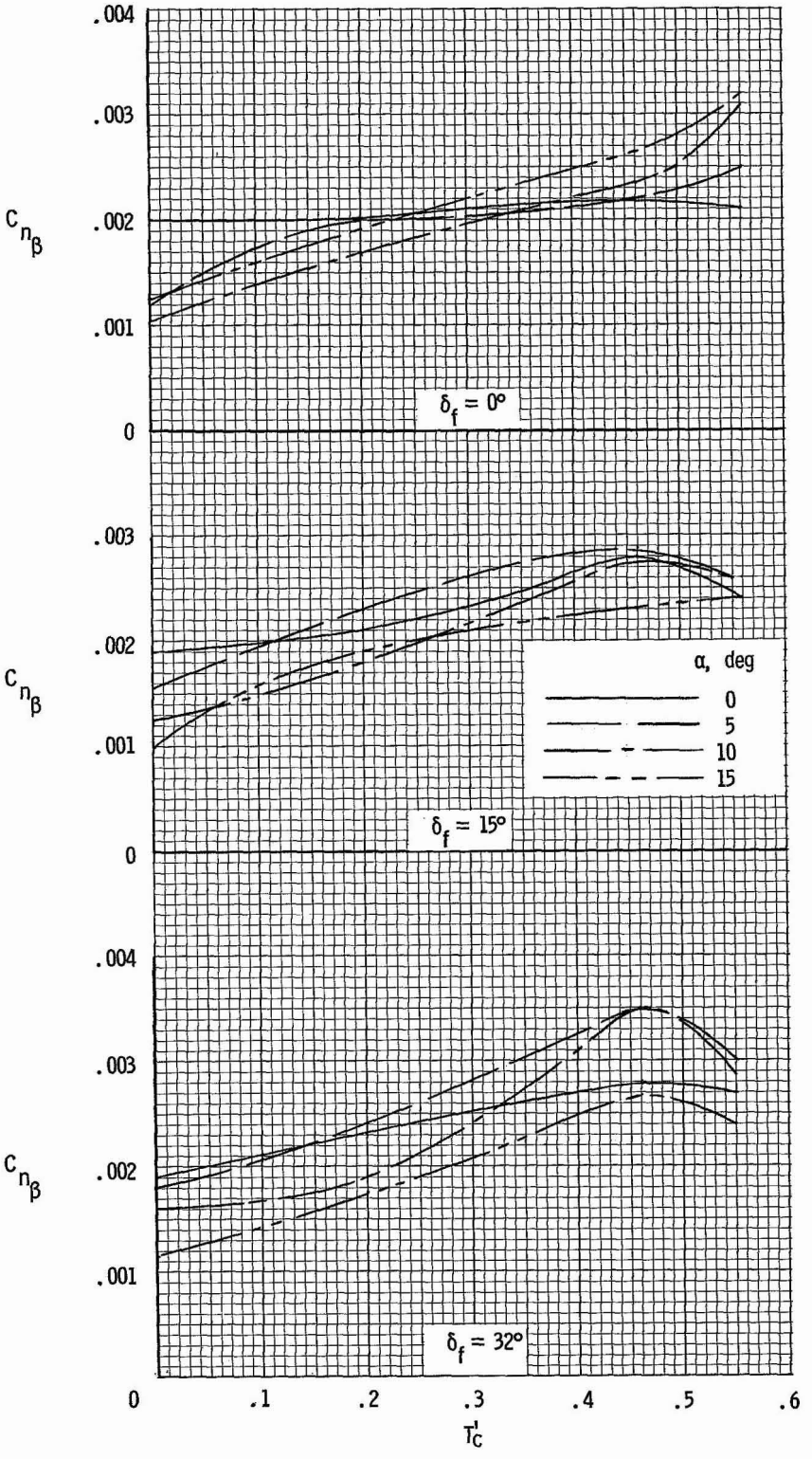


Figure 46.- Effect of power on directional stability parameters.

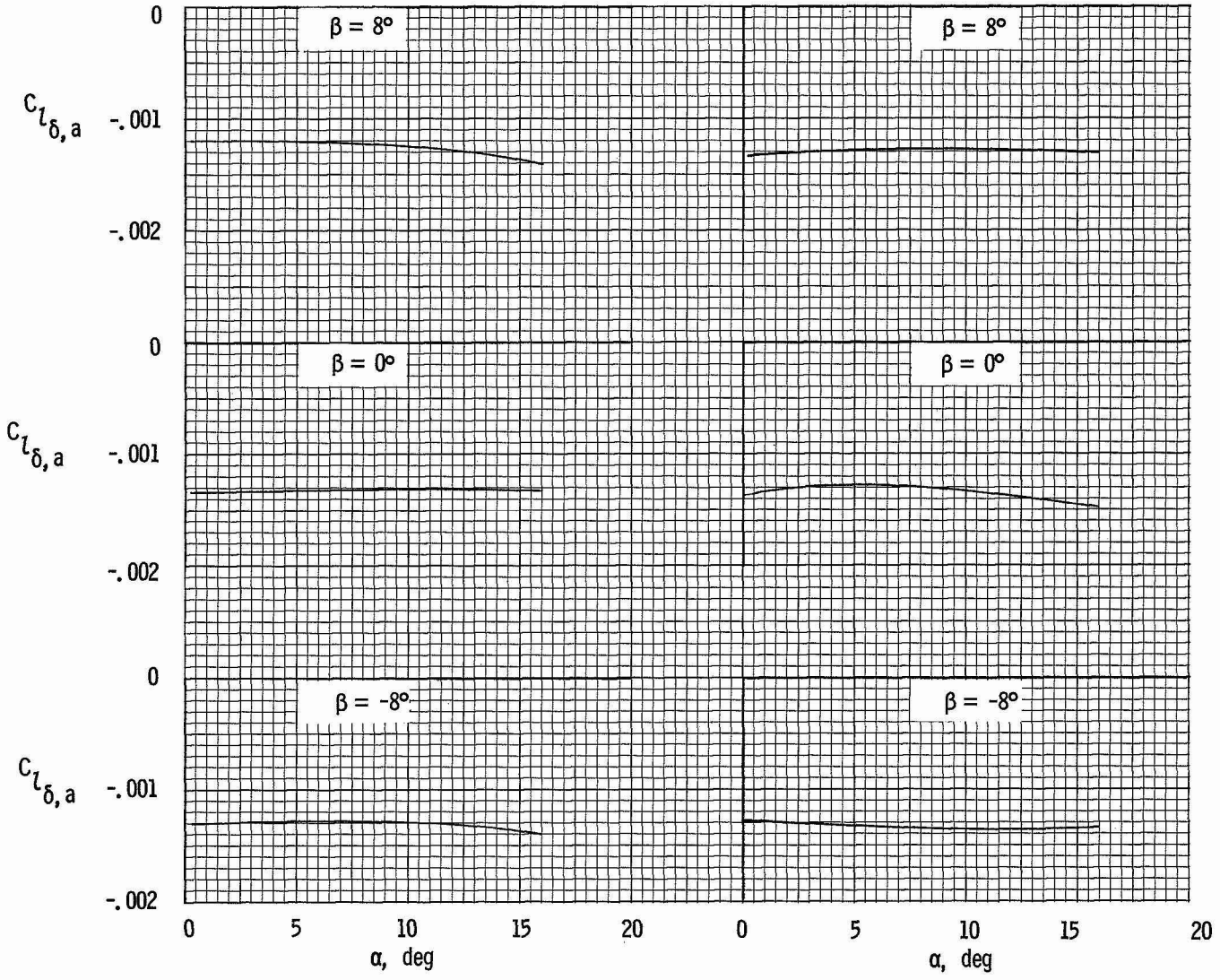


(a) $T_c' = 0$; $\delta_f = 0°$.

(b) $T_c' = 0.46$; $\delta_f = 0°$.

Figure 47.- Variation of aileron effectiveness with angle of attack for several sideslip angles and flap deflections.

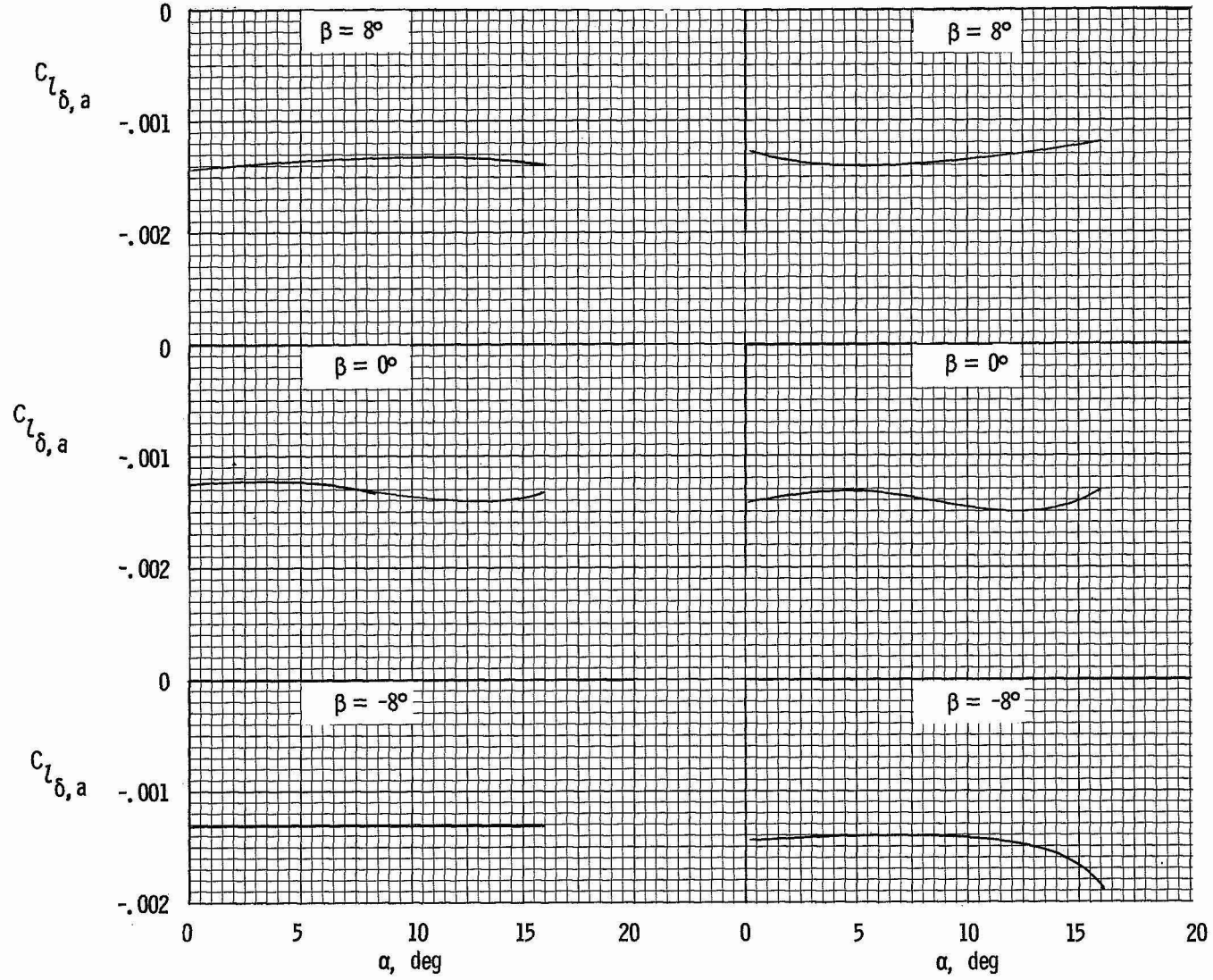


(c) $T_c' = 0$; $\delta_f = 32^o$.

(d) $T_c' = 0.46$; $\delta_f = 32^o$.

Figure 47.- Concluded.

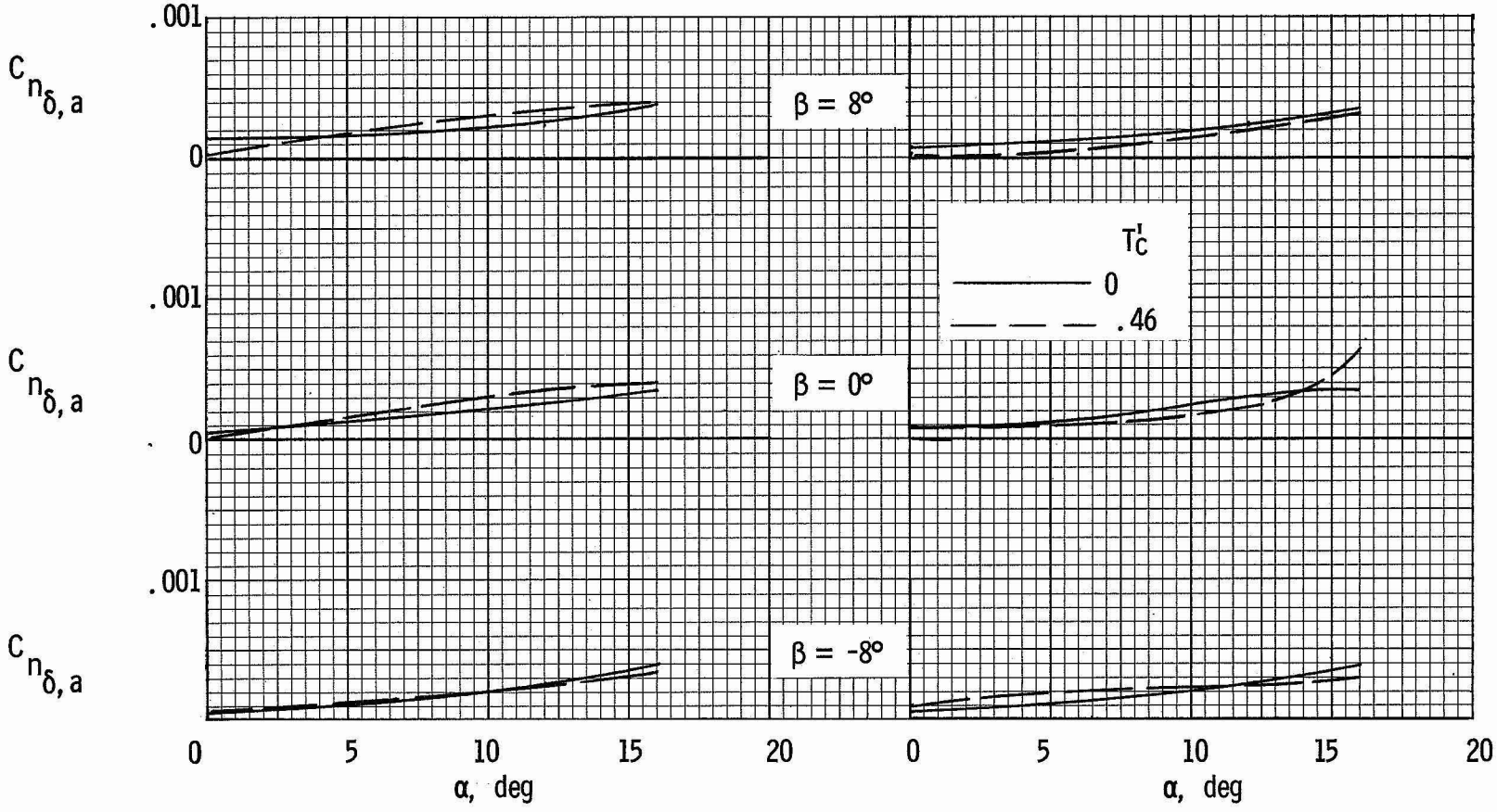


Figure 48.- Effect of aileron deflection on yawing-moment coefficient.

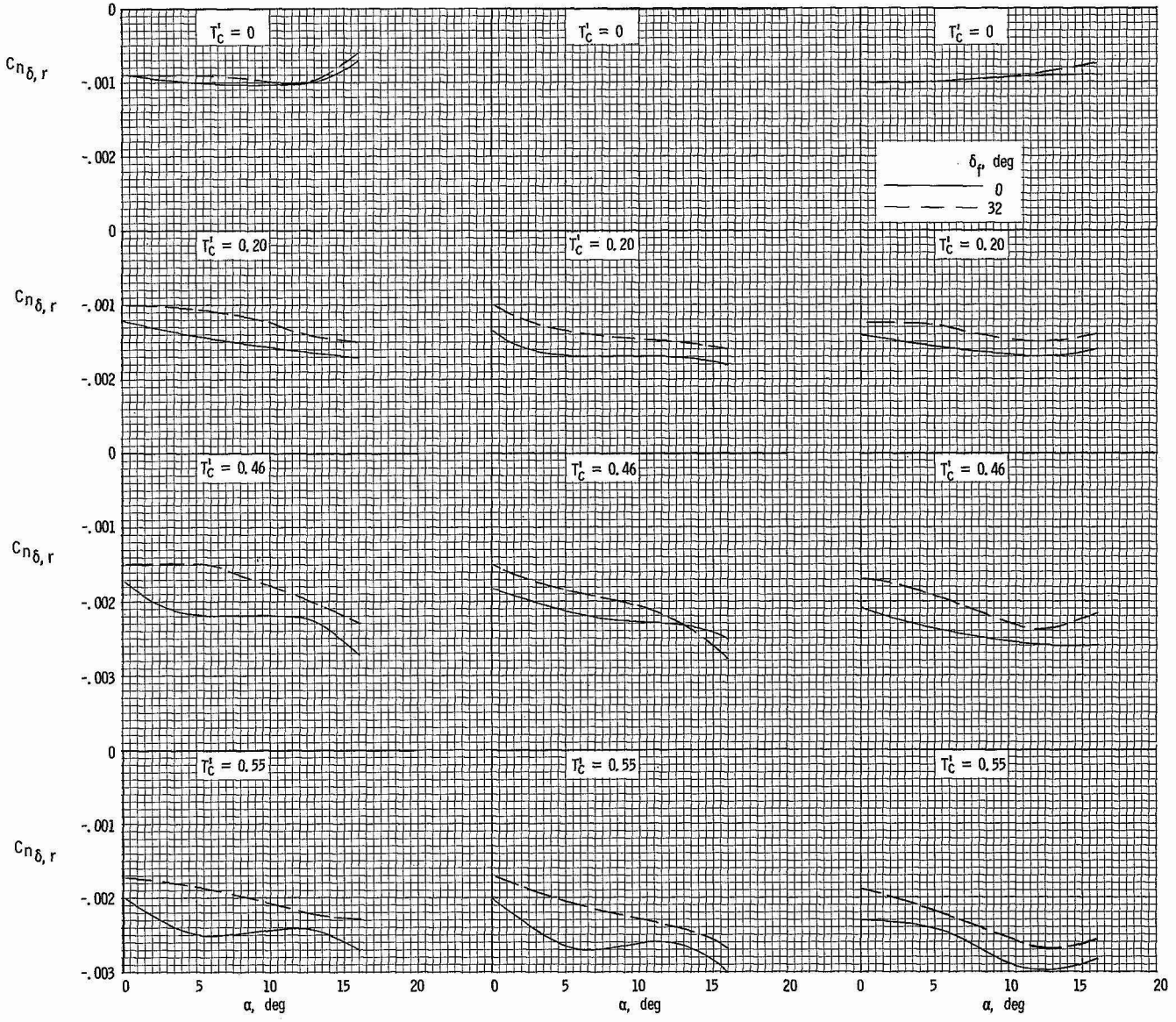


(a) $\beta = 8^0$. (b) $\beta = 4^0$. (c) $\beta = 0^0$.

Figure 49.- Variation of rudder effectiveness with angle of attack for several sideslip angles and flap deflections.

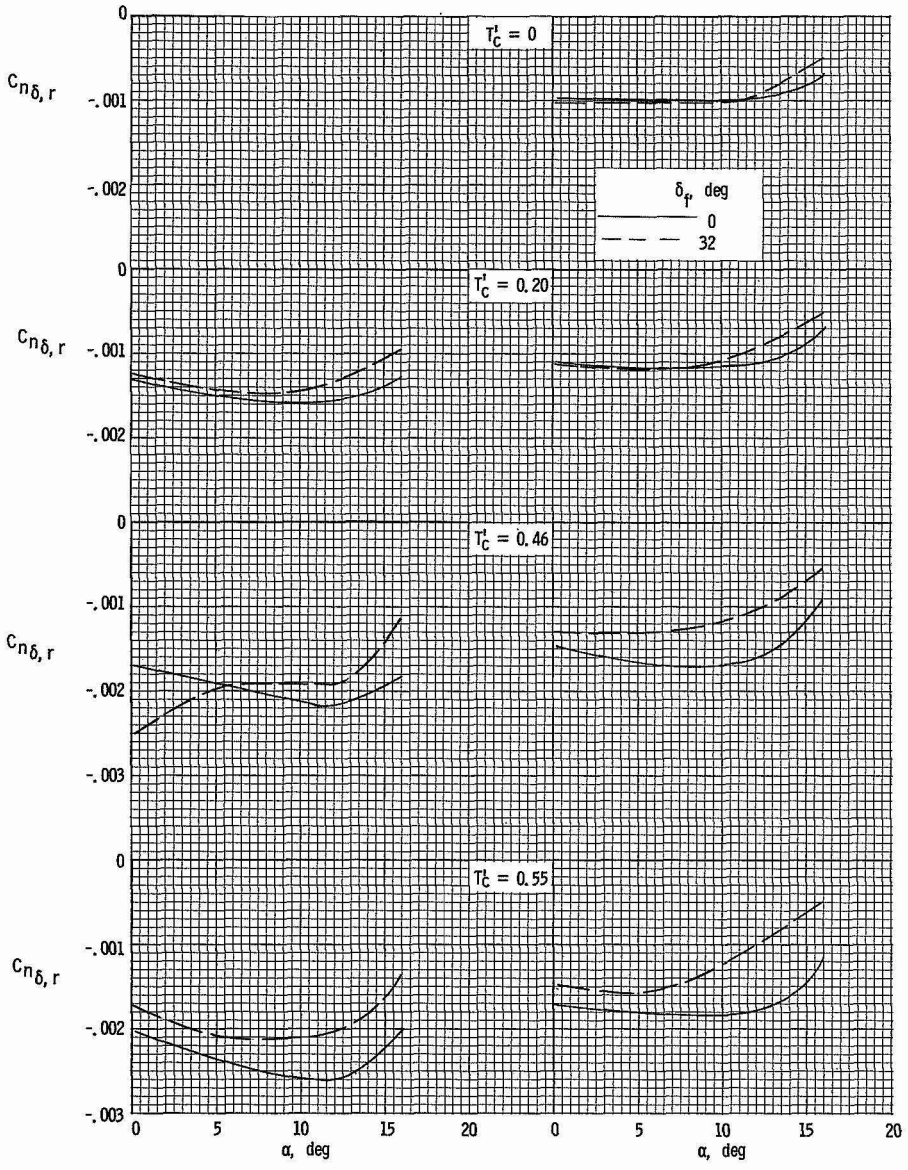


(d) $\beta = -4^{0}$.

(e) $\beta = -8^{0}$.

Figure 49.- Concluded.

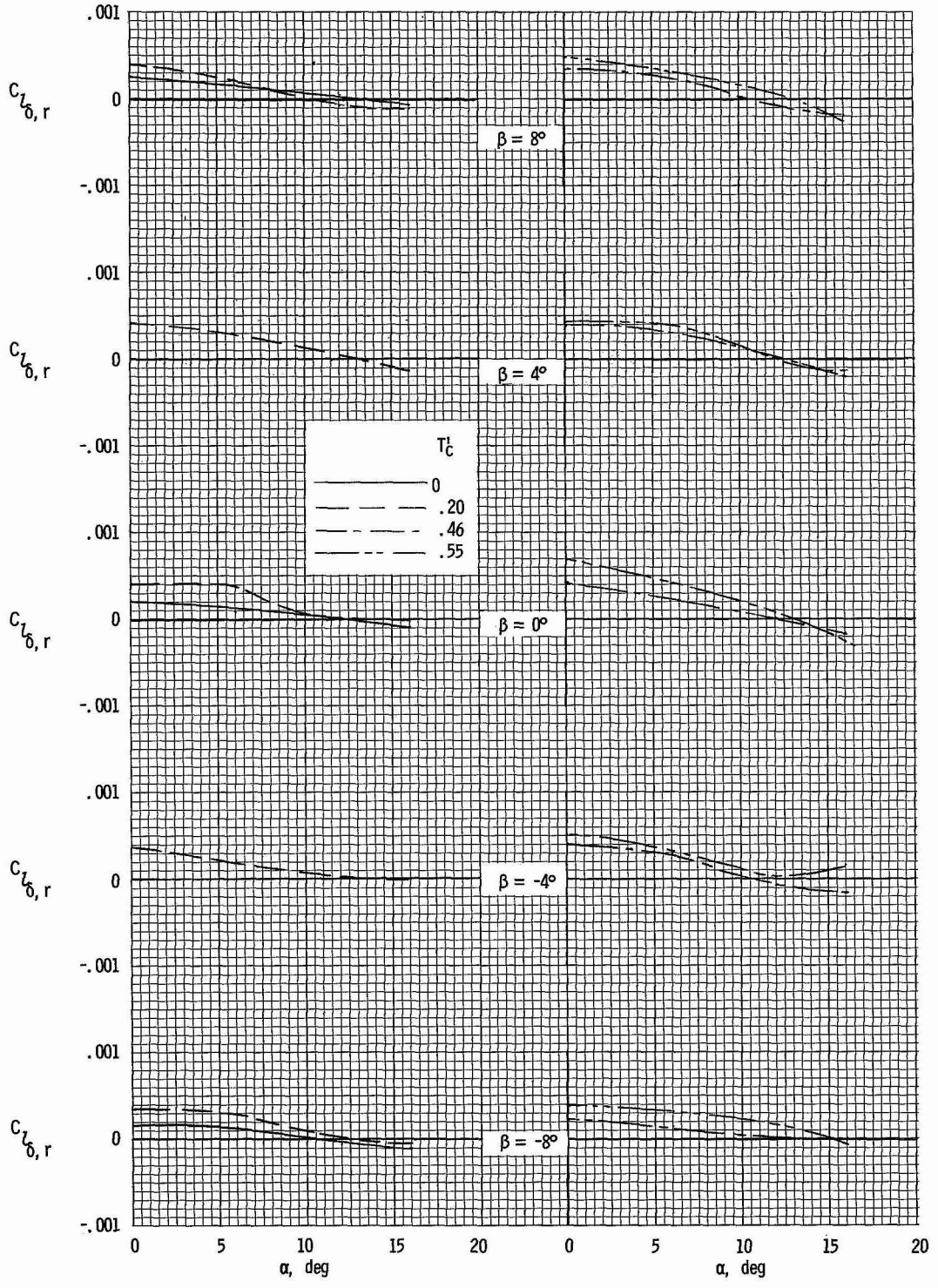


(a) $\delta_f = 0^0$.

Figure 50.- Effect of rudder deflection on rolling-moment coefficient.

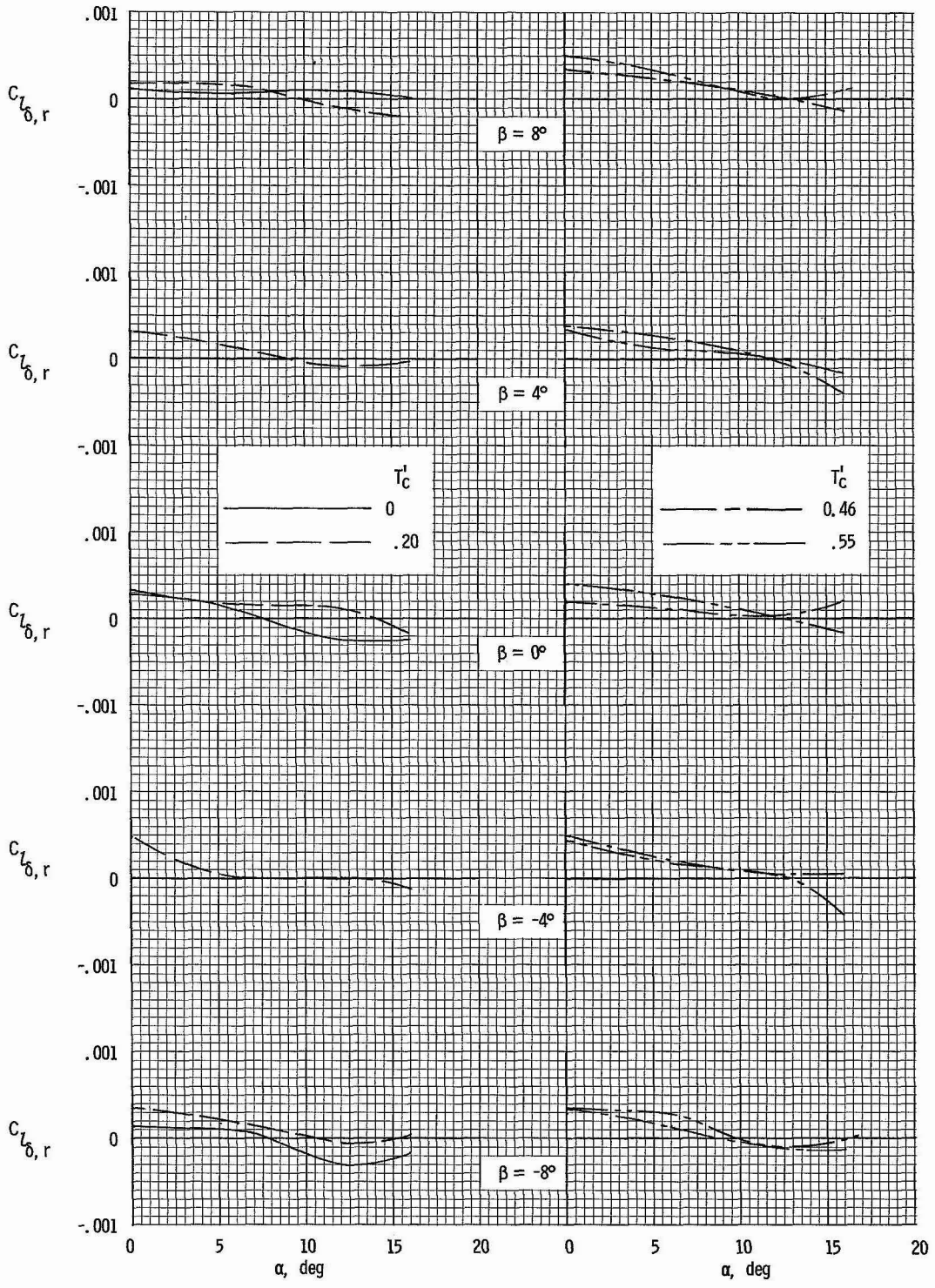


(b) $\delta_f = 32^0$.

Figure 50.- Concluded.

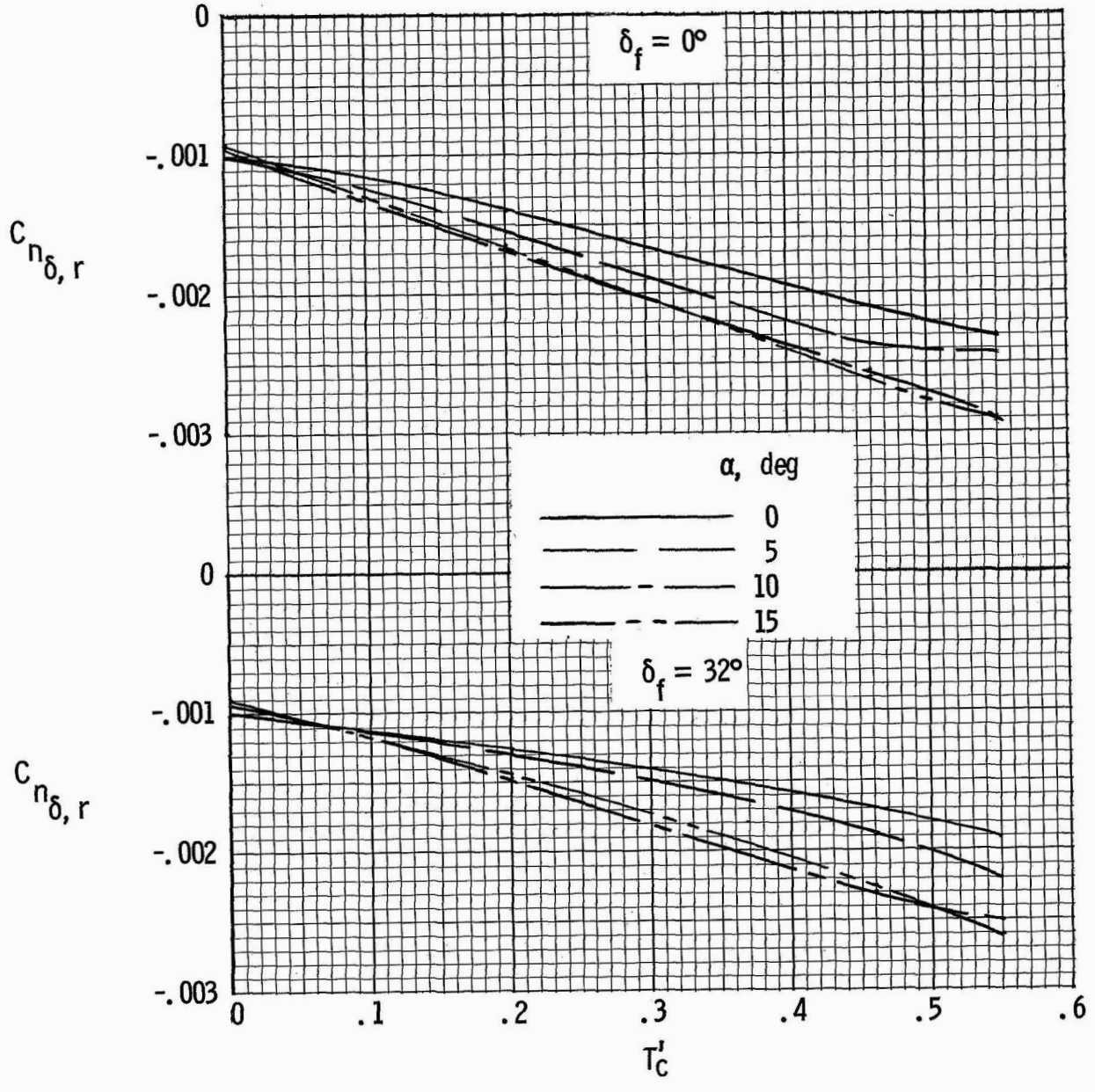


Figure 51.- Effect of power on rudder effectiveness.

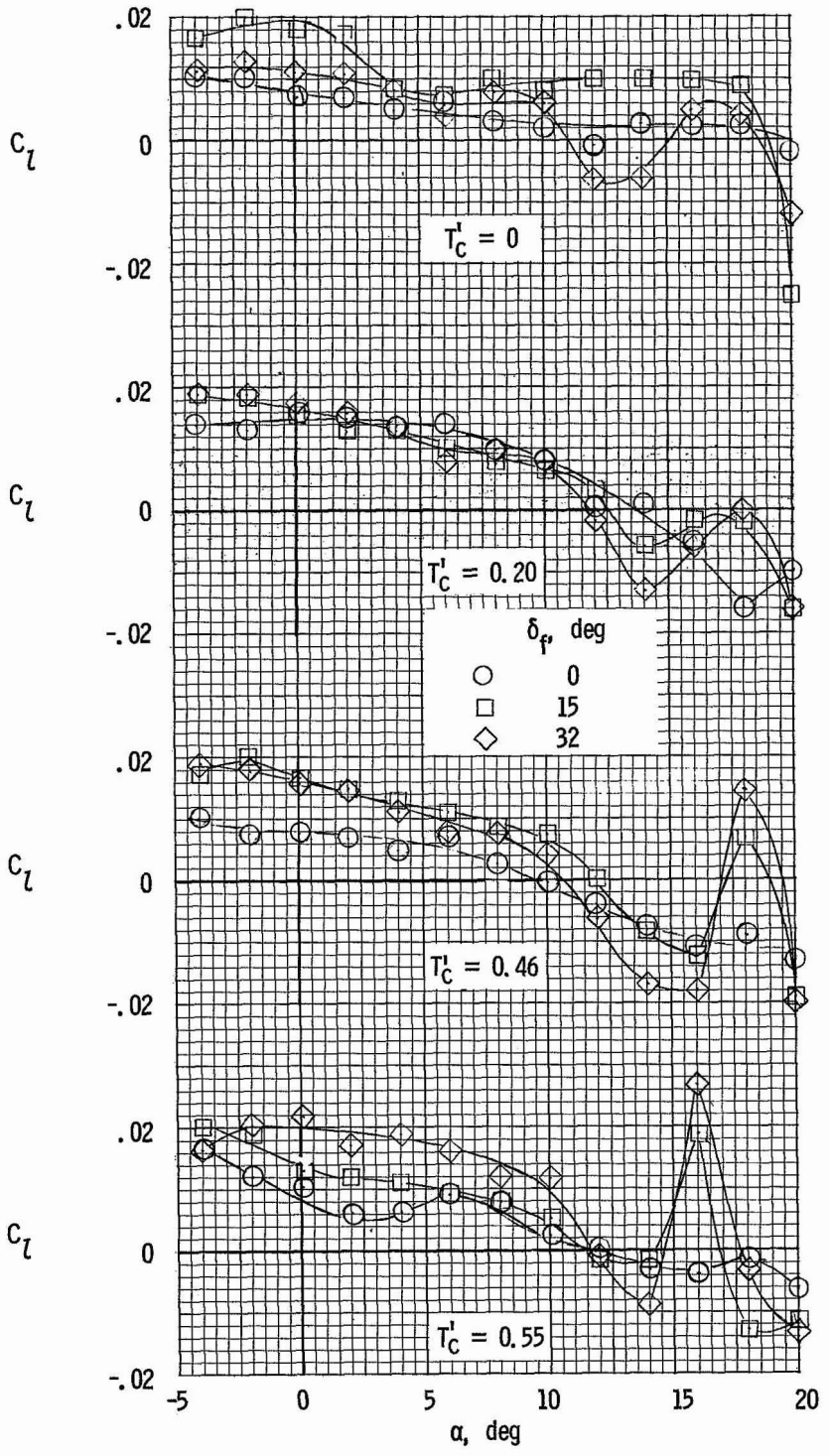


(a) Rolling-moment coefficients.

Figure 52.- Variation of rolling-moment and yawing-moment coefficients with angle of attack. $\beta = 0^o$.

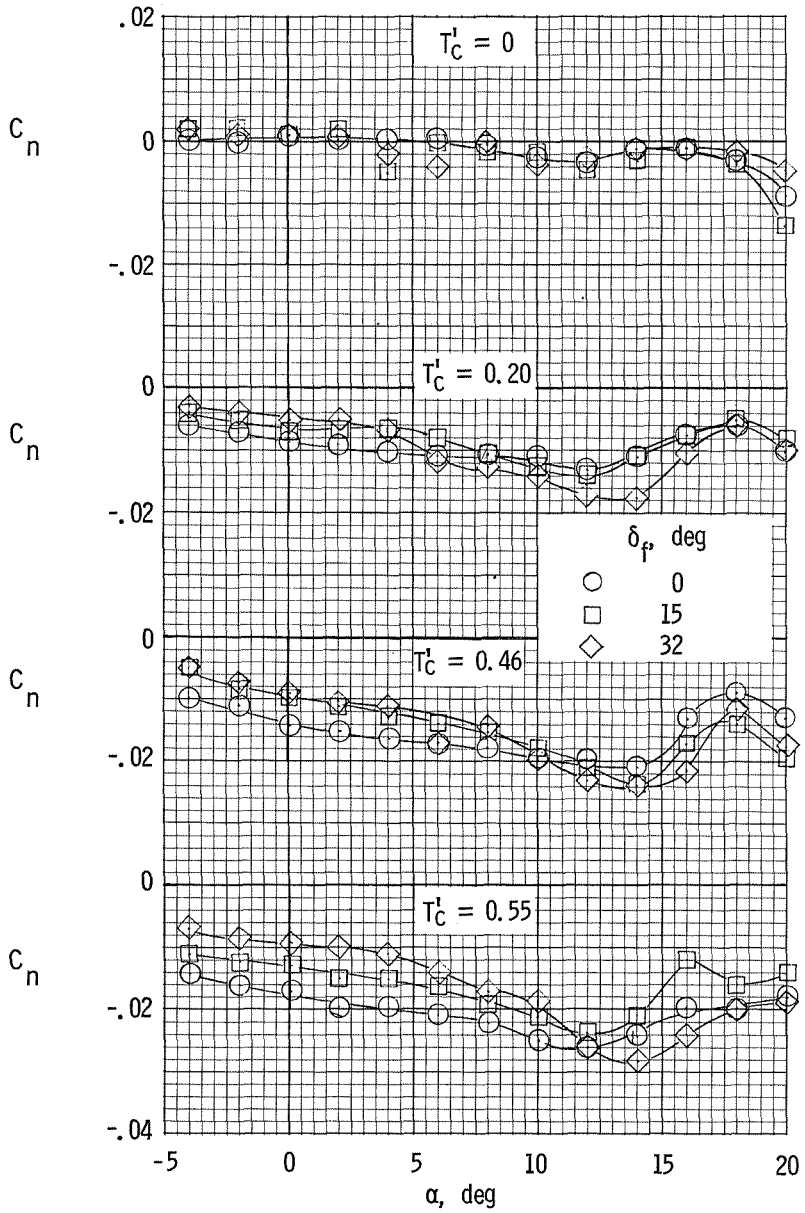


(b) Yawing-moment coefficients.

Figure 52.- Concluded.

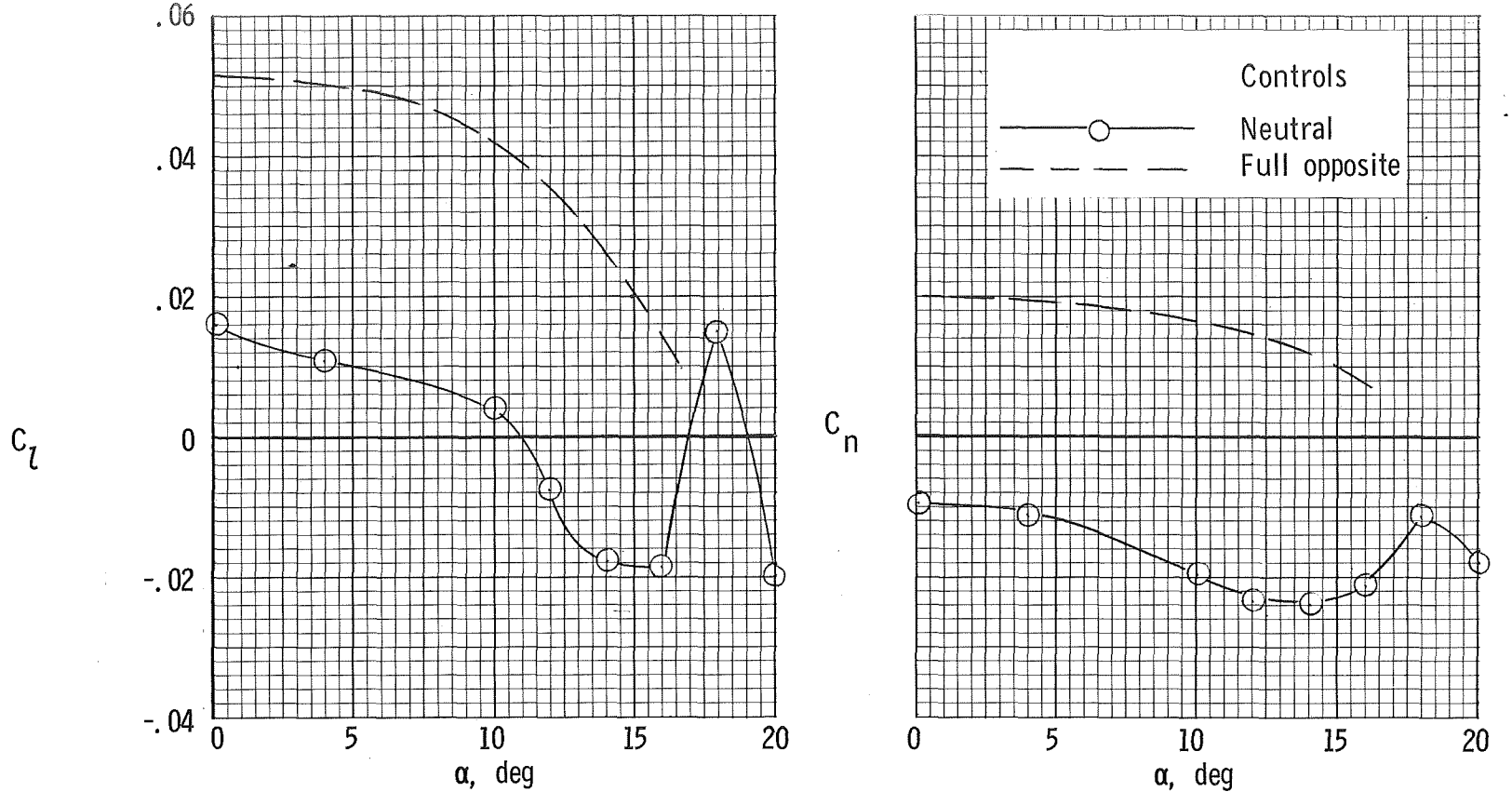


Figure 53.- Control capability for overcoming lateral moments. $\delta_f = 32^o$; $T_C' = 0.46$; $\beta = 0^o$.